

From bio-inspired locomotion models To controllers for lower-limb exoskeletons

Thèse N° 9344

Présentée le 28 février 2019

à la Faculté des sciences et techniques de l'ingénieur

Laboratoire de biorobotique

Programme doctoral en robotique, contrôle et systèmes intelligents

pour l'obtention du grade de Docteur ès Sciences

par

Florin DZELADINI

Acceptée sur proposition du jury

Prof. K. Aminian, président du jury

Prof. A. Ijspeert, directeur de thèse

Prof. M. Daley, rapporteuse

Prof. H. Geyer, rapporteur

Prof. S. Micera, rapporteur

2019



ÉCOLE POLYTECHNIQUE
FÉDÉRALE DE LAUSANNE

Acknowledgements

I first would like to thank my Thesis director, Prof. Auke Ijspeert, for giving me the opportunity to pursue my Ph.D. at the Biorob, for his encouragement, continuous support and enthusiasm. While allowing me to explore my own ideas and hypotheses, he has always been present to provide me with inputs when needed. He has brought together a team of wonderful people, creating a friendly atmosphere within the lab members. Working in at the Biorob has been truly enriching.

I would like to thank the members of my thesis jury Prof. Aminian Kamiar, Prof. Monica Daley, Prof. Hartmut Geyer and Prof. Sivestro Micera for offering their time to read and evaluate my work.

I am grateful to the Symbitron project which gave me the chance to collaborate with several groups across Europe, giving me the opportunity to meet and work with various scientists, broadening my research experience and allowing our work to reach higher levels. A very special thank goes to all the Symbitron partners, for their hospitality, their involvement, specifically I would like to thank Gijs van Oort, Tycho Brug, Herman van der Kooij, Edwin van Asseldonk, Victor Sluiter, Amber Emmens, Heide Witteveen from University of Twente; Cor Meijneke, Heike Valery, Shiqian Wang from Delft University; Nevio Luigi Tagliamonte, Federica Tamburella, Iolanda Pisotta, Marcella Masciullo, Matteo Arquilla, Marco Molinari from Santa Lucia Fondation; Arash Arami, Androw Pennycott, Huang Hsien Yung and Etienne Burdet from Imperial Collegue; Freygardur Thorsteinsson from Ossur.

A very special thanks goes to my colleagues Amy Wu and Daniel Renjewski with whom I shared many flights and visits all over Europe and shared the amazing cultural and culinary experiences it offers.

The work presented here would not have been possible without the contribution and enthusiasm of numerous students. A special thank to Jean Gschwind, Arnaud Desvachez, Bastien Martin, Nicolas Metteraux, Amandine Grappe, Audrey Schenker, Corentin Puffay, Chiheb Boussema and Rui Vasconcelos.

I also thank all the past and current members of the lab, which I have had the chance to meet, for the opportunity to learn from them and fruitful discussion we have had. Specifically: Alessandro Crespi, Tomislav Horvat, Behzad Bayat, Anne Koelewijn, Kamilo Melo, Hamed Razavi, Amy Wu, Olivier Michel, Philippe Müllhaupt, Romain Baud, Jonathan Arreguit, Andrea

Acknowledgements

Di Russo, Salman Faraji, Jessica Lanini, Mehmet Mutlu, Laura Páez, Amalric Ortileb, Sylvie Fiaux, Francois Longchamp. And past members : Susanne Lipfert, Renaud Ronsse, Andrej Bicanski, Jérémie Knüsel, Andrej Gams, Kostas Karakasiliotis, Sébastien Gay, Soha Pouya, Yannick Morel, Jesse van den Kieboom, Daniel Renjewski, Mostafa Ajallooeian, Stéphane Bonardi, Luca Colasanto, Massimo Vespignani, Alexandre Tuleu, Tadej Petrič

I am also grateful to my friends and peers Sebastian Savidan, Hamza Ouared, César Ferreira, Berat Denizdurduran, Emanuele Formento for the very exciting discussion on control, machine learning, artificial intelligence and neuroscience.

Finally, I would like to thank my family. My parents Catia and Xhevat for encouraging me all along my studies and the Ph.D. My two sisters, Flora and Donika, for their love and good energy.

My dear son Noam for teaching me the art of now and Nadine, for making all this possible.

Bhavatu Sabba Mangalam

Lausanne, 17 Décembre 2018

F. D.

Abstract

Human locomotion shows fascinating abilities which are the results of the interplay between the environment, the biomechanics, the spinal cord, and modulation from higher control centers. How the different structures interact to generate meaningful behavior is an active field of research, and understanding the key principles underlying bipedal locomotion could have a strong impact and important implications in several fields related to both medicine and robotics, such as improved rehabilitation procedures, predicting surgery outcome or facilitated human-robot interaction.

In this context, the development of biologically relevant bipedal models that faithfully recapitulate human locomotion are urgently needed. Existing such bio-inspired models usually rely on one of the two following principles: the Central Pattern Generators (CPGs) and the reflexes. In the first part of the thesis, we present a method to introduce a CPGs as feedforward components in a feedback based (i.e. reflex) model of human walking, named neuromuscular model (NMM). The proposed strategy is based on the idea that, in a feedback driven system, the feedforward component can be viewed as a feedback predictor. We implement the feedback predictors using morph oscillators as abstract models of biological CPGs. Thanks to the intrinsic robustness inherited from the feedback pathways, modulation of CPGs network's frequency and amplitudes becomes possible, over a broad range, without affecting the overall walking stability. Furthermore, the modulation of the CPGs network's parameters allowed smooth and stable gait modulation (such as changes in speed and adaptation to increasing slope) suggesting that the idea of using feedback predictor as gait modulator can be extended to a large range of applications, highlighting the role biological CPGs could play on top of a reflex-based rhythmic movement.

Building on the NMM, we present, in the second part of the thesis, the implementations of the models as controllers on different orthoses and exoskeletons. Wearable devices designed to assist abnormal gaits require controllers that interact with the user in an intuitive and unobtrusive manner. Here, we rationalized that such a neuromuscular controller could be implemented based on the NMM models. The implementation of NMM model on a controller (NMC) was demonstrated for human healthy subject and was confirmed with experiment on SCI subjects with different devices. Overall, the bio-inspired NMCs successfully demonstrated remarkable versatility in generating gait patterns tuned to the subjects' dynamics and producing near-physiological gait at near-normative speeds. The positive SCI subject-machine

Acknowledgements

interaction stemmed from replacing the subject's impaired function with dynamical virtual muscles that require few sensors.

These preliminary but auspicious results have important implications towards the exploitation of natural walking dynamics through understanding human biological behavior in the design of controllers for wearable devices that are amenable to various environmental conditions and promote intuitive and unobtrusive human-machine interaction.

Résumé

La locomotion humaine montre des capacités fascinantes qui résultent de l'interaction entre l'environnement, la biomécanique, la moelle épinière et la modulation des centres de contrôle supérieurs. La manière dont les différentes structures interagissent pour générer un comportement significatif constitue un domaine de recherche actif, et la compréhension des principes clés de la locomotion bipède pourrait avoir un impact important et des fortes implications dans plusieurs domaines liés à la fois à la médecine et à la robotique, tels que l'amélioration des procédures de rééducation, la prédiction des résultats de chirurgie ou l'amélioration des interfaces homme-robot.

Dans ce contexte, il est urgent de mettre au point des modèles bipèdes biologiquement pertinents qui reproduisent fidèlement la locomotion humaine. Les modèles bioinspirés existants reposent généralement sur l'un des deux principes suivants : le réseau locomoteur spinaux (CPGs) et les réflexes. Dans la première partie de la thèse, nous présentons une méthode pour introduire un CPG dans un modèle de marche humaine basé sur les réflexes, appelé ici modèle neuro-musculaire (NMM). La stratégie proposée est basée sur l'idée que, dans un système basé sur des boucles réflexes, le CPG peut être considéré comme un prédicteur des boucles réflexes. Nous implémentons ces prédicteurs en utilisant des "morph oscillateurs" comme modèles abstraits de CPG biologiques. Grâce à la robustesse intrinsèque héritée des réflexes, la modulation de la fréquence et des amplitudes du réseau de CPG est possible, sur une large plage, sans affecter la stabilité globale de la marche. De plus, la modulation des paramètres du réseau de CPG permet une modulation de marche continue (comme des changements de vitesse et une adaptation à la pente croissante), ce qui suggère que l'idée d'utiliser des CPG comme modulateur de marche peut être étendue à une large gamme d'applications, soulignant le rôle que les CPG biologiques pourraient jouer au-dessus d'un mouvement rythmique basé sur les réflexes.

En nous appuyant sur le NMM, nous présentons, dans la deuxième partie de la thèse, des implémentations de contrôleurs inspirés de ces modèles sur différentes orthèses et exosquelettes. En effet, les exosquelettes conçus pour assister les démarches anormales nécessitent des contrôleurs qui interagissent avec l'utilisateur de manière intuitive et discrète. Nous montrons qu'un tel contrôleur neuro-musculaire (NMC) pourrait être mis en œuvre sur la base des modèles NMM. La mise en œuvre du modèle NMM sur un contrôleur (NMC) a été démontrée pour plusieurs sujets en bonne santé et a été confirmée par des expériences sur des sujets

Acknowledgements

paraplégiques avec différents dispositifs. Dans l'ensemble, les NMC ont fait preuve d'une polyvalence remarquable en générant des schémas de marche adaptés à la dynamique des sujets et en produisant une démarche quasi physiologique à une vitesse presque normative. L'interaction positive sujet-machine des sujets paraplégiques provient de l'effet des muscles virtuels qui complètent les capacités restantes du sujet.

Ces résultats préliminaires montrent l'importance que la compréhension du comportement biologique humain peut apporter à la conception de contrôleurs pour exosquelettes, en particulier pour le développement de contrôleurs pouvant être soumis à diverses conditions environnementales et promouvant une interaction homme-machine intuitive et naturelle.



Keywords

Human locomotion, particle swarm algorithm (PSO), neuromuscular model, reflex, central pattern generator (CPG), spinal cord injury, paraplegia, rehabilitation, exoskeleton, orthese



Mots-clefs

Locomotion humaine, optimisation par essais particuliers (OEP), modèle neuromusculaire, réflexe, réseau locomoteur spinal, synchronisation, lésion de la moelle épinière, paraplé-
gie, rééducation, exosquelette, orthèse

Contents

Acknowledgements	iii
Abstract/Resume	v
Keywords/Mots-clefs	ix
List of Acronyms	xvi
List of Figures	xvi
List of Tables	xix
Introduction	1
1 Context	1
2 Physiological aspects of locomotion	3
2.1 Spinal cord's reflex circuits	3
2.2 Spinal central pattern generators	4
2.3 Upper brain structures	6
2.4 Musculo-skeletal system	10
2.5 Sensory system	13
3 Analysis and modeling of walking	14
3.1 Top-down approaches	14
3.2 Bottom-up approaches	15
3.3 Neuromechanical approaches	15
4 Control aspects of CPGs and current use in robotics	17
4.1 Background	17
4.2 CPG design methodology	18
5 Robotic training controller for spinal cord injury	28
5.1 Spinal Cord injury	28
5.2 Robotic training after neurologic injuries	29
5.3 Assistive control	30
5.4 Adaptive control	31
6 Thesis objectives	33
7 Contributions	35

I	On NeuroMechanical modeling of locomotion control	39
1	Learning and optimization of walking gaits	43
1.1	Introduction	43
1.2	particle swarm optimization (PSO)	43
1.2.1	PSO algorithms	44
1.2.2	Stage PSO objective function	46
1.2.3	Optimization criteria	46
1.2.4	Practical consideration when optimizing walking controller	50
2	A reflex based neuromuscular model of human walking	53
2.1	Introduction	53
2.2	Methodology	55
2.2.1	Spinal cord	56
2.2.2	Simulation environment and Optimization	59
2.3	Results	63
2.3.1	Metabolic cost analysis	63
2.3.2	Golden ratio analysis of gait harmony	64
2.3.3	Gait analysis	64
2.4	Discussion	65
3	Pattern in the central nervous system	69
3.1	Introduction	69
3.2	Methodology	70
3.2.1	CPG Model	71
3.2.2	3FBL models	75
3.2.3	3FBL modulation: model of supraspinal influences	75
3.3	Results	76
3.3.1	Feedback and feedforward study	77
3.3.2	3FBL Models: Systematic study of supraspinal signal modulation and their effects on gait	81
3.4	Discussion	82
3.4.1	CPG modulations on both proximal and distal muscles allow speed control	82
3.4.2	Stable locomotion is produced even with a significant decrease in feedback activity	84
II	On symbiotic control of exoskeleton	89
4	Neuro-Muscular Controller (NMC) concept validation	93
4.1	Introduction	93
4.2	Materials and methods	94
4.3	Results	96
4.4	Discussion	100

5 NMC constraints and design methodology and use cases	105
5.1 Introduction	105
5.2 Exoskeleton for paraplegics	105
5.3 Modularity and tailoring aspect	109
5.3.1 Neuromuscular control parameters	109
5.3.2 NMC customization for subject-specific control	111
5.4 Gait initiation	112
5.5 Real-time system requirements	113
5.5.1 Limitation of hill muscle model	114
5.6 Torque tracking	114
6 Applications	117
6.1 Introduction	117
6.2 I : NMC for incomplete SCI on the Achilles exoskeleton	118
6.2.1 Pilots general information	118
6.2.2 Objectives	120
6.2.3 Methods	120
6.2.4 Results	123
6.2.5 Summary of achievements	125
6.3 II : NMC for incomplete SCI on the WE1 exoskeleton	127
6.3.1 Pilots general information	127
6.3.2 Objectives	127
6.3.3 Methods	127
6.3.4 Results	130
6.3.5 Summary of achievement	136
6.4 IV : NMC for complete SCI on the LOPES gait trainer	138
6.4.1 Introduction	138
6.4.2 Material and Methods	139
6.4.3 Results	146
6.4.4 Discussion	152
6.5 III : NMC for complete SCI on the WE2 exoskeleton	156
6.5.1 Pilot general information	156
6.5.2 Objectives	156
6.5.3 Methods	156
6.5.4 Results	158
Outlook	162
III Appendix	167
A Software	169
1.1 Simulink/Matlab neuromuscular controller	169

Contents

1.1.1	Library description	169
1.1.2	Example of Ankle Knee reflex modules used with WE1	172
B	Hardware	175
2.1	Ethercat	175
2.1.1	Etherlab and Symbitron wiki	175
2.1.2	Low level simulink library	176
2.2	Exoskeleton devices	176
C	Mathematical models	177
3.1	Musculoskeletal system	177
3.1.1	Ligament model	177
3.1.2	Muscle model	178
3.1.3	Sensors model	179
3.2	CPG models	182
D	Supplemental experiments	191
4.1	Neuromuscular ankle controller modeled as an impedance controller	191
E	Clinical aspects	193
5.1	Subjects	193
5.1.1	Incomplete paraplegics	193
5.1.2	Complete paraplegics	194
5.2	Assessments	194
5.2.1	training procedure	194
5.2.2	Clinical assessment	198
	Bibliography	219
	Curriculum Vitae	221

List of Figures

1	Paraplegic subject undergoing epidural stimulation of lumbar spinal cord . . .	7
2	Central nervous system involved in locomotion. Overview	9
3	Type of possible decerebration	10
4	Illustration of the skeletal muscle anatomy and contraction process.	11
5	Schematic representation of muscle force-length force-velocity relationship . .	12
6	Inverted pendulum and SLIP model ground reaction forces	16
7	Taga CPG Bipedal model overview.	20
1.1	Random push environment description.	52
1.2	Wavy ground environment description.	52
2.1	Schematic view of the state machine used in the reflex model [79]	54
2.2	Closed loop information flow of the FBL model	55
2.3	FBL model biomechanical comparison to human	66
2.4	FBL optimization cost of transport and golden ratio.	67
3.1	Schematic representation of feedback-feedforward relative importance for one specific pathway	71
3.2	Schematic representation of the spinal network and supraspinal control of the CPG network in the 3FBL model	72
3.3	CPG synchronization mechanism with the environment	74
3.4	$I_{N_{sen}}$ signals (dotted lines) and the reproduced signals (thick lines) for the the worst gait	77
3.5	One by one feedback and feedforward combination effect on gait	85
3.6	$3FBL_{fdb}^{min}$ and FBL model comparison	86
3.7	Systematic search study of CPG parameters (supraspinal influences) for the different 3FBL models	87
4.1	Schematic view of the control achitecture of the Ankle controller	95
4.2	Measured exoskeleton torque on Achilles experiment with healthy subject . . .	97
4.3	Muscle activity recording during Achilles experiment with healthy subject . . .	98
4.4	Net metabolic power with different level of assistance on Achilles experiment with healthy subject	99
4.5	Ground reaction forces in Achilles experiment with healthy subject	100

List of Figures

4.6	Total moment and power, estimation of subject contribution in Achilles experiment with healthy subject	101
4.7	Peak moment and push-off power in Achilles experiment with healthy subject	102
5.1	Schematic view of the neuromuscular controller	106
5.2	Average time histories of joint angles for subject walking on a treadmill	108
5.3	Neuromuscular controller customization	110
5.4	Flow chart of assistance selection process through PUI Assessment	112
5.5	WE1 experiments - Torque tracking error	115
6.1	Group1 Test pilots	119
6.2	Achilles experiment - Training procedure	120
6.3	Achilles experiment - PUI results	122
6.4	Achilles experiment - 10MWT and 6MWT average with the achilles	124
6.5	Achilles experiment - 10MWT free walking	125
6.6	Achilles experiment: ankle kinematics	126
6.7	WE1 experiment - Training procedure	128
6.8	WE1 experiment - Box of walking speeds at T0	131
6.9	WE1 experiment - Boxplot of walking speeds across experiment	132
6.10	WE1 experiment - Plot of speed and stride length	134
6.11	WE1 experiment - Ground reaction forces at T0	135
6.12	WE1 experiment - Joint angles, torques for the different joints	137
6.13	Lopes experiment - Schematic overview of (A) the NMC and (B) the LOPES gait trainer	140
6.14	Lopes experiment - SCI speed and step length over a range of speeds	145
6.15	Lopes experiment - Knee and hip angles and NMC generated moments, torques, power, and work	147
6.16	Lopes experiment - EMG patterns of the different subject walking with NMC.	148
6.17	Lopes experiment - SCI positive and negative joint work over a range of speeds.	149
6.18	Lopes experiment - joint angle trajectories and EMG	151
6.19	Lopes experiment - Knee and hip angles, moments, powers, and work from the right leg of S2D	152
6.20	Muscle force (F_m), contraction velocity (V_{ce}), and length (L_{ce}) from four virtual muscles of the NMC with S2D (complete SCI injury) walking in LOPES	153
6.21	WE2 experiment - Anthropometric customization	159
6.22	WE2 experiment - Speed, Step length and time per step across the experiment for the two subjects.	161
A.1	NMC for WE1. Control interface overview 1	172
A.2	NMC for WE1. Control interface overview 2	172
A.3	NMC for WE1. Control interface overview 3	173
B.1	Picture of different exoskeletons	176

C.1	Segments weight and length distribution based on anthropometric data from [225].	177
C.2	Schematic view of a muscle tendon unit (MTU) in the Hill muscle model.	179
C.3	Schematic view of sensory pathways involved in the reflex model	180
C.4	CPG Models classification	183
C.5	Simple pendulum controlled by an HCO	186
D.1	Estimated stiffness and damping during gait cycle in the Achilles experiment with healthy subject	192

List of Tables

1	Adaptive control: typically affected control variable	32
1.1	Lexicographic PSO objective function used to optimize the FBL model	46
2.1	Vector representation of the FBL control loop	59
2.2	List of the FBL sensory interneurons	60
2.3	List of muscles used in the FBL model	61
2.4	FBL model parameters list and their respective range	62
3.1	Description of the CPG-FDB combination map for the different 3FBL models	76
3.2	Feedback replacement study	78
3.3	Feedback sensitivity for 7 solutions.	79
6.1	Group I Test pilots epidemiological data	118
6.2	Clinical scales used in Achilles training with groupI pilot	123
6.3	WE1 experiment - Walking condition	128
6.4	NMC adjustable parameters for WE1.	129
6.5	WE1 experiment - Biomechanical assessment measurements and instruments	130
6.6	WE1 experiment - Range of walking speeds	133
6.7	Lopes experiment - virtual muscles of the neuromuscular controller	141
6.8	Lopes experiment - Subject characteristics	142
6.9	Lopes experiment - NMC subject experiment settings	144
6.10	Lopes experiment - Step length s and knee and hip joint work	150
C.1	Joint angle range of motion in the FBL model	178
C.2	Properties of relative to main CPG type	184

Introduction

Context

Human locomotion shows fascinating abilities which are the results of the interplay between the environment, the biomechanics, the spinal cord, and modulation from higher control centers. How the different structures interact to generate meaningful behavior is an active field of research, and understanding the key principles underlying bipedal locomotion could have a strong impact and important implications in several fields related to both medicine and robotics, such as improved rehabilitation procedures, predicting surgery outcome or facilitated human-robot interaction.

In this context, the development of biologically relevant bipedal models that faithfully recapitulate human locomotion are urgently needed. Existing such bio-inspired models usually rely on one of the two following principles: the Central Pattern Generators (CPGs) and the reflexes. CPGs are networks of neural cells that can generate coordinated rhythmic patterns in the absence of sensory feedbacks. The idea that CPG control locomotion in lower vertebrates has been widely accepted for several decades [88], while their presence in bipedal locomotion has been a matter of debate for more than 20 years [47, 140]. Several models have demonstrated the potential role that CPGs could play in human locomotion [196, 197, 199, 196, 198, 115], while others have developed neuro-musculo-skeletal model solely driven by reflex loops [79, 78, 191, 192]. We hypothesized that combining a reflex model with models of CPG would allow enhanced control of the gait properties, such as the gait speed and the step length. To achieve this goal, we developed a variety of models combining CPG and feedbacks in different manners to study the relative importance of the different feedbacks/feedforward pathways. This work is presented in the first part of the thesis; I. *On biological modeling of spinal control of locomotion*.

The second part of this thesis (II. *On symbiotic control of exoskeleton*) results from a team effort created by the *Symbitron - Symbiotic man-machine interactions in wearable exoskeletons to enhance mobility for paraplegics* project¹. The Symbitron project - now successfully completed - was part of the "Future and Emerging Technologies (FET)" program of the European Commission². The main goals of the Symbitron were threefolds:

¹EU FP7 funded project. Website : <http://www.symbitron.eu>.

²<http://ec.europa.eu/digital-agenda/en/future-emerging-technologies-fet> (funding: European Union's Seventh

Introduction

1. Develop a bio-inspired exoskeleton that enables Spinal Cord Injured (SCI) subjects to walk without assistance, by complementing their remaining motor function, in a tailor-made, symbiotic manner.
2. Establish training protocols and create training environments for both SCI subjects and their clinicians, and
3. Perform a proof of concept study regarding the safety and functionality of the system in a clinical environment.

In this project, the role of the Biorob laboratory - and thereby an important aspect of this thesis - was to develop and test the controller of the exoskeleton. More precisely, we aimed at developing a controller that would be able to compensate for the lacking motor functions of paraplegic subjects suffering from both complete and incomplete SCI (see Section 5.1), in a made-to-measure manner. This imposed specific design choices both at the mechanical and control level. The targeted control strategy was to use a bio-inspired controller that would mimic the forces produced by an intact neuromuscular system. The main hypothesis was that the generation of proper dynamic aspects of the leg movement and of spinal-like pattern and reflexes during walking would allow a seamless symbiotic man-machine interaction between the subject and the exoskeleton.

The thesis is organized as follow: The introduction discusses the state-of-the-art knowledge on the modeling of human locomotion, starting with a general overview of the human locomotion physiology and development, followed by an analysis of the modeling possibilities of bipedal walking and concluding on more specific aspects related to Symbitron: paraplegia, man-machine interactions and exoskeletons for rehabilitation purposes.

The first part of the thesis (*I On biological modeling of spinal control of locomotion*) presents different aspects of the biological modeling of spinal control of locomotion. In most models, several parameters are unknown and researchers often rely on learning and optimization tools to find the aforesaid parameters. Chapter 1 discusses them. In Chapter 2 we introduce a reflex controller (re-implementation of Geyer et al, 2010 model [79]), and in Chapter 3 we present a CPG extension controller inspired from pattern matching and proposes a generic strategy to move away from steady state walking. Finally, in Chapter 4 we propose a formalization and unification of the CPG and reflexes models.

The second part of the thesis (*II On symbiotic control of exoskeleton*) presents our neuromuscular controller (NMC) which translates our bio-inspired control strategy (described in part I) for the control of wearable exoskeletons. Chapter 5 is a proof-of-concept validation of the NMC control with healthy subjects. Chapter 6 introduces our neuromuscular controller in terms of architecture, properties and tailoring aspects. Chapter 7 illustrate the various possibilities raised by our controller through its application onto three different devices.

The thesis concludes with a general discussion of what has been presented and the future step of development that should be undertaken to bring this solution to the market.

Framework Programme FP7-ICT-2013-10, ID 661626), as a collaborative project between EPFL, Switzerland, the University of Twente, Netherlands, the Technical University of Delft, Netherlands, Imperial College of Science, Technology and Medicine, United Kingdom, the Santa Lucia Foundation, Italy and Össur, Iceland.

Physiological aspects of locomotion

Modelling locomotion would not be possible without understanding the different parts of the nervous system and the body devoted to that function and without describing how they are involved in locomotion and interconnected. Locomotion is generated by the neuromuscular system, which as the name implies, is made of a musculo-skeletal system that is controlled by a neural system. More specifically, bones are attached together through ligaments that constraints the movement between two bones. Muscles are attached to the bones through tendons and can be electrically stimulated to produce - always - contractile forces. This stimulation comes from specialized neurons in the spinal cords called α motoneurons. The body would not be able to move without a representation of its state in the environment. This representation is created by a myriad of specialized neurons called sensory neurons. On the many existing types of sensory neurons, only a small subset is directly involved in locomotion. This subset includes sensory neurons relying information on contact (free nerve endings), on local orientation of the different segments (muscle spindles), on the exerted forces on the tendon (golgi tendon). The quest is therefore to understand how the brain and the spinal cord use this sensory representation to produce the adequate α motoneuron activity to generate a stable locomotion.

Humans are able to send rockets to space, to make little modules land on the soil of asteroids, but still the versatility and diversity of the movement produced by nature's personal motor - the muscles - remains a mystery. Behind this seemingly simple and trivial question of human walking, one has a beautiful example of the nervous system magics in action. What is a voluntary action ? And how voluntary are our actions ? How voluntary is walking ? When one walks, one has no need to bring to consciousness the details of how it legs moves to produce walking. One simply starts walking. But how much is one responsible for the way walking happens at the level of the muscle? Experiments on decerebrate cat showed that without cerebrum, cats were still able to walk on a treadmill and even exhibited gait transitions [53]. Lower brain structures and the spinal cord must therefore be key in generating walking. But are likely to be tightly coupled to upper brain structures for their modulation.

Spinal cord's reflex circuits

Locomotion consists of cyclic events controlled by interneurons networks located within the spinal cord, which are under the continuous influence of descending signals and peripheral inputs [86],[6]. Early work of SC. Sherrington confirmed the leading role played by the spinal cord in the generation of locomotion [186]. Through his experiments, he could establish the predominant role of muscles afferents in the generation of rhythmic activity and introduce the term "reflex walking" to describe his view that locomotion was limited to a succession of reflex loops.

A large part of the sensory information comes from the muscle spindles (type Ia and II fibers) and the golgi tendon (type Ib fibers), see Section 2.5. Their effects on locomotion have been

Introduction

studied either by isolating the spinal cord from upper brain inputs [85], therefore turning off afferent information [96] or by selectively stimulating some sensors (for instance using techniques such as muscle vibration, which selectively activates Ia fibers [173]). The first described reflex circuit was the action of those sensors to produce a muscle response proportional to the sensor changes. In this context, Ia reflexes act as overall system stabilizers, by tending to hold muscle length constant, while Ib reflexes are protective reflexes preventing damage to the tendon, by inhibiting synergistic muscles activity when the tension in a tendon reaches a given threshold [84],[103].

This simple aspect of reflex loops has shown to be generally true for group Ia afferents fibers on synergistic muscles. Ib reflex action, which is mediated through interneurons, is more complex³[17]. Despite this complexity, in immobile decerebrate cat, the reflex action of extensor Ib afferents generally inhibits extensor activity in the limb and promotes flexor activity, in agreement with a negative force feedback [16].

The complex role of afferents has been highlighted by a series of experiments that showed how sensory feedback from the limbs are closely integrated into the activity of the spinal networks generating the locomotion. An example is the role of phasic afferents signals in phase transitions generalized to many vertebrates and invertebrates [152]. The question of whether this transition was load or position-dependent in mammals was answered by experiments performed on cats [53], where it was shown that if the extensor force was kept above a certain level, the extensor activity was maintained and the swing phase delayed. It became later clear that this effect was mediated by Ib afferents positive feedback [152]. The effect of this positive force feedback has been studied in the context of muscle control where it showed an effective and surprisingly stable way of controlling load-bearing tasks, such as locomotion [163]. This is further supported by results showing that the stability of bouncing gaits is greatly increased by the presence of positive force feedbacks [80]. Further experiments in humans concluded that there is a inhibition of Ib inhibitory and an activation of Ib extensor facilitatory pathways [45]. In terms of control, this phase dependent triggering is useful because it ensures that the neural system stays synchronized with the body environment dynamic.

Spinal central pattern generators

It is relatively intuitive that efficient moving is a key feature for animal survival. For this reason, locomotion must have emerged early in evolution, and thus must be implemented in primitive structures of the nervous system. Corroborating this hypothesis, several groups have reported the existence of neural circuits able to generate rhythmic locomotor activity, both in invertebrate and vertebrate species [101]. Although locomotor circuits are ancient structures of the nervous system, understanding the misleadingly simple automated movement of

³1. for many muscles, the reflex action of flexor Ib afferents diverge for many muscles, 2. individual Ib interneuron receive inputs from Ib afferents of other muscles, from Ia afferents, as well as descending input from the rubrospinal tract, 3. flexor Ib afferents are much weaker and variable than extensor Ib afferents.

locomotion has been – and still is – a challenge for neuroscience. Indeed, walking is the result of a complex motor activity that requires high level of coordination between the trunk and limbs muscles and joints; each limb movement involves rotations at several articulations, Degrees Of Freedom (DoF), as well as the activation of many other muscles, while maintaining perfect body balance. Over the past century, scientists have tried to understand how this is performed by the nervous system. One hypothesis - validated in many invertebrate and vertebrate species - is that movement patterns generator circuits (MPG) localized in the spinal cord are responsible for the emergence of locomotion, whereby the spinal cord would be more than a simple “relay station”. These MPGs could consist of central pattern generators (CPGs), which are neural networks capable of producing self-sustained periodic rhythmic pattern endogenously, i.e. without sensory or central input [101]. Alternatively, several groups have proposed that MPGs emerge from simple reflex loops [79], without the need of neural oscillators (i.e. CPG network). Most likely, and consistent with biological findings, the reality might be somewhere in between; the CPG might control the basic rhythms and patterns of motoneuron activation during locomotion, while reflexes would adapt the CPG outputs to the specific state of the body, in a specific environment.

Seminal work on the existence of locomotor spinal networks goes back to the 19th century, with the observation that spinally transected dogs displayed rhythmic stepping movements upon lifting of a limb [186]. In the beginning of the 20th century, from the observation that cats transected at the brain stem level could perform stepping movements, Sir Charles Scott Sherrington [186] suggested that the basis of motor pattern could result from a combination of reflexes from proprioceptors onto spinal centers, introducing the notion of “reflex-based walking”. Although he already proposed that there must be some specialized spinal neurons able to transform the peripheral input into a stepping pattern, it is his student, Thomas Graham Brown [19], who proposed the hypothesis that basic locomotor movements of posterior limbs could be initiated by the spinal cord itself without any descending drive or sensory inputs and introduced the concept of "half-centres", which since then have been classified as a subtype of Central Pattern Generator (CPG).[20]. His work was based on the observation that transected and deafferented cats (i.e. with cut afferent from hind limbs muscles) could also generate rudimentary stepping movements, in the absence of reflexes, which led him to hypothesize that the alternate flexion and extension of the leg muscles observed during walking could be generated by rhythmic central circuits (the half-centers oscillators) in which antagonist muscles were activated by neurons that inhibited each other (see Section 3.2). Since then, various evidence of the existence of a CPG have been reported in lower vertebrates (lampreys, salamanders) [88] and in cats [85]. The presence and role of CPG have been a strong drive in the emergence of bio-inspired robots to test neuro-physiological hypotheses [105], and in parallel led to the emergence of many different models and bio-inspired architectures used to control and stabilize different types of gait.

However, due to the limited possibility of investigating the “CPG question” in human, the existence of locomotor CPGs in human is still a matter of debate. Nevertheless, most researchers agree that the spinal cord plays a key role in generating and modulating gaits in

Introduction

most vertebrates including humans (i.e. the spinal cord is not simply a relay station for conveying signals from higher brain regions) [85, 124, 47, 126, 35]. However, how the different components affect the control of locomotion remains unclear. Based on an evolutionary point of view, there should be no fundamental difference between biped and quadrupeds locomotor mechanisms, as the basic spinal cord organization is conserved [42]. However, human walking requires specific mechanisms to maintain the body upright, and the corticospinal tract is more important in primates compared to lower species, suggesting less autonomy of the spinal cord. Evidence of a spinal stepping generator and/or a sensory feedback (i.e. reflexes) in normal human locomotion comes from experiments on the locomotor capacity of Spinal Cord Injury (SCI) subjects where it was shown that complex bilateral muscle activation and coordinated stepping movements could be induced by partially unloading the subjects [44]. Another study on partial body weight support showed that the amplitude and duration of the EMG bursts could be modulated by varying treadmill speed and the level of body weight support, suggesting that - as it is the case in decerebrate cat [53] - peripheral sensory inputs associated with locomotor-like behavior can switch the lumbosacral spinal network from non functional to highly functional state [49]. Further evidence comes from a study from M. Dimitrijevic et al. (see Fig. 1 for details) where it was shown that non-patterned electrical stimulation of the posterior structures of the lumbar spinal cord in subjects with clinically complete SCI induce patterned and locomotor-like behavior [47]. More precisely, their findings showed that a lumbosacral spinal cord isolated from upper brain control can - in humans - respond with a motor pattern of flexor / extensor alternation if patterned sensory input associated with load-bearing stepping are provided. Rhythmic activity was induced when the electrical train was between 5 and 9 V and the frequency between 25-50 Hz, while higher stimulation generated tonic muscle activity. The electrical stimulation site was important in the generation of stepping-like behavior. Indeed, stepping behaviors were observed when the stimulation was on the L2 segments. When the electrode was moved higher or lower, only rhythmic activity but no stepping behavior were observed, see Fig. 1. Interestingly, the interburst latency between flexor and extensor activity (i.e. tibial anterior and triceps surae) was dependent on both the frequency of the electrical stimulation and the tension. This change in frequency of flexor / extensor alternation strongly suggests that a more complex mechanism than a simple reflex loops is involved. The authors concluded that the train of stimuli activated a locomotor CPG and that additional peripheral inputs were used to shape the motor outputs.

Section 4 reviews the use of CPG for the the generation of robotic walking controller in bipedal models.

Upper brain structures

The information conveyed by the somatosensory system flows in the nervous system through the peripheral system, which makes connections to the spinal cord via the different spinal nerves. Only a small subset of the peripheral system is involved into locomotion, this includes the sense of touch and proprioception (including the sense of position and movements of

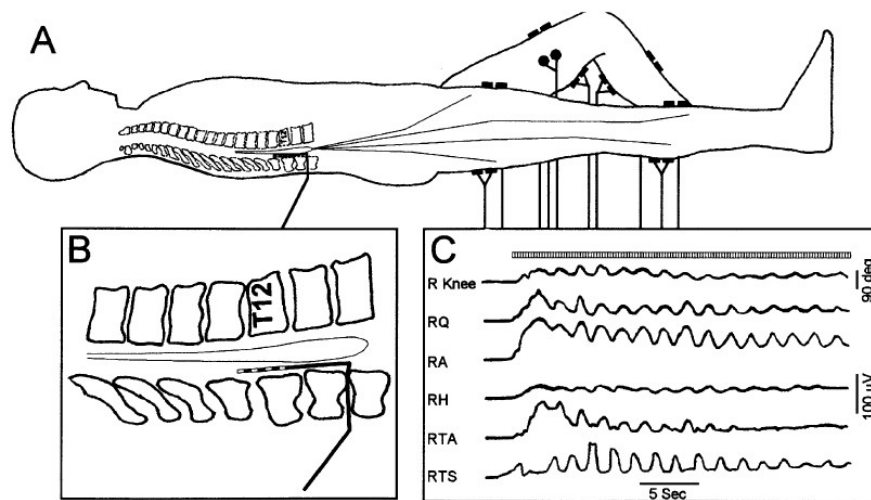


Figure 1 – Sketch of the experimental design in [47]. A) Paraplegic subject under examination is lying down and the epidural electrode stimulation is placed above the lumbar cord. Pairs of surface electrodes for EMG recording are placed over both quadriceps, adductors, hamstrings, tibial anterior and triceps surae muscle groups. B) Diagram of the quadripolar epidural electrode placed within the spinal canal above the posterior lumbar cord structures. C) EMG recording of rhythmic activity from the right lower limb during stimulation of the upper segments of the lumbar cord, with position sensor trace recording movement of the knee during flexion and extension of the lower limb.

Introduction

the body in the environment and of the different segments) which are conveyed by different sensors (described in Section 2.5).

On top of and structurally continuous with the spinal cord is the brainstem, the most posterior part of the brain (see Fig. 2), one of the most important region of the brain, as all descending and afferent pathways pass through it. It also plays a major role in regulating different cyclic functions such as sleep cycle, heart rate, breathing and eating.

A dedicated part of the midbrain called the Mesencephalic locomotor region (MLR) has the role of initiating and modulating locomotion. This very specific role was first observed by comparing cats decerebrated at different levels and stimulating the MLR. Indeed, four different types of decerebrate cat have been used, depending on the location of the cut: the decorticate cat, the premammillary cat, the postmammillary cat and the classic decerebrate cat [223]. The first one keeps the thalamus and basal ganglia intact and can walk spontaneously. The second one is cut between the top of the brainstem and the mammillary body of the hypothalamic region of the diencephalon, but mammillary bodies are not removed, this cat can walk spontaneously when put on a treadmill and exhibits righting reflex. The third type is cut right after the mammillary body, see Fig. 3. This cat also called the mesencephalic cat, does not walk by default but can exhibit stepping and even show gait transition when the MLR is stimulated. The last type is obtained similarly to the previous type except that only the inferior colliculus are kept. This cat, initially described by Sherrington in [187], cannot exhibit walking through stimulation of the brainstem because of extensor muscles high tone.

Reticular Formation

The reticular formation consists of hundreds of interconnected nuclei located throughout the brainstem (see Fig. 2). Those nuclei are involved, for example, in sleep phases control, pain modulation, consciousness, breathing and swallowing CPG. It has an important role during locomotion; its descending pathway to the spinal cord (so-called "reticulospinal tract") has a major role in maintaining the body posture during locomotion, by creating both inhibitory and excitatory connections on both α and γ motoneurons of the trunk proximal limbs muscles [69].

Vestibular sensors

The vestibular system (Fig. 2) acts in the management of balance and conveys information regarding body orientation and movements to the Central nervous system (CNS). The vestibular system is made of two main structures: the otolith organs and the semi-circular canal. The otolith organ is sensitive to linear acceleration and can thus detect the direction and magnitude of the gravity, as well as other linear accelerations due, for example, to movements. The semi-circular canals are sensitive to angular acceleration [169]; There are three semi-circular canals that are oriented orthogonally to each other. By combining the information from the three different canals, the CNS generates a 3D representation of the head instantaneous

2. Physiological aspects of locomotion

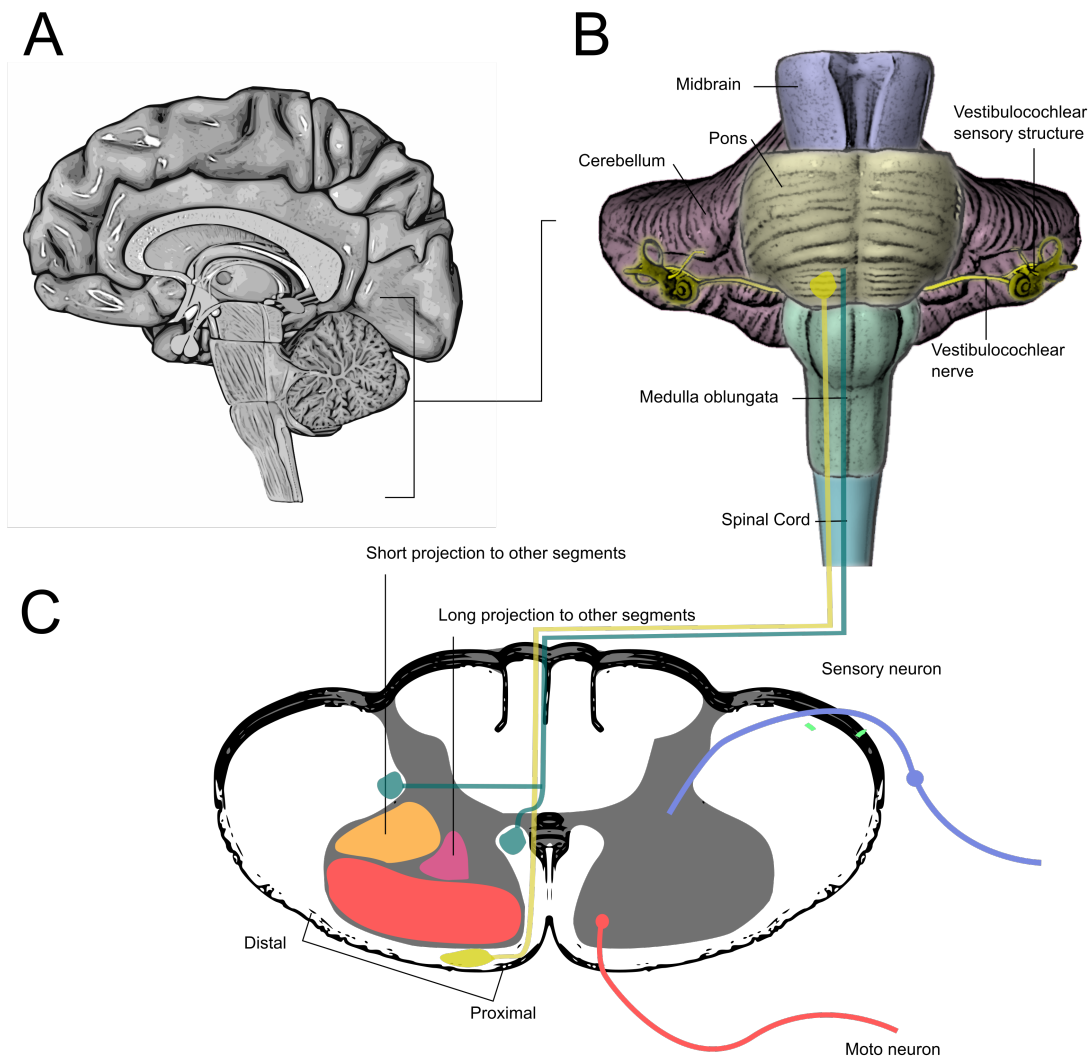


Figure 2 – A: schematic view of the upper brain, B: schematic view of the brainstem together with the cerebellum. The brainstem is composed of three regions, the midbrain, the pons and the medulla oblongata. All the cranial nerve make their connection in the brainstem, the Vestibulocochlear nerve that conveys information on posture and balance, crucial to locomotion is shown in yellow. C: Spinal cord cross section and schematic view of the effect of vestibulospinal and reticulospinal tracts on the spinal cord [165]. The sensory information enters the spinal cord by the dorsal part while motoneurons project to muscles through the ventral part of the spinal cord. Small interneuron networks exist in the spinal cord with vertical projections to other segments. Fig. adapted from [165]

speed [104]. The action of the vestibular system on movements is conveyed through the vestibulospinal tract whose neurons are located in the vestibular nuclei (see Fig. 2). It acts on motoneurons of extensor muscles. It also innervates muscles of the trunk, thus helping in coordinating postural adjustments [165].

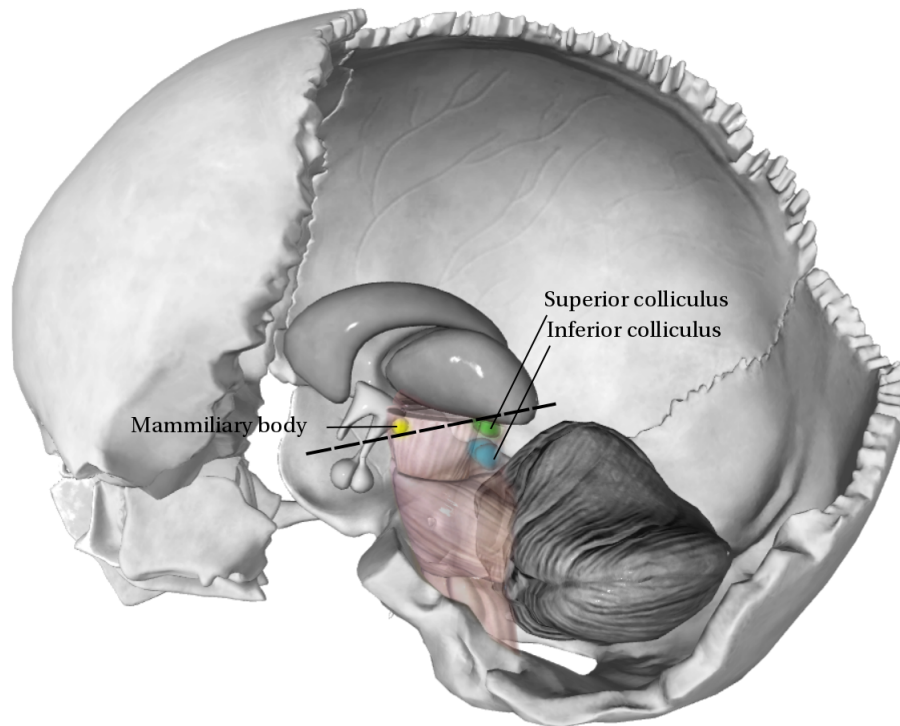


Figure 3 – The mesencephalic decerebration is made by cutting before the mammillary body and after the superior colliculus, dashed line in the Figure. When cutting between the superior and inferior colliculus the cat cannot exhibit locomotion because extensors often show a high tone [187], this phenomenon was referred to as decerebrate rigidity by the author.

Musculo-skeletal system

The spinal cord circuitry receives control signals from upper brain structures and sensors of the peripheral system and plays a key role in the control of locomotion, as discussed in the previous sections. But how does it contract muscles of the body to move the skeleton? This is done by specialized neurons called motoneurons located in the ventral part of the gray matter in the spinal cord, see Fig. 2 C). They directly control the level of contraction of the muscles by innervating extrafusal muscle fibers. The connection between extrafusal muscle fibers and motoneurons is done by the neuromuscular junction, a very specialized connection allowing the transmission of hundred of thousands of neuro-transmitters through vesicle release in a very short amount of time (delay of 0.5 to 0.8 msec). Those neuro-transmitters will then induce the release of calcium ion in the muscle fibers allowing them to contract.

Muscles

Skeletal muscles are made of multiple bundles named the fascicles, each of which contains many muscle fibers, the individual muscle cells. Within the muscle cells are the myofibrils,

2. Physiological aspects of locomotion

which are the muscle contractile units. They are themselves made of repeating units: the sarcomeres, which consist of organized actin and myosin filaments which, by sliding along each other shorten the fiber, provoking the muscle contraction (see figure 4). The active force generated by the contraction of the sarcomeres can be modeled at the muscles level by a bell shaped curve with a maximum occurring close to muscle resting length. When stretched beyond a certain length, the elastical property of a protein called titin (which is part of sarcomere) generates, at the muscle level, a passive repealing force in the opposite direction (e.g. acting against its elongation) [81].

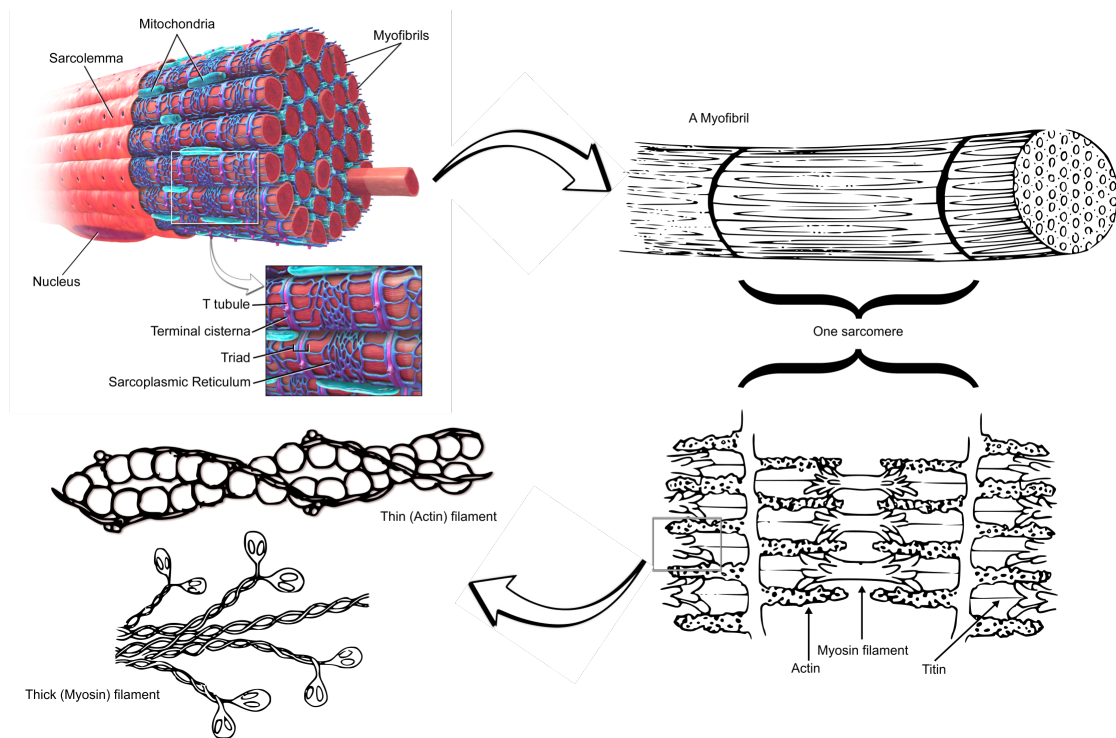


Figure 4 – Illustration of the skeletal muscle anatomy and contraction process. Adapted from [178]

Force-length relationship The relation between the length of a muscle and the force generated can be understood by looking at the property of sarcomeres to generate an active force with a bell shaped profile and a passive repealing force when stretched beyond a certain length. The resulting shape of the muscle force-length relationship is shown in figure 5, left panel.

Force-velocity relationship The relationship between the shortening velocity during concentric contractions (shortening contractions) and the force generated by the muscle represents the dynamic property of the actin - myosin interaction cycle. The force-velocity profile has a inverted sigmoidal shape. The force generated is maximum when the muscle is lengthening and goes to zeros when the muscle is shortening [97]. The right panel of figure 5 shows

Introduction

a plot of the force-velocity relationship.

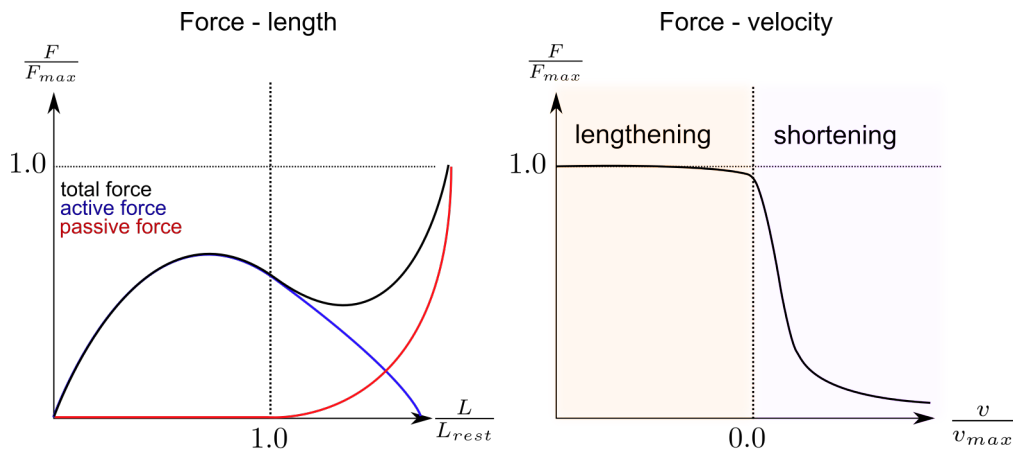


Figure 5 – Schematic representation of muscle force and muscle length relationship in the two-filament sarcomere model or Hill type muscle model (i.e. model neglecting the role of a titin filaments into producing activity dependent muscle stiffness modulation, see [95]). Left: schematic representation of muscle force-length relationship. Right: muscle force-velocity relationship. F refers to the force generated by the muscle, F_{max} is the maximal force that can be generated by the muscle, L is the muscle length, L_{rest} is the muscle reference length, v is the muscle contractile velocity, v_{max} is the maximum muscle velocity.

Muscle fibers types Skeletal muscles are composed of two types of fibers: the type I and type II fibers, called slow and fast twitch fibers, respectively. Fast twitch fibers are activated faster than slower ones and can produce more energy but they fatigue more quickly. This difference is due to the fiber composition; slow twitch fibers composition favors aerobic metabolism (i.e. they contain many mitochondria and are surrounded by many capillaries), whereas fast twitch fibers have a composition which favors anaerobic metabolism (mostly lactic acid fermentation) [184]. In order to understand why the type II fibers contract faster but fatigue quicker than the type I fibers we have to look at the mechanisms by which cells produce energy. Cells produce energy mainly by regenerating their stock of Adenosine triphosphate (ATP) from Adenosine di and monophosphate (respectively ADP and AMP). In animal cells, this can be achieved through different processes, depending on the presence or absence of oxygen. One of the main reaction chain used in both aerobic (with oxygen) and anaerobic (without) conditions to regenerate the ATP is the transformation of oxygen into pyruvate. This is done through a reaction chain called glycolysis. Then, in the presence of oxygen, the pyruvate will be transformed to acetyl-CoA and enter in the krebs cycle (a chain of 10 reactions that involves many different compounds) while in absence of oxygen, pyruvate undergoes a process of fermentation which oxidizes the NADH by-product of glycolysis back to NAD^+ , thus regenerating the NAD^+ needed by the glycolysis.

Therefore, what makes the muscles fibers II faster than fibers I is the fact that the fermentation is much faster in regenerating the NAD^+ stock than the electron transport chain. However

the fermentation process produces lactic acid which accumulates and makes prolonged effort painful.

Sensory system

The sensory nervous system is the part of the nervous system dedicated to the processing of sensory information, thereby allowing the transduction of the physical world to the perception. It consists of: 1) sensory receptors which receive the sensory stimuli, 2) neural pathways which carry the stimuli to the central nervous system, and 3) brain centers that interpret the stimuli allowing the perception.

Free nerve endings

The skin of vertebrates is abundantly innervated with sensory afferent nerve fibers. Some of these fibers are unspecialized, unencapsulated and have no complex sensory structures. These are referred to as “free nerve ending”, in opposition to specialized encapsulated receptors, such as the Pacinian and Meissner’s corpuscles. Free nerves ending resemble plant’s roots that infiltrate the middle layers of the dermis and surround hair follicles. They function as cutaneous mechanoreceptors, thermoreceptors and nociceptors and account for the large majority of human nerve ending. They transform mechanical energy to electrical energy through changes in membrane permeability, resulting in an impulse that is transmitted to the central nervous system by an afferent fiber.

Muscle spindles

Muscle spindles are sensory receptors found in the central part of the muscles, which provide sensory feedback information to the central nervous system (CNS). They are composed of two different afferent fibers called primary (type Ia) and secondary (type II) nerve fibers. The first type reacts quickly to muscle length and velocity changes and conveys information related to the rate of muscle length changes. The second type reacts much slowly and fires when the muscle is static. The Golgi tendon (type Ib) provides information regarding the current tension exerted on the muscle. [164]. The response of the primary and secondary fibers muscle spindles to change in velocity and length, respectively, can be modulated by efferent neurons called γ motoneurons.

Golgi tendon organ

Golgi tendons are proprioceptive stretch sensory receptor organs that are activated upon contraction or stretch of skeletal muscles. They sense changes in muscle tension and transmit this information to the central nervous system. They consist of a thin capsule of connective tissue that enclose strands of collagen that are connected to the muscle fibers at one end

Introduction

and merged into the tendon proper at the other end. The collagenous fibers within a capsule are innervated by afferent type Ib sensory fibers, whose terminal branches intertwine with the collagenous fibers. Upon muscle contraction, the sensory terminals are compressed. The ensuing Ib afferent nerve deformation leads to an opening of stretch-sensitive ion channels, thus depolarizing the Ib neuron resulting in an impulse that is transmitted to the central nervous.

Analysis and modeling of walking

People have been interested in understanding human walking since antiquity [7]. The complexity of this activity seamlessly performed by animals has always intrigued and inspired scientists, inventors and artists. Mathematically speaking, animal locomotion results from complex, high dimensional, non-linear, dynamically coupled interaction between an organism and its environment [73]. Understanding locomotion is complex because of the high number of components involved. But since the body obeys the rules of physics, all this complexity can be observed at higher levels of representation. And this is what scientists and researchers did, looking at locomotion by its effect on macroscopic variables such as the center of mass or the ground reaction forces [ref needed here]. We will review below the history and modelling of locomotion using a top down approach, e.g. starting from the center of mass to more detailed model including different segments. The analysis will be made from the view point of energy storage (potential energy) and release (kinetic energy). This choice is made because equation of motions - of great interest for the analysis of walking - can be derived from the flow between kinetic and potential energy and because animals generally try to minimize their energy.

The components of locomotion are highly redundant at many levels [27]: at the kinematic one (i.e. animals usually show a high level of kinematic redundancy and have many more DoF than the minimal number theoretically needed to move the Center Of Mass (CoM)), at the actuator one (e.g. the knee joint which could be theoretically actuated by 2 muscles is at least actuated by 23 muscles), at the neural one and at the sensory one (e.g. how different afferents converge at an interneuronal level to form multisensory reflex feedback systems [124]).

All the modeling work done to understand the control of animal locomotion has focused on two different modeling approaches: (i) top-down, concentrating on simple models - called template models and (ii) bottom-up, concentrating on models integrating neuro-physiologic observations, able to answer very specific questions on the organization of spinal circuitry.

Top-down approaches

Top-down approaches seek at reproducing or explaining the global dynamics of the system. This approach is driven by biomechanists and engineers, which - with ideas borrowed from Newton dynamics - seek an understanding of the basic physical principle behind animal locomotion and legged dynamics. They gave rise to simple models, sometimes called template

models [73]. Two examples of template models for locomotion are the inverted pendulum proposed for walking [190] and the Spring Loaded Inverted Pendulum (SLIP) [182] model initially proposed to explain running, see Fig. 6. Those models were useful in many regards, one of which was the implementation of several successful strategies for the creation and control of legged robots (e.g. the passive dynamic walker [133] or the monopeds robots developed by Raibert [166]).

Bottom-up approaches

While top-down approaches are driven by bio-mechanics and has a very long history (since antiquity), the bottom-up approaches are driven by neuro-physiologists discoveries. It seeks at shedding light on the possible organization of spinal networks responsible for stepping [47],[126], on the role of sensory afferent on the shaping and timing of the locomotion [153],[49], on the specific influence of afferents on the CPG [128],[177] or on the role of CPG by simulating fictive locomotion [177]. While efforts in integrating all the observations in more complex models exist (e.g. the development of a complex neuromuscular system to investigate the effect of spinal cord injury [151]), usually, models following an integrative approach have to be limited to very specific questions in order to keep the model tractable in terms of number of parameters.

Neuromechanical approaches

Because template models are simple with regards to the number of parameters, they can be used to generate predictions that can be easily verified with experiments which can in turn be used to improve or propose alternative template model. Once a model is validated, more complex model that keep this dynamic fidelity can be proposed and indirectly validated up to the extent that they produce the same dynamics. An example is the discrediting of the inverted pendulum as template of human walking by experiments on the movement of CoM in humans [25] and ground reaction forces [78] (Fig. 6). These limitations were circumvented by adding a spring between the point mass, representing the CoM, and the ground. This led to the creation of the SLIP template which is in agreement with in phase fluctuations of the CoM kinetic and gravitational potential energy observed in running animals [26]. The model was able to predict the reaction forces observed during running.

Template models can also be easily extended to shed light on important mechanical principles, when merged with bottom-up approaches. An example is the implementation of the swing leg retraction mechanism - a commonly observed behavior in legged animals - implemented as a simple extension to the SLIP model, that confirmed the stabilizing effect of this behavior on the produced locomotion [185]. It was later shown that the same model can also generate walking again producing reaction forces strikingly similar to those observed in human walking [78]. The validity of the SLIP model in both walking and running drove the emergence of neuromechanical models (Neuro-Muscular Model (NMM)) based on leg compliance principles. After

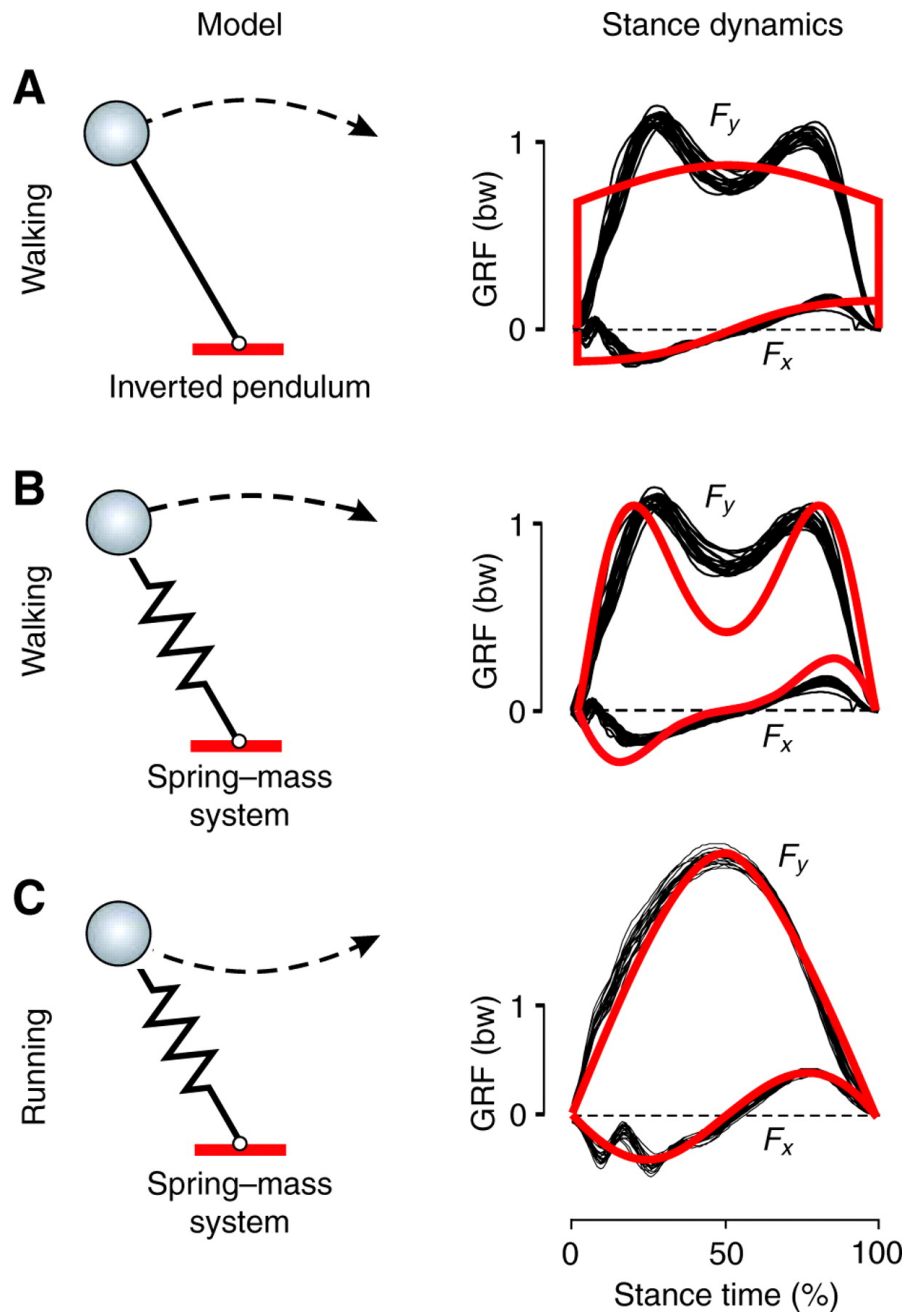


Figure 6 – Ground reaction forces in the inverted pendulum and the SLIP template model of legged locomotion. Left: model schematic, right: ground reaction forces. A. Walking as inverted pendulum, B. Walking as spring mass system, C. Running as spring mass system. Fig. from [78].

the introduction of a neuro-mechanical principle of leg compliance, named "positive force feedback" [78], Geyer and Herr [79] developed a detailed 2D 6 degrees of freedom model producing kinematics, torques, center of mass dynamics and ground reaction forces similar to healthy human walking.

Control aspects of CPGs and current use in robotics

This section will dig into more concrete examples of models of spinal circuits used as walking controller for biped simulation and two-legged robots control and present a methodology for the design of such controller. This methodology is applied in chapter 3 to introduce the CPG in a reflex-based walking controller.

As discussed in section 2, spinal control relies on a combination of both reflex loops and CPG. When applied to bio-inspired robotics, those components are often used as building blocks for the generation of walking controllers. From a mathematical viewpoint, CPG are dynamical systems exhibiting limit cycle behaviors, which offer several advantages when applied to the locomotion of robots. One of their main advantages is that they can be dynamically coupled to the mechanical system, which can enforce the synchronization of the CPG network with the body and the environment, through mechanical entrainment using resonance tuning or through explicit learning of the frequency components and the phases of an external signal. Moreover, they permit easy modulation of the gait speed and incorporation of gait transition mechanisms. The recovery from perturbations is also inherently encoded in the system, and the need for an accurate model of the robot is often not required. Finally, if the CPG controller is implemented in a distributed fashion, e.g., on several microcontrollers, it allows simplified reconfiguration or adaptation of the robot to a missing or a nonfunctional part.

Background

CPG-based controllers were first used as tools to validate or disprove hypotheses based on biological observations ([87], [177], [106]). However, over the past two decades, CPGs have been increasingly used to design controllers for the locomotion of autonomous robots, from snakes and multi-legged insect-like to humanoids bipedal robots.

Regardless of whether CPGs are involved in human locomotion, several properties of the CPGs make them good candidates for the implementation of walking robots. Indeed, some inherent features of the CPG, such as the drastic dimensional reduction of control signals and the robustness to sensory noise, makes it of particular interest for the development of walking robot, as a tool, and thus independent of the physiological relevance of the specific CPG network implemented. For instance, when used as trajectory generators, CPG can be coupled to different learning schemes making them useful to encode movement patterns: these are called Rhythmic dynamic motor primitives (rDMP) [22], [74], [142] and make use of CPGs properties with little or no link to biological CPGs.

CPG control of locomotion in robotics

It is quite remarkable how biological systems can resolve the complex problem of locomotion control, i.e. nonlinear, high dimensional control problem, redundancies at the actuator level, sensory noise, transmission delays and instabilities. Therefore, it is not surprising that modeling of the spinal circuits responsible for the locomotor activity is not restricted to the validation of biological observations, but can also inspire robotics engineers. Indeed, modeling of locomotor CPGs for human can have two distinct aims; either to validate biological findings and hypotheses, or to take advantage of and explore their unique features, to implement functional and robust controllers for walking robots, prosthesis or exoskeletons. Obviously, these two goals do not share the same requirements and do not require the same level of abstraction. When implementing controller for walking robots, it does not need to be based on existing biological networks. Rather, it is the properties of the CPGs allowing the implementation of a robust robot that are put forward. In such cases, the models tend to be more abstract, and the CPGs are used as tools. Because of these various applications, CPGs models are of many types and level of abstraction.

Regardless of the goal of a CPG model, it presents some unique advantages over other control approaches, such as position control based on zero moment point (ZMP) [219] or virtual model controls [161]. Indeed, their descriptions as limit cycles can allow mechanical entrainment between the controller and the body and structural stability of the controller to internal transient perturbations. Furthermore, the low number of control parameters permits dimensionality reduction and facilitates optimization, while their modular aspect (i.e. they are composed of several interconnected dynamical systems) enable increased modulation and is well suited for a distributed implementation. Finally, they can easily to integrate sensory feedbacks.

While some tools exists to facilitate the design of CPGs network with desired behaviors that we will review in this contribution, some difficulties and problems still exists when trying to combine CPG control with other aspects that needs to be considered when designing controller for real robot application, such as the combination of CPG with high level planning and discrete movements, the choice of feedback and CPG parameters, the shape of the CPG output or the choice of the controller output (end effectors, joint angles, joint torques, muscle activities).

CPG design methodology

When designing a CPG controller for a robotic application, abstract models of CPGs, relying on oscillators modeled as simple dynamical systems, such as the Matsuoka oscillators, the ACPO or the Hopf oscillator, are preferred to less abstract models, such as spiking neurons. Indeed, the most abstract models already captures most of the features required for robotic applications, including limit cycle behavior, explicit phase/frequency control, arbitrary limit cycle shape generation, synchronization mechanisms between oscillators, and between the

CPG network and the environment. These properties make CPGs perfect candidates for any rhythmic activities encoding. The pattern generated by CPGs for locomotion control can be motoneurons or muscle activation (in the cases of bio-inspired controllers), joints torques, angle trajectories, end-effector trajectories or motor voltages. CPGs can be used on their own or combined with other control methods, such as Zero-Moment Point (ZMP) [148], reflex-based controllers [209], passive dynamic walkers [216] or inverse kinematics [65].

To be used to control humanoid walking robots, design methodologies should be followed to facilitate the design of CPGs exhibiting the desired behavior. Two approaches have been proposed; the first, that we will call “self-organized oscillatory patterns”, is based on the work of G.Tagar et al. and focuses on the interaction between the CPG, the mechanical system, and the environment. In this case the output of the CPG signals is not known but is rather the result of the interaction between the oscillators, the mechanical system and feedback signals. The main idea is that locomotion emerges from the interaction of the neural, sensory, and musculo-skeletal systems which behave synergetically (i.e. cooperatively) to adapt the system to the environment in real time. This approach fits in the general framework of resonance tuning. The second approach, that we will call “explicit oscillatory patterns”, focuses on specific oscillatory patterns where the emphasis is on the control of the pattern generated, its frequency and its phase. This approach falls in the framework of rhythmic DMPs, Morph oscillators and the two-layered imitation framework. Note that while both approaches start from different perspectives – one focusing on self-organization through dynamic feedback to the oscillator and the other one focusing on the shape of the produced pattern – in practice several tools can be used to bridge the gap between those two strategies. These two approaches are discussed in the next two sections.

Self-organized oscillatory patterns

Initial work by Tagar In a seminal study published in 1991 and in subsequent work, G.Tagar et al. [199] investigated how human locomotion is generated by the central nervous system with a totally novel perspective. The question addressed was whether the motor behaviors of animals were pre-programmed by the central nervous system and executed by the musculo-skeletal system, or whether they were generated as a result of the emergent properties of the system. This group successfully demonstrated that locomotion can emerge from the interaction of the neural system, the musculo-skeletal system and the environment. This interaction can lead to a stable limit cycle behavior, in which the whole system (controller+body) is able to resist small perturbations. The initial model, inspired by the work of Matsuoka [131], combined sensory information and CPGs in the form of an entrained non-linear dynamical system of coupled oscillators. More specifically, they proposed to use a CPG controller entrained by the mechanical system to generate stable locomotion on a simulated 6 DOF lower limb model of a human body constrained to the sagittal plane (Fig. 7). The model had no feet (during stance, the connection between the ankle and the ground was considered as a perfect revolute joint). Non-linear friction forces were assumed at the hip and knee joints to model the energy

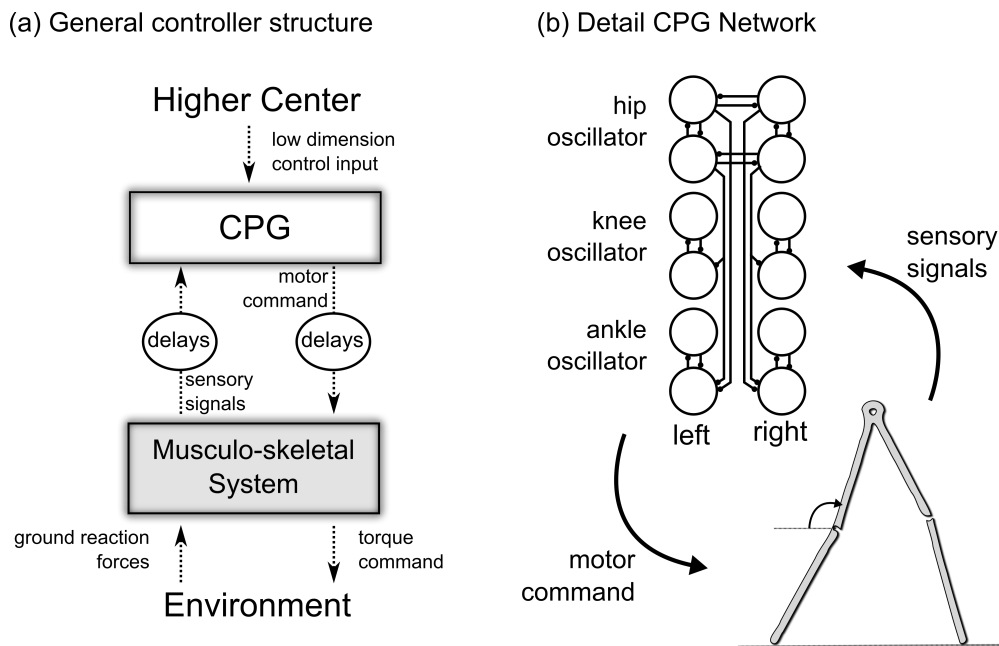


Figure 7 – Overview of Taga’s model (adapted from [199]). (a) The controller is separated into three different layers: 1) higher center, 2) CPG and 3) musculo-skeletal system. The higher centers send low dimensional input to the CPG network in the form of external input in the CPG. The CPG network communicates with the musculo-skeletal system with a delay representing the neural communication speed (CPG sends motor command and receives sensory signals). The musculo-skeletal system then generates torque commands by combining the CPG extensor and flexor outputs from the CPG units to all the controlled DoFs. (b) Detailed CPG Network. The CPG network is composed of Matsuoka oscillators, each joint is controlled by a pair of neurons inhibiting each other, one generating a flexion and the other an extension torque. Interlimb coordination is ensured by connections between the hip oscillators, ensuring a phase delay of π between the two legs. Intralimb coordination is ensured by connections between the kneen and ankle oscillators.

dissipation of muscles and human joints. An elastic force was also added to the knee joint to restrict the motion of the knee (i.e. restricted bending). Ground was modeled as a two dimensional spring and damper. Each joint was controlled by two coupled Matsuoka neurons with self-inhibition (forming an oscillatory unit).

The torque generated at the joint was proportional to the output of the corresponding flexor and extensor neurons. The parameters of the oscillatory units and of the network interconnections were chosen in order to reproduce the motion observed in human walking. The design of the feedback pathways used to enforce synchronisation were chosen following a principle derived from the stretch reflex observed in vertebrates; cross joint stretch reflexes were added to enforce the phase relationship between hip/knee and hip/ankle. The stretch reflex was assumed to be a function of the joint angle in the global reference frame, playing an important role in the stability of the locomotion. This assumes a transformation of local

4. Control aspects of CPGs and current use in robotics

sensory information by global information of the body orientation coming from the vestibular system and visual information. See Fig. 7 for an general overview of Taga's 1991 model. The initial model was able to produce stable walking/running gait in the sagittal plane, resist to both mechanical perturbations and environmental changes without any parameter changes, and switch between walking and running by playing with one single parameter.

In 1993, the same group investigated the stability and flexibility of the global limit cycle generated by the model, when subjected to spatio-temporal changes in the environment (resistance to perturbations, uneven ground, presence of another walker) [195]. They observed that the dynamic stability to mechanical perturbations varied depending on the level and timing of the perturbations. Moreover, the model was intrinsically stable against slow changes in the environment. Finally, through coupling at the level of the higher centers (i.e. the non specific input parameter to the neural system) between two walkers, synchronization of two identical bipeds could be ensured.

In a later study [196], the same group set out to study the effect of time delays in transporting and processing information between the neural rhythm generator and the musculo-skeletal system. The system was resistant to variations in time delay, up to a certain limit, above which the system exhibited a chaotic behavior.

While the emergent properties of the proposed models showed intrinsic adaptability to unpredictable changes in the environment, which would have many benefits for real robots applications, it was still not clear how such a system could be combined with planned anticipatory response when confronted to drastic changes in the environment, such as the presence of obstacles. To tackle this problem, the same group [198] added a discrete movement generator receiving input from the Rhythm Generator (i.e. the CPG) and the visual information, and generated discrete signals that had the capacity to modify the basic gait pattern. The control problem of the clearance of obstacles was divided into two parts: 1) the preparation of obstacle clearance through the modulation of the step length, done by modulating the activation and timing of the ankle and hip extensor (i.e. if the obstacle is far the step length is increased, if the obstacle is close the step length is diminished), and 2) the modification of the basic gait pattern during the clearance of the obstacle. Based on the observation that a reorganization of motor strategies toward active knee flexion occurs during obstacle avoidance in humans, the authors assumed that, during obstacle avoidance, the muscle activation pattern was determined by a weighted sum of the signals from the CPG and the discrete movement generator. The model was able to pass over obstacles of different height and different positions.

Taga model extension Several groups have since developed models based on the work initiated by Taga et al. For instance, in 2002, Hase and Yamazaki [93] proposed a 3D biomechanical model of the entire human body. The controller was based on Taga's hypothesis that bipedal walking emerges from the cooperation between rhythmic patterns from the neural system and rhythmic pendulum-like motion of the locomotion, and proposed an

Introduction

extended 3D model of the entire body able to perform stable walking. Passive spring and damper elements were assumed at the 14 joints. The model comprised 60 muscles, with no passive components. Models of the force-length and force-velocity relation of the muscle were used. The parameters were optimized through Genetic Algorithm (GA). The fitness function was minimizing the energy expenditure while maximizing the smoothness of the movement (by minimizing the muscle tension). The simulation results were consistent with real human walking in terms of joint kinematics and energy consumption. However, the robustness of the motion to external forces or environmental variations was low when compared to Taga's model (explained by the increased complexity of the model).

To tackle this problem, Kim et al. [115] suggested to use a postural controller in parallel with the CPG controller to improve the robustness of the gait. The idea was to add a feedback controller that would generate a torque command to move back the joints to the reference trajectory generated by the neuro-musculo-skeletal model. They successfully used Principle Component Analysis (PCA) to reduce the dimensionality of the feedback control problem, whereby the feedback controller controlled only four states (i.e. the four principal components of the steady-state joint angle trajectories). This strategy significantly improved the robustness of the generated gait against environmental changes and external perturbations. The feedback controller was thought to model the effect of upper brain structures. Indeed, the use of a reduced number of dimension to recover the walking motion can be compared to the idea of motor primitives where a low bandwidth is sufficient to generate complex coordinated behavior (e.g. constant drive to brainstem is sufficient to initiate walking in decerebrated cat, see Section 2.3).

In parallel to the more bio-inspired work of Hase et al., Izumi et al. proposed an improvement of Taga's initial model based on the addition of a new inhibitory connection between the extensor and flexor of the knee joints to the flexor of the ankle joints, first with fixed weights [123] and later with adaptable weight depending on descending drive [90]. With this new mechanism, the biped was able to move up- or down-hill, simply by modulating the descending drive, while all other CPG parameters were kept constant and the robustness to external perturbation was conserved.

For all the model described in this section, the understanding of the underlying principles that generate stable and flexible movements in a self-organized manner, despite unpredictable changes in environmental conditions, remains challenging, given the complexity arising from the interaction among the different components. Indeed, since in these cases the locomotion emerges from the mutual interaction between highly interconnected systems (i.e. neural system, musculo-skeletal system, environment), it is difficult to identify which sub-component is the cause and which is the effect.

Resonance tuning This section provides an overview of the work done on the coupling between the CPG and the mechanical system to ensure global entrainment (i.e. resonance tun-

4. Control aspects of CPGs and current use in robotics

ing), with an emphasis on the role of entrainment in the minimization of energy consumption, which is a major concern for the design of effective autonomous biped walking robots.

In order to achieve energy-efficient rhythmic movement, the brain needs to inject energy at the right moment into the system. Assuming that the building blocks of rhythmic movements is a CPG, it needs to be in synchrony with the natural frequency and relative phase of the rhythmic movements, in the same way a children on a swing needs to push at the right moment in order to maximise the transfer of energy between him and the swing and consequently minimizing the overall energy expenditure of the movement. Studies showed that during rhythmic movements, the brain regulates joint stiffness so that the natural frequency of the total muscle-limb system matches the instructed movement frequency [1]. In other words, the hypothesis is that by modulating the joint stiffness, the CPG has an automatic ability to control a limb in its resonance frequency. This phenomenon is termed *resonance tuning*.

In a study published in 1998, Williamson et al. [224] used Matsuoka oscillators to control the rhythmic movement of robot arms. The positional feedback fed into the oscillator was able to ensure synchronisation of the CPG into the resonance frequency of the limb when the endogenous frequency of the CPG was lower than that of the CPG. In 2006, Verdaasdonk et al. [216] applied resonance tuning to a simplified limb model composed of one hip joint. The CPG used was a Matsuoka oscillator and the output of the CPG were torques. The CPG received input from the state of the limb (angle, velocity and integrated angle). The authors proposed to use a Proportional-Integral-Derivative (PID) type feedback instead of the simple proportional feedback proposed in Williamson's model. This greatly increased the synchronisation capabilities of the system: the positional feedback provided resonance tuning when the frequency of the CPG was lower than that of the limb, and the integral feedback provided resonance tuning when the frequency of the CPG was higher or equal to that of the limb and the velocity feedback compensated for time delays in the feedback loop.

In 2009, the same group applied these results to a more complex system: the minimal input to be added to a simulated passive dynamic walker in order to control it [217]. The results showed an increased basin of attraction due to the entrainment of the CPG by the limb dynamics with an excellent energy efficiency at low speed (the lack of ankle and knee could explain the decreased energy efficiency at higher speed). The velocity could be modulated by changing the proportional afferent strength and the hip stiffness values (i.e. the gain that translates CPG outputs into moments). Increasing the afferent feedback increased the speed by increasing the stride length and increasing the hip stiffness decreased the speed by decreasing the stride length. The resistance to perturbations was achieved by increasing swing leg velocities (achieved by a larger stride length generated by a modulation of the afferent signals due to the perturbation). A suggestion proposed to improve the robustness of the gait was the use of non-linear feedback gain.

Link to robotic systems Several features and hypothesis proposed by Taga et al. and subsequent work have impacted the design of controllers for the locomotion of real legged robots. For instance, the fact that global entrainment can be used as a method of intra-systems communication (i.e. change in speed, synchronization with the mechanical system in the environment), but also as a method of inter-systems communication [195], have applications in robot-to-robot or human-to-robot interactions. Furthermore, the idea of replacing the traditional idea of “planning and execution” with “planning and emergence” offers the advantage that the process of planning becomes independent of the time and state of the dynamical system from which a behavior emerges, which might enlight new planning principles. Based on their results (see Section 4.2), Taga proposed three generalized principles for locomotor control:

1. Self-organized relationships among nonlinear oscillators in a locomotor system are the basis of flexible generation of motor patterns : the alternation of flexion and extension phases produces alternative limb oscillation.
2. The dynamic stability of the locomotor system is produced by a global entrainment between the control system (nonlinear oscillators) and the controlled system (with oscillatory dynamics). The entrainment generates a global limit cycle in the whole system including the environment.
3. Gait patterns can be controlled through changes of a nonspecific parameter. The changes in the system take the form of bifurcations between different types of global limit cycles.

The main idea is that the controller, sensors, and the robot body behave synergistically (i.e. cooperatively) to adapt to the system in real time. In this context, gait transitions can be viewed as a non-equilibrium phase transitions of a synergetic system [181]. This offers new perspective for the implementation of gait transitions in robotics.

Explicit oscillatory pattern.

Methods to design CPGs for explicit oscillatory behaviors are presented in this section. Different tools can be combined to create a CPGs of desired properties in terms of stability, frequency/phase control, synchronisation behavior and coupling architecture. Details can be found in the presentation of two-layered movement imitation system framework [74]. Many applications of this framework exist, e.g. for bipedal walking [142], [172], frequency tuning of a hopping robot [23], drumming task, table wiping, robotic rope tuning or EMG based human-robot synchronization [158]. The general idea is to start from a basic oscillator (such as those presented in Section 3.2), and improve it using the methods described below. The main criteria to consider in the design of a robust CPG for explicit oscillatory behavior are a) stability, b) easy modulation of the frequency and amplitude of the pattern produced,

c) synchronisation between CPGs and the environment, d) encoding of multi-dimensional periodic patterns, and e) coupling architecture. The two first requirements ((a) and (b)) can be guaranteed by the use of simple models with infinite basin of attraction, and the use of oscillators that can be represented in polar coordinates (such as the ACPO or the Hopf oscillator). State of the art solutions to resolve the last three requirements ((c), (d) and (e)) are presented below:

1. Environment synchronization

Any CPG used in robotics must interact with the environment, which is why ensuring that the CPG synchronizes with the environmental dynamic is crucial. While, in case of resonance tuning, this synchronization is done through global entrainment of the oscillators, the mechanical system and the environment, in case of explicit oscillatory behavior, the synchronization can be ensured by: 1) having the frequency of the CPG matching that of the gait cycle and 2) having the CPG and the locomotion cycle in phase. Several mechanisms have been proposed to ensure synchronization between the CPG and the environment in the context of CPG for explicit oscillatory behavior.

A simple solution is to use phase resetting or accelerating/decelerating mechanisms; when the CPG is faster than the gait frequency, a deceleration mechanism engages, ensuring that the CPG does not start a new cycle before the gait cycle actually ends. Likewise, when the CPG's frequency is too slow compared to the gait frequency, an acceleration mechanism ensures that the new cycle does not start before the CPG cycle ends. In its simplest form, the acceleration mechanism consists in a resetting of the phase [142], [4] (i.e. the acceleration is infinite).

Another elegant mechanism developed to guarantee environment synchronization and that can be combined to the previously described approach, consists in adapting the frequency of the oscillator to the frequency of the gait cycle using an online adaptive mechanism. The models implementing such mechanisms are called Adaptive Frequency Oscillators (AFO) and have the property of being able to dynamically adapt their frequency to any periodic driving signal [23], [171] [157]. These oscillators dynamically modify their parameters in order to have an intrinsic frequency that corresponds to the frequency of the input. In order to understand how this is implemented, let's consider an oscillator with two state variables, one of the variable forced by a periodic input signal F .

$$\begin{cases} \dot{x} = f_1(x, y, w) + \epsilon F(t) \\ \dot{y} = f_2(x, y, w) \end{cases} \quad (1)$$

x, y are the cartesian state variables of the oscillator and ω its frequency. In this case, the oscillator effective frequency will be modified toward that of the input signal. If this frequency is not too far from the intrinsic oscillator frequency, the oscillator will converge to the oscillation frequency and both signals will be synchronized, a mechanism called *phase locking*. The idea behind AFO is to describe the frequency as a state

variable whose equation is forced by the input signal F :

$$\dot{w} = -\epsilon F(t) \frac{y}{\sqrt{x^2 + y^2}} \quad (2)$$

This equation has a dynamic on a slower time-scale than the oscillator's dynamic and guarantees that the oscillator will adapt its frequency to one of the frequency components of any periodic signal, for any initial conditions. Moreover, as the rule is encoded in a differential equation, the oscillator will dynamically track and adapt to any change of input frequency. The generic aspect of the method makes it applicable to various oscillators [23], [171]. The main difference with the synchronization occurring through coupling (as in the case of self-organized oscillatory patterns) is that in this case the frequency is learned by the system, therefore when the teaching signal is removed ($F(t) = 0$) the frequency will not be lost (i.e. w will not change, since $\dot{w} = 0$).

2. Encoding periodic patterns

Encoding patterns - or trajectories - as limit cycles is of great interest for the control of robots and highly beneficial in systems and controllers design, as they allow to combine the advantages of using nonlinear oscillators - in terms of stability, due to their dynamical system origin - with the capacity of implementing any desired control reference signal using functions of desired shapes.

One solution to create an arbitrary limit cycle shape - and thus an arbitrary periodic pattern - is to use a pool of AFOs [172], where each oscillator captures one of the frequency component of the teaching signal (i.e. signal with the desired shape), the output of the model being the weighted sum of each oscillator output. This approach learns both the frequencies and shape of the input signal but has several drawbacks when the signal to be learned has a complex frequency spectrum. Indeed, in this case a large number of oscillators will be needed in order to reproduce the desired shape, and consequently: 1) the choice of the oscillator which captures the main frequency of the input signal is not trivial and 2) the learning process will be time consuming and will thereby limit online implementations. Another approach allowing the generation of custom limit cycles is to use one oscillator per dimension of the input signal and to transform its output into an arbitrary wave form, for instance using a single oscillator and higher harmonics of the extracted frequency [158] or using virtual linear springs that are forced to generate the desired periodical output. This second approach can be implemented using rhythmic Dynamical Movement Primitives (rDMP), as proposed by Ijspeert et al. [108], [107], who provided an elegant formulation of a phase oscillator with an arbitrary limit cycle shape using locally weighted regression. A mathematical formalisation and several extensions of this approach are described in Ajallooeian et al [2], where a more general scheme is proposed to convert any existing phase oscillator into the desired nonlinear phase oscillator, with well-defined and controllable properties. The methodology to obtain the desired limit cycle behavior is based on morphing the limit cycle of existing phase oscillators using phase-based scaling functions. More

specifically, and given a desired limit cycle shape encoded in a periodic function f , any oscillator that can be represented in polar coordinate can be morphed to have the limit cycle shape defined by f . The general equation of the compensated morphing (i.e. the compensated form used to obtain a system whose dynamics are closer to the original system when the state is far from the limit cycle, see [2] for details) for an oscillator is given below:

$$[\dot{\theta}, \dot{r}]^T = \left[\omega, \frac{r}{f(\theta)} \dot{f}(\theta) + f(\theta) \cdot g\left(\frac{r}{f(\theta)}\right) \right]^T \quad (3)$$

where $f(\theta)$ is the desired oscillator shape, and g is the radial equation of the oscillator. For example, morphing the ACPO (where $g = c(r_0 - r)$) leads to:

$$[\dot{\theta}, \dot{r}_{new}]^T = [\omega, r_0 \dot{f}(\theta) + c(r_0 f(\theta) - r_{new})]^T \quad (4)$$

where r_{new} is the output of the morphed ACPO and follows the shape of f . The advantage of this method is that any continuous signal can be directly encoded in the system and therefore no learning is needed. In practice, any discrete signal can be used, provided that they can be represented by second order splines.

3. Coupling

In the design of locomotor CPGs, a good control of the phase relationship between the different oscillators is crucial to ensure the coordination between the different muscles, joints and limbs. Therefore, being able to easily control phase relationships between oscillators is an important feature of locomotor CPGs. In case of oscillators that can be written in polar forms, the generation of complex networks of coupled oscillators with desired phase relationship becomes trivial. This has been proven useful in the design of networks of lower vertebrates, such as the lamprey or the salamander, or in quadrupeds, where they can be used to study different gait patterns, gait transition and coordination of movements within and between limbs. For an oscillator that can be described in polar form (see equation C.12), the equation of any oscillator i in the CPG can be written as follow:

$$[\dot{\theta}_i, \dot{r}_i]^T = \left[\omega_i + \sum_j \left[w_{ij}(\Delta\theta_{ij} - \phi_{ij}) \right], g_i(r_i) \right]^T \quad (5)$$

where w_{ij} is the coupling weight between oscillator i and oscillator j , g_i is the radial function and ϕ_{ij} is the desired phase relation between oscillator i and oscillator j . Using this representation, the phase relationship between all oscillators can be summarized in a matrix Φ . In order to ensure that the network will converge to the desired phase relationship, reciprocal phase shift (i.e. $\phi_{ij} = -\phi_{ji}$) can be used.

Robotic training controller for spinal cord injury

Spinal Cord injury

Description

Thanks to the coordinated interaction between muscles, reflexes, spinal oscillators and higher-level brain areas, humans are able to walk, run, jump and generally move around in various environments. Given its central role in locomotion, lesions in the spinal cord - such as those occurring following spinal cord injuries (SCI) - affect these coordinated, symbiotic interactions, often resulting in the loss of walking capability. In addition, SCI subjects also suffer from bowel and bladder dysfunctions, impairments in autonomic functions, and several other secondary conditions, such as pain and ulcers, all of which becoming devastating for the subject's life quality. On a socio-economic level, SCI negatively impacts various areas, such as social care and employment [3]. Indeed, with 11'000 individuals diagnosed with SCI in Europe every year [230] and an average medical cost of €11'000-€22'000 per subject per year [72] SCI drives a total yearly cost of €2.5 to €3 billion in Europe.

Various approaches aim at restoring and compensating walking impairments in SCI subjects, such as epidural electrical stimulation and robotic exoskeletons. Moreover, spontaneous recovery may occur. These different approaches are discussed below.

Spontaneous motor recovery

The ultimate goal of rehabilitation therapy is to reestablish functional connections between the spinal network below and above the lesion, by promoting neural growth at the lesion level. Interestingly, depending on the lesion level and severity, both sensory motor and autonomic functions can spontaneously recover to various extents in both humans and animals. This recovery is called Spontaneous Motor Recovery (SMR) [147]. Originally, it was thought that recovery after SCI required long-distance axonal regeneration [221]. While this effect might exist to some extent, it has recently been shown that the recovery observed in SMR is correlated with the establishment of intraspinal detour circuits [8],[221],[34]. It was further shown that the mechanism by which SMR occurred was related to neurons of the Dorsal Root Ganglia (DRG), in agreement with the idea that repetitive movements during rehabilitation training can induce an enhanced sensory activity which suffices to engage local spinal circuits. These conclusions were drawn from experiments on mice lacking muscle spindles afferents. The lack of spindle afferents did not affect basic motor abilities but severely restricted SMR after incomplete SCI [200].

The ability of the muscle lacking muscle spindles to generate almost normal locomotion is striking. Since the mice grew up with functional muscle spindles and the degeneration occurred postnatal some self organization mechanism might have taken place in the spinal cord during development (as suggested by recent work showing that Spontaneous Motor

5. Robotic training controller for spinal cord injury

Activity (SMA) can lead to coordinated behavior [130]), leading to functional spinal networks able to generate locomotion even in the absence of muscle spindle afferents - the main source of sensory input in DRG.

Epidural electric stimulation

Epidural Electric Stimulation (EES) - patented in 1974 - was first designed as a method for pain management and it was successfully used for pain relief of different diseases [205],[143]. A study, on 25 subjects with SCI showed that while the success rate of pain relief was high after short test periods it dropped consequently after 3 years of test [28] It was later shown that stimulation can be used to control the effect of spasticity in subjects with chronic SCI [46]. These results provided evidence that simple stimulation of the spinal cord could activate latent residual control circuitry and place the network in a more normal physiological state [46].

More recently, both rhythmic and tonic effects of EES were observed in subjects with clinically complete SCI. Stepping was also observed when the stimulation site was on the upper segments of the lumbosacral spinal cord (L2), see Section 2.2 for details. Harkema et al. studied the effect of EES of the lumbosacral spinal cord on voluntary movements, standing and assisted stepping on one subject with clinically complete motor SCI [92]. In the presence of stimulation and after 18 months of training, the subject recovered standing (active control of full weight-bearing for 15 to 20 minutes), stepping (stepping patterns observed, although coordination was not sufficient to accomplish full weight-bearing), voluntary control of both lower legs and showed an increase in muscle mass. While all these locomotor recoveries manifested only in the presence of epidural stimulation, the voluntary control of the bladder occurred several months post-implantation and did not require the simultaneous presence of epidural stimulations. In a review published the same year, the authors highlighted the evidence that the network below the lesion could retain its capacity to generate complex behaviors in both rats, cats and humans. The network is able to control very complicated movements provided that the excitability of the network is enhanced with EES and that the spinal network receives appropriate sensory input [61].

Robotic training after neurologic injuries

Following neurological injuries, such as SCI, subjects will typically follow a phase of rehabilitation, whereby the subjects train the production of movement, usually with the assistance of a physical therapist. There are several rationals behind this rehabilitation procedure: reduced weakening of the bio-mechanical structure, induction of somatosensory inputs in a way that correlates with motor output and reinforces normative sensory-motor pathways [127]. Upon completion of this rehabilitation phase, the subjects' capacities are considered stable, while they may still require walking assistance, usually by the means of wheelchairs or crutches. Wearable exoskeletons could theoretically be used for both the rehabilitation phase and walking assistance, depending on the specific exoskeleton's characteristics.

Introduction

The first role of robotic devices has been to contribute to the rehabilitation phase, by assisting the physical therapist (assistive control). Such exoskeletons present several limitations, such as their lack of adaptability to the specific subjects' capacities and their lack of stability for the subject, which therefore requires additional external stabilizers (such as crutches).

Recent advances in understanding how human locomotion occurs and how balance is maintained during walking makes it now possible to include adjustability options and stabilizing components in the design of wearable exoskeletons. In order to improve the beneficial aspects of the devices on the rehabilitation procedure, the addition of an extra layer of control has been recently proposed, which allows online adaptation of the control parameter (adaptive control), to account for the subject's impairment specificities and subject's improvement in performing the task.

We review here the most common assistive control strategies and describe the most common algorithms for implementing adaptive controllers.

Assistive control

Neurological injuries induce a broad range of impairments, which makes any subjects different. Furthermore, the impairment is not static but evolves with time. Even though the dynamics of a neurological injury is highly subject-specific, changes can be separated into two classes: the physical and neural changes.

- Physical changes:
The reduced recruitment of the muscles in turn reduces the strength of the bio-mechanical structure: the muscles become weaker, bones and ligaments become fragile and soft tissues show an increased stiffness.
- Neural changes:
The sensory-motor map is disturbed by the injury often inducing spasticity (i.e. reflex stiffness). In the long term, this distribution leads to a reorganization of the affected neural pathways. However, it has been shown that - even in complete motor paralysis and years after the injury - the structure below the lesion can remain intact. (as discussed in section 5.1) This intact network can be reactivated if it receives the appropriate external drives, see Section 5.1.

In order to decrease those effects and favor motor recovery, a common practice performed by physiotherapists and by robotic devices consists in actively assisting the movement. There are several rationals behind active movement assistance [127]. First, the movement itself will reduce the stiffness of soft tissue and the weakness of the bio-mechanical structure. It will also provide somatosensory stimulation that will help inducing brain plasticity [213],[160],[176]. Second, even though the subject may be able to contract his / her muscles, the contraction may be so weak that no movement is observed. Therefore, by helping the subject performing the

5. Robotic training controller for spinal cord injury

movement, the somatosensory input is increased in a way that correlates with motor output. In the context of locomotion, if the induced movement is close to physiological movement, it will also reinforce normative sensory-motor pathways, thus reducing undesired neural changes and facilitating the reestablishment of a normative pattern of motor output [91],[168].

Interestingly, some researchers have shown that, in some cases, assistance might have negative effects. This work on assistive control can be grouped in two different classes: the guidance hypothesis [36] and the slacking hypothesis. The guidance hypothesis suggests that physically guiding the movement may actually decrease motor learning for some tasks. The idea is that physical assistance of the movement changes its dynamics. The task learned is therefore not the target task inducing undesirable neural changes [180]. The slacking hypothesis suggests that the active assistance might decrease the recovery if it encourages slacking, i.e. decrease in motor output, effort and energy consumption.

To address these negative effects of providing too much assistance, a class of controller have been developed to provide “assistance-as-needed”. Many studies present assistive based controllers that rely on position feedback strategy: if the subject moves along a desired trajectory, the robotic device should not intervene, and if subject deviates from the desired pattern the robot should create a restoring force, usually generated by a specific mechanical impedance [215],[9]. An other strategy is to use EMG-based assistance. In this case the assistance is driven by surface electromyography signals (sEMG). For lower limb devices, sEMG signals are used as an assistive force generator. In this case, the generated force is proportional to the amplitude of the processed EMG (*proportional myoelectric control*). One advantage is that the subjects control their own movements, since they decide the movement to be performed. The robotic device plays the role of a force amplifier, compensating for the weakness of the subjects. This has been successfully used in the HAL device for both able-bodied and impaired subjects [94] and also by Ferris and al. with an ankle-foot orthosis powered by artificial pneumatic muscles [67]. The limitation of this methods comes from the sensitivity of EMG recording. Indeed, sEMG are very sensitive to electrode placement, skin properties and may be also affected by the overall neurologic condition of the individual. The consequence is that the EMG needs to be re-calibrated for every individual and for each experimental session. The method must also take into consideration abnormal, uncoordinated muscle activation patterns, often observed after neurologic injury to prevent undesired movement.

Adaptive control

The term “adaptive control” refers to control algorithms that adapt controller parameters based on online measurements of the subjects’ performance. Adapting the control parameters has the potential to cope with both short-term (e.g. spastic state, fatigue) and long-term individual changes (induced by neural changes, either directly induced by the device itself or by external treatment) [117],[113]. An example of adaptive control have been presented in

Introduction

Adaptive control parameter	Implementation for lower limb
Impedance modulation	[138],[64],[14]
Desired movement time modulation	[5],[66],[218]
Desired movement path modulation	[170]
Sum of error and effort minimization	[63]

Table 1 – Typical variable affected by the adaptive control in different research applied to lower limb rehabilitation.

the *subject-cooperative training* developed first for the Lokomat, where the robot, rather than imposing an inflexible control strategy, adapts its control based on current subjects intention. More precisely, the desired stepping trajectory, as well as the robot impedance is shaped based on participant interaction forces [170].

Most of the adaptive strategies fall in a common framework, where the control parameter is changed in an error-based fashion that adjusts the control parameter from cycle to cycle based on measured participant performance. The linear version of the error-based adaptive control has the following form :

$$P_{i+1} = fP_i - ge_i \quad (6)$$

Where, P is the control parameter being is adapted (see Table 1), i refers to the i^{th} movement and e_i is a performance error measure (e.g ability to initiate a movement, reach a target, generate a desired position or a given force pattern), f and g are the forgetting and gain factors, respectively. The inclusion of a forgetting term addresses the possible issue that the subject would slack in response to assistance. Indeed, with a forgetting factor of 1 (i.e. $f = 1$), if the performance error is zero, the parameter will not be changed anymore and the participant is not further challenged (this is a consequence of the fact the the performance error is usually a combination of the robots plus subject performance). Introducing a forgetting factor (i.e. $0 < f < 1$) will reduce the control parameter when performance error is small thus challenging the participant [63],[226],[138].

An example, applied to gait training following SCI, where the control parameters modulated the impedance at different percentage of the step trajectory during walking, showed that the subject could step with greater variability while still maintaining a physiologic gait pattern. By adapting the impedance along the step trajectory, the control algorithm was able to cope with subject impairment specificity [64].

Concerning paraplegia, adapting the control parameters would be important in two aspects. First, regarding the high variability of SCI (the level of injury, the depth of the injury) adapting the control parameters would permit to have a “per subject” controller. Second, regarding the dynamical aspects of paraplegia following SCI (e.g. the existence of SMR, the improvement

of impairment condition following rehabilitation, the described effect of electro-enabled motor control), the need to create controllers for orthoses and exoskeletons that can adapt the control parameters has great potential to improve the effect of rehabilitation and is a needed feature of any devices that is designed to be used on daily basis.

Thesis objectives

The understanding of complex locomotor injuries such as stroke or SCI and the creation of the next generation exoskeleton and orthoses requires a deeper understanding of complex questions that involves both the biomechanical (body-environment dynamics, musculo-skeletal structure) and neuro-physiological (muscles, sensors, neural networks) aspects. The questions to be answered involve different layers of complexity (e.g. the role of segmented leg, the recruitment of the muscles, the role of feedback pathways and the organization of the neural networks responsible for locomotion). The increase in computational power, the generalization of physical simulations and the advances in robotic systems offer new opportunities to study and create more complex models.

In order to gain further understanding of the locomotion in general and allow the development of exoskeletons, we sought to develop a dynamical NMM model of the neuromuscular system that would be accurate enough to account for the effect of bones, ligaments, muscles and neural structure and able to produce walking with some degree of fidelity and thus could be implemented on a controller. To reach this goal, we proposed to run the simulation online and in real time, that is, using inputs from the environment to derive the models state and in turn use this state to generate the muscles forces that could then be sent as torque command to the motor. This is to be contrasted with more traditional position, speed or acceleration control of joint states.

We then further developed this model through the introduction of CPGs as feedforward components. The proposed strategy was based on the idea that, in a feedback driven system, the feedforward component can be viewed as a feedback predictor. We implemented the feedback predictors using morph oscillators as abstract models of biological CPGs. Thanks to the intrinsic robustness inherited from the feedback pathways, the modulation of CPGs network's frequency and amplitudes were possible, over a broad range, without affecting the overall walking stability. Furthermore, the modulation of the CPGs network's parameters allowed smooth and stable speed changes and adaptation to larges increase in slope. In this thesis, we present these models and discuss the advantages and implications of using feedback predictors as gait modulators, and highlight the role that biological CPGs could play on top of a reflex-based rhythmic movement.

To date, existing wearable exoskeletons still fail to restore SCI subjects' ability to walk without any external assistance and while promoting the use of residual motor functions. The purpose of the Symbitron project was to overcome the technical limitations of existing exoskeletons, to improve the life quality of partially or fully paralyzed SCI subjects and to enhance the state-of-

Introduction

the-art knowledge on human locomotion and balance, and on man-machine interaction.

Leveraging on our NMM model, we propose a unique approach, whereby the exoskeleton is tailor-fitted to complement the remaining functions specific to each subject, by compensating for the lost motor function. This subject-centered approach therefore requires the design of a customizable solution to complements the unique residual functionality of each individual subject. To reach this goal, the exoskeletons are given adaptable human-like neuromuscular properties to restore the symbiotic interactions naturally occurring between the legs and the rest of the body. Indeed, to allow a bi-directional, symbiotic interaction between paralyzed body parts (to be compensated for by the exoskeleton) and the rest of the body, the exoskeleton replicates physiological neuromuscular functionality, while integrating remaining human motor capacity, such as muscle characteristics and reflexes. This novel approach drives a paradigm shift in the field of robot-assisted locomotion and we believe will achieve substantial breakthrough in the application of wearable exoskeleton technology for SCI-subjects.

We hypothesized that integrating biological layers to the controller could benefit the model in three aspects, which are evaluated in this thesis: First, the mechanical constraints imposed by the muscles and ligaments would provide a natural safety layer. Second, the muscle level would separate the action of extension and flexion forces, allowing more complex behaviors while keeping a simple control scheme and third, the use of a spinal cord model would allow to propose and test hypotheses regarding the spinal organization in a totally new environment. Thanks to the bio-inspired aspects of the controller, subjects wearing the device were able to walk on different terrains (ground, ramp ascent / descent, stairs) in a manner comparable to healthy subjects and without the difficulty of explicit terrain sensing [62]. The results demonstrated the potential of Neuro-Muscular Simulation (NMS) in the controller design of lower limbs rehabilitation devices.

Contributions

This thesis would not have been possible with the Financial support provided by the European Union research program FP7-ICT (SYMBITRON grant #611626). The content is partially compiled from fragments of published journal papers, conferences papers, reviews and technical reports. Below are given, for each chapter, the different documents that were used and the corresponding contributors in decreasing level of importance.

Introduction

Relevant documents

- Florin Dzeladini, Nadine Ait-Bouziad, and Auke Ijspeert. Cpg-based control of humanoid robot locomotion. *Humanoid Robotics: A Reference*, pages 1–35, 2018 (**book chapter**)
- Karen Minassian, Ursula S Hofstoetter, Florin Dzeladini, Pierre A Guertin, and Auke Ijspeert. The human central pattern generator for locomotion: Does it exist and contribute to walking? *The Neuroscientist*, 23(6):649–663, 2017 (**review**)

Chapter 1

Relevant documents

- Florin Dzeladini, Jesse van den Kieboom, and Auke Ijspeert. The contribution of a central pattern generator in a reflex-based neuromuscular model. *Frontiers in Human Neuroscience*, 2014 (**journal article**)
- Florin Dzeladini. Implementation of a Human Feedback-based Locomotion and its Control by means of a Feedforward Component inspired by Central Pattern Generators. 2013 (**master thesis**)

Contributions and resources

- Development of the optimization framework : Jesse Van Den Kieboom
- Development of stage PSO : Jesse Van Den Kieboom
- Maintenance of the framework and cluster infrastructure : Florin Dzeladini

Chapters 2 and 3

Relevant documents

- Florin Dzeladini, Jesse van den Kieboom, and Auke Ijspeert. The contribution of a central pattern generator in a reflex-based neuromuscular model. *Frontiers in Human Neuroscience*, 2014 (**journal article**)

Introduction

Contribution and resources

- First implementation of Geyer Model in Webots : Steve Berger
- Implementation of the C++ model and CPG extension : Florin Dzeladini [54]

Chapter 4

Relevant documents

- Florin Dzeladini, Amy R Wu, Daniel Renjewski, Arash Arami, Etienne Burdet, Edwin van Asseldonk, Herman van der Kooij, and Auke J Ijspeert. Effects of a neuromuscular controller on a powered ankle exoskeleton during human walking. In *Biomedical Robotics and Biomechanics (BioRob)*, 2016 6th IEEE International Conference on, pages 617–622. Ieee, 2016.

Contributions and resources

- Initial Simulink reflex model : H.Geyer [79]
- Development of the initial NMC Achilles controller : Daniel Renjewski, Florin Dzeladini
- Development of the NMC Library for Simulink : Florin Dzeladini, Bastien Martin
- Development of Achilles controller's using the NMC Library : Florin Dzeladini, Amy Wu
- Device : Achilles from UT-Twente [134]
- Infrastructure : UT-Twente (Enschede, NL)

Chapter 6.1,6.2

Relevant documents

- N.L Tagliamonte, F. Tamburella, I. Pisotta, M. Masciullo, M. Molinari, A. Wu. Report on clinical evaluation of the Achilles exoskeleton (*Symbitron deliverables*).
- N.L Tagliamonte, F. Tamburella, I. Pisotta, M. Arquilla, M. Masciullo, M. Molinari, T. Brug. Report on clinical evaluation of WE1 prototypes (*Symbitron deliverables*).
- A. Wu, F. Dzeladini. NMCs for WE1 prototypes for SCI group I subjects and test report (*Symbitron deliverables*).

Contributions and resources

- Addition of tailoring capabilities in the NMC Library: Florin Dzeladini
- Improvement of NMC Achilles controller to account for subject specificity: Amy Wu, Florin Dzeladini
- Device : Achilles and WE1 from Delft University and UT-Twente [134] - Infrastructure and clinical team : Santa Lucia Foundation (Rome, IT)

Chapter 6.4

Relevant documents

- Amy R Wu, Florin Dzeladini, Tycho JH Brug, Federica Tamburella, Nevio L Tagliamonte, Edwin HF Van Asseldonk, Herman Van Der Kooij, and Auke J Ijspeert. An adaptive neuromuscular controller for assistive lower-limb exoskeletons: A preliminary study on subjects with spinal cord injury. *Frontiers in neurorobotics*, 11:30, 2017 (*journal article*)

Contribution

- AW, FD, and EA designed the study and performed the experiment with FT, NT, and HK.
- AW and TB analyzed and interpreted the data.
- AW wrote the manuscript, and FD, TB, FT, NT, and EA participated in the design and drafting of the manuscript.
- EA, HK, and AI were involved in critical revision of the manuscript.

Contributions and resources

- Development of Lopes NMC controller : Florin Dzeladini
- Improvement of NMC to account for subject specificity: Amy Wu, Florin Dzeladini
- Device : Lopes II from UT-Twente [136]
- Infrastructure : UT-Twente
- Clinical team : Santa Lucia Foundation (Rome, IT)

Chapter 6.5

Relevant documents

- N.L Tagliamonte, F. Tamburella, I. Pisotta, M. Arquilla, M. Masciullo, M. Molinari, T. Brug. Report on clinical evaluation of WE2 prototypes (*Symbitron deliverables*).
- A. Wu, T. Brug. NMCs for WE2 prototypes for SCI group II subjects and test report (*Symbitron deliverables*).

contributions and resources

- Development of WE2 NMC controller : Tycho Brug, Amy Wu, Florin Dzeladini
- Device : WE2 from Delft University and UT-Twente
- Infrastructure and Clinical team : Santa Lucia Foundation (Rome, IT)

Appendix B and E

Relevant documents

- N.L. Tagliamonte, F. Tamburella, I. Pisotta, M. Arquilla, M. Masciullo, M. Molinari, T. Brug. Report on clinical evaluation of WE2 prototypes (*Symbitron deliverables*).
- A. Wu, T. Brug. NMCs for WE2 prototypes for SCI group II subjects and test report
- Edwin van Asseldonk. Evaluation report on different (virtual) WE2 (control) designs and man-machine interfaces in healthy control and SCI subjects with higher lesions - Section B: 2.1 Is from Herman van der Kooij, Edwin van Asseldonk, Gijs van Oort, Victor Sluiter, Amber Emmens, Heide Witteveen, Nevio Luigi Tagliamonte, Federica Tamburella, Iolanda Pisotta, Marcella Masciullo, et al. Symbitron: Symbiotic man-machine interactions in wearable exoskeletons to enhance mobility for paraplegics. In *International Symposium on Wearable Robotics*, pages 361–364. Springer, 2018 (*Symbitron deliverables*).

Affiliations

The affiliation of the Symbitron Team can be found in [207]⁴. Jesse Van Den Kieboom was PhD student with BioRobotics laboratory (EPFL, 2014), Steve Berger was Master student with BioRobotics laboratory (EPFL, 2013), Bastien Martin was Semester student with the BioRobotics laboratory (EPFL, 2015)

⁴https://link.springer.com/chapter/10.1007/978-3-030-01887-0_69

On NeuroMechanical modeling **Part I** **of locomotion control**

Without movement, sensing would be very limited and without sensing, movement would be impossible. This relationship allows the brain to hierarchically create very complex model of the reality. This relationship can go from simple to very complex dynamic responses (integrating visual stream and auditory processing to accurately predict the position of a prey and use this clue to optimize the next actions).

How is this complexity built up ? Which portion is genetically encoded and which portion self-organizes in response to the environment? To understand this complexity, a key strategy is to use realistic neuromuscular simulation to investigate the control of increasing complexity, following a bottom-up approach that goes from very simple to more complex and realistic sensory-motor relationship . A first step is to classify biological movements into three different types of increasing complexity: reflex responses, oscillatory movements, and fine conscious movements.

Fine conscious movements differ from reflexes and oscillatory movements in the sense that they use cortico-spinal pathways that act directly on motoneurons, and therefore do not rely on lower brain circuitry (such as the spinal cord).

Reflexes represent the simplest relationship that can exist between a sensory stream and a muscle: an action and a trigger, we call this a reflex arc. The action and trigger are always a transformation of some sensory inputs. Both action and trigger can be as complex as needed. This reflex arc can be grouped by trigger to generate what we call a reflex map. Several reflex maps can then be combined and associated to generate more complex behaviors. An example of what we call a reflex map is the "withdrawal reflex". In this case, the trigger signal (i.e. impulse from a pain receptor) will trigger several arc reflexes (involving several muscles) to generate a movement from the source of pain (withdrawal). Moreover, a single pain receptor will generate different response depending on the initial state of the body at the onset of the reflex, and therefore the action generated depends on the sensory state.

Interneuron populations specialized into the generation of oscillatory output called CPGs are involved in the generation of movements. CPGs are common structures found in the animal kingdom and play role in diverse functions associated with oscillatory motor response, such as breathing, swallowing, locomotion or digestion. Although the concept of CPGs controlling locomotion in vertebrates is widely accepted, how important are CPGs in human locomotion is still a matter of debate. As discussed in the introduction (4.2), an interesting numerical model developed in the 90s' demonstrated the importance CPGs could play in human locomotion, both in terms of stability against perturbations, and in terms of speed control.[199] Recently, a reflex-based neuro-musculo-skeletal model has been proposed by H.Geyer et al.[79] showing a level of stability to perturbations similar to the previous model, without any CPG components. Although exhibiting striking similarities with human gaits, the lack of CPG makes the control of speed/step length in the model difficult.

Herein, we hypothesize that a CPG component would offer a meaningful way of controlling the locomotion speed. We first describe our optimization procedure (1), and re-implement the H.Geyer model[79] using this optimization procedure. After introducing a CPG component in the reflex model, a simple model for gait modulation is presented. The results highlight the advantages of a CPG in terms of gait modulation.

1 Learning and optimization of walking gaits

Introduction

Any mathematical model has parameters associated to it. If equation are one side of the coin then parameters are the other one. They capture the state of the system. Some parameters are known or can be inferred from literature. This is true for muscles, ligaments and bones. Other parameters such as reflex weights are unknown and have to be obtained by other ways. One way of getting them is by using optimization techniques. In that case, all unknown parameters are combined in a vector. Any set of values satisfying the constraints are called solution and a criterion is chosen to evaluate the quality of a given solution. The goal is then to find an optimum solution maximizing the criterion. A commonly used criterion for locomotion models is the minimization of the energy spent while walking, the rational behind this is the fact that as resources are limited, minimizing energy is a very important selective factor in evolution. A very important aspect to keep in mind is that nature does not only minimize energy, it does it under the constraint of keeping robustness as high as possible. While energy can be estimated quite easily using simple energy consumption model, robustness is hard to quantify. One good approach to tackle this problem is to put an external pressure in the environment during the optimization, such as random pushes or uneven ground. Results show that the basin of attraction of the produced limit cycle is increased while similarity with human locomotion characteristics is maintained.

In the next section we present the type of optimization algorithms that we have selected to optimize our models: the particle swarm optimization (PSO).

particle swarm optimization (PSO)

Optimization can be viewed as finding one particular solution of a subset of solutions that satisfies some criteria. Most of the optimization problems can be formulated mathematically

as finding the minimum of a given fitness function or objective function, i.e.

$$[x \in A, \forall y \in A, f(x) = \min(f(y))], f(x) : A^n \rightarrow \mathbb{R}, A \in \mathbb{R}$$

In order to use the framework of iterative optimization algorithms, we need a) a set of parameters, usually from a subset of the multidimensional space of real numbers (noted A in the previous equation, often referred to as the search space) that controls the behavior of the system and b) a way to evaluate the system.

Various optimization techniques can be used, such as genetic algorithm, particle swarm optimization (PSO) or gradient descent algorithm. Here we chose PSO because it has been shown to give good results to resolve similar problems (see work of Steve Berger, former master student at Biorob [12]), and because its low computational cost is small and easy implementation.

PSO algorithms

PSO algorithm is a method used for the optimization of non linear continuous functions, but adaptations to discrete space exists [193, 188, 99]. It is inspired by the movement of swarm observed in nature, hence the name. PSO algorithm is an iterative optimization algorithm. It starts with a set of solutions (randomly chosen or not) in the search space A . After each iteration, the performance of each particle is evaluated using an objective function f . Then, each particle moves in the search space with a speed direction and amplitude that takes into account

- the personal best performance noted x_{pb}
- the best performance of the whole swarm so far x_{gb}

At each iteration, the whole swarm moves in the search space and particles smoothly influence each other. The speed v_i and the position x_i of particle i at iteration t are given by [167]:

$$v_i(t+1) = \omega v_i(t) + c_1 \text{rnd}() (x_{pb} - x(t)) + c_2 \text{rnd}() (x_{gb} - x(t)) \quad (1.1)$$

$$x_i(t+1) = v_i(t+1) + x_i(t) \quad (1.2)$$

Where,

- v_i and x_i are respectively the speed and the position in the search space A of particle i
- c_1 and c_2 are the “cognitive factor” and the “social factor”, respectively. If c_1 is too large compared to c_2 , each particle will converge to another direction and the whole swarm will not converge to a specific solution. If c_2 is too large compared to c_1 , the algorithm will converge prematurely. Here $c_1 = c_2 = 2.05$ (adapted from [167])
- ω is the constriction factor. $\omega < 1.0$ and prevent failure to converge due to unbounded increase of the speed. In our optimization procedure, we define: $\omega = 0.729$. We further

limit the maximum normalized velocity v_n to 0.3, where the component on dimension d of v_n is given as $v_{nd} = v_d / |\max(A_d) - \min(A_d)|$.

Multi-objectives functions evaluation

The objective function often combines different criteria. The consequence is that it is not always easy to manage interactions between the different criteria. A simple solution is to prevent interaction by using multiplicative parameters of different order of magnitudes for each objective (criteria with highest magnitude order parameters (C_{high}) will be optimized first, while criteria with lowest magnitude order parameters (C_{low}) will be optimized last). However, in presence of noise, some criteria might never be optimized. In practice, it is very unlikely - and difficult to verify - that the C_{low} will be optimized at all. Indeed, if any criterion has a variability larger than the magnitude order of the next criteria, those criteria will never be optimized. This motivates the introduction of the Stage PSO presented in the next section, and that we used to optimize our models.

Stage PSO

The stage PSO algorithm is a simple extension of the PSO algorithm (developed by Jesse Van den Kieboom at BioRob and available in the liboptimization framework¹) that uses Lexicographic ordering to manage multi-objectives functions. Lexicographic ordering can be used only if the objectives can be written as constraints and ensures that the multi-objective optimization remains on the Pareto Front [122, 37], that is, no objective can be improved without sacrificing at least one other objective. .

Instead of using a unique multi-objective function (the usual average weighted sum or product of the multiple objectives can become difficult, due to the interaction between the different objectives), the different objectives are decoupled in single objective functions, that are sequentially optimized in corresponding stages. All except the last stage are constraint optimization. Each solution is evaluated according to one single objective function, following a sequential order. The solution is evaluated using the objective function of a given stage until the constraint of that stage is fulfilled. Therefore, each evaluated solution is defined by a tuple (s, v) , where s is the stage reached and v is the fitness value obtained using the objective function of this stage. The solutions are then ranked according to their stages s and, within a stage, according to the value of the associated objective function v . In other words, assuming maximization, the following conditions hold:

- The stage are ordered so that a solution in a higher stage is always considered fitter.
- A solution can be in only one stage.
- Solutions in the same stage s_j are ordered using the fitness function f_j associated to

¹see <https://biorob.epfl.ch/page-36418-en.html>

that stage

- A solution is in stage s_i with $i > 0$, if all the constraints associated to stage $j < i$ are fulfilled but not the one of stage i .

Stage PSO objective function

In stage PSO, the objective function is defined as a serie of stages. All stages except the first one should have an “entrance criterion” that says when the previous stages is close enough to the desired value. Note that criteria for whom a clear desired value is not know (for example the criterion of energy consumption minimization) should be evaluated at the last stage. Using d_{lim} as stopping criteria (SC), we defined an objective function composed of the following five stages for our walking models:

- Stage 0 : maximize the traveled distance
- Stage 1 : bring the speed in a given range -item Stage 2 : minimize pain term
- Stage 3 : minimize energy

The objective functions corresponding to each stage, as well as the entrance conditions are detailed in table 1.1.

Table 1.1 – The 3 stages used during optimization of the FBL. All evaluated criteria are maximized. d is the distance covered by the simulated biped, d_{lim} the maximum distance (simulation stops when $d \geq d_{lim}$), v is the mean speed, v_{opt} the desired mean speed, E is the energy expenditure, P is a penalty term accounting for knee overextension (see [80] for details).

stage	fitness fct	entrance condition
1	d	
2	$ v - v_{opt} $	$d \geq d_{lim}$
3	$-P$	$ v - v_{opt} < 0.05$
4	$-E$	$P < 0.01$

Optimization criteria

The different optimization criteria defined above are further discussed in this section.

1. Control gait speed and step length size

Here, constraints on gait characteristics - namely speed and step length - are introduced. In both cases, the function chosen should present a unique maximum at the desired speed $v_{desired}$ or step length $sl_{desired}$. The simplest function presenting this

characteristic is the absolute function. The constraint for speed is thus written as :

$$C_{speed} = -|v_{desired} - v| \quad (1.3)$$

where v is the mean of the step lengths during one run. Similarly, the constraint for step length is written as

$$C_{steplength} = -|sl_{desired} - sl| \quad (1.4)$$

where sl is the mean of the step lengths during one run.

2. Energy minimization constraint

In order to minimize the energy spend, we need to estimate it. We use a model of muscle energy expenditure to estimate the energy spent by the muscles. The energy consumption model is inspired from [13], as described in [220]. The model also separates the activation heat rate and the maintenance rate in two terms: one for slow twitch fibers, and one for fast twitch fibers. Slow twitch fibers are activated more slowly than fast twitch fibers (see section 2.4 of the introduction for details). The full model of energy of one MTU M with :

- m : mass
- t_I : type I fiber percentage
- s : neural stimulation
- a : muscle activity
- F : active force generated by the muscle
- F_t : the total force generated by the MTU

can be written as:

$$E = A + M + S + W \quad (1.5)$$

Where:

- $A = m \cdot f_A(s)$ is the activation heat rate, with :

$$f_A(s) = 40 \cdot t_I \cdot \sin(\pi/2 \cdot s) + 133 \cdot t_{II} \cdot (1 - \cos(\pi/2 \cdot s)) \quad (1.6)$$

- $M = m \cdot g(l_{ce}/l_{opt}) \cdot f_M(a)$ is the maintenance heat rate, with :

$$g(l) = \begin{cases} 0.5 & \text{if } 0.0 \leq l \leq 0.5 \\ 1 & \text{if } 0.5 < l \leq 1.0 \\ -2l + 3 & \text{if } 1.0 < l \leq 1.5 \\ 0 & \text{else} \end{cases} \quad (1.7)$$

$$f_M(a) = 74 \cdot t_I \cdot \sin(\pi/2 \cdot a) + 111 \cdot t_{II} \cdot (1 - \cos(\pi/2 \cdot a)) \quad (1.8)$$

$$\begin{aligned}
 - S &= \begin{cases} 0.25 \cdot F_t \cdot v_{ce} & \text{if } v_{ce} > 0.0 \\ 0.0 & \text{else} \end{cases} \text{ is the shortening heat rate,} \\
 - W &= \begin{cases} F \cdot v_{ce} & \text{if } v_{ce} > 0.0 \\ 0.0 & \text{else} \end{cases} \text{ is the work rate. } v_{ce} \text{ is the shortening speed, } l_{ce} \text{ the} \\
 &\text{muscle length and } l_{opt} : \text{ the optimal muscle length.}
 \end{aligned}$$

The change in energy consumption at time t is given by:

$$dE = dt \cdot \sum_{m \in \text{muscles}} E_m, \text{ with } E_m = A_m + M_m + S_m + W_m$$

We have developed other criteria for specific use, which are described here for completeness purpose.

1. Increase similarity with human gait

When optimizing using the objective function described above, the produced gait can significantly differ from human gait, both in terms of joint angles and produced torques. In order to increase resemblance with human gait, we introduced a similarity criterion: the correlation $corr$ between joint angle data of walking human (data from [225]) and joint angle of the robot.

$$corr(X, Y) = \frac{cov(X, Y)}{\sqrt{var(X)var(Y)}} \quad (1.9)$$

Where:

- The covariance between to dataset of the same length is given by :

$$cov(X, Y) = \frac{1}{N-1} \sum_{i=1}^N (X_i - \bar{X})(Y_i - \bar{Y}) \quad (1.10)$$

- The variance of a dataset is given by :

$$var(X) = \frac{1}{N} \sum_{i=1}^N (x_i - \bar{x})^2 \quad (1.11)$$

The $corr$ is calculated for each joint of one arbitrarily chosen limb (we assume that the gait is symmetric) over the last full walking cycle. Note that because the correlation is calculated between two sequences of the same length, the angles extracted from the robot are linearly interpolated to have the same length as the human angle sequence. The final criterion is the minimum correlation of the three joints. Because the measure of correlation is not sensitive to the mean of the signal, the difference in mean angle between robot and human could be added in the criterion. Optimizations run with and without the criterion accounting for the difference in mean angle between robot and human joints shows no real improvement in the resulting gait. The similarity is

therefore simply chosen as:

$$C_{angles} = \min\{corr_{ankle}, corr_{knee}, corr_{hip}\} \quad (1.12)$$

2. Increase step length stability

In order to avoid step length variation, a measure of the stability of the step lengths is used: the signal to noise ratio (SNR) of the step length during the trial is calculated. The SNR is defined as:

$$SNR = \log\left(\frac{\bar{X}}{var(X)}\right) \quad (1.13)$$

Where \bar{X} is the mean of the vector X and $var(X)$ is the variance of the vector X The criterion for step length stability is given as :

$$C_{steplengths} = SNR(sls) \quad (1.14)$$

Where sls is the vector of all the step lengths.

3. Minimizing cost of transport

This criterion is used as last stage of stage PSO optimization, when optimizing for robustness. It takes into account not only the energy expenditure, but also the traveled distance, so that it favors increased travelled distance, but only if the increase in energy consumption rate is not too high. The criterion is defined as :

$$C_{cot} = \frac{d}{E} \cdot d \quad (1.15)$$

Where $\alpha = 0.001$ is a normalizing factor, E is the energy expenditure, d is the traveled distance.

4. Maximizing left and right step length similarity

This criterion has been designed to maximize the gait symmetry. It was used at early stages of the project to prevent symmetry issues, but appeared not to be necessary. The criterion is based on the comparison of left and right steplength. Given two sequences x and y of the same length, the similarity criterion is:

$$SNR(x, y) = \log\left(\left|\frac{\bar{x}}{var(x)} - \frac{\bar{y}}{var(y)}\right|\right) \quad (1.16)$$

Where \bar{x} is the mean of the vector x and $var(x)$ is the variance of the vector x The criterion for step length stability is given as :

$$C_{left_right} = SNR(sl_{left}, sl_{right}) \quad (1.17)$$

Where sl_{left} is the vector of left limb step lengths, sl_{right} is the vector of right step lengths.

5. Trunk leaning prevention

This criterion was designed in order to prevent optimized gait to have their trunk leaning forward when optimizing for high speed or for perturbed environment. The criterion is defined so as to be maximized when $0 < C_{trunk} < 0.105$.

$$C_{trunk} = \begin{cases} |\bar{\theta}_{trunk} - 0.105| & \text{if } \bar{\theta}_{trunk} > 0 \\ 0 & \text{else} \end{cases} \quad (1.18)$$

Practical consideration when optimizing walking controller

Initial conditions

The choice of the model initial state is crucial for the subsequent optimization to be effective. Usually, the question of the initial conditions is handled by optimizing the initial joint positions and velocity, together with the control parameters. Here, we have opted for a different strategy. Motivated by the final goal of our work - that is, to drive a person's limb movement with an exoskeleton - we wanted to maximize the robustness of the controller to external changes. Mathematically, we aimed at maximizing the volume of the basin of attraction of the model. Consequently we propose two initial conditions:

- Start in standing position

With the reflex model used as a starting point of this thesis, starting from a standing and straight position is possible with a very small change of the system. Indeed, we simply force the state of one of the leg to swing, disregarding its actual state, until the leg touches the ground again. This feedforward change of the gating mechanism allows the foot - artificially considered in swing - to detach from the ground and activates other feedbacks, generating locomotion. Although stable locomotion can be found with this condition, the final gait obtained after optimization will consume more energy than a gait whose initial joint speeds and positions were learned with optimization.

- Start with an non-zero initial velocity

In order to circumvent the issue of high energy consumption due to the above-defined condition, we further propose to start with a walking gait (obtained from optimization with the standing position as initial condition), and then change the parameters after a few steps (when the limit cycle of the starting gait is reached). This solution presents the advantage of minimizing the initial perturbation of the system. However, the robustness of the system will be reduced.

Gait robustness

Given that our goal is to use the model as an controller, gait robustness to perturbations is a very important feature to maximize. The easiest way to maximize gait robustness, which does not require any modification in the optimization criteria, is to simply add perturbation in the environment during the evaluation. Two types of "perturbed environment" are defined :

1. Random pushes on flat ground: a serie of random pushes are applied at random time to the robot (see details below).
2. Wavy ground: the robot walks on an environment made of wave of increasing slope at random length (see details below).
3. Increasing slope

Random pushes Pushes are modeled as short forces occuring at random time, applied at different position and with different orientations. The force amplitude of the push increases with time. The duration between two pushes is randomly chosen following a F-distribution. The parameters of each push (position, orientation, duration) follow different probability distributions (see figure 1.1). The amplitude follows a normal distribution with mean increasing push after push toward a maximum mean amplitude f .

Wavy ground The wavy ground is modeled as a serie of small trapezoidal structures. The angles of the structures increase structure after structure towards a maximum angle. The length of each structure and the space between them follows a Gaussian probability distribution. (see figure 1.2).

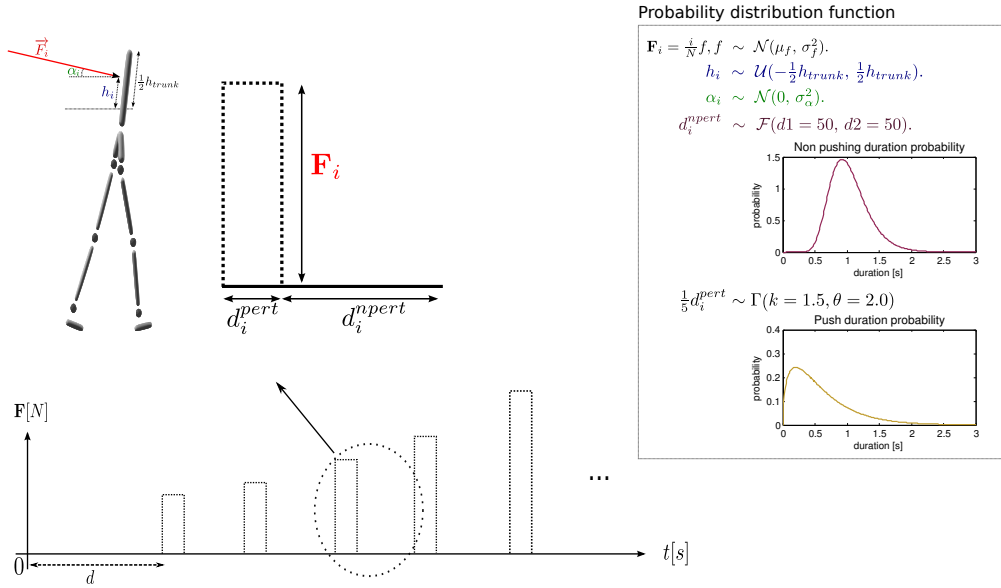


Figure 1.1 – The force of the i^{th} push is modeled has a constant input of amplitude F_i and duration d_i^{pert} , where the amplitude of the force is follows a normal distribution. The mean and standard deviation increase linearly push after push. The duration of the push follows a gamma distribution. The angle of the force with respect to the ground follows a normal distribution with mean 0 and standard deviation of $\pi/2$. The height of the push follows a uniform distribution with a range equal to the trunk height. Finally, the duration of the resting period follows a F-distribution with parameters chosen so that pushes arises every second in average.

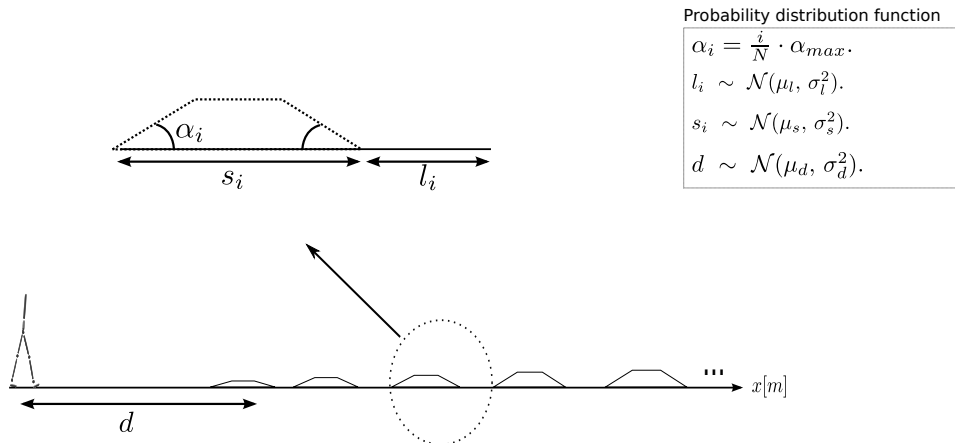


Figure 1.2 – The length of each structure and the space between the different structures follow a normal distribution. For each trapezoidal structure, the up and down angles are the same, and increase between structures, toward a maximal angle α_{max} .

2 A reflex based neuromuscular model of human walking

Introduction

The pure feedback-based neuromuscular model of human locomotion, which we call FBL model, refers to a bio-inspired neuromuscular bipedal walking model developed by H.Geyer & H. Herr [79]. H.Geyer's reflex-based model defines different reflex loops depending on the gait cycle. Moreover, ground contact is used to switch between stance and swing. During stance, the reflex loops induce higher activity in extensor muscle, in order to favor weight bearing support. When the swing phase is initiated, reflexes induce a reduction of extensor activity and an increase of flexors activity (see Fig. 2.1 for a general description of the state machine driving the model). Although the spinal architecture responsible for locomotion proposed by H.Geyer is neuro-physiologically incomplete, the dynamics of the produced gaits are in striking agreement with physiological observations of healthy human walking. More precisely, ground reaction forces, joints angles and torques patterns are surprisingly close to those observed in humans, as shown in the results from our reimplementation of the model, see Fig. 2.3. This agreement is also observed at the muscle level, where similar patterns to those recorded in humans with surface EMG are observed. It is important to note that the muscle activity observed corresponds to normal walking speeds. However, typical features observed at very slow walking speeds [145] are not recapitulated in the model in its current form (lower bound for speed is 0.5 [m/s]).

In this chapter, a C++ implementation of H.Geyer's model is presented using the stage PSO algorithm presented in Chapter 1. The following description is thus largely inspired by their work. Any differences with the original model will be explicitly stated. This model demonstrates that simple delayed feedback loops (i.e. delayed linear mapping between sensors state and muscles activities) are sufficient to generate walking at various frequencies and step lengths. Furthermore, when the objective function used for the optimization process includes a metabolic cost minimization criterion, the generated angles, torques and muscles activation are comparable to human walking data (thus replicating results found in [79] and [220]).

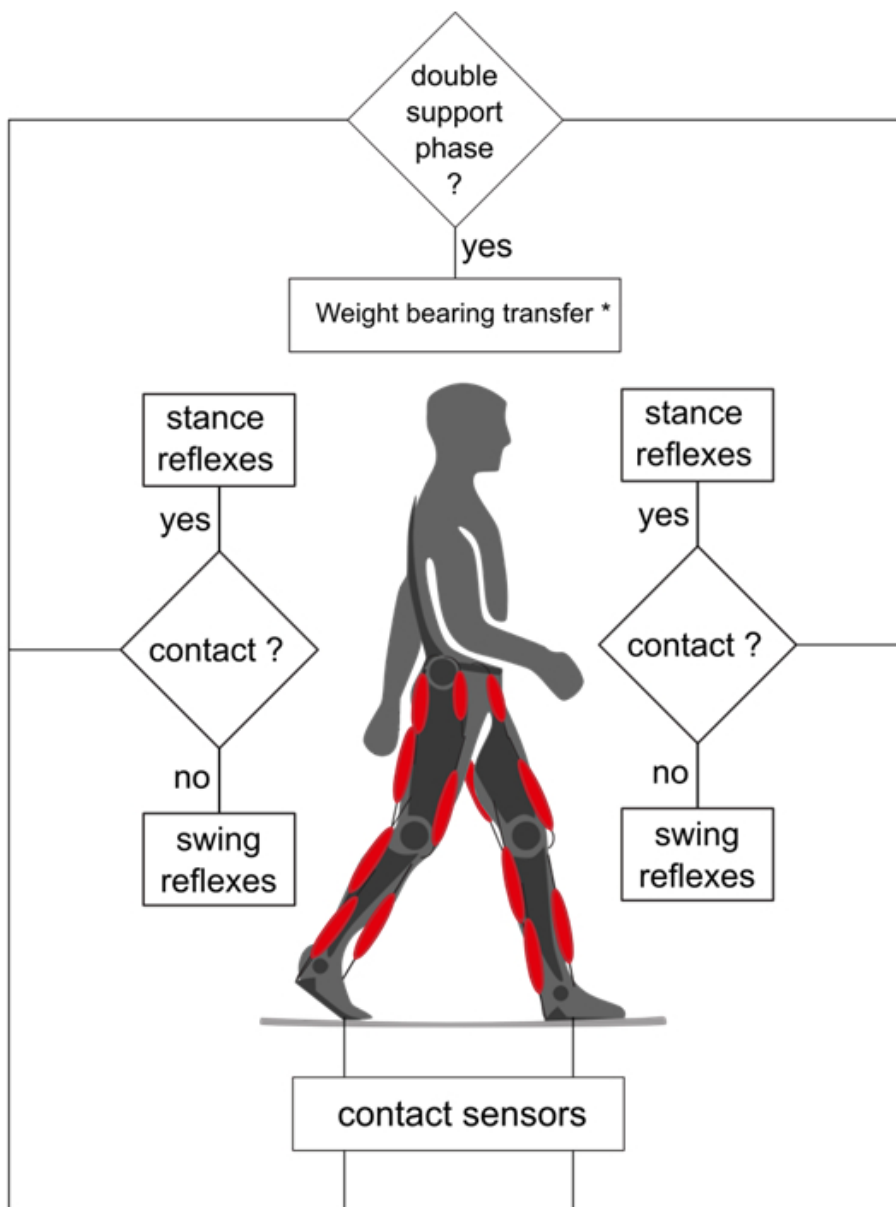


Figure 2.1 – Schematic view of the state machine behind the reflex model of H.Geyer. Ground sensors are used to detect whether the limb is on stance or swing phase. Then, depending on whether the limb is in contact with the ground, different reflex rules are generated (Table 1 in [59] shows the different reflex loops acting depending on the gait phases). An extra term is added to the hips flexor (i.e. HF) and hips extensor (i.e. GLU) to facilitate the weight bearing transfer during the end of the stance, when the other limb touches the ground (i.e. during the double stance support). Fig. inspired from [79].

Methodology

FBL model description

The FBL model uses feedback rules connecting different sources of sensory information (comprising muscle force and length feedbacks, ground reaction forces and joint angles) to Hill-type muscle models (details concerning the muscle model can be found in [80]), which in turn generate effective joints torques.

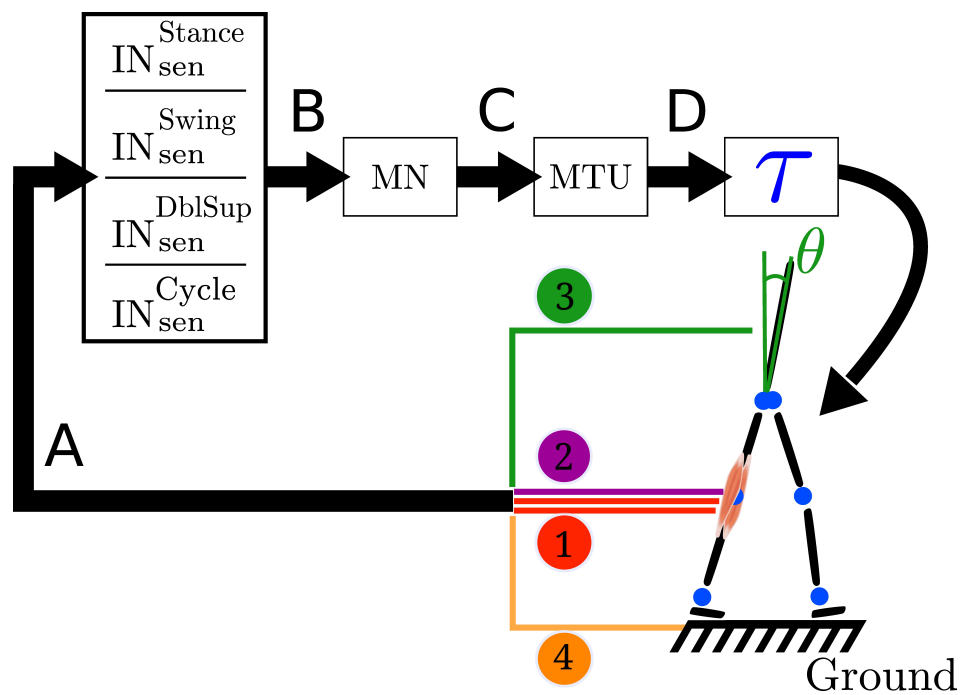


Figure 2.2 – Closed loop information flow of the FBL model. A) Sensors signals stimulate (see Eq. 2.2) a set of sensory interneurons (IN_{sen}). The sensors signals are represented by the colored line; 1 represents the muscle sensors, 2 represents the joint overextension/flexion prevention sensors, 3 represents the stability sensor generating a signal to maintain the trunk upright and 4 represents the ground sensors. There are four different types of sensory interneurons: IN_{sen}^{stance} which are active only during stance, IN_{sen}^{swing} only during swing, IN_{sen}^{dblsup} , only during the double support phase and IN_{sen}^{cycle} during the whole cycle. B) Each IN_{sen} is connected to a unique motoneuron (MN). However a given MN receives inputs from several IN_{sen} . Connections between IN_{sen} and MN follow Eq. 2.3. C) In turn, each MN stimulates its corresponding muscle tendon unit (MTU). D) Each MTU contributes to a torque (τ) on one or two joints, depending on whether it models a uni- or bi-articular muscle. Finally, the action of all the muscles on the body generates a movement, which induces a change in the sensors state and thereby closes the loop. Note that in the original model the link between sensors states and muscles activities is direct (i.e. no intermediary stage), while here the sensors to muscles mapping is separated in three more biologically relevant stages: sensory interneurons (IN_{sen}), motoneurons (MN) and muscle tendon units (MTU). Note that both the original and the FBL model are computationally equivalent.

Chapter 2. A reflex based neuromuscular model of human walking

A state machine is used to switch between two sets of feedback rules: one to generate the stance phase control (mainly extensor muscles activity) and one to generate the swing phase control (mainly flexor muscles activity). Ground sensors placed under the feet are used to detect the state transition (takeoff and touchdown). The generation of the gait cycle is done through reflexes represented by a sequence of time delayed reactions (see Fig. 2.2). Details of the musculoskeletal can be found in Appendix 3.1.

Spinal cord

While in the original model the link between sensors states and muscles activities was direct (i.e. no intermediate stage), in our work we separate the sensors to muscles mapping in three more biologically relevant stages (see Fig. 2.2 for details): sensory interneurons (IN_{sen}), motoneurons (MN) and muscle tendon units (MTU). The intermediate stages are added in order to prepare the extension of the model and makes no functional differences with the original model, as long as the overall delay between sensors and muscle activities is identical in both models. Stages A, B, C are implemented using the connection model defined in Section 2.2.1.

Connection model

in the FBL, walking is generated by a sequence of time delayed reactions (or feedback loops) that connect sensory interneurons to muscles stimulation. The state of the output (y_j) is modeled as an affine transform of the sum of delayed weighted inputs ($\tilde{x}_i = x_i(t - T_{i,j})$):

$$\begin{aligned} y_j &= f(W' \tilde{X}) = f\left(\sum_{i \in Input} (w_{j,i} \tilde{x}_{i,j})\right) \\ &= \min\left\{1, \max\left\{0, \sum_{i \in Input} (w_{j,i} \cdot x_i(t - T_{i,j})) + x_j^0\right\}\right\} \end{aligned} \quad (2.1)$$

Where the i -th index refers to input i and j -th index refers to the output j . Input-Output pairs are sensory neurons-sensory interneurons (stage A), sensory interneurons-motoneurons (stage B) and motoneurons to MTUs stimulation (stage C) shown on figure 2.2. $\tilde{x}_{i,j}$ represent delayed input neuron activities meaning that a change in an input neuron will not affect the output neuron instantaneously but does so after a delay $T_{i,j}$ (modeling the fact that traveling speed of spikes depend on the properties of the nerve fiber). The delays are estimated assuming an average nerve fiber conductance of 80 m/s and estimated length between sensors and spinal cord. Note that the conductance of 80 m/s is the lower bound of extrafusal muscle fibers, golgi tendon organ and muscle spindle Ia conduction velocity [189]. We use three different delays. A 2.5ms delay to model the delay from hip muscles sensors and trunk stability sensors to their corresponding sensory interneuron and from the hip motoneurons to hip muscles. A 5ms delay to model the delay from knee muscles sensors and knee joint angles sensors to their corresponding sensory interneurons and from the knee motoneurons to knee muscles and finally. A 10ms delay for the ankle muscles sensors and ground sensors to

their corresponding sensory interneuron and from the ankle motoneurons to ankle muscles. We assume no delay between sensory interneurons and motoneurons. $w_{j,i}$ is the connection weight from input x_i to output y_j and x_j^0 is the basal activity of the output (in vector format W is the vector of weights and \tilde{X} is the vector of delayed input activity). The output is always constrained to the $[0, 1]$ interval. For a neuron it can be viewed as its normalized firing frequency (1 meaning the neuron is firing at its maximum rate and 0 the neuron is not firing at all), for an MTU it can be viewed as a percentage of maximum muscle stimulation.

Sensor to torque mapping

The sensors to torque mapping noted A to D (schematically represented in Fig. 2.2) are presented below (see Table 2.1 for a description of the different vector/matrices used):

A Sensors to Interneurons

The activity of all interneurons can be written, in matrix form as:

$$X_{\text{in}_{\text{sen}}} = \min\left\{1, \max\left\{0, W \tilde{X}_{\text{sen}}\right\}\right\}^T \quad (2.2)$$

Where $X_{\text{in}_{\text{sen}}}$ is a vector of sensory interneurons activities, \tilde{X}_{sen} is a vector of delayed sensors activities. W is the connection weights matrix linking the sensors and the interneurons. Table 2.2 gives the list of the sensory interneurons present in a given limb.

B Interneurons to Motoneurons

Given limbs state $s = (S_{\text{left}}, S_{\text{right}})$ (with $S_{\text{left}}, S_{\text{right}} \in S = \{\text{ST}, \text{STend}, \text{SW}\}$, where ST, SW and STend stand for stance, swing and double support finishing stance respectively) the activity of all the motoneurons can be written, in matrix form as:

$$X_{\text{mn}} = G^s X_{\text{in}_{\text{sen}}} + X_{\text{mn}}^0 \quad (2.3)$$

Where: X_{mn} is the vector of motoneurons activities acting on limb L , $X_{\text{in}_{\text{sen}}}$ is a vector of sensory interneurons activities, in this case we assume no delay between interneurons and motoneurons (i.e. $\tilde{X}_{\text{in}} = X_{\text{in}}$). X_{mn}^0 is a vector of basal motoneurons activities. G^s is a boolean matrix representing the connection state from interneurons to motoneurons given a limb state s . It ensures that the interneurons act on the motoneurons only when needed (i.e. stance feedback loops are active only during stance, swing feedback loops only during swing. For example if the interneuron $i = 18$ is connected to a motoneuron $j = 3$ and active only during left swing then $G^s(3, 18) = 1$ if $s = (\text{SW}, \cdot)$. Given a limb state s , the state of the considered limb S_{limb} , where limb can be either left or right is defined as a function of the level of the vertical ground reaction forces GRF_{limb}^y and the state of the contralateral limb S_{contra} . When $GRF_{\text{limb}}^y < 0.1$, the limb is considered in swing ($S_{\text{limb}} = \text{SW}$). If $GRF_{\text{limb}}^y \geq 0.1$ and S_{contra} switches from SW to ST then the current limb is in finishing stance ($S = \text{STend}$) otherwise the limb is in stance ($S_{\text{limb}} = \text{ST}$).

C Motoneurons to muscle activities

A motoneuron acts on only one MTU, consequently the equation linking motoneurons to the MTUs stimulation is simply given by:

$$X_{mtu} = \tilde{X}_{mn} \quad (2.4)$$

Where: X_{mtu} is a vector of MTUs stimulation and \tilde{X}_{mn} is a vector of delayed motoneurons activities. The MTU stimulation is constrained to the $[0.01, 1]$ interval. The lower bound of 0.01 is there to model the muscle tone (i.e. a minimal level of tension always produced by the motoneurons innervating a muscle). Its purpose is to permit quicker recruitment of muscles by maintaining a minimal non zero level of tension. The MTU activation level A constrained to the $[0, 1]$ interval is linked to the MTU stimulation level by a first order differential equation modeling the excitation-contraction coupling:

$$\frac{dA}{dt} = \tau_A (X_{mtu} - A), \tau_A = 100[s^{-1}] \quad (2.5)$$

D Muscle activities to joint torques

The overall torque τ_j acting on joint j is given by :

$$\tau_j = \sum_{m \in j} \tau_{m,j} + \tau_j^{ligament}$$

Where $\tau_j^{ligament}$ is the torque generated by the ligaments of joint j , $\tau_{m,j} = F_m \cdot r_m(\phi_j)$ is the torque generated by a MTU m on joint j , F_m is its force and r_m is the moment arm between MTU m and joint j (constant r_0 for hip joints and $r_0 \cos(\phi - \phi_{max})$ for knee and ankle joints, the r_0 and ϕ_{max} values associated to each muscle-joint couples are given in Table 2.3).

State machine as a gating principle

It is clear that what a leg does during walking is different if the leg is in contact with the ground or not. Indeed, a general extension is needed from the leg in contact with the ground to bear the weight, while a general flexion is needed from the leg in swing phase, to bring the leg forward. This is modeled by a state machine which makes the activity of the motoneurons dependent on the cycle phase in which the leg of the ipsilateral side is. The cycle phase can be divided in three parts : Stance phase (st), Swing phase (sw), Stance end phase (stend). The ground sensors (Eq. C.7) are used to detect the state of the limb (i.e. st / sw). A threshold is put on the summed signals from toe and heel ground sensors. If reached, the limb is assumed to be in st phase. The stend phase corresponds to the double stance support phase when the contralateral limb just touched the ground. Fig. 2.1 shows a schematic view of the state machine.

Table 2.1 – Summary of the main vectors / matrices used in the control loop. The model uses a total of 26 sensors (9 muscle sensors, 1 knee joint angle sensors and 2 ground sensors per limb plus 2 trunk sensors). Each sensory interneurons receives connection from one sensor (except the stability sensory interneuron that receives input from the trunk angle and ground reaction forces). The number of sensory interneurons is of 15 per limb see Table 2.2 for details. The number of effective CPG is 9 for the 3FBL models (only the muscle feedbacks are considered) and 13 otherwise (muscle feedbacks + stability feedbacks considered).

Vector / matrices summary

	Dim	Description
X_{sen}	26x1	Vector of sensors states
W	30x26	Connection weight between sensors and sensory interneurons
$X_{in,sen}$	30x1	Vector of sensory interneurons states
$X_{in,cpg}$	30x1	Vector of CPG interneurons states
G^s	14x30	State machine matrix wiring interneurons to motoneurons
X_{mn}^0	14x1	Vector a basal motoneuron activities
X_{mn}	14x1	Vector of all motoneurons states
X^{MTU}	14x1	Vector of all MTU stimulation
A	14x1	Vector of all MTU activation level

Simulation environment and Optimization

The model is implemented as described in [80] and [79], i.e. 6 degrees of freedom all constrained to the sagittal plane and 7 Hill type based muscles per limb. Simulations run with a time step of 1ms. All differential equations are solved with a fourth order Runge–Kutta method, except for the muscle velocity which is integrated using the Euler method (as described in [80]). As already observed by other researcher, the standard Hill muscle model has In order to ensure convergence of the integration process, the integration time step of the muscle is reduced by a factor of 20 in comparison to the simulation time step (this is due to instabilities of the Hill muscle due to lacking damping structure, see section 5.5.1 for details).

Concerning the optimization, the open parameters of the system are the motoneurons basal activities (X_{mn}^0 in Eq. 2.3), the sensors parameters (trunk reference angle of the stability feedback, muscle length feedback offsets) and the feedback gains (non-zero values of matrix $W_{in,sen}$ in Eq. 2.2). The full model has 25 open parameters (the parameters and their associated ranges are given in Table 2.4). In [79], the parameters values were hand-tuned. When using those parameter values in our implementation, the produced gait shows a velocity of 1.1 [m/s]. The generated angles have a correlation with human data of 0.6, 0.7 and 0.9 for the HIP, KNEE and ANKLE joint, respectively. The differences in produced gait between the original Geyer model and our implementation (for a given set of parameters) can be explained by the fact that we use a different simulation environment, bringing differences in the contact model

Chapter 2. A reflex based neuromuscular model of human walking

Table 2.2 – List of the FBL sensory interneurons. The first column gives the abbreviation of the interneuron. The abbreviation indicates from which sensor the interneuron receives input from and to which MN it sends its output and is constructed as follow: MN←INsen_TYPE, ACTIVE_DURING. MN represents the motoneuron onto which the interneuron acts. If not specified, the motoneuron onto which the interneuron acts is on the same side as the sensors side (i.e. ipsilateral). INsen_TYPE represents the interneuron type. There are six different sensory interneurons; MFF (MTU force feedback), MLF (MTU length feedback), GSIF (ground and stability ipsilateral feedback), GCF (ground contralateral feedback), OPF (overextension prevention feedback), TLF (trunk lean feedback). ACTIVE_DURING indicates when the feedback is active; ST: feedback is active during stance, STend: feedback is active during double support finishing stance, SW: feedback is active during swing, CY: feedback is active during the whole cycle, AO: the feedback is active only when the angle of the corresponding joint goes beyond a certain limit, this is used only for the knee joint where the limit is fixed and set to 170 degree. The second column gives the type of the interneuron, as described in section 3.1.3. The third and fourth columns indicate the start and target of each feedback pathway. The last column specifies in which part of the cycle the feedback is active, the (-) sign refers to a inhibitory effect.

Sensory Interneurons

Abbreviation	Type	From	To	ACTIVE_DURING
GAS←GAS MFE, ST	1b	GAS	GAS	Stance
GLU←GLU MFE, SW	1b	GLU	GLU	Swing
HAM←HAM MFE, SW	1b	HAM	HAM	Swing
SOL←SOL MFE, ST	1b	SOL	SOL	Stance
TA←SOL MFE, ST	1b	SOL	TA	Stance (-)
VAS←VAS MFE, ST	1b	VAS	VAS	Stance
TA←TA MLF CY	1a	TA	TA	Cycle
HF←HAM MLF SW	1a	HAM	HF	Swing (-)
HF←HF MLF SW	1a	HF	HF	Swing (-)
HF←GSIF ST	3,4	iFoot,Trunk	HF	Stance
HAM←GSIF ST	3,4	iFoot,Trunk	HAM	Stance
GLU←GSIF ST	3,4	iFoot,Trunk	GLU	Stance
VAS←GCF STend	4	cFoot	VAS	Stance end (-)
HF←TLF SW	3	Trunk	HF	Swing
VAS←KNEE OPF	2	KNEE	VAS	Angle off (-)

Table 2.3 – List of the seven different muscles used in the FBL and derived models: GLU for gluteus, HF for hip flexor, VAS for vasilus, GAS for gastrocnemius, TA for tibialis, HAM for hamstring and SOL for soleus. The last two rows (HAM and GAS muscles) corresponds to bi-articular muscles (i.e. they span two joints), other rows are for uni-articular muscles. The second column shows the resulting action on the joint(s) onto which the muscle acts. The third column corresponds to the lever arm used for torque calculation. The fourth column gives the angle at which the action of the muscle on the joint is maximum (absent for the hip joint). The last column gives the reference angle of the muscle (i.e. the angle that corresponds to the muscle rest length).

MTUs list and joints related parameters

	Action	r_0 [m]	ϕ_{\max} [deg]	ϕ_{ref} [deg]
GLU	hip ext.	0.1	-	150
HF	hip flex.	0.1	-	180
VAS	knee ext.	0.06	165	125
SOL	ankle ext.	0.05	110	80
TA	ankle flex.	0.04	80	110
HAM	hip ext. knee flex.	0.08	-, 180	155, 180
GAS	ankle ext. knee flex.	0.05	110, 140	80, 165

Chapter 2. A reflex based neuromuscular model of human walking

and ground sensors. In almost all subsequent articles on FBL enhancement, optimization algorithms are used to set the parameters values. For example, in [191], the parameters were optimized to generate gaits of different speeds. The parameters were then analyzed in order to study the possibility to generate a speed controller through the direct modulation of reflex gains. The objective function used took into account the difference between target velocity and current velocity, a penalty term accounting for knee overextension and an energy expenditure term based on [13].

Table 2.4 – FBL model parameters list and their respective range. The parameters are tuned by optimization. ks_* and δ_{ref} are the stability feedback related parameters. wf_* are muscle force feedback gains, wl_* muscle length feedback gains and l_* muscle length offsets. s^0_* are the muscle basal activities. $k_{\delta knee}$ is the gain of the knee overextension prevention feedback. ΔS is a constant term added to the HF and subtracted from the GLU during stance.

Name	Range	Name	Range
wf_{sol}	[0.8; 1.6]	ks_{lean}	[0.0; 2.0]
$wf_{ta_{sol}}$	[0.1; 0.8]	ks_{bw}	[0.8; 1.4]
wf_{gas}	[0.3; 1.6]	ks_{p1}	[0.8; 1.4]
wf_{vas}	[0.9; 1.8]	ks_{p2}	[0.5; 1.4]
wf_{ham}	[0.2; 1.0]	ks_d	[0.8; 1.4]
wf_{glu}	[0.2; 0.9]	s_{sol}^0	[0.01; 0.1]
wl_{ta}	[1.0; 3.0]	s_{ta}^0	[0.01; 0.1]
wl_{hf}	[0.2; 1.5]	s_{gas}^0	[0.01; 0.1]
wl_{ham}	[0.0; 3.0]	s_{vas}^0	[0.01; 0.1]
l_{offset}^{ta}	[0.0; 1.0]	s_{ham}^0	[0.01; 0.1]
l_{offset}^{hf}	[0.2; 1.0]	s_{glu}^0	[0.01; 0.1]
l_{offset}^{ham}	[0.7; 1.0]	s_{hf}^0	[0.01; 0.1]
		$k_{\delta knee}$	[0.0; 3.0]
		ΔS	[0.0; 1.05]

In the present work we also use optimization to instantiate parameters values of the FBL model. Since at least two criteria are always used (i.e. the minimization of energy and the penalty term accounting for knee overextension, and more as soon as one wants to optimize for an extra parameter, such as speed or step length), a good handling of multi-criteria evaluation is mandatory. We use a lexicographic ordering extension on top of the PSO (Particle Swarm Optimization [114]) algorithm (stage PSO) to handle multi-objectives fitness functions. As described in Chapter 1, in stage PSO, the different objectives are decoupled in single objective functions, that are sequentially optimized in corresponding stages, instead of using a unique multi-objective function (the usual average weighted sum or product of the multiple objectives can become difficult, due to the interaction between the different objectives).

Here we used 4 stages whose associated fitness functions and continuation criterion are given

in Table 1.1. The first stage optimizes for a walking gait that can cover at least a distance of d_{lim} . Since the model can generate gaits of various speeds, we added a second stage to constrain the speed of the walking solution so as to facilitate further comparison between the different solutions obtained. The third stage minimizes a penalty term accounting for knee overextension to favor human-like gaits.[80] The fourth stage minimizes the metabolic energy expenditure. The criterion associated with each of these stages are described in section 1.2.3.

Since our final goal is to add a feedforward component to modulate the gait, the initial model should have the capacity to manage changes in acceleration, deceleration or step lengths, i.e. it should be robust. However, optimizing for energy consumption on a flat ground will not favor the emergence of such gaits. In order to circumvent this issue and favor robust solutions, we optimized the feedback parameters on an environment with increasing and decreasing slope. The increasing/decreasing slope are modeled as simple trapezoidal structure (with max slope 5%). Furthermore, the length, slope and distance between trapezoidal structure are randomized (as described in Chapter 1). During the optimization process, each solution is evaluated on 5 different randomly generated environments, and only the worst fitness score is considered.

Results

In order to determine the ability of our optimization process to generate stable gait, we performed 10 runs of the same optimization process (as described in Section 2.2.2) with different random initial conditions. We observe that the optimization process always converges to a stable and symmetric walking solution, but to different solutions (local optima), hence leading to visually different gaits. Fig. 2.3 F gives a snapshot of the solution 1 during two cycles. Note that the presented results are, in terms of joint angles, joint torques and muscles activities, qualitatively similar to those presented in the paper describing the original model [79].

Metabolic cost analysis

When comparing the cost of transport (CoT) between the 10 different solutions, we observed a value ranking from 2.2 to 3.5 [$\text{Jm}^{-1}\text{kg}^{-1}$] (CoT is defined as E/md , where E is the energy consumed during the run, m is the mass of the model, d is the traveled distance), see Fig. 2.4. Five solutions show a CoT less than 25% higher than the net metabolic transport cost of $2.1[\text{Jm}^{-1}\text{kg}^{-1}]$ found in human subjects of similar heights, weights and walking at the same speed [222]. This increase is comparable to the one found in [13] and can be explained by the fact that, in our model, the upper body is modeled as a single rigid body, while the experimental values used for comparison are for walking with arm swing. Indeed, it has been shown that, despite the fact that arm muscles consume energy to produce movement, they can still reduce the walking metabolic cost up to 12% [30]. An other reason explaining the higher CoT could be the lack of feedbacks for stance preparation. Indeed, as most of the metabolic cost of walking comes from the stance phase, optimizing the properties of the limb joints

before touchdown will affect the efficiency of walking, as shown in [52]. Finally, the observed very low energy consumption of eccentric contraction in real muscles not recapitulated in the Hill model could explain the higher CoT level, see Section 5.5.1.

Golden ratio analysis of gait harmony

As demonstrated in [109], the ratios between cycle/stance durations (noted GR0, commonly referred to as the duty factor), stance/swing durations (noted GR1), and swing/“double stance support” durations (noted GR2) is similar in healthy humans of different size, corpulence and age walking at preferred (self-chosen) speed, and satisfy the golden ratio ($\phi = \frac{1+\sqrt{5}}{2}$). Note that the variability of GR1 is higher than GR0, and the variability of the GR2 is higher than GR1. We measured those three ratios in our 10 solutions, and observed that GR0 converges to ϕ in all cases, GR1 converges to values close to ϕ with higher variability and a bias to slightly smaller values, and GR2 is more variable, with a bias to values higher than ϕ . The bias observed in the cases of GR1 and GR2 indicates that there is a tendency to generate gaits with longer swing and shorter double stance support phases. This overestimation of the swing duration can be explained by the fact that our model does not have toes; the length of the foot being shorter, the legs tend to enter the swing phase earlier.

Gait analysis

We then compared the joint angles and torques trajectories of the 10 solutions, with human data [225]. A correlation analysis revealed that all joints angles and torques are comparable to human data (see Fig. 2.3 A and C, if not stated otherwise, the solutions are ordered with increasing CoT). While the ANKLE torques show high correlation with humans, the HIP and KNEE torques correlations are substantially lower. This can be explained by the fact that, in our model, the HIP is completely fixed to the trunk. We thus do not model the characteristic pelvis movement observed in human walking. Regarding the joint angle correlations, we can see that the ANKLE angle correlation is not perfect. The low correlation can be explained by the differences in shape in late stance and early swing (see Fig. 2.3 B, right), which is due to the fact that the toe is not modeled. Indeed, the lack of toes will make the leg enters in swing earlier, thereby explaining both the reduced minimum angle and the earlier slope inversion (i.e. the swing/stance transition). Another interesting difference between the model and human data can be noted at the ANKLE angle level during early stance. Indeed, while humans show an initial passive extension during early stance of about 1/10th of stance duration (black dotted line in Fig. 2.3 B right), the model does not show this behavior. When looking carefully at the ANKLE angle pattern for solution 1 an initial passive extension is visible. However, this initial passive extension is very short and almost not visible in the figure (blue line in Fig. 2.3 B right, the ANKLE angle does not start at the same place due to a very fast and quick passive extension). The solution 10 (orange line in Fig. 2.3 B) does not show this behavior at all: the foot touches the ground horizontally. Several elements can explain this behavior, such as the lack of mechanism (e.g feedback, CPG) for stance preparation, a shorter swing range (due to

smaller HIP range or an under-extension of the knee) or the way the swing-stance transitions are designed, i.e. state machine with discrete transition.

When comparing muscles activities of solution 1 (see Fig. 2.3 E), we note that all the ANKLE muscles and HF muscle are close to human data. However, the GLU, VAS and HAM muscles do not show the typical activity observed during late swing in humans. This is in agreement with the conclusion drawn in the previous paragraph concerning the lack of a mechanism for stance preparation. Another explanation could be the use of Hill-type muscle models, which do not account for all of the predominant intrinsic muscle dynamics, see Section 5.5.1 for a discussion.

Discussion

The analysis of gaits generated by the optimized FBL model highlighted several similarities to healthy humans. Moreover, some solutions of different runs from the same optimization process showed ANKLE kinematics similarities to children suffering from cerebral palsy, highlighting the role that the FBL model could play in terms of modeling locomotion diseases. Children with cerebral palsy show a typical ANKLE flexion (instead of extension) in the early stance, followed by a double bump, visible at both the angle and torque level [110]. This is conceivably linked to a reduced hip range of motion, a weakness of tibialis anterior and/or a hypertone of gastrocnemius. Surprisingly some of the solutions such as solution 10 (orange line in Fig. 2.3 B and D right), show both features observed in children with cerebral palsy, i.e. ANKLE flexion in early stance and the double bump visible in both the torque and the angle. Furthermore, solution 10 shows a smaller HIP range of motion compared to solution 1. Finally, the tibialis anterior was found less active at the beginning of gait cycle compared to human physiological gait, as reported for children with cerebral palsy. Conversely, the double bump noted in the model seemed not to be related to an increased muscular activity of gastrocnemius. These interesting similarities, as well as the potential role of the model in disease/injury modeling should be further investigated.

Despite the interesting properties of the model presented in this chapter, an important limitation is that, once a walking gait at a given speed and step length is obtained, the only way to modulate it is by the tuning of the multiple feedback gains. The gait modulation strategy proposed in the next chapter is based on evidence from lower vertebrates and quadrupeds suggesting that simple low dimensional descending signals are sufficient to modulate walking (speed changes and gait transitions) [88].

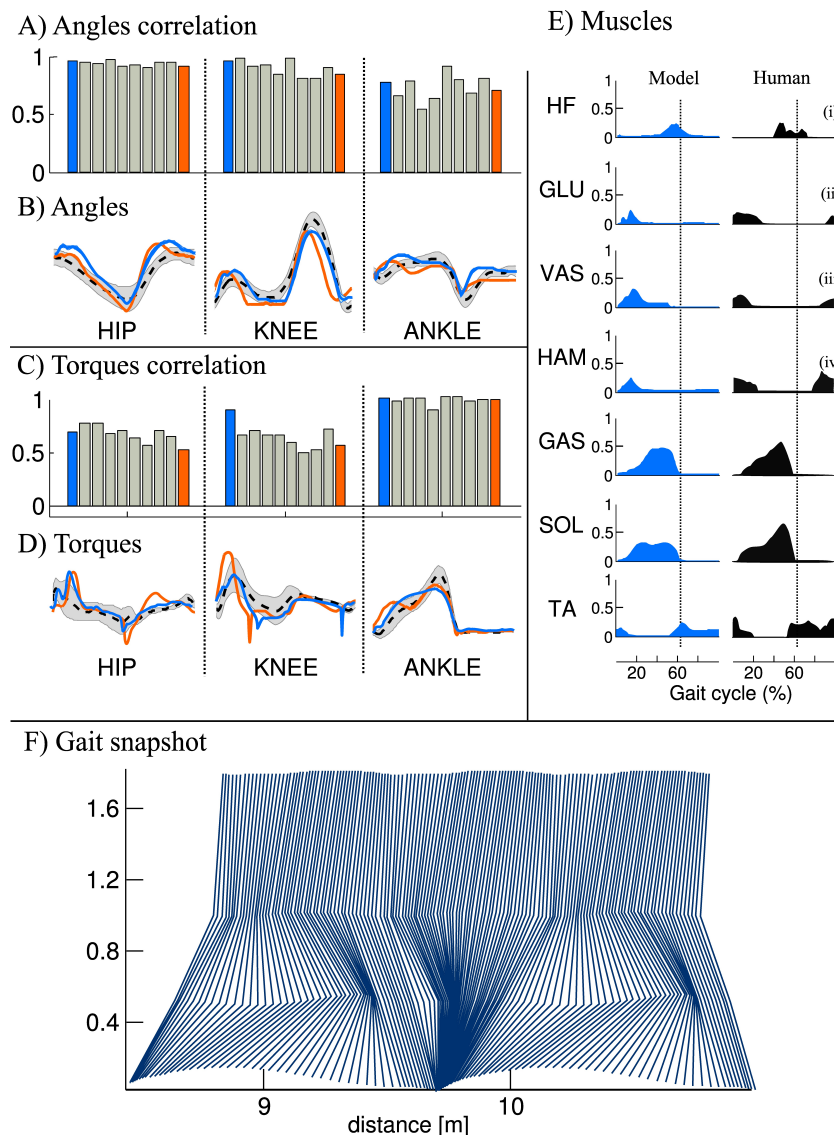


Figure 2.3 – Comparison of joints angle, joints torque and muscles activity extracted from the FBL models (10 optimization runs), with human data. Human joints angle and torque are taken from [225], muscles activities are adapted from [155], as presented in [79]. A) Joint angle correlation with human, B) Average joint angle compared to human, C) Joint torque correlation with human, D) Average joint torque compared to human, E) average muscles activity of solution 1 compared to human and F) Gait snapshot of the solution 1 over two cycles. In A) and C), the bar plots show the correlation with human for the different solutions and for the different joints. In B) and D) are shown typical human trajectories (black dotted line:mean, gray: standard deviation) and two mean trajectories from solution 1 and solution 10, blue and orange lines respectively. Each bar corresponds to one solution of the same optimization process (optimized for a stable gait walking at 1.3 m/s), the different solutions are ordered with increasing energy consumption (same as in figure 2.4). The correlation were calculated on data extracted from 50 strides of steady state walking (sampling frequency of 1Khz), spline interpolation was used to normalize the length of the vectors to 1000 points. The average of the normalized vector was then correlated with average human data. In E) the subscripts show the compared muscles: (i) adductor longus, (ii) upper gluteus maximum, (iii) vastus lateralis, and (iv) semimembranosus. The data was extracted from a model walking on a flat terrain without noise and external perturbations.

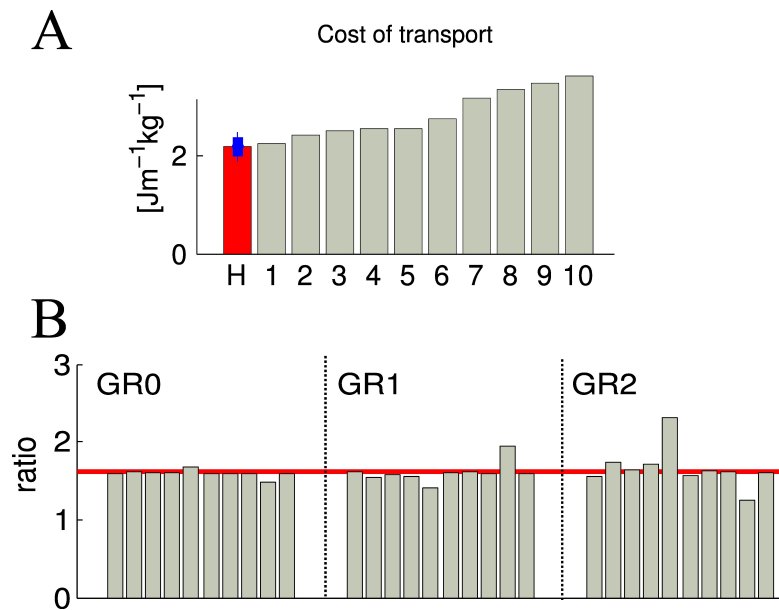


Figure 2.4 – Each gray bar corresponds to one solution of the same optimization process (optimizing for a stable gait walking at 1.3 m/s). A) Normalized cost of transport. The red bar corresponds to the normalized cost of transport of human subject of the similar weight and walking speed as our obtained gait (data from [222]), the blue bar shows the estimated standard deviation. B) Duration proportion of the different gait phases. GR0 corresponds to the ratio between cycle duration and stance duration, GR1 corresponds to the ratio between stance duration and swing duration and GR2 corresponds to the ratio between swing duration and double stance support. The red line corresponds to the golden ratio $\phi = \frac{1+\sqrt{5}}{2}$. GR0, GR1 and GR2 are known to be statistically similar to the golden ratio in human walking at their preferred speed [109].

3 Pattern in the central nervous system

Introduction

As discussed in details in the thesis introduction (section 4, a model developed by G.Taga demonstrated the role that CPGs could play in human locomotion. It was shown that walking and running could emerge from a rhythmic interaction (modeled by coupled oscillators, i.e. CPGs), between the central nervous system, the musculo-skeletal-system and the environment. The CPGs were modeled as a network of oscillators, coupled with the environment through joint angles and ground reaction forces [196]. The intriguing robustness of the generated gaits against mechanical perturbations and changes in the environment was attributed to the use of CPGs and feedbacks, respectively, highlighting the important role of both components.

While in G.Tagas model, speed was controlled by a simple unique variable (the frequency of the oscillators), such a strategy is inapplicable in the FBL model. Although a preliminary speed control strategy has been proposed by [191], its complexity compared to the very simple descending signals, originating from the brain stem, able to control locomotion (found in lower vertebrates, such as the lamprey and the salamander, and even in cats) makes their relevance, from a biological point of view, questionable.

Given the striking properties of the FBL, we wanted to study the possible benefits that a CPG would add to the model. We hypothesized that the reflex model would benefit from the presence of CPGs in terms of gait speed / step length control. The CPG component is derived from the feedback pathways, following an idea from [118], where CPGs are viewed as feedback predictors. We use a variety of models combining CPG and feedbacks in different ways to study the relative importance of the different feedbacks/feedforward pathways. Finally, taking advantage of the properties of the CPG, a simple model for speed modulation is presented.

Methodology

The extended model is a hybrid feedback and feedforward model, referred to as 3FBL. The CPG component (IN_{cpg}) generation is based on an idea from [118], where feedforward signals produced by the CPGs are considered as feedback predictors. A direct way of combining such CPGs with feedbacks is to use a proportional term to control the relative importance of the CPG versus the feedback it predicts, i.e. given the vector of CPG activities $X_{\text{in}_{\text{cpg}}}$, equation 2.3 representing the motoneurons states becomes:

$$X_{\text{mn}} = G^s \left(\vec{\alpha} X_{\text{in}_{\text{sen}}} + (1 - \vec{\alpha}) X_{\text{in}_{\text{cpg}}} \right) + X_{\text{mn}}^0 \quad (3.1)$$

Where: G^s , X_{mn} , X_{mn}^0 and $X_{\text{in}_{\text{sen}}}$ are the same as in equation 2.3. $X_{\text{in}_{\text{cpg}}}$ is the vector of feedforward interneurons activities. Note that here $X_{\text{in}_{\text{cpg}}}$ and $X_{\text{in}_{\text{sen}}}$ have the same dimension but all the components of $X_{\text{in}_{\text{cpg}}}$ referring to non-modeled sensory interneurons are set to 0. In the 3FBL models, only the sensory interneurons related to muscles sensors are modeled with CPGs. Thereby, limiting the effective number of CPGs to 9 per limb. $\vec{\alpha}$ is a vector controlling the relative importance of sensory versus CPG interneurons: a value of 0 in any of the α_i components will make the corresponding pathway exclusively feedforward-driven, whereas a value of 1 would make it solely feedback-driven (see Fig. 3.1). Thus, when $\vec{\alpha} = \mathbf{1}$, the 3FBL becomes the FBL model. Conversely, when $\vec{\alpha} = \mathbf{0}$, the activity of all the sensory interneurons is ignored and the model becomes a purely feedforward-driven model.

Any IN_{cpg} is by definition a model of the underlying feedback pathway IN_{sen} . In this work, we used two different abstract models of biological CPGs: a dynamical model $IN_{\text{cpg}}^{\text{osc}}$, generating a periodic time varying signal, and a constant model $IN_{\text{cpg}}^{\text{cst}}$, generating a constant signal (see section 3.2.1 for details). Both $IN_{\text{cpg}}^{\text{osc}}$ and $IN_{\text{cpg}}^{\text{cst}}$ can be viewed as a linear model of the underlying IN_{sen} . The former is a model capturing the shape, timing and average activity, while the latter only captures the average activity. Therefore, their combination with IN_{sen} can be viewed as a linearization of the underlying feedback pathways. Indeed, equation 3.1 can be rewritten as:

$$X_{\text{mn}} = G^s \left(X_{\text{in}_{\text{cpg}}} + \vec{\alpha} (X_{\text{in}_{\text{sen}}} - X_{\text{in}_{\text{cpg}}}) \right) + X_{\text{mn}}^0 \quad (3.2)$$

This representation highlights the fact that, in the 3FBL model, the equation governing the activity of the motoneurons can be viewed as a linear feedforward term, plus a corrective term (i.e. the difference between the IN_{sen} and IN_{cpg} states). As expected, the effect of a $IN_{\text{cpg}}^{\text{osc}}$ - IN_{sen} combination is different from the one of a $IN_{\text{cpg}}^{\text{cst}}$ - IN_{sen} combination. On the one hand, increasing the proportion of $IN_{\text{cpg}}^{\text{cst}}$ can be viewed as reducing the amplitude of the underlying IN_{sen} , without affecting its mean activity. In other words, the proportion of $IN_{\text{cpg}}^{\text{cst}}$ *versus* IN_{sen} controls the flatness of the IN_{sen} . On the other hand, the combination of IN_{cpg} and IN_{sen} will neither significantly affect the shape, nor the average activity of the IN_{sen} , but will affect the timing.

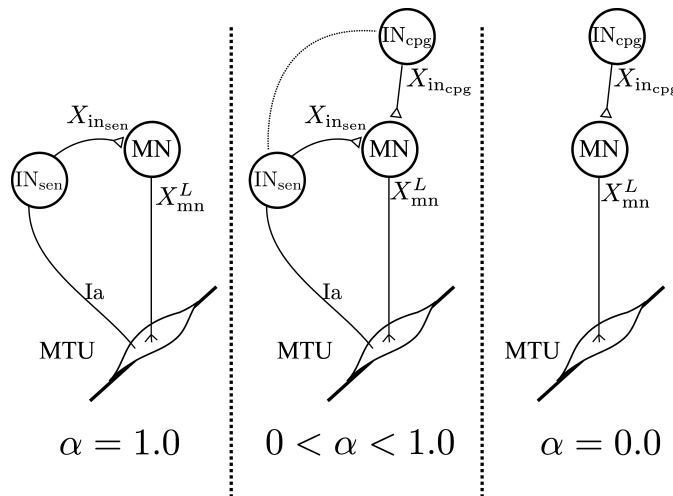


Figure 3.1 – Schematic representation of feedback-feedforward combination for one specific pathway. The value of α controls the proportion of feedback versus feedforward. With $\alpha = 1.0$ the feedback pathway is solely feedback-driven. With $\alpha = 0.0$ the feedback pathway becomes a feedforward pathway. All values in-between create a feedback/feedforward pathway.

CPG Model

CPG-Constant model

In order to test whether a very simple model of feedback could already capture enough information to permit modulation, we decided to implement a CPG-Constant model, denoted IN_{cpg}^{cst} . IN_{cpg}^{cst} state is a constant signal, whose value equals the average underlying IN_{sen} state. The average is calculated only on the part of the cycle where the feedback is active (e.g. for feedback active only during the stance, the average is calculated only during stance). This type of feedforward signal captures the average activity of the underlying feedback pathway. When combined with feedbacks, the net effect is a flattening of the original feedback signal.

CPG-Oscillator model

In the oscillatory model, denoted IN_{cpg}^{osc} , each feedback predictor is modeled as a dynamical system reproducing the average shape and amplitude of the original feedback signal. In other words, CPGs can be viewed as a dynamical approximation of the sensory interneurons states $X_{in_{sen}}$ (see Eq. 2.2). The dynamical system used for this purpose is a morphed oscillator (MO) [2]. This oscillator is able to produce any shape, as long as this shape can be represented by a function that is both 1-periodic and derivable. The differential equation governing the oscillator is the following:

$$\dot{\theta} = \omega \quad (3.3)$$

$$\dot{x} = \gamma(g(\theta) - x) + \frac{dg}{d\theta} \cdot \dot{\theta} + K \quad (3.4)$$

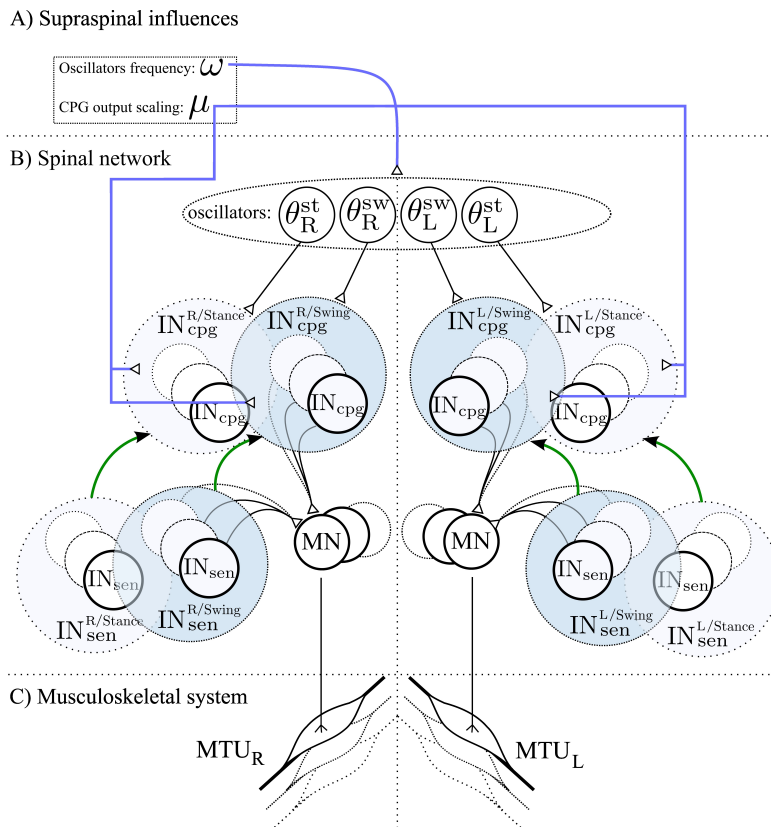


Figure 3.2 – Schematic representation of the spinal network and supraspinal control of the CPG network in the 3FBL model. The network is symmetric: left/right part of the figure corresponds to the part of the network acting on right/left limb muscles respectively. A) Supraspinal influences: μ represents the activity modulation pathway and ω the frequency of the CPG network. All 4 oscillators share the same ω , but each CPG can have a different μ . If not stated otherwise, all IN_{cpg}^{osc} and IN_{cpg}^{cst} share the same amplitude modulation μ_{osc} and μ_{cst} , respectively. B) Spinal network. 4 oscillators, differing in their synchronization mechanism with the environment, drive the different IN_{cpg} . $\theta_R^{st}, \theta_R^{sw}, \theta_L^{sw}$ and θ_L^{st} are used by IN_{cpg} starting at right limb stance, right limb swing, left limb stance and left limb swing respectively. IN_{cpg} and IN_{sen} action on MN follows Equation 3.2. The green arrow between Sensory and CPG Interneurons pathway highlights the fact that each CPG pathway is a model of one sensory pathway. C) Musculoskeletal system, there is one muscle corresponding to each individual motoneurons.

Where θ is the frequency of the oscillator, γ (here set to 100) controls the speed of convergence of the oscillator output x toward the shaping function $g(\theta)$, and $g(\theta)$ is the nominal function that shapes the output of the oscillator, this function is extracted from IN_{sen} states, see next paragraph.

Pattern generation In order for the stability condition of the MO to be fulfilled, the pattern of the CPG must be represented by a first order differentiable 1-periodic function. Based on our hypothesis that CPGs can be viewed as feedback predictors, this function should reproduce the typical shape of the corresponding feedback pathway, for each cycle. The typical shape is derived as follow: 1) the sensory signals are recorded from a stable walking solution, 2) each sensory signal is split into cycles using the ipsilateral limb takeoff event (for feedback pathways active during swing), or the ipsilateral limb touchdown event (for all other feedback pathways), 3) each resulting sub signal is normalized in the temporal domain, in order to obtain a set of N signals of the same length $p(\theta, i)$, $i = [1, \dots, N]$, 4) the shaping function $g(\theta)$ is then derived using a third order spline interpolation of the mean signal.

$$g[\theta] = 1/N \sum_{i=1}^N p[\theta, i] \quad (3.5)$$

CPG coupling with the environment All oscillators have the same frequency ω initially set to an estimate of the FBL gait frequency from which the feedback patterns were extracted. In order to ensure that CPGs stay synchronized with the gait phases on which they should act, a coupling has to be defined. This coupling should ensure that:

1. IN_{cpg} will always start at the beginning of the gait phases during which it acts, at the touchdown / takeoff events of left limb for IN_{cpg} acting during left stance / left swing respectively, same holds for right limb. This event is called the synchronization event.
2. IN_{cpg} will never starts a new period before the gait phases on which it acts ends.

Consequently, there should be four different oscillators driving the different IN_{cpg} , i.e. two for each limb: one that uses touchdown as synchronization event (used by IN_{cpg} acting during stance or whole cycle) and another one that uses takeoff as synchronization event (used by IN_{cpg} acting during swing), Fig. 3.2 B shows the organization of the spinal network. Each oscillator is coupled to the environment using the following frequency adaptation mechanisms implementing the two requested coupling properties:

1. If the oscillator is too slow compared to the walking frequency, the phase of the central clock is simply restarted and set to 0.0 at the synchronization event (see Fig. 3.3 A)
2. If the oscillator is going too fast compared to the walking frequency, a slowing down mechanism takes action before the expected synchronization event (see Fig. 3.3 B). It

Chapter 3. Pattern in the central nervous system

ensures that signals generated by the MOs will not start a new cycle before they should (e.g. for oscillators active during stance, before the limb touches the ground).

With both mechanisms turned on, the phase of oscillator i is defined as:

$$\dot{\theta}_i = \begin{cases} \omega & \text{if } t_i < p \cdot \frac{1}{\omega} \\ c(t_i) & \text{else} \end{cases} \quad (3.6)$$

$$\theta_i = 0 \text{ if } t_i > \frac{1}{\omega} \quad (3.7)$$

Where: θ_i is the phase of oscillator i , t_i is the time since the last synchronization event and p is the percentage of the phase at which the slowing down mechanism is turned on. $c(t)$ is a slowing down function that ensures that $\theta \leq 1.0, \forall t \in \mathbb{R}$. For the slowing down mechanism to enter in action after 90% of the period of the oscillator (i.e. $p = 0.9$), we can use the following function:

$$c(t_i) = 10\omega \cdot \exp(-10\omega t_i - \ln(10) + 9)$$

Details on how $c(t)$ is derived can be found in [56].

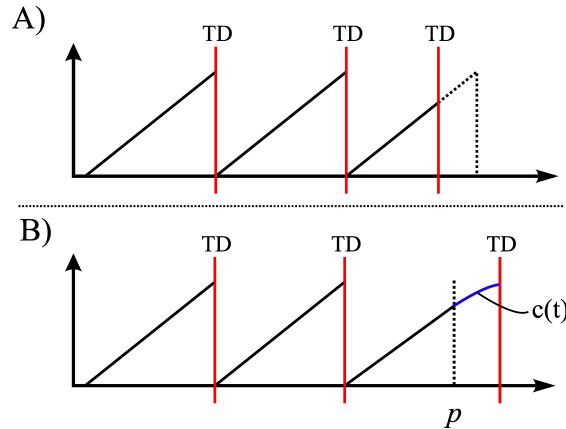


Figure 3.3 – CPG-OSC synchronization mechanism. A) If the central clock is too slow compared to the walking (i.e. the touchdown/takeoff event occurs before the oscillator has finished its period) the phase is simply reset. B) If the central clock is too fast compared to the walking, a slowing down mechanism enters in action. The mechanism enters in action at a defined percentage of the period ($p = 90\%$), ensuring that the oscillator will not finish its period before the synchronization event (SE) occurs.

Feedback sensitivity scale

For a feedback pathway i , the feedback sensitivity definition is noted $FDB_i^{sen} = 1 - \alpha_i$ and corresponds to the point at which the gait becomes unstable when 1) all other feedback pathways are kept as feedbacks (i.e. $\alpha_j = 1$ for all $j \neq i$) and 2) the feedback pathway i is combined with an IN_{cpg}^{osc} . A feedback sensitivity of 0 means that the feedback can be fully

replaced by its cognate $IN_{\text{cpg}}^{\text{osc}}$ predictor without destabilizing the stability of the generated gait.

3FBL models

In order to demonstrate the effect of feedback and CPG combinations, we created different models combining CPG and feedback components in different ways. Here we present only the 5 models exhibiting the most interesting properties in terms of speed modulation. The 5 models differ in their CPG-feedback combination vectors $\vec{\alpha}$ (see Table 3.1 for details). Contrary to what might be expected, a 3FBL model with a $IN_{\text{cpg}}^{\text{osc}}$ - IN_{sen} combination vectors of 0.5 for all muscle feedbacks pathways did not perform well in terms of speed modulation when considering global control variable acting on all CPGs. The first 4 models study the effect of a CPG addition on different group of muscles, namely the $3FBL_{\text{ankle}}^{\text{osc}}$, $3FBL_{\text{hipA}}^{\text{osc}}$, $3FBL_{\text{hipB}}^{\text{osc}}$ and $3FBL_{\text{biArt}}^{\text{osc}}$. The fifth model was designed to study the properties of gait with minimal feedback activity. That model was obtained as follows: IN_{cpg} are added starting from pathways acting on distal muscles. Pathways acting on distal muscles use CPG-CST models ($IN_{\text{cpg}}^{\text{cst}}$) and pathways acting on proximal muscles use CPG-OSC models (IN_{cpg}), using the lowest possible α (in the $[0, 1]$ range). This methodology was chosen, with the aim of finding a gait with the minimal number of feedbacks. Note that other CPG-FDB combinations might be found using different methodologies. The $3FBL_{\text{fdb}}^{\text{min}}$ was generated using this methodology. The resulting model can generate stable walking with a global feedback activity reduced from 100% to 45% (the feedback activity is defined as $\frac{\sum_i(\alpha_i)}{N}$, where N is the number of feedbacks), see Section 3.3.1 for more details.

3FBL modulation: model of supraspinal influences

We hypothesize that the use of a CPG component would facilitate speed control. Indeed, it is known that simple supraspinal signals are sufficient to modulate gait frequency in lower vertebrates and in mammals, as demonstrated by experiments on decerebrated cat walking on a treadmill, where speed changes and gait transitions can be elicited by varying the stimulation of the mesencephalic locomotor region. Therefore, we modeled two different kinds of descending pathways (see Fig. 3.2):

- Frequency : ω
Controls the frequency of the CPG-OSC (ω value in Equation 3.6). This variable affects all oscillators as they share the same frequency.
- Activity modulation : μ
Modulates the CPG activity of both CPG-OSC and CPG-CST. Effectively, the CPG output $X_{\text{in}_{\text{cpg}}}$ becomes $\mu \cdot X_{\text{in}_{\text{cpg}}}$, with $\mu > 0$ controlling the activity of the CPG.

Chapter 3. Pattern in the central nervous system

Table 3.1 – Description of the CPG-FDB combination map for the 5 different 3FBL models. Each row shows for a given feedback pathway, the type of CPG used (Osc stands for IN_{cpg}^{osc} and Cst for IN_{cpg}^{cst}) and the level of CPG-FDB (i.e. α) for the 5 different 3FBL models. The four first columns shows the most interesting 3FBL models in terms of speed control: $3FBL_{ankle}^{osc}$, with CPGs acting on distal extensor muscles, $3FBL_{hipA}^{osc}$ and $3FBL_{hipB}^{osc}$, with CPGs acting on HIP muscles and $3FBL_{biart}^{osc}$, with CPGs acting on the HAM bi-articular muscles. The last column shows the combination vector for $3FBL_{fdb}^{min}$ (i.e. the minimum feedback model). Note that the $3FBL_{fdb}^{min}$ also replaces the “VAS←GCF STend” and “HF←TLF SW” pathways by a CPG-CST predictor. Note that only the pathways related to muscle feedbacks are shown. Even though a full replacement of the “VAS←GCF STend” pathway by CPG-CST is possible without affecting the produced gait, the effect of a modulation produces no significant effect on the resulting gait (data not shown). This pathway is thus not used, except for the $3FBL_{fdb}^{min}$. The KNEE overextension prevention pathway (“VAS←KNEE OPF”) and the pathways related to stability (i.e. “HF←GSIF ST”, “HAM←GSIF ST”, “GLU←GSIF ST” and “HF←TLF SW”) are not used, as their role as feedback is evident. Moreover, even though a combination with CPG generates stable walking, walking becomes unstable even with very small modulation of the CPG parameters (data not shown).

		$3FBL_{ankle}^{osc}$		$3FBL_{biArt}^{osc}$		$3FBL_{hipA}^{osc}$		$3FBL_{hipB}^{osc}$		$3FBL_{fdb}^{min}$	
		type	$1 - \alpha$	type	$1 - \alpha$	type	$1 - \alpha$	type	$1 - \alpha$	type	$1 - \alpha$
ANKLE	SOL←SOL MFF, ST	Osc	0.5								
	TA←SOL MFF, ST									Cst	0.9
	TA←TA MLF CY									Cst	0.9
KNEE	GAS←GAS MFF, ST	Osc	0.5							Cst	0.9
	VAS←VAS MFF, ST										
	HAM←HAM MFF, SW			Osc	0.5	Osc	0.5	Osc	0.5	Osc	1.0
HIP	HF←HF MLF SW					Osc	0.5	Osc	0.5	Osc	1.0
	GLU←GLU MFF, SW					Osc	0.5			Osc	1.0
	HF←HAM MLF SW					Osc	0.5			Osc	0.0

Results

The results are separated in two parts. In the first part (section 3.3.1), we present an analysis of the different feedback pathways of one specific solution of the FBL model. Each feedback pathway is analyzed separately. For each of them the effect of a combination with their feedforward predictor is studied. In the second part (section 3.3.2), we analyze the model of supraspinal influences in terms of speed control.

Feedback and feedforward study

IN_{sen} signal analysis and prediction

Since the produced gaits are all symmetric and stable (i.e. close to perfectly periodic), the feedback signals should be very similar between cycles. Consequently, the quality of the feedback prediction should be very high (i.e. IN_{cpg}^{osc} should be very close to IN_{sen}). In order to study the quality of the prediction, we generated the IN_{cpg}^{osc} (as described in Section 3.2) and ran them in a passive mode (no action on muscles, i.e. no link between IN_{cpg}^{osc} and MN). Fig. 3.4 shows the actual IN_{sen} signals (dotted lines) and the reproduced signal (thick lines) over one step, for the worst gait (in terms of feedback prediction quality, i.e. similarity between IN_{sen} and IN_{cpg}^{osc}). We can see that the prediction is very close to the feedback signals; the lowest correlation between the original and the reproduced signals is of 0.98. Differences are noted as shifts and amplitude differences, and are due to small asymmetries in the gait. It is interesting to note that, even if those asymmetries are visible at the level of the feedbacks, their effects on the gait are very small. However, even small asymmetries between the IN_{sen} and their predictors (IN_{cpg}^{osc}) can create instabilities which makes their replacement difficult.

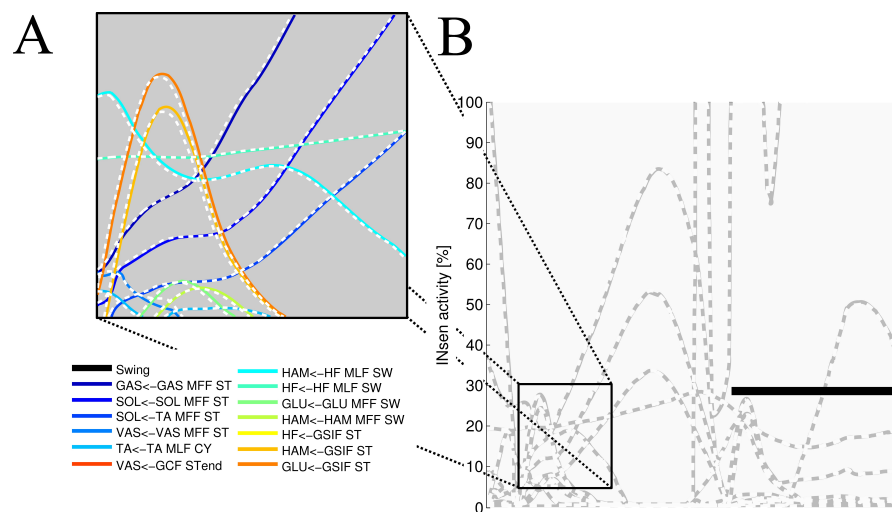


Figure 3.4 – Actual IN_{sen} signals (dotted lines) and the reproduced signals (thick lines) for the the worst gait, in terms of IN_{sen} - IN_{cpg} similarity. A) zoom in a subpart of the IN_{sen} activity. We clearly see that the errors between the reproduced signal and the real one are very small. B) IN_{sen} activity over one cycle. Note that we do not reproduce the “HF←TLF SW” and the “VAS←KNEE OPF” IN_{sen} , because their roles as feedback is clear: the first gives stability to the gait by generating larger steps when the body leans forward, and the second because it prevents knee overextension.

Feedbacks replacement

In order to study the possibility of replacing the feedbacks (IN_{sen}) by their full predictors (IN_{cpg}^{osc}), we ran a systematic search in which we increase $\beta = 1 - \alpha$ (i.e. the proportion of IN_{cpg}^{osc}) from 0 to 1.0 using the combination strategy shown in Fig. 3.1. The systematic search is done for each feedback pathway i , where β_i is increased from 0 to 1 in steps of 0.1. All the others pathways are kept as feedbacks (i.e. $\beta_j = 0, j \neq i$).

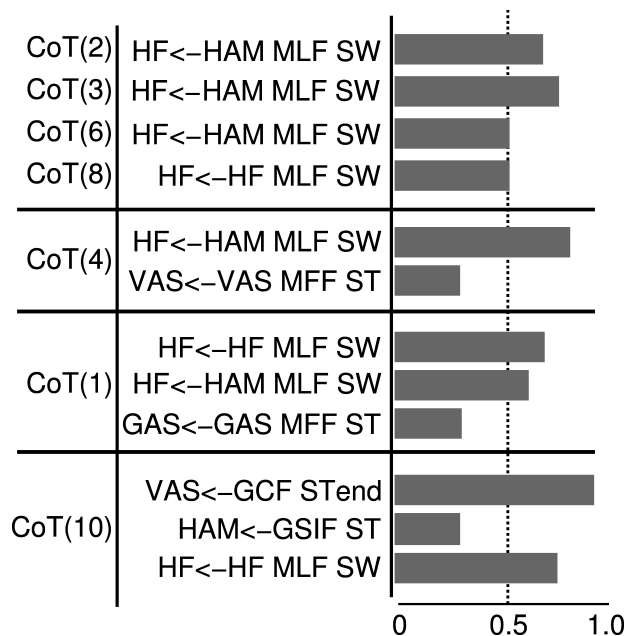
Table 3.2 shows, for each gait, the number of feedback pathways that could not be fully replaced (i.e. the feedback pathways that have a $FDB_i^{sen} \neq 0$). Table 3.3 shows the feedback sensitivity of the 7 best gaits, in terms of the number of feedback pathways that can be replaced, i.e. in terms of feedback replacement capacity (see section 3.2.1 for details on the feedback sensitivity scale). It is interesting to note that feedback pathways acting on ANKLE muscles have a zero feedback sensitivity value which means that they can be fully replaced by a IN_{cpg}^{osc} model without loss of stability. The muscle length feedback pathway from HAM bi-articular muscle acting on the HF muscle always shows a high sensitivity (for gaits showing meaningful CoT), highlighting its importance for the stability of the gait. Even though feedback related to trunk stability (stability sensor, type 4) are crucial to ensure stable walking and to enhance gait resistance to perturbations, they are not part of sensitive feedbacks. However, a gait with only one trunk stability feedback replaced is stable only in steady state walking; as soon as small perturbations (pushes and/or change in slope) are exerted on the model, the gait becomes unstable and falls.

Based on these results, we focus on the second gait in terms of CoT consumption (i.e. first row in Table 3.2) for further analysis as it shows a good correlation with human data (see Figure 2.3, a CoT in the range of human CoT (see Figure 2.4) and a low feedback sensitivity (see Table 3.2).

Table 3.2 – Summary of solution rank in terms of CoT and number of IN_{sen} that could not be replaced by a IN_{cpg} model while keeping other pathways purely feedback (i.e. $\alpha = 1$). The first column gives the solution rank in terms of CoT (1 corresponds to minimal CoT), see Figure 2.4 for the actual CoT values.

CoT	IN_{cpg}^{osc}	IN_{cpg}^{cst}
2	1/13	7/13
3	1/13	7/13
6	1/13	7/13
8	1/13	8/13
4	2/13	7/13
1	3/13	8/13
10	3/13	8/13
9	5/13	7/13
5	5/13	8/13
7	6/13	6/13

Table 3.3 – Feedback sensitivity (see Section 3.2.1) for the best 7 solutions (in terms of IN_{sen} replacement capacity, i.e. percentage of IN_{sen} that can not be replaced by a CPG-OSC model). The first column shows the solution, ranked in term of cost of transport (CoT). The second column gives the name of the feedback pathway. The third column shows the feedback sensitivity (FDB^{sen}).



Feedbacks combination

Fig. 3.5 A shows the effect on the generated gait (in terms of CoT, stride length and speed) of an increase in the proportion of feedforward versus feedback signal for one specific pathway while maintaining all the other pathways purely feedback driven (this was implemented by decreasing the feedback proportion by steps of 0.1 of one component of the $\vec{\alpha}$ vector at a time while keeping all other components at 1). Fig. 3.5 A left and right panels show the combination analysis of feedbacks with IN_{cpg}^{cst} and IN_{cpg}^{osc} respectively. As expected, the replacement of IN_{sen} by a constant model (i.e. IN_{cpg}^{cst}) has more effect on the gait characteristics, compared to the replacement of the IN_{sen} by an oscillatory model (i.e. IN_{cpg}^{osc}). This confirms that the latter captures more information from the IN_{sen} (i.e. the shape, timing and amplitude).

Despite the higher sensitivity of the IN_{cpg}^{cst} - IN_{sen} combination (i.e. percentage of IN_{sen} that could not be replaced by a constant model (IN_{cpg}^{cst}), several interesting effects of the IN_{cpg}^{cst} - IN_{sen} combination are noted, as shown in Fig. 3.5. We observe that, for the “SOL←-TA MFE, ST” and the “HF←-HF MLF, SW” feedbacks, changes in α (i.e. proportion of IN_{cpg}^{cst} versus IN_{sen}) produce large variations in speed and stride length. In the case of “SOL←-TA MFE, ST”, there is a linear relationship between the IN_{cpg}^{cst} proportion level and both the speed and the stride length. A decrease in stride length and speed is observed with the increase in IN_{cpg}^{cst} level, as shown in Fig. 3.5 B.

3FBL_{fdb}^{min}: Minimal Feedbacks gait

We have shown that all feedbacks can be combined with their CPG predictors, and that interesting properties, such as speed and step length variation, could be achieved by playing with the CPG-FDB combination level when using CPG-CST predictors. But are all those feedback really needed to produce stable locomotion? Here the question of the minimal number of feedback needed to produce stable walking is addressed. The 3FBL_{fdb}^{min} model is able to produce stable walking with a global feedback activity reduced from 100% to 45%. More specifically 3 over 4 proximal muscle feedbacks are fully replaced by IN_{cpg}^{osc} (i.e. $\alpha = 1.0$) while 3 over 5 distal muscle feedbacks can be replaced by IN_{cpg}^{cst} with $\alpha = 0.9$. The fact that distal feedbacks cannot be fully replaced could be explained by the limitation of the Hill muscle model 5.5.1. Its average speed on flat ground is 1.35[m/s] (3% increase compared to the underlying FBL model). When comparing the joint angles, torques and muscles activities between the two models, almost no differences can be observed at the HIP joint (see Fig. 3.6C). However, differences are noted at the level of the ANKLE joint (see Fig. 3.6A). Indeed, all muscles activities acting on the ANKLE joints show different muscle activation patterns than the corresponding FBL model. Interestingly, the differences observed in muscles activities do not produce important changes in the shape of the torque and angle patterns of the ANKLE joint. Nevertheless, the increase in extensor muscles activities produces a steeper increase in joint torque during stance. This increase in torques explains the observed increased ANKLE angle at takeoff. In turn, this increase in ANKLE angle also increases the duration of the stance phase, thereby explaining the observed shift of the KNEE peak angle in early swing.

The SOL muscle shows a different muscle activation pattern, while the “SOL—SOL MFE, ST” pathway, the only one acting on it, has not been replaced by a CPG (i.e. kept as pure feedback, $\alpha = 1$). Since the 3FBL_{fdb}^{min}'s feedback / CPG combination map does not permit a combination of CPG-OSC with feedback for this specific pathway (even with $\alpha = 0.95$, i.e. pathway kept almost purely feedback), this change in activity is necessary to ensure a stable walking gait. This highlights the important stabilizing role that muscle feedbacks play in locomotion. It is important to note that, while in a stable walking regime reducing as much as possible the proportion of feedback signals for specific pathways does not significantly affect the generated gait, the replacement of feedbacks considerably reduce the gait robustness to perturbations. Indeed, recovery after 0.25[s] pushes is reduced from 40[N] to 28[N] compared to the original gait.

This highlights the importance of feedback to adapt to perturbations. Even though the 3FBL_{fdb}^{min} is valuable, as it shows that a large part of feedbacks can be removed from the FBL model, while a stable walking gait is still produced, it is not surprising that its modulation is almost impossible. Indeed, since a large part of the feedbacks are removed, even small modulations of CPG parameters render the gait unstable. This instability could potentially be reduced by self stabilization mechanism acting at the level of the muscles, see Section 3.4.2.

3FBL Models: Systematic study of supraspinal signal modulation and their effects on gait

Using the model of supraspinal influences presented in section 3.2.3, we ran a systematic search on the effect of CPG amplitude and frequency modulation on the 4 different 3FBL models presented in the previous section namely $3FBL_{\text{ankle}}^{\text{osc}}$, $3FBL_{\text{hipA}}^{\text{osc}}$, $3FBL_{\text{hipB}}^{\text{osc}}$ and $3FBL_{\text{biArt}}^{\text{osc}}$, using ω and μ_{osc} as parameters (the parameters are split into 11 values across a given range ([0.2, 2.5] for ω and [0.1, 4.0] for μ_{osc}).

The systematic search on the 4 chosen models acting on different group of muscles (see Fig. 3.7 A) indicates that all the models are stable in a large range of amplitudes and frequencies, except the $3FBL_{\text{hipA}}^{\text{osc}}$, that shows a more restricted region of stability. This can be due to the fact that the $3FBL_{\text{hipA}}^{\text{osc}}$ has more oscillators than the three other models.

Note that the restricted region of stability does not imply a restricted range of speed. Indeed, small variations in ω (while μ_{osc} remains fixed) induces noticeable change in speed in this model; an increase in speed is observed with an increase in frequency. In other words, changing the frequency of the $3FBL_{\text{hipA}}^{\text{osc}}$ is sufficient to entrain the whole musculoskeletal system. Interestingly, this model - which is the only model with a high number of CPGs acting on proximal muscles - is the only one that shows an increase in speed when increasing the CPG network frequency. This suggest that CPGs acting on proximal muscles are required to produce a frequency-driven entrainment of the system.

Interestingly, the $3FBL_{\text{hipB}}^{\text{osc}}$ - which has only two CPGs acting on proximal muscles, compared to four in the case of the $3FBL_{\text{hipA}}^{\text{osc}}$ - shows almost no change in speed when the frequency ω is modulated (while μ_{osc} is fixed). Possibly, the frequency modulation of only two CPGs at the HIP level is not sufficient to produce a frequency-driven entrainment of the system. However, increasing μ_{osc} leads to a significant decrease in gait velocity. This decrease in speed with increasing amplitude is likely an effect of the “HF←HF MLE, SW”, as this effect is not observed in the $3FBL_{\text{biArt}}^{\text{osc}}$, which differs from the $3FBL_{\text{hipB}}^{\text{osc}}$ model only by the absence of a CPG component for this feedback pathway. Indeed, the “HF←HF MLE, SW” is a negative feedback, and thus increasing the amplitude of its associated CPG (i.e μ_{osc}) will reduce the activity of the HF muscle, reducing the HIP flexion velocity and hence increasing the duration of the swing, which in turn decreases the gait speed (as the stride length does not change significantly).

Surprisingly, as little as one oscillator is sufficient to allow significant changes in speed (shown by the $3FBL_{\text{biArt}}^{\text{osc}}$, see Fig. 3.7 B). The changes in speed are mainly induced by a modulation of the amplitude μ_{osc} , but with an opposite effect compared to the $3FBL_{\text{hipB}}^{\text{osc}}$ (i.e. an increase in μ_{osc} leads to an increase in the gait velocity). However, since this effect is accompanied with a shortening of the stride length, this model is unlikely to be relevant; in humans, an increase in speed is usually concomitant to an increase in stride length [141].

Note that small changes in speed are still possible with a modulation of the frequency ω , both in the case of the $3FBL_{\text{biArt}}^{\text{osc}}$ and $3FBL_{\text{hipB}}^{\text{osc}}$, but to a lesser extent than the $3FBL_{\text{hipA}}^{\text{osc}}$. This is expected, as a lower number of CPG - acting on proximal muscles - will have a lower frequency-driven entrainment capacity.

Chapter 3. Pattern in the central nervous system

Concerning the pathways acting on distal muscles (i.e. the $3FBL_{\text{ankle}}^{\text{osc}}$ model), large changes in speed and step length are observed. However, contrary to what might be expected, an increase in frequency produces a decrease in speed. This is an artifact only possible because of the synchronization mechanism used to ensure the lock-in of the CPG with the mechanical system (see Section 3.2.1). This effect is thus mainly related to a change in the duration of the burst of the feedforward signal (induced by the change in frequency), rather than to an entrainment between the two systems (i.e. CPG and musculoskeletal system). In other words, the observed gait modulations are due to a modulation of the shape of the signal (change in amplitude and/or duration).

Importantly, increases in speed induced by supraspinal influences on the different 3FBL models do not have the same effect on the gait characteristics (i.e. stride length and step duration). Modulation of the $3FBL_{\text{hipA}}^{\text{osc}}$ or $3FBL_{\text{hipB}}^{\text{osc}}$ parameters induce very little change in stride length (< 5%). This is explained by the fact those CPGs are active only during swing and modulate the swing speed, but do not impact the swing length (and hence the stride length). Conversely, an increase in speed in the $3FBL_{\text{ankle}}^{\text{osc}}$ induces a significant increase in stride length, as increasing the propulsive force will increase the swing length and thereby the stride length. As previously mentioned, the opposite effect is observed for the $3FBL_{\text{biArt}}^{\text{osc}}$ (i.e. a decrease in stride length).

In real humans, it is known that, up to a certain point, increases in speed are usually accomplished by a decrease in step duration (i.e. increase in frequency), as well as by an increase in stride length [141]. As expected, the 4 models exhibit a decrease in step duration with the increase in speed. Interestingly, only a modulation occurring on distal muscles also shows an increase in stride length, suggesting the propulsive force modulation as a means of velocity control. Taken together, these results suggest two ways of controlling speeds: 1) frequency modulation of CPGs acting on proximal muscles, 2) modulation of burst duration, amplitude and timing of CPGs acting on distal muscles.

Discussion

A dynamical system model of CPGs playing the role of feedback predictors offers an easy and intuitive way of studying the relative importance of the different feedback pathways, and allows to highlight several interesting aspects regarding locomotion control.

CPG modulations on both proximal and distal muscles allow speed control

Mixing a constant predictor (CPG-CST) and feedbacks for as little as one pathway already enables speed and step length control. Increasing the level of CPG-CST for one specific pathway results in a flattening of the original feedback signal. Flattening the “SOL←SOL MFE, ST” feedback (i.e. the SOL positive muscle force feedback, active during stance) induces a clear decrease in both the gait speed and stride length, while flattening the “HF←HF MLE, SW” feedback (i.e. the HF negative muscle length feedback, active during swing) induces a clear

decrease in the gait speed, but has little effect on the stride length (see Fig. 3.5 B). Those two observations confirm the intuition that speed changes would arise differently, depending on whether the control is applied during stance or swing. While speed control arising from stance control would more likely use extensor distal muscles, a speed control arising from swing control would more likely use proximal muscles. On the one hand, to be effective, a control acting during the stance should affect the propulsive force, which is mainly controlled by extensor muscles acting on the ankle joint (i.e. SOL and GAS muscles). It is thus not surprising that a modulation of feedback pathways acting on ankle extensor muscles during the stance affects the speed of locomotion (see Fig. 3.5 A). The effect on stride length is understood as the result of the modulation of the propulsive force: decreasing the propulsive force will decrease the swing length and thereby decrease the stride length. On the other hand, for the control acting during the swing at the level of the HIP flexors, the decrease in speed is not accompanied with any clear reduction in stride length (see Fig. 3.5 B green), meaning that it is the speed of the swing, but not its amplitude that induced the change in speed.

Similarly, the 3FBL models with CPG components acting on different groups of muscles confirm that speed control can arise from distal muscles extensors during the stance phase, and proximal muscles during the swing phase. We show that changes in speed, induced by a modulation of feedforward signals acting at the level of the ankle muscles, is unlikely due to a modulation of the frequency of the CPG network (see section 3.3.2), but rather induced by changes in burst duration and timing, which could be potentially triggered by upper brain structures [119]. Conversely, the results from a control acting during the swing at the level of proximal muscles shows that they could, indeed, be due to a modulation of the frequency of a CPG network. This proximo-distal gradient in joint neuromechanical control has already been observed experimentally on perturbation experiment conducted on the helmeted guinea fowl *Numida meleagris* by M.Daley [39].

When the CPG activity is modulated, the rest of the system (i.e. the remaining feedbacks) should adapt to the new conditions. Therefore, it is the combined effects of both CPGs and feedbacks that changes the gait properties (such as speed, step length, step duration). It has already been demonstrated that feedbacks acting at the level of the ankle produce such speed-adaptive behaviors [129]. Here we show that this is true regardless of whether the control is applied at the level of proximal or distal muscles.

The proposed spinal architecture was able to generate speed transition ranging from 0.75 to 1.35 [m/s]. While this can seem relatively small compared to the controller proposed in [191], in which speed transition ranging from 0.8 to 1.6 [m/s] were obtained, the strategy proposed in this article has the advantage that changes in speed can be obtained without changing the reflex parameters. Furthermore, as the proportion of feedbacks versus CPGs (i.e. α vector) of the 3FBL models were hand tuned, larger range of speed could be obtained through optimization. Finally, co-optimizing the feedback and feedforward components could also increase the range of speed. Indeed, as already stated, the 3FBL can be viewed as a system made of two components: a feedforward component and a corrective term, accounting

for the differences between the feedback and the feedforward pathways (see Section 3.3.1). In this context, the FBL model is a 3FBL model where the feedforward component is zero: the feedback parameters of the FBL are thus optimized for a model without any feedforward component. In this regard, since the 3FBL models were designed on top of an existing FBL model, the feedback parameters are not optimized to work with a non-zero feedforward component. This could also explain the low robustness of the $3FBL_{fdb}^{\min}$ model. Furthermore, in a biological point of view, it is obvious that the feedforward components should evolve together with the feedback components. Consequently, in the future, we will investigate the co-evolution of the feedforward and feedback components.

Stable locomotion is produced even with a significant decrease in feedback activity

The $3FBL_{fdb}^{\min}$ model shows that stable locomotion can be produced despite a significant decrease in feedback activity. Indeed, stable walking is produced even with a 65% percent reduction in muscle feedback activity. As expected, this large decrease in feedback activity reduces the robustness of the gait to external perturbations (pushes and slope variation), and also considerably reduces the possibilities to control the gait (change in speed and stride length are not possible). This shows that some pathways are more important than others regarding their role as gait stabilizers, which can be beneficial to both perturbation resistance and control of the gait. This high sensitivity is not in agreement with recent experimental evidence of intrinsic stabilization mechanism in the muscles themselves (sometimes referred as preflexes [212]) that act faster than reflexes but together with them). The higher instability of the $3FBL_{fdb}^{\min}$ could suggest that the muscle model used does not capture this self stabilization mechanism, see Section for a discussion on possible alternative to Hill muscle model 5.5.1.

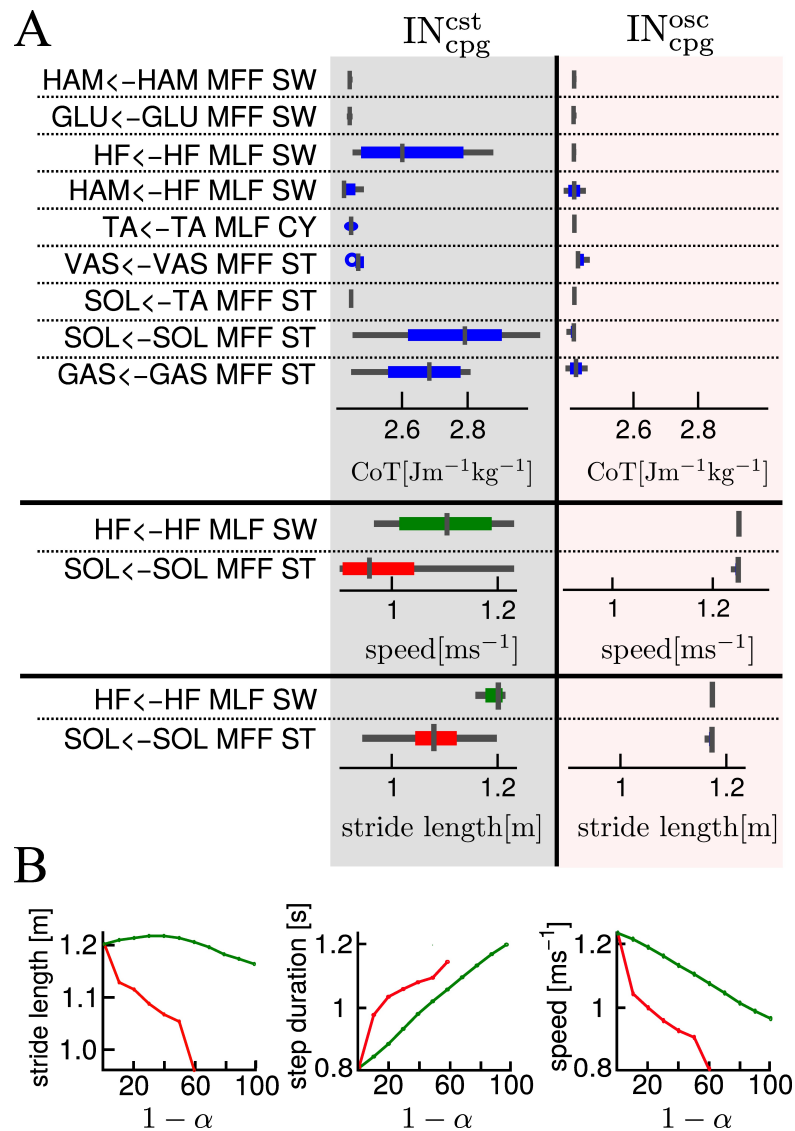


Figure 3.5 – A) One by one feedback and feedforward combination effects on cost of transport, stride length and speed, for gait number 1. The first column gives the name of the feedback pathway considered. The second and third columns show for an $IN_{sen} - IN_{cpg}^{cst}$ and an $IN_{sen} - IN_{cpg}^{osc}$ respectively, a box plot of the variation of a measured variable when α varies from 1 to 0. In the first part of the table the considered variable is the cost of transport (CoT), in the second part, the speed and in the third part, the stride length. We show the speed and stride length box plot only for the two most interesting pathways in terms of feedback and feedforward combination effect on CoT. The box plot read as follow: the middle line is the median, the colored line represents 99% of the data assuming the data are normally distributed and the gray horizontal bar shows the range of the measured variable. A very thin box plot (no colored line visible) means that the variation of α had no effect on the considered variable, feedback pathway and IN_{cpg} model. As expected the $IN_{sen} - IN_{cpg}$ combination for any α in the $[0, 1]$ interval has very little effect on the CoT. B) Relationship between IN_{cpg}^{cst} proportion and gait variables, for two selected feedbacks (red, “SOL \leftarrow TA MFF, ST” and green, “GAS \leftarrow GAS MFF, ST”). Left panel: relationship between stride length and $1 - \alpha$ (i.e. the IN_{cpg} proportion), middle panel: relationship between step duration and $1 - \alpha$ and right panel: relationship between speed and $1 - \alpha$.

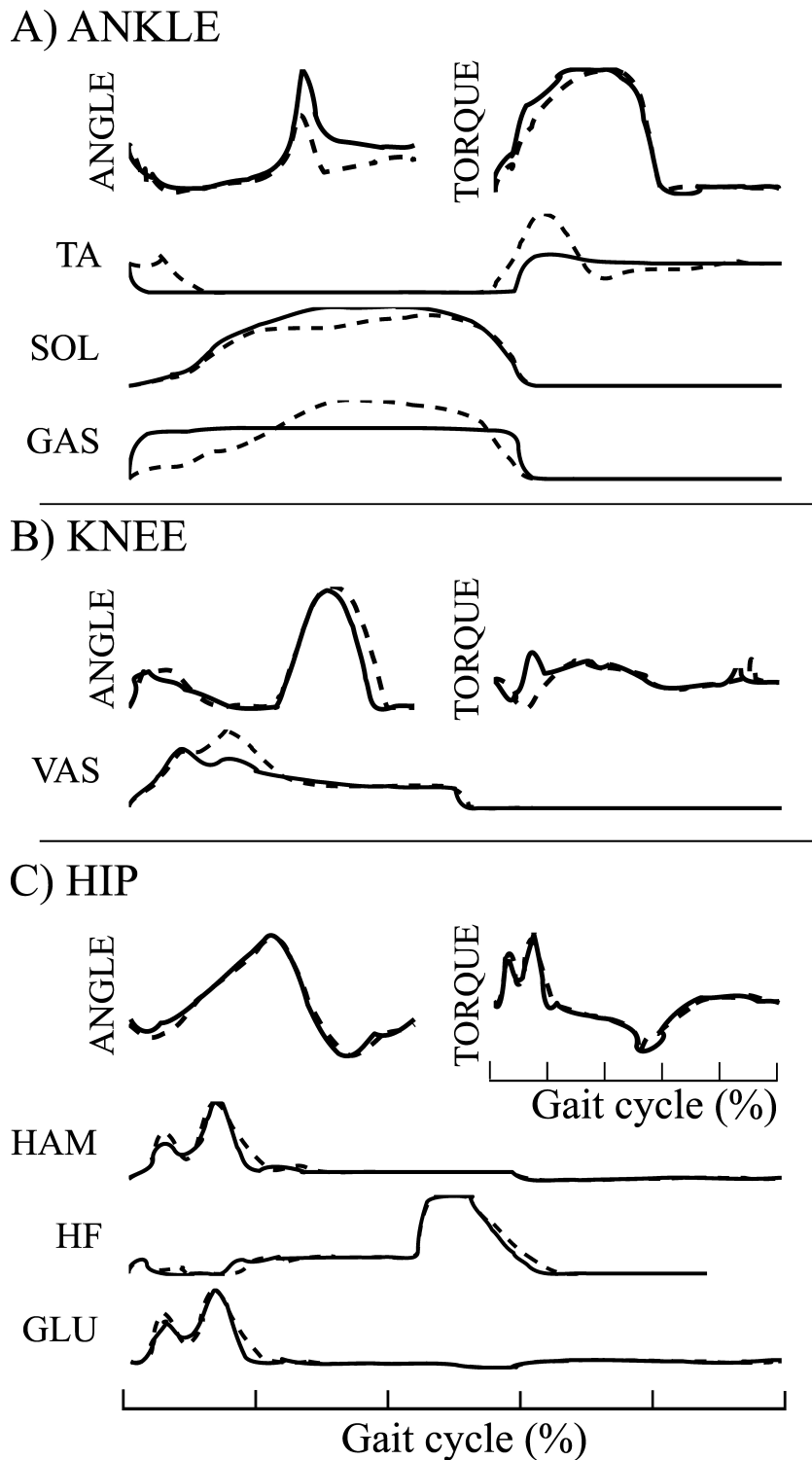


Figure 3.6 – Comparison of average joint angles, joint torques and muscles activation pattern between the $3FBL_{fdb}^{min}$ (black line) and the FBL models (dashed line) for solution 1. A) ANKLE angle, torque and associated muscles activation level, B) KNEE angle, torque and associated muscles activation level, and C) HIP angle, torque and associated muscles activation level.

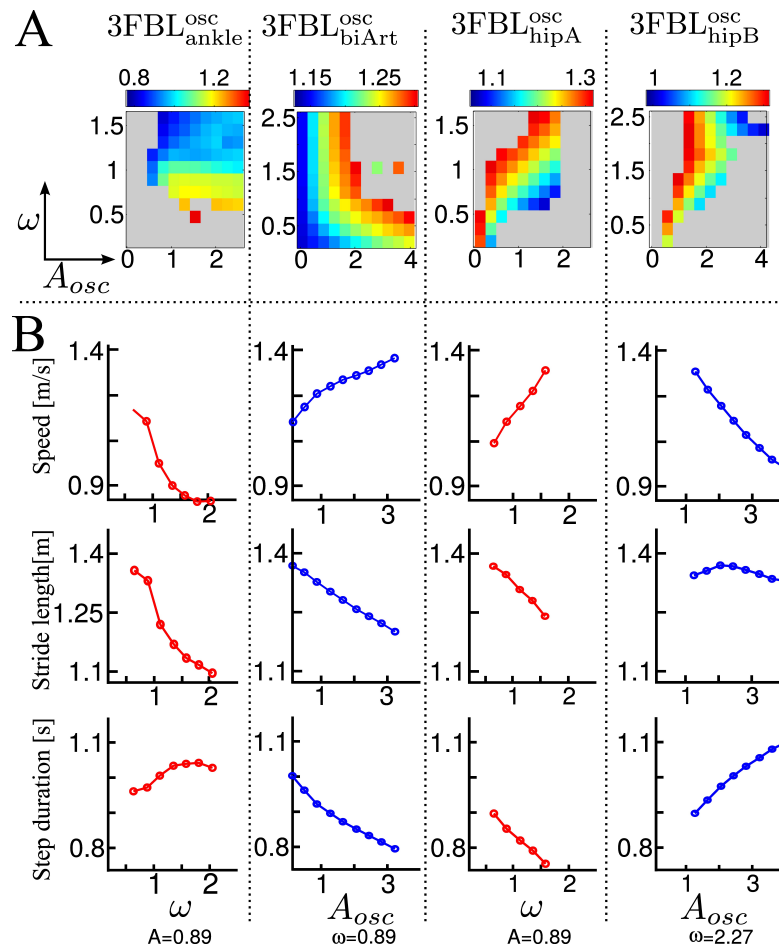


Figure 3.7 – Systematic search study of CPG parameters (supraspinal influences) for the different 3FBL models. The systematic search is done for two parameters: ω , the frequency of the CPG network and μ_{osc} , the CPG-OSC amplitude modulation. Each column corresponds to a given 3FBL model (name at the top, see Table 3.1). A) Heat map of the systematic search. The color indicates the speed of the gait for a given (μ_{osc}, ω) pair (gray color means that the gaits was unstable or asymmetric). B) Highest variation in speed possible while maintaining one of the parameters constant (based on the heat map). A red/blue line means that (μ_{osc}/ω) is kept constant, respectively. The value of the constant parameter is indicated at the bottom. The first row shows the speed, the second the stride length, and the third the step duration. Note that the 3FBL_{fdb}^{min} is not shown as its modulation is almost not possible.

On symbiotic control of exoskeleton **Part II**

A widely accepted practice in gait rehabilitation by physiotherapists and robotic devices entails active assistance of lower body movement [32, 100]. This yields several positive effects, such as soft tissue stiffness reduction, increase in muscle strength, and increase in brain plasticity by providing somatosensory stimulation that correlates with motor output [231, 160, 176]. As robotic devices increase in popularity for both gait training and gait assistance, interaction control (i.e. shared control) between the orthese/exoskeleton and the human becomes important for recovery, understanding user intention, and adaptation to outside environments. Some researchers have shown that lack of interaction control can reduce the recovery capacity, such as when the assistance encourages slacking (slacking hypothesis [180]). To address the negative consequences of the slacking hypothesis, researchers have developed a new class of controllers to provide "assistance-as-needed", such as strategies based on impedance modulation [194, 14] - helping the subject only when away from a reference pattern (kinematic in most cases) - or proportional myoelectric control [179, 68, 70, 94], where the control output is directly proportional to the magnitude of surface electromyography (EMG) signals [94]. One advantage of proportional myoelectric controllers is that they do not require a reference, as their control signals are directly derived from muscle activation patterns. This type of interaction control may be robust to environmental changes and thus suitable for wearable devices. Myoelectric controller also promotes neural plasticity, as device wearers can actively initiate and modulate the device's actions. However this method relies on clean and reliable EMG signals from existing and functional muscles, which is often difficult to obtain and may limit their application for certain subject groups.

The first part of the thesis was devoted to the bio-inspired modeling of human locomotor system. This was done with one concrete and practical objective : using this knowledge to create a paradigm shift and build better "assistance-as-needed" controllers for lower-limb orthoses and exoskeletons. Specifically, we aimed at designing biomimetic walking controllers for wearable orthoses and exoskeleton that assist altered and/or pathological gaits.

To reach this goal, a deeper understanding of the complex dynamics that involves both the biomechanical (i.e. body-environment dynamics, musculo-skeletal structure) and the neuro-physiological (i.e. muscles, sensors, neural networks) level is required. Therefore the controller should ideally not only have a good dynamics fidelity, but also emulate the properties of the neuro-physiological components (e.g. muscles, sensors, neural networks). Our proposed control approach utilizes models of human muscles and tendons in order to generate motion that is compliant with both the user's abilities and natural walking dynamics. The hypothesis is that the functional biomimetics will promote active recruitment of the user's own neuromuscular system.

Building on the bio-inspired NMM model presented in the first part of the thesis, we propose here a novel controller, referred to as neuromuscular controller (NMC), that has the capacity to work in parallel with the remaining subject's locomotor function, without impeding its function and while only using few sensory inputs. The novelty of the control paradigm is to base the controller on functional models of dynamic elements in the human leg (i.e. coming from the NMM) rather than observed properties of human gait, such as libraries of desired

joint trajectories. This offers several advantages compared to other approaches:

- **Robustness & adaptability:** With no predetermined pattern, walking emerges as a result of the interaction of the body with the environment. A consequence is that the exact same controller (with same parameters) can be used under a variety of conditions, such as different speeds and different terrains [59].
- **Modularity:** As a consequence of the use of a physiologically realistic controller framework, the structure of the model (with use of local feedback/feedforward control) enables ease of control and assistance of specific components of the walking gait. This can be either joint-based (e.g. ankle controller to assist push-off, or hip controller to assist a subject with weak hip function) or muscle-based (e.g. assist only ankle extensors, or assist only mono-articular muscles components).
- **Simple sensors:** Due to the dynamics of the muscle models, modules only need ground contact detectors and joint angles to reproduce walking. The hip modules also require trunk angle relative to gravity, which can be viewed as a simplified representation of the vestibular system.

In the first part of the thesis, we have demonstrated that the reflex-based NMM model was sufficient to recapitulate important properties of the human locomotion, while a CPG component could allow locomotion modulation. With the goal of developing exoskeletons for rehabilitation purposes of partially SCI subjects, we hypothesized that the CPG component of our NMM model would be accounted for by the subject's remaining proximal functions, while the lost distal functions should be partially provided by the reflexes component, in a subject-specific manner. For this reason, the NMC implementation presented herein is solely based on the reflex component of the NMM. However, one should bear in mind that a CPG component could be easily added on top of the reflex component in the design of MNC controllers for complete SCI subjects.

To this aim, we created a library comprising both reflex and CPG control modules that can be combined to generate different types of assistive controllers. The library permits controller designs, in a drag-and-drop fashion with Simulink (Mathworks, Natick, MA, USA). The Simulink models is available to researchers on gitlab¹. More details are available in the Appendix 1.1. We present here several applications of our NMC controller. Specifically, in Chapter 4, we perform a proof-of concept validation of the implementation of such NMC controller on an ankle orthese (Achilles), and evaluate its performances on healthy subjects. Then, we review the design constraints required in order to translate our controller to ortheses and exoskeletons dedicated to SCI subjects (Chapter 5). Finally, in Chapter 6, we present several applications of our MNC for the rehabilitation therapies of SCI subjects using the following exoskeletons developed by the University of Twente: Achilles and the Lower-extremity Powered ExoSkeleton II (LOPES II), and two Symbitron prototypes: wearable exoskeleton 1 and 2 (WE1 and WE2).

¹https://gitlab.com/symbitron_simulink_nmc

4 NMC concept validation

Introduction

Reproducing the dynamics of human locomotion does not imply that the neuro-physiological structure of the extended model is valid, but demonstrates that it would be sufficient to produce the desired dynamics. This dynamic fidelity makes the models good candidates for the design of controllers for robotic devices, where the robustness and flexibility of this approach have been successfully demonstrated in the control of a prosthetic ankle device [62]. The bio-inspired aspects of the controller enabled amputee subjects wearing the device to walk on different terrains (e.g. flat ground, ramp ascent / descent, stairs) in a manner comparable to healthy subjects, without the need for explicit terrain sensing [62]. These results demonstrated the potential of NMM in the controller design of lower limbs rehabilitation devices. Indeed the flexibility and robustness of the controller implies compliance with both healthy subjects and subjects with remaining function.

In this Chapter, we demonstrate the first example, to our knowledge, of the application of this principle for the control of orthotic devices. We tested our control paradigm by implementing the ankle module on a powered ankle exoskeleton (Achilles) and investigated the effects of the controller on the gait of healthy subjects. We expected that the NMC would not adversely affect walking mechanics. Instead, we anticipated less plantarflexor activity around push-off, lower joint power at the ankle, and less energetic cost overall.

Specifically, we present (i) an ankle reflex controller for the Achilles exoskeleton derived from our Simulink library, and (ii) the mechanics and energetics of healthy subjects walking with an actuated ankle orthosis using the proposed controller. As this controller was designed to mimic human reflex patterns during locomotion, we hypothesized that walking with this controller would lead to lower energetic costs, compared to walking with the added mass of the device only, and allow for walking at different speeds without explicit changes in the control parameters. Indeed, we have demonstrated in Chapter 3 that the reflexes were able to cope with different speeds without having to modify their parameters, as modifications in the CPG component would be sufficient to generate such changes. Here, since the controller only

accounts for the reflex component (in the case of healthy or only partially SCI subjects, the CPG is considered to be accounted for by the input from the subject), changes in speeds are consciously decided by the subjects and thus the controller adapts to these changes, while its parameters are not explicitly modified. Our results suggest that the neuromuscular controller does not disturb walking dynamics in both slow and normal walking cases, and can also reduce the net metabolic cost compared to the transparent mode of the device. Reductions in tibialis anterior and soleus activity were observed, suggesting that the controller could be suitable for augmenting or replacing walking functions. We also investigated the impedance patterns generated by the neuromuscular controller. The validity of variable impedance controller, particularly in stance phase, can facilitate serving subject-specific features by linking joint impedance measurement and neuromuscular controller.

Materials and methods

Ankle module for exoskeleton control

As mentioned previously, we have created a Simulink library of reflex and CPG control modules that can be combined to generate different types of assistive controllers. Here, our controller was implemented on an ankle exoskeleton, and therefore only the distal reflex modules were used. In particular, the control loops of the tibialis anterior and soleus muscles were implemented, see Fig. 4.1. The virtual gastrocnemius, a bi-articular muscle, was omitted to avoid a shared control issue, as torques would have been created at both the ankle and absent knee joint. Both the tibialis anterior and soleus control loops were used in pure reflex mode, without the CPG component, as previous studies showed the CPG component is more critical for proximal joints, in particular, the hip joint [59]. The parameters used for the control were the same as presented in [79], except for the soleus muscle resting length, which was decreased to 0.3 cm to account for the difference in morphology between the model and the subjects. At the time of testing, we did not scale the controller in respect to the subjects' body weight or height, and we applied the same controller to different subjects at various speeds as an indirect test of robustness.

A gain multiplying the normal torque output of the ankle controller was used to control the level of assistance of the controller. The gain was either 0%, 50%, or 100%, corresponding to Zero, Low, and High levels of assistance. A High level of assistance corresponded to the contribution of the tibialis and soleus muscles required for the neuromechanical simulation of the lower limb model walk in steady-state at 1.3 m/s.

Experimental setup

We investigated the mechanics, energetics, and muscle activity of young, healthy subjects walking with ankle exoskeleton controlled by the NMC. Subjects ($N=2$) wore the Achilles [134], a motorized ankle exoskeleton which provided various amounts of bilateral torque assistance.

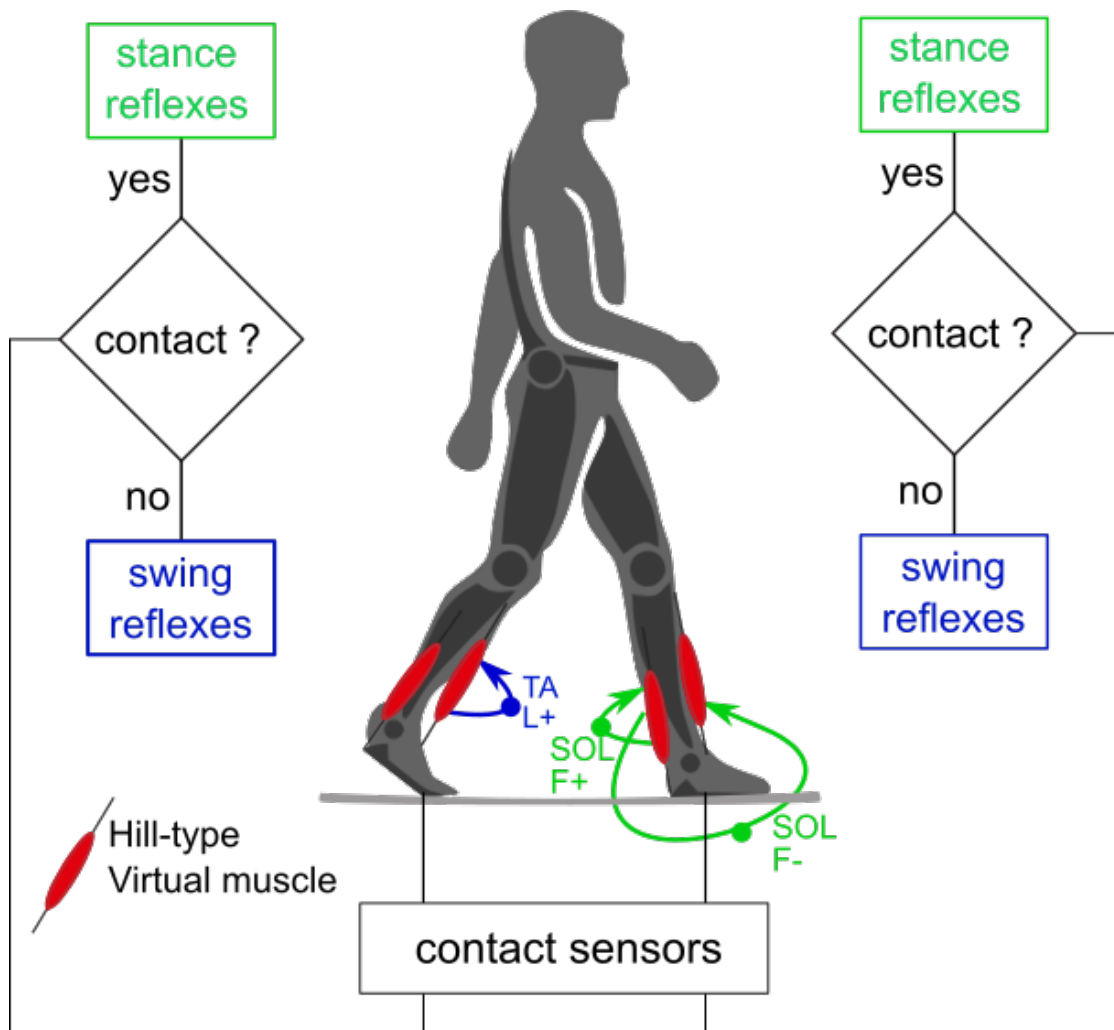


Figure 4.1 – Schematic view of the ankle module based on the reflex walking model from H. Geyer. Ground sensors are used to detect whether the limb is on stance or swing phase. Then, depending on whether the limb is in contact with ground or in swing, different reflex rules are generated, stance reflexes in green and swing reflexes in blue (Table 1 in [59] shows the different reflex loops acting depending on the gait phases). Here, only the soleus and tibialis muscle modules are used. During stance a positive force feedback (F+) increases the tension in the soleus muscle, and a negative force feedback (F-) decreases the tension on the tibialis anterior to prepare for push off. During the whole gait cycle, a positive length feedback (L+) tries to return the tibialis anterior muscles to a predefined length. Fig. inspired from [79].

Subjects walked at their preferred speed (self-selected speeds, 1.06 m/s, 1.08 m/s) and at a slow speed (0.58 m/s) on an instrumented split-belt treadmill. At self-selected speeds, three different levels of torque assistance were provided (Zero, Low, and High), and two were provided at slow speeds (Zero, Low). The Zero condition corresponded to the transparent mode of the device, with no input from the NMC. The High condition for slow speed was not performed by one of the subjects due to time constraints, and therefore that trial is not included here. The trials were six minutes each and randomized. Subjects' age was 28 and 37 years, their body mass was 80 kg and 77 kg, and their leg length was 0.92 m and 0.92 m. All subjects provided written informed consent prior to the study, according to Institutional Review Board procedures.

We measured metabolic power, electromyography, and gait biomechanics using standard procedures. We recorded the rate of oxygen consumption and carbon dioxide production (CareFusion Oxycon Pro, San Diego, CA USA) and calculated the steady-state metabolic power (in W) from the last two minutes of each trial using standard conversion factors [18]. Net metabolic power was calculated from subtracting the metabolic power for quiet standing (108 W, 106 W) from the gross metabolic power. We also recorded electromyography (EMG) in the tibialis anterior (TA), soleus (SOL), and medial gastrocnemius (MG) of the left leg (Delsys, Boston, MA, USA). All signals were high-pass filtered with a 20 Hz cutoff frequency (fourth-order Butterworth filter, zero-lag), full-wave rectified, and then low-pass filtered (fourth-order Butterworth filter, cutoff frequency 6 Hz, zero-lag) to obtain the linear envelope of each EMG signal. Kinematic data was measured for one of the subjects with motion capture (Phoenix Technologies Visualeyex, Canada), and 6 DOF ground reaction forces were measured from both subjects with an instrumented dual-belt treadmill (Motekforce Link, Amsterdam, the Netherlands). Gait event detection provided to the controller was calculated from the ground reaction forces. Kinematics and inverse dynamics (OpenSim, Stanford, CA, USA) yielded ankle angles, moments, and powers. As with metabolic power, only the last two minutes of the trial were used for analysis.

Results

Our results indicate that the controller reduced the energetic cost of walking and lowered soleus and tibialis anterior muscle activities. The subjects' overall walking dynamics were not significantly altered by the controller. In particular, the ground reaction forces and joint angles were qualitatively similar, and no systematic changes in step length or step time were observed.

As the gain on torque assistance increased from Zero to High, the measured torque from the exoskeleton also increased (Fig. 4.2). Peak plantarflexion torque occurred at around 55% of the gait cycle, and peak dorsiflexion occurred around 6% and 65% of the stride. Since the NMC torque is dependent on stance and swing phases and ankle angles, walking with different levels of assistance induces gait changes that inherently influence the commanded torques.

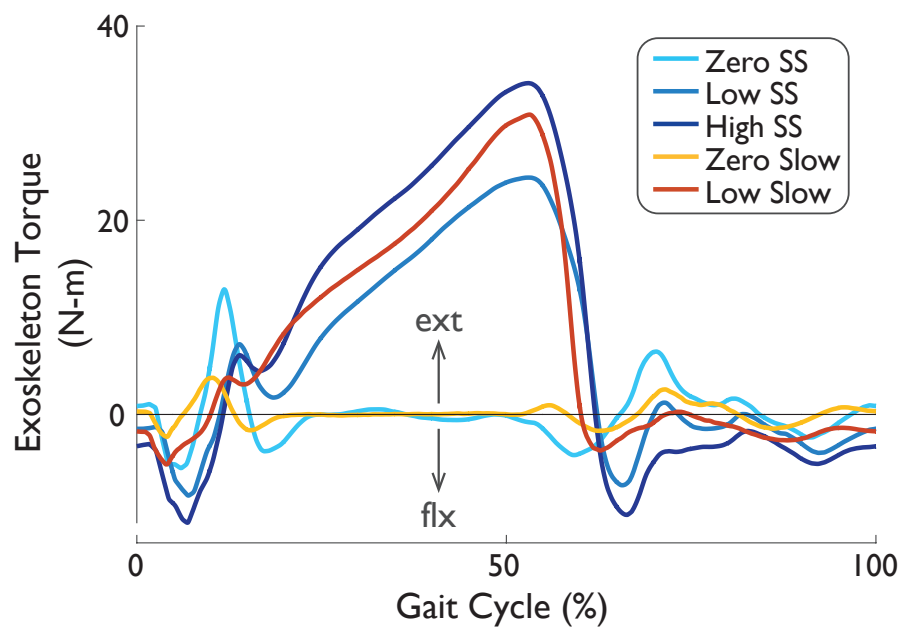


Figure 4.2 – Measured exoskeleton torque from the Zero to High conditions at self-selected speeds (SS) and for Zero and Low at slow speeds (Slow) from subject B. At Zero, the commanded torque from the neuromuscular controller was not provided, and thus the torque command defaulted to zero torque mode. Peak plantarflexion and dorsiflexion torques increased as controller contribution increased. The gait cycle is defined as a full stride starting from heel-strike.

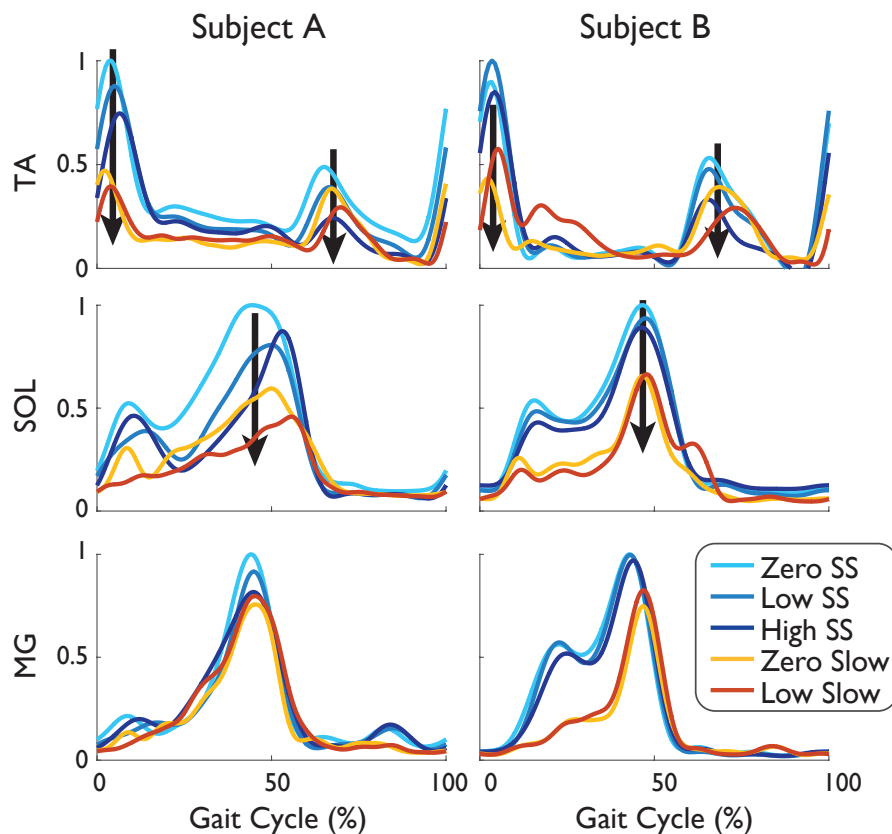


Figure 4.3 – Muscle activity ($N=2$) of the tibialis anterior (TA), soleus (SOL), and medial gastrocnemius (MG) over a range of torque assistance conditions. TA activity decreased near heel-strike, and SOL activity decreased near push-off. EMG signals were normalized to peak activation among the muscles for each subject.

Speed-related changes in ankle kinematics, such as lower peak plantarflexion angle [233], also affect the commanded torque. Hence, the peak torque at Low is not expected to be half the amount at High, and indeed the peak torque at Low is 70% of the High torque (24 N-m for Low, 34 N-m for High).

As an indication of muscular effort, muscle activity of the tibialis anterior, soleus, and medial gastrocnemius were measured. We found decreased activity at the tibialis anterior and soleus (Fig. 4.3), which explains at least part of the observed metabolic reduction. The subjects' tibialis anterior (TA) activity decreased near heel-strike and after toe-off. Hence, the controller assisted the subjects' dorsiflexion during heel-strike and for ground clearance during swing. Both subjects' soleus activities also decreased near push-off, and, as the controller provided more assistance, the plantarflexion generated by the subjects decreased. A similar, albeit less clear trend was also observed for the medial gastrocnemius. However, this muscle assists in both ankle plantarflexion and knee flexion, and therefore the effect of an ankle exoskeleton on this biarticular muscle is expected to be less straightforward.

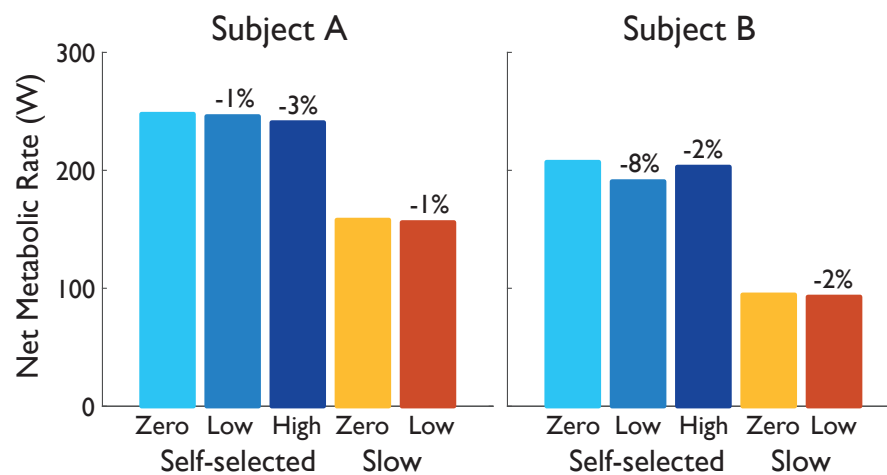


Figure 4.4 – Net metabolic power ($N=2$) with Zero to High levels of torque assistance. Both subjects decreased their energy expenditure rate with NMC at both slow and self-selected speeds. The reduction ranged from 1 to 8%, compared to the Zero condition.

Subjects also expended less energy to walk with the reflex controller. Compared with the Zero condition (i.e. the transparent mode of the device), the NMC conditions reduced the net metabolic rate between -1% to -8% for self-selected speeds and up to -2% for slow speeds (Fig. 4.4). Hence, the overall cost of walking with Achilles was reduced, and this could be reflected in the human-like torque profiles provided by the controller. Presumably, as the exoskeleton provides some of the ankle torque that the subjects would normally exert, the subjects can choose to use less of their own ankle muscles.

While the controller reduced metabolic cost and EMG activity, it did not greatly alter the subjects' overall walking dynamics. In particular, ground reaction forces (Fig. 4.5) were relatively unchanged. Qualitatively, the characteristic double hump of the vertical forces was intact with no apparent changes in force loading. Speed had a greater effect, as the initial vertical loading was shallower at slow compared to self-selected speeds. Similarly, there was also no observable trend for changes in step parameters among conditions, except for speed-related changes of shorter step length and longer step time with slower speeds. At self-selected speeds, mean step length was 0.64 m and mean step time was 0.60 s, and at slow speeds, mean step length and step time was 0.50 m and 0.86 s, respectively.

Observations of the total and exoskeleton ankle moments and powers revealed that the subjects' own contribution decreased as exoskeleton assistance increased (Fig. 4.6). Biological ankle moment and power were calculated from subtracting the exoskeleton measurements from the total moment and power provided by inverse dynamics. With greater exoskeleton assistance, both the subject's peak biological ankle moment and push-off power decreased to a maximum of -43% and -54%, respectively (Fig. 4.7). Hence, with increased assistance by the exoskeleton, the subject provided less push-off power, which could partially explain the lower metabolic cost we measured.

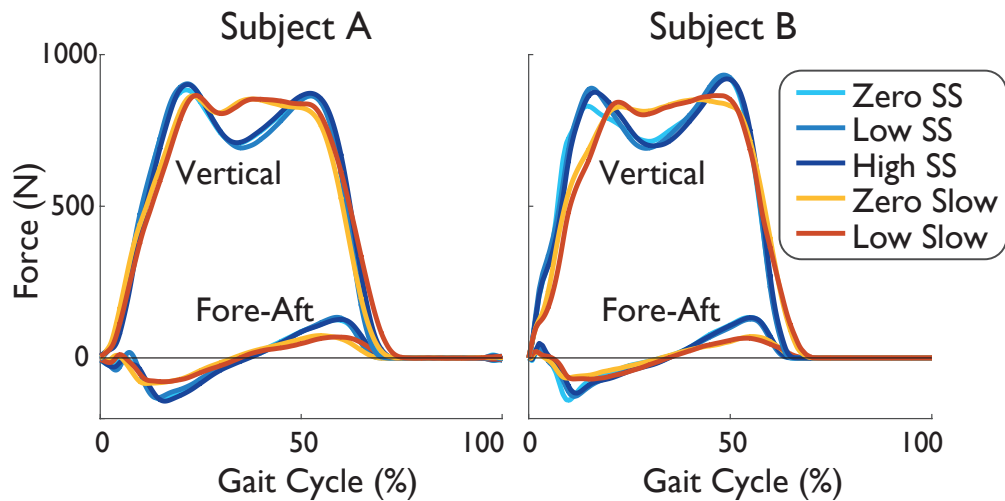


Figure 4.5 – Fore-aft and vertical ground reaction forces ($N=2$) at different torque levels over two different speeds. Qualitatively, minimal changes were observed with increased torque gain. Greater changes occurred between the two speeds, especially in the loading slopes.

Discussion

We had hypothesized that the bio-inspired controller would be intuitive for subjects and be adaptable without the need for extra sensors. To test this hypothesis, we measured healthy subjects walking at two different speeds with the controller on the Achilles' powered ankle exoskeleton. Our results demonstrate that as the controller provides more torque, the overall cost of walking is reduced for both speed conditions. Reductions were observed in soleus and tibialis anterior muscle activity and net metabolic cost. The controller did not appear to adversely affect walking dynamics, since only negligible changes were observed in the ground reaction forces and in step parameters.

While the experiment had a limited number of subjects, the results indicate a reduction in metabolic cost of walking and lowered EMG activity. The implemented controller was also not tuned for specific subjects, for specific speeds, and did not account for the weight of the Achilles device. Hence, the reductions could be even greater than those observed here. In addition, we measured a third subject, whose results were not included as the subject's anthropometric dimensions were not fully compatible with the device. However, we also observed less soleus activity with greater torque assistance for that subject. This suggests that the bio-inspired controller proposed could have an inherent capacity to provide subject-specific assistance by automatically adapting to the environmental conditions and subjects' state.

Anecdotal evidence from one subject also suggests that the controller may enable faster recovery from perturbations. This subject experienced anterior-posterior perturbations (in the form of 200ms impulse of different magnitude generated by a pushing device) at the pelvis while wearing the device and felt that the controller enabled less effort to recover. Preliminary

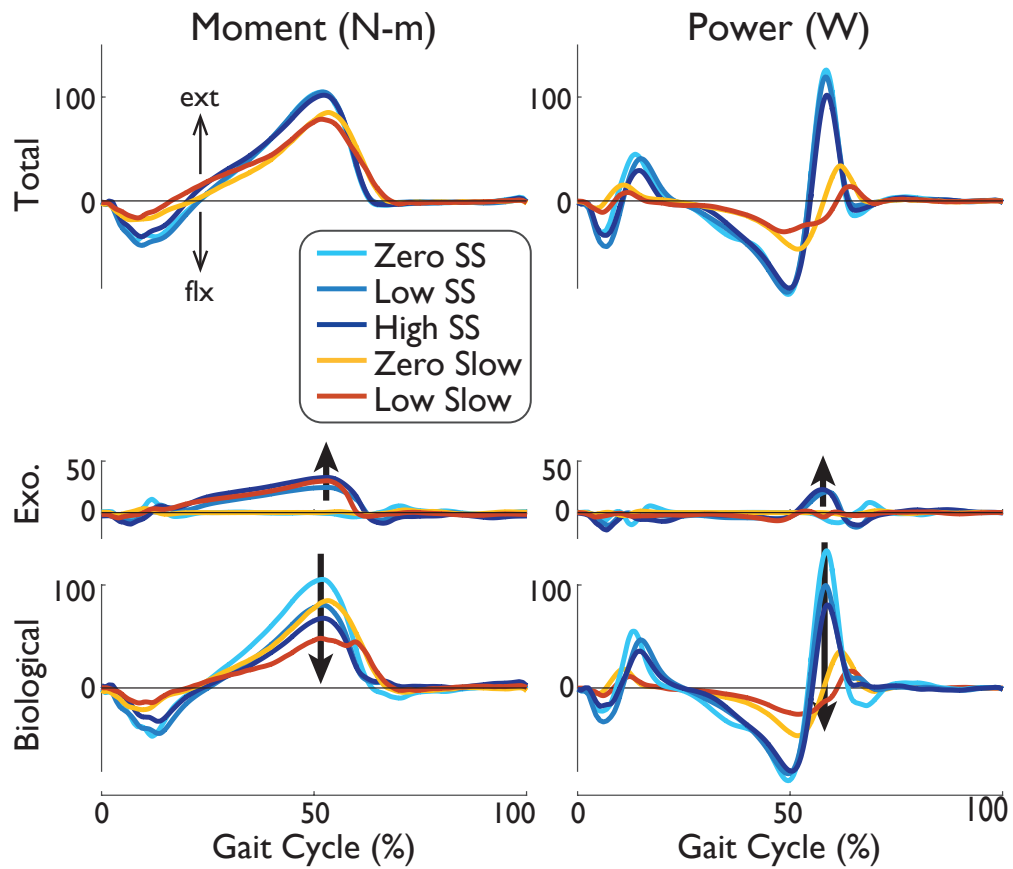


Figure 4.6 – Total moment and power, as determined by inverse dynamics, measured exoskeleton torque and power, and the difference as the subject's own contribution (Subject B) for a range of torque assistance conditions. With greater assistance, the subject provided less ankle moment and power near push-off.

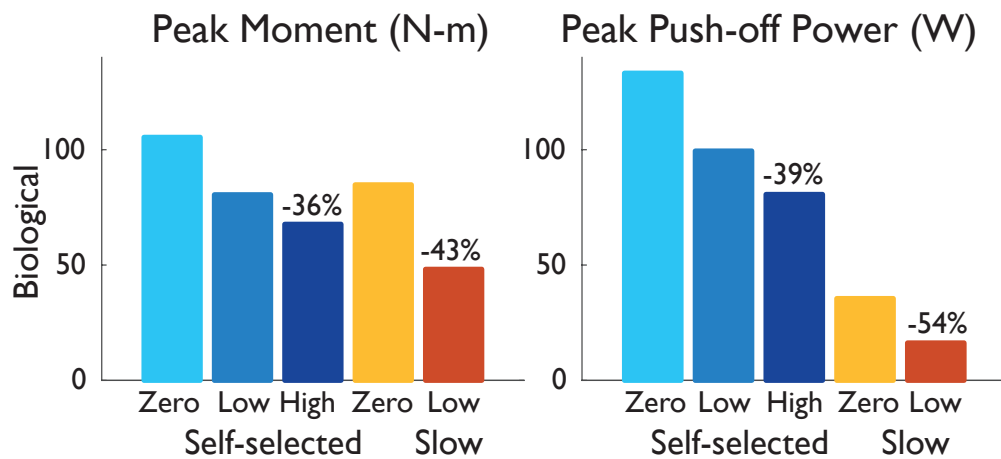


Figure 4.7 – Peak moment and push-off power produced by Subject B’s ankle for different assistance levels. With greater assistance, the biological ankle provided less moment and power near push-off. Percentage decreases (compared to Zero) reach up to 43% for moment and 54% for power.

observation of fore-aft ground reaction forces for these perturbation trials suggests peak recovery forces are reduced with controller assistance. Interestingly, similar observations were also made for SCI subjects (see Section 6.4).

It may be difficult to compare the energetic savings of our controller and the Achilles with that other devices and control algorithms, as exoskeleton weight and actuator limitations also impact metabolic cost. One possible measure is the exoskeleton performance index of 0.25 times net metabolic power savings over average exoskeleton positive mechanical power [179], but this does not capture controller robustness or complexity. Here, the NMC only needed a minimal set of sensors to reliably and robustly provide human-like ankle power at two different speeds.

We also compared our NMC ankle module with an impedance controller derived from a simulated perturbation experiment. The effect of the NMC in stance phase could also be approximated by an impedance controller which would facilitate subject-specific tuning of the NMC. The details of this study is presented in the Appendix D.

In this Chapter, we presented a bio-inspired modular controller robust to different walking conditions and requiring very few sensors. The controller we developed is part of a control library for the neuromechanical simulation and was tested at the ankle joint level on healthy subjects wearing a powered ankle exoskeleton. The success of this proof-of-concept experiment on a ankle orthese tested on a small group of healthy subject strongly support the idea that such a controller could be implemented as a rehabilitation strategies for SCI subjects. Indeed, the similarity between the bio-inspired model and the intact neuromuscular system could have the potential to improve subject’s recovery by adapting the control to the specificity of the subject’s remaining functions. Therefore we further tested implementations of the NMC

controller on spinal cord injury subjects using different exoskeletons: Achilles, the LOPES II robot [136]), and on the novel exoskeletons developed within the framework of the Symbitron project. These applications are presented in Chapter 5. Before that, the NMC characteristics, properties and constraints required to implement such a controller in the context of stroke or SCI subjects rehabilitation must be carefully evaluated. This is the topic of the next Chapter.

5 NMC constraints and design methodology and use cases

Introduction

Building on our Proof-of-concept validation that the implementation of a NMC controller based on our NMM model on healthy subjects presented in Chapter 4, we further explored the possibilities of utilizing such controllers for the development of orthoses and exoskeleton as rehabilitation strategies for strokes or SCI subjects. In this Chapter, we discuss the controller specificities required and propose a methodology for its design.

The hypothesis is that an exoskeleton controlled by such a NMC would be intuitive to use by the subject, as it would offer gaits and responses similar to what the intact neuromuscular system would normally offer. This similarity with the intact neuromuscular system has also the potential to improve the subject's recovery by adapting the control to the specificity of the SCI subjects remaining functions (such as flexor/extensor or left/right asymmetries).

Practically, one obtains a NMC by running the simulation partially online, that is, using inputs from the environment to derive the models states and in turn use these states to generate the muscles forces that are then sent as torque commands to the motors, see Fig. 5.1. This is to be contrasted with more traditional position, speed or acceleration control of joint state ¹.

Exoskeleton for paraplegics

Many neurologically impaired subjects would benefit from a personalized exoskeleton able to reproduce a walking gait, while coping with the subject's gait specificities. One challenge of such a controller is the ability to recover only the missing torques of the impaired gait, without injuring the wearer. In addition to standard safety criteria such as joint angles and torque limits, impairment-specific features should be accounted for. Indeed, impaired gait often

¹Since the goal is to mimic an intact neuromuscular model, we need our exoskeleton to accept torques as input. This brings constraints on the motors that needs to be able to follow the commanded torque as discussed in the Appendix B.

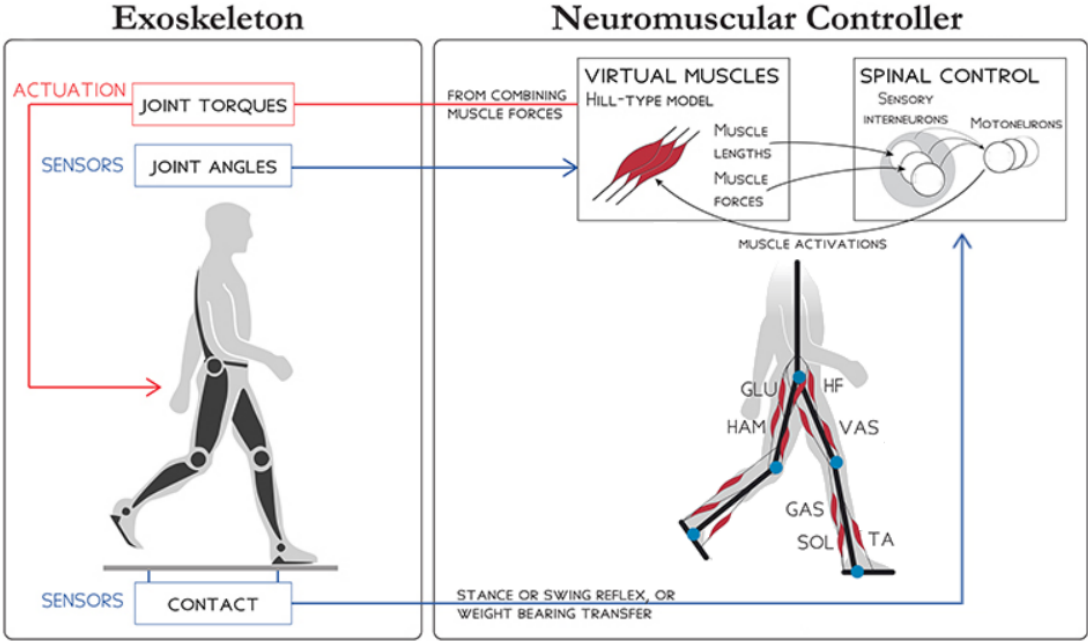


Figure 5.1 – Schematic view of the neuromuscular controller, and its use with an exoskeleton device. The joint angles and contact sensors of the exoskeleton are fed in the neuromuscular controller. Joint angles are used to derive the virtual muscle state and associated model of Ia and II fibers. The contact information is used as a state machine to switch between different reflex maps. The resulting muscle forces are then transformed into torques and applied at the different motor joints.

exhibits features that act to constrain the locomotion, for example, owing to the increased muscle or joint stiffness or spastic states frequently observed in stroke and SCI subjects. Such features, if not taken into account, can result in discomforts for the subjects or even injuries. Therefore, impairment characterization is a crucial step in the generation of a personalized exoskeleton controller.

One means of characterizing the impairment is by examining the net effect of the impairment on muscle contraction. In this context, an impairment can be classified as one of two main categories: Remaining locomotor features (RLF) and Features constraining locomotion (FCL). RLF refers to features inducing an overall reduced muscle activity due to muscle weakness and decreased activity level of the spinal networks responsible for locomotion. FCL refers to contracture and the increased overall joint stiffness often present in injury and disease that affect ambulation [146], [203]. FCL constrains the range of motion that can be realised by the limbs and the torques that can be applied at the different joints. In order to guarantee safety, the corrections of the RLF should only be performed within the constrained range of motion determined by the FCL, which is likely to be markedly different from healthy gait, owing to typical gait impairment features. We therefore needed to implement a controller that would constrain the range of motion to the physical limits of the subjects (i.e the FCL), while leveraging on its RLF to improve the gait performances.

An interesting feature of the neuromuscular model is its ability to also model gait which deviates from healthy subject. This can be achieved by adding extra constraints to the optimization process. An example is given below where the range of motion of a SCI subject is used to constraint the optimization to generate a stable walking solution within this range. The model is developed using data from treadmill walking of a male SCI subject aged of 64 years suffering from an incomplete C1 injury. The subject's height and weight are 1.86 m and 95 kg, respectively. The subject walked without assistance at a speed of 1 m/s while kinematic data from the hip, knee and ankle joints were collected. The angle ranges for the three joints corresponding to the collected data are $[-5.62, 43.6]$, $[10.3, 61.8]$ and $[-11.0, 13.5]$ for hip knee and ankle, respectively. Fig. 5.2 compares the time history plot of the hip, knee and ankle joint angles of the SCI subject and a healthy human (healthy gait data from [225]). In the SCI subject, we observe small asymmetries between the left and right limbs, as a result of the injury. The ranges of the hip angles for both right and left limbs are substantially higher than in the healthy subject (caused by a bending of subject's trunk). Ankle angles show the same trend as the hip angles, with the differences being larger during the stance compared to the swing. While the knee angles resemble the healthy kinematics, a reduced maximum extension can still be noted. The kinematic data are used to generate the FCL that the constrained gait should fulfill (see Fig. 5.2 A). The FCL are modeled here as minimum and maximum ranges of the different joints.

Fig. 5.2 B shows the resulting hip, knee and ankle angles of the optimized model under the constraints imposed by the FCL derived from the subject. As expected, the angles fall within the specified angle range constraints; these angle ranges are significantly lower than those

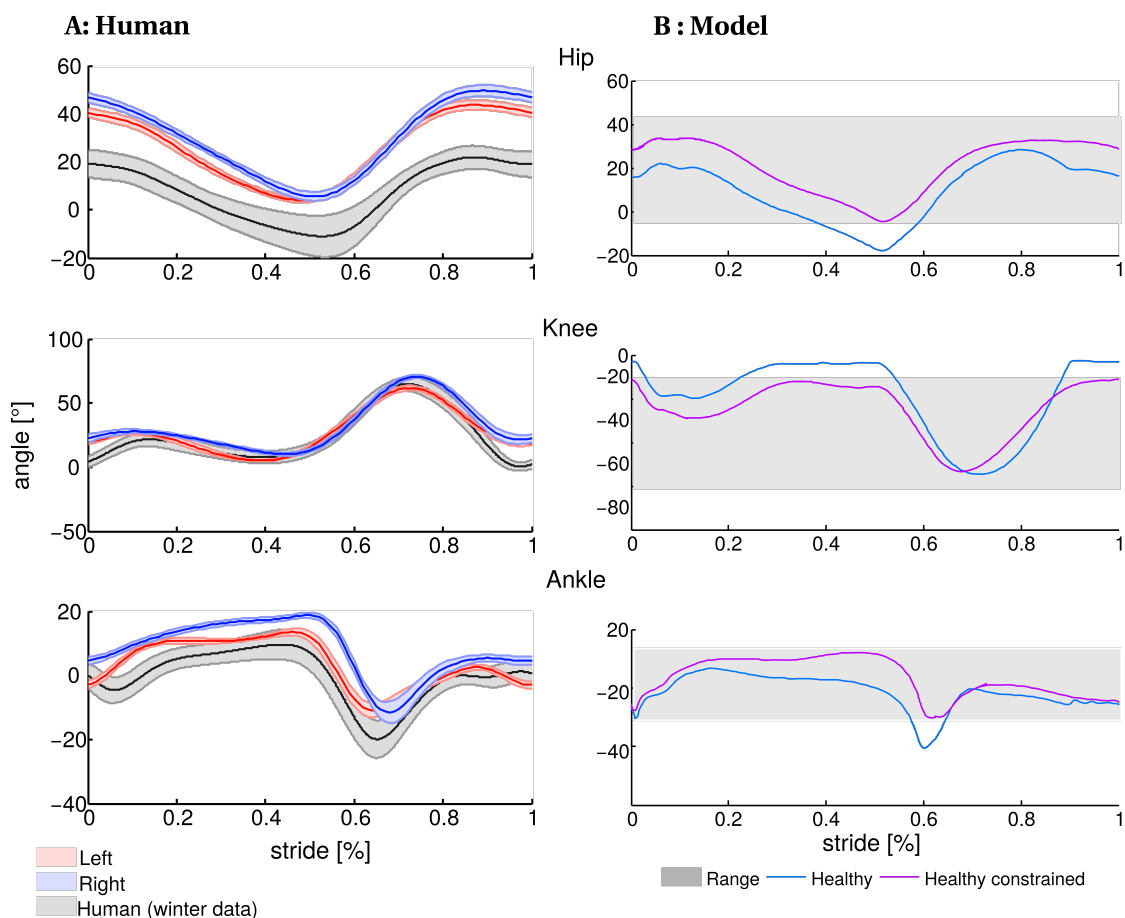


Figure 5.2 – A. Average time histories of joint angles during gait of the subject walking on a treadmill. Thick lines show the average angles +/- standard deviation. Angles from left/right legs of the subject are in red/blue respectively, healthy human gait angles are in grey (taken from [225]). Top: hip angles, Middle: knee angles, bottom: ankle angles. B. Average time histories of joint angles (as percentage of stride) for a healthy model in dashed blue (i.e. no FCL) and a healthy constrained model in purple (i.e. with FCL). The FCL, corresponding to results with range constraints extracted from subject kinematics shown in A., are in grey. The healthy constrained gait fulfills the constraints imposed by the FCL.

of the typical gait pattern of an healthy subject. The results demonstrate that the applied method successfully reproduces some aspects of impaired gait, and can therefore be used to implement a NMC controller tailor-made for subjects with specific FCL. There are other typical gait features of subjects with neurological impairment, including reduced joint torques, asymmetry and altered timing of joint kinetics, which could also theoretically be taken into account using different optimization of our controller.

However, in order to facilitate the tests of the control paradigm, subjects were selected so as to limit the FCL. Patients were clinically evaluated and selected by the Symbitron partner the

Santa Lucia Foundation in Rome (see details in AppendixE). For instance, the range of motion of the joints had to be relatively large and the level of spasticity had to be as low as possible so has not to preclude natural movements. Then, assuming that the subjects are chosen so that FCL could be disregarded, the subject specificity of the controller can be simply obtained by modulating the strength of different modules, so as to compensate for the specifically lost features. Thanks to the neuromuscular nature of the control architecture, the modularity can be done at the level of joints, by only using muscles spanning the joints of interest or at the muscle group level, by selectively modulating some muscles (e.g. if an flexion / extension asymmetries are noticed). Moreover, left/right asymmetries are easily taken into account at both the joint and muscle levels.

Modularity and tailoring aspect

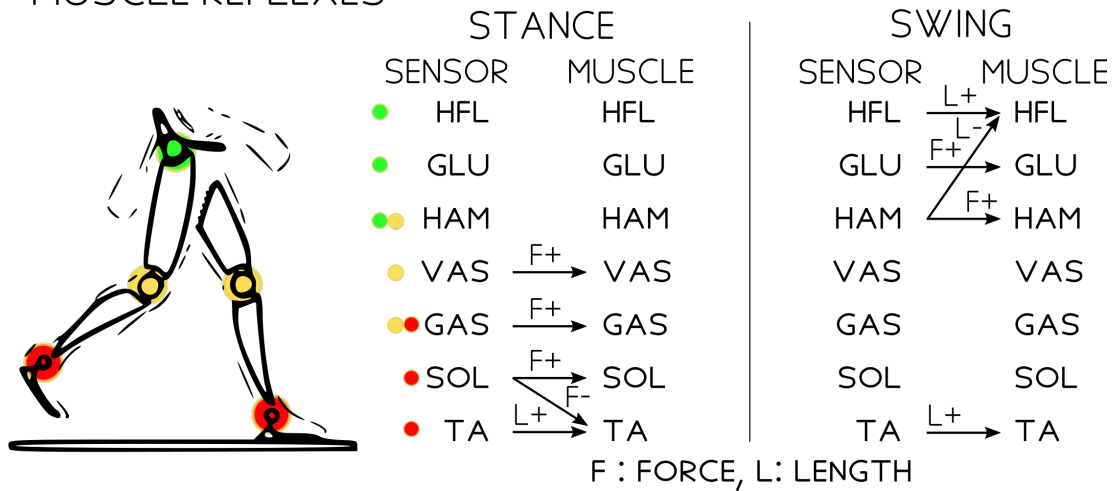
Since our NMC model is derived from the hypothesis that reflex-chains can generate walking, modularity automatically follows, as shown in Fig. 5.3. The top panel of the Fig. shows the different muscle reflex loops used in the model, one can observe that: 1) a state machine switches between different set of reflexes (or reflex maps) depending on the state of the ipsilateral limb, and 2) most of the reflexes are homonymous reflexes (see horizontal arrows in the Figure) or reciprocal inhibition reflexes. This allows for a simple first level modularization, which is to consider only the group of muscle involved in the controlled degrees of freedom. This strategy proved to be successful, as highlighted in the bottom panel of the Fig. 5.3, where four different MNC were implemented using this principle and tested on dedicated devices.

Neuromuscular control parameters

As described in the Appendix 1.1, the NMC was implemented as a Simulink interface by modularizing the initial model developed by H.Geyer, see Chapter 2, to which we included the CPG component presented in Chapter 3. This allowed us to test the controllers in simulation or in a data-driven manner, as well as to drive the different low-level controllers through a provided Simulink library and example controllers. Every NMC comes with a set of control and tailoring parameters that are presented below:

- Overall level of assistance
The overall level of assistance, set in percentage, modulates the overall torque sent to the motors.
- Joint limit
The soft limit ligaments switch can be used to enable / disable the joint ligament models. This module is always active as it offers an extra and smooth safety layer (smooth when compared the mechanical safety layer as it will not turn off the motor but create compensatory torques instead)
- Torque limiter

MUSCLE REFLEXES



CONTROLLED DEVICES

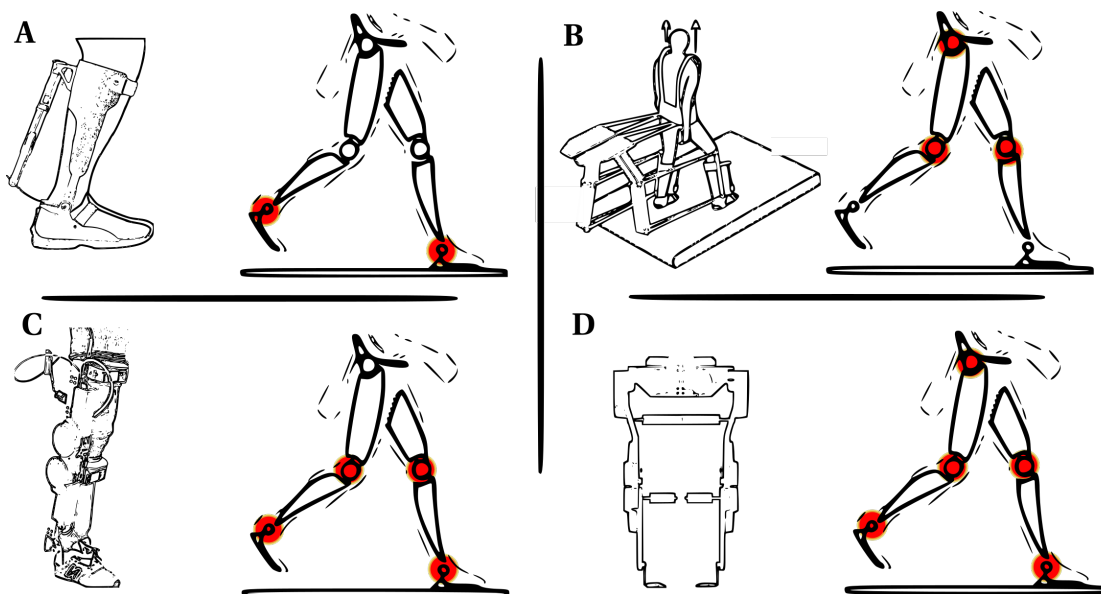


Figure 5.3 – Top: the different muscle reflex loops available in the NMC. Bottom: the different controllers designed for different devices, with different actuated degrees of freedom. A) Achilles actuating the ankle [134], B) The Lopes actuating the hip and knee [136], C) The WE1 symbitron prototype actuating ankle and knee, D) WE2 symbitron prototype actuating hip, knee and ankle.

The torque limiter allows to change the relative impact of specific joint to account for joint level weaknesses

- Muscle limiter
the muscle limiter allows to change the relative impact of specific muscles to account for muscle level weaknesses.

The last two parameters (torque and muscle limiters) have been implemented to allow a tailoring of the controller to the specificity of subject's impairment. Both limiters can be applied in a symmetric/asymmetric fashion.

The controller is set to provide joint torques for a human simulation model to walk at 1.3 m/s. Controller gains, given as a percentage, modify these nominal torques as needed for each test pilot, allowing customization. The NMC control also provided the option to apply controller gains symmetrically (to both left and right legs) or asymmetrically (see Fig. A.1 a). The torque limiter is then used to specify global torques for either both legs or a different set for the left or right (Fig. A.1 b). In addition, each joint and muscle action can be modified separately.

Our approach presents the advantage that the controller uses the same language as the one used by physiotherapists to describe the subject: the muscles, the segments, symmetric / asymmetric compensation. This greatly facilitates the interaction between engineering and clinical teams, and proved useful in the applications of our NMC, see Chapter 6.

NMC customization for subject-specific control

Walking customization aims at adjusting the NMC settings based on the walking abilities of each subject. To achieve this goal, the customization procedure starts with the maximum level of assistance and then reduces it gradually, using the control parameters described above. The reduction of the assistance level is driven by the online assessment of the Performance and Usability Index (PUI), which is conceptually illustrated in Fig. 5.4. Note that for the Achilles experiment, the PUI was simply measured with five different settings and the resulting matrix was used to select the NMC assistance configuration (further detailed in Chapter 6).

The PUI takes into account a usability and a performance components. The performance component was assessed in term of the velocity reached during the tests. We assessed usability component in terms of safety, comfort and perceived assistance. these 3 domains were selected as they are the most important for the user's positive attitude toward devices, thus allowing us to optimize the evaluation process as much as possible by reducing the time of evaluation without loss of reliability. The following questions were used to account for these three components: 1. I feel completely safe and confident in using this device; 2. This modality of walking is very comfortable for me; 3. This level of assistance helps me to walk properly, which were to be rated on a 7-point Likert-type scale. This instrument was designed to capture users' perception of the device, without any influence from his demographic or social background

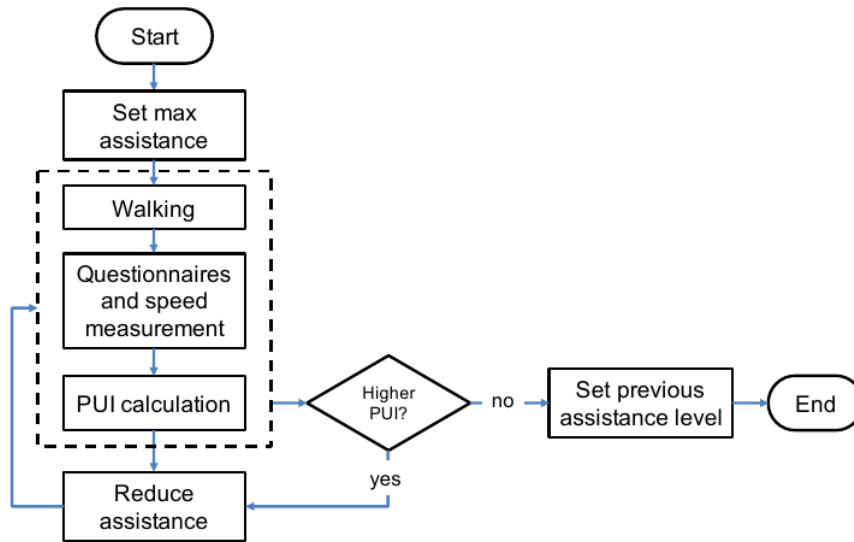


Figure 5.4 – Conceptual flow chart for the process of assistance reduction driven by PUI assessment. For simplicity, assistance increases, which are permitted for single joints, are not depicted in the flow chart.

The PUI, ranging from 0 to 1, was then calculated using the following equation:

$$PUI = 0.4S + 0.3C + 0.2V + 0.1A \quad (5.1)$$

sub-scores S (safety), C (comfort), A (assistance) and V (velocity) were normalized to range from 0 to 1, and the weights were selected by clinicians (highest importance given to safety and lowest given to perceived assistance).

For each setting under testing, subjects were asked to walk three times on a 10-meter path with self-selected Walking Index for Spinal Cord Injury (WISCI) level while wearing the device. For each test, the speed was measured as an index of performance, and after each test, the questionnaire was administered to scale perceived usability. Usability and performance results were combined to obtain the PUI. Each step of the process is stopped when the PUI stops decreasing. In case of equal PUI scores, the configuration with the minimal level of assistance is preferred.

Gait initiation

Usually, to allow for gait initiation, optimization of NMM include parameters related to the initial velocity and position of the different segments. Another method proposed by S. Berger in his master thesis[12] was to lift the body so that both legs are in swing and provide a velocity at the center of mass level only. The reasoning was that providing an initial velocity would give

enough kinetic energy to the system to initiate walking. This proved successful. Alternatively and as presented in Chapter 2, we propose to start with a model with both feet on the ground and a trunk leaning forward (with a small angle of 10 degrees). In that condition, both legs are in stance. Then, by forcing one of the legs to be the leading leg, stable walking can be obtained. As such, the NMM presents an inherent capacity to start walking on its own, rendering the above-mentioned optimization methods unnecessary and suggesting that the same would apply to the NMC.

This observation was confirmed in experiments with subjects presenting limited impairments (see Chapter 6 section 6.2 and 6.3. However for subjects with severe impairments (see Chapter 6, section 6.5 and section 6.4), another strategy had to be implemented to initiate the gait. In this case, the legs of the subjects were moved by two physiotherapists, and the level of activity of the NMC was increased step by step ,together with the treadmill speed until the NMC level and treadmill speed were high enough to move the leg. This strategy was then extended and the help provided by the physiotherapists was replaced by a position control algorithm. More specifically, we started with only the position control algorithm to initiate walking and then introduced a smooth transition between the two controllers by reducing the activity of the position control and increasing the activity of the NMC at every steps.

Real-time system requirements

While using the controller designed from the NMC library on real devices, we noticed that the resolution of the muscle model was unstable at 1 kHz (the rate at which we control the devices). These instabilities create vibrations which can be felt by the device wearer. This was practically solved by filtering the output. This was done without affecting the control scheme by reducing the neural delays used in the model to compensate for the delay induced by filtering.

Although the filtering changes did not alter the resulting gait, this still brings interesting questions. What is missed by filtering? How important are the non-linearities of the muscle model? How important is the internal dynamic of the muscle for the model? We initially addressed these questions in [208], where another approach to circumvent the instabilities noticed at 1 KHz was presented. The muscle model was simplified by neglecting the muscle-velocity relationship, linking the muscle length, the muscle-tendon length and the activity of the muscle to the rate of change of muscle length. This relationship is highly non-linear, and therefore requires small integration time step, wich might lead to computational issues when transferring this model to realtime controllers. The muscle model approximation was obtained by neglecting the effect of the muscle-velocity relationship, thereby considering that the muscle was so fast that it directly converged to its steady-state value. The results show that (i) neglecting the dynamics of proximal muscles does not affect the obtained gait and (ii) neglecting all muscles dynamics did alter the gait, but a robust gait could be recovered if the parameters were re-optimized, and the obtained controllers were stable even above 3 ms.

This strongly suggest that neglecting the muscle-velocity relationship dynamics has indeed a very limited impact on the length contractile element (lce) profile and on the overall dynamic. This holds true for the NMC, because the clock frequency of the high-level controller is inherently limited by the low-level controller and motor properties.

Limitation of hill muscle model

The neglecting of muscle velocity effect is a computational trick that does not make sense biologically. The instability of the hill muscle model has already been shown to be linked to the descending limb of the force length relationship (see Figure 5) which models the actin/myosin interaction [232]. Strong evidence suggest that the "two-filament sarcomere model" (i.e. accounting for acting / myosin interaction in the scaromere, as proposed in the Hill Muscle model) is missing a third filament made of titin proteins that interacts with actin [121, 102]. This interaction could prevent the instability of the cross-bridge [95] and could also explain the observed low energetic cost of eccentric contraction [144] and the evidence suggesting that intrinsic muscle compensation dynamics allow to rapidly adjust leg mechanics to keep from falling without help from the brain [38]. This strongly suggest that the creation of a better muscle model accounting for titin-actin interaction should be developed.

Torque tracking

While the NMC can command desired torques, the exoskeleton must execute these torques as closely as possible. We define torque tracking error as the measured torque from the device minus the NMC commanded torque. As an example, the quality of torque tracking during NMC trials with the WE1 is shown in Fig. 5.5, see Section for details on the experiment 6.3. The torque tracking error was quantified by the average of the root mean square error (RMSE) per stride and of the maximum error per stride. We found that torque tracking was quite good with RMSE mean +/- standard deviation of 6.78 +/- 1.10 N-m (Fig. 4).

However, at some points (e.g. S1 left knee around 9.5 s), the torque error can still be large, see Fig. 5.5A. This is by design and results from the knee being in the end stop. Here the end stop controller, which minimizes the penetration beyond end stop, takes precedence over the torque tracking goal (which minimizes torque error). For S1, the end stop was reached because the test pilot nominally walks with a hyperextended left knee during stance (compare W-F-T0 and W-R-T0 left knee joint angles in Fig. 6.12). Max error generally occurred from mid to late stance and was more variable in timing for the knee joint than the ankle joint.

5.6. Torque tracking

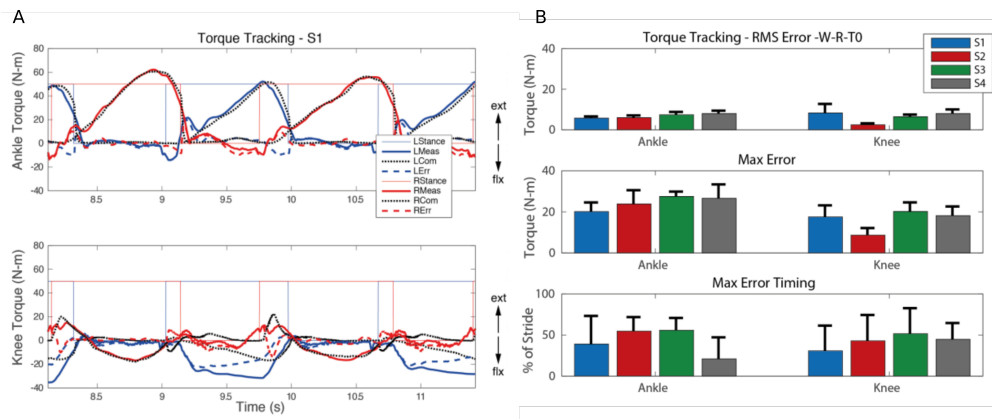


Figure 5.5 – A) Close-up of torque tracking for left (blue) and right (red) legs. LStance and RStance indicate stance on (1) or off (0). Meas: Measured torque, Com: Commanded torque, Err: Error (measured-commanded). Pos: ext, neg: flx. B) Torque tracking error between NMC commanded torque and WE1 measured torque, quantified by root mean square of the error (top) and maximum error (middle). Timing of max error per stride (bottom) is a function of gait cycle percentage.

6 Applications

Introduction

Building on the design constraints established in Chapter 5, to implement our controller for use on exoskeletons dedicated to SCI subjects, this chapter presents the results on the use of the NMC control principle for SCI subjects. The experiments presented were conducted at the University of Twente (Netherlands) and at the Santa Lucia Foundation (Italy) with the help of Symbitron's clinical and hardware partners,[207] and the experiments are the results of a collective effort.

The experiments were conducted on subjects (here referred to as "test pilots") that were separated into two groups: The first group included subjects with a distal deficit at lower limbs and the second group includes subjects with proximal (and therefore distal) deficit at lower limbs. The subjects of the second group have less residual motor abilities and were tested on distinct devices. The test pilots data are detailed in the Appendix E Fig. 5.3 gives a schematic overview of the different devices used and the corresponding controlled degrees of freedom. Group 1 was first tested on Achilles [134] (which actuates only the ankle in sagittal plane) and then on the wearable exoskeleton (WE) 1 prototype (which actuates both the ankle and the knee). The experimental setups and the results of group II on the Achilles and WE1 are presented in Sections 6.2 and 6.3, respectively.

A first set of test pilots from group II were trained on the Lower-extremity Powered ExoSkeleton (Lopes) II gait trainer [136]. The device provides a safe environment thanks to lateral bars, a weight bearing system and a shadow leg (creating a mechanical safety layer constraining the range of motion of the knee and hip). The Lopes actuates both the knee and the hip joints. Since the subject of Group II have no control of distal muscles, spring straps were used to prevent a drop foot effect during swing phase by pulling toes upward. The experimental setups and the results of the Lopes tests are presented in Section 6.4.

Another set of test pilots from the group II were then trained on the wearable exoskeleton (WE) 2 prototype, which actuates the ankle, knee and hip. The experimental setups and the results of the WE2 tests are presented in Section 6.5.

I : NMC for incomplete SCI on the Achilles exoskeleton

Pilots general information

Data collected in the clinical/neurological preliminary assessment of the five enrolled test pilots are reported in Table 6.1. Taking into account the inclusion criteria “ability to ambulate over ground, also with some aids if necessary”, WISCI level at the enrollment is also reported. The pictures of the five test pilots involved in the experiments are shown in Fig. 6.1. Three subjects underwent both the Achilles and the WE1 trial. The top part of the Fig. shows the Manual Muscle Test (MMT) and gives an appreciation of the residual motor capacity of the subject at each joint (0-5 scale, 0/no movement, 5/normal power).

It can be appreciated that each test pilot has different muscle force for each joint and also differences between left and right sides: Test pilot S1: has the highest force level at the hip joints and right knee, while the most affected joint was the left ankle. Test pilot S2 has the highest force level at the knee joints, in particular the left one, while the most affected joint was the right hip. Test pilot S3 has a similar force level at both hip joints, with minor differences, and the most affected joint was the right ankle. Test pilot S4 is the less affected test pilot; the force was very high for the knee and hip joints, while the right ankle was the most affected joint. Test pilot S5 has a similar force levels a the hip and knee joints, while the right ankle was the most affected. This pilot presents different force levels between extensor and flexor MMT, and is the most affected test pilot.

Table 6.1 – Epidemiological data of the 5 enrolled test pilots.

	S1	S2	S3	S4	S5
Age	48	69	47	36	42
Lesion Date	Nov 2013	Feb 2016	Nov 2016	Jul 2017	Jul 2015
AIS level²	D	D	D	D	D
Lesion level	C7	T10-T11	L4-S3	L3	T11-T12
Aethiology	Traumatic	Traumatic	Ischemic	Disc L3-L4 herniated	Traumatic
WISCI level	20	16	16	20	20

6.2. I : NMC for incomplete SCI on the Achilles exoskeleton

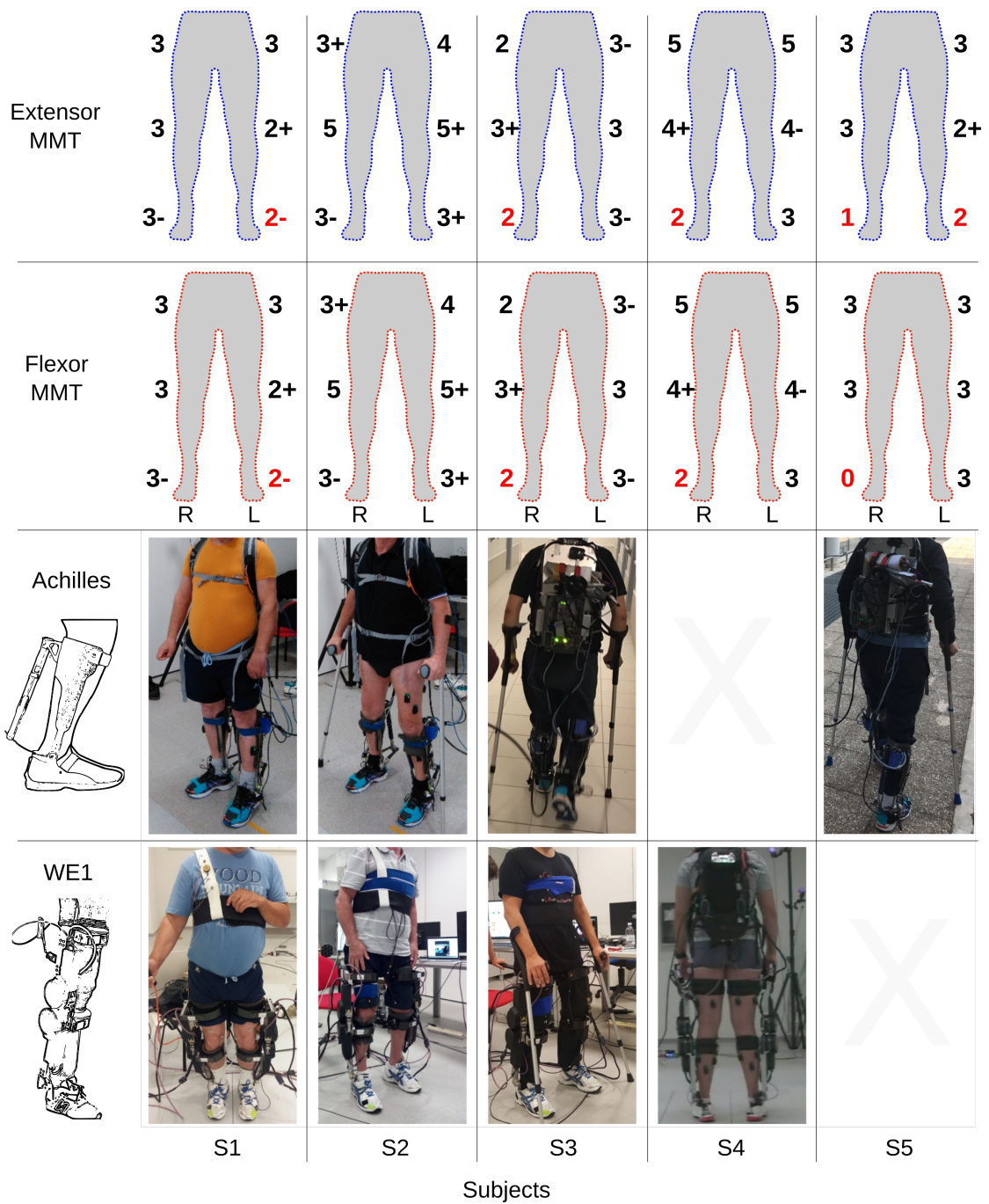


Figure 6.1 – Test pilots of group I (S1 to S5) involved in the experiments wearing Achilles or WE1. Top part shows the MMT for Flexor and Extensor muscle of the different subject before the trial

Chapter 6. Applications

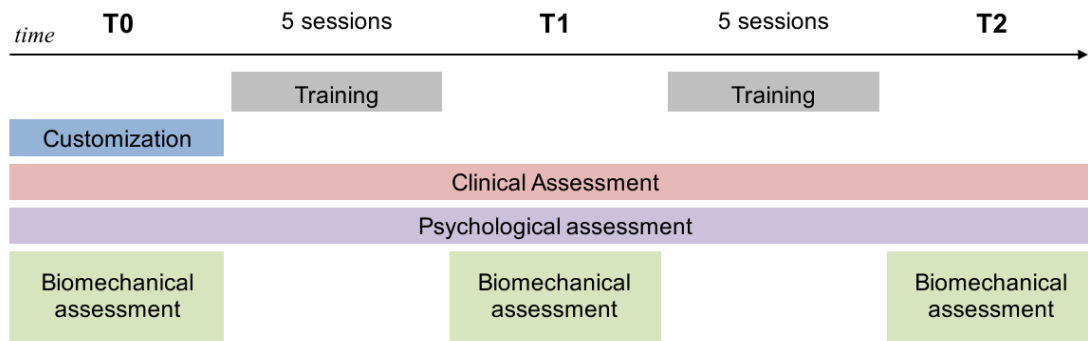


Figure 6.2 – Overview of the timing for the experimental protocol for the clinical evaluation of the Achilles Exoskeleton.

Objectives

We present herein the implementation of the NMC for the Achilles, which requires the ankle module. Tests were performed on group I test pilots by our consortium partner at the Santa Lucia Foundation. We also provided a simple user interface for the NMC and assistance when needed. The experiments performed on Achilles had the following objectives:

- To customize the Achilles NMC parameters settings to properly fit the SCI test pilots needs in terms of residual motor functions. This subject-specific approach was based on the measured performance during walking and on subjects' feedback on usability, as presented in section 5.3.2.
- To train test pilots to the use of the Achilles with NMC.
- To perform clinical, psychological and biomechanical evaluation of test pilots before, during and after the training, in order to verify the effectiveness of the training and the usability of the robot.
- To derive and fine-tune a method for the customization, training and assessment of the Achilles to be extended to the clinical validation experiments on the WE1, which will be presented in section 6.3.

Methods

An overview of the timing of the protocol is reported in Fig. 6.2. The customization phase corresponds to the selection of the best NMC setting based on a PUI, as described in Section 5.3.2 and further detailed below. The training, clinical and biomechanical assessment phases are described below.

NMC customization procedure

The customization process was devoted to adjust the NMC settings based on the features of each test pilot. For each setting to be tested, test pilots were asked to walk four times on a 5-meter path with self-selected WISCI level while wearing the Achilles. The 5 NMC settings under testing were selected randomly and are described below:

3 symmetric settings:

- 0 % Assistance (0L-0R);
- 50 % Assistance (50L-50R);
- 100 % Assistance for Left and Right side (100L-100R);

2 asymmetric settings:

- 100 % Assistance on the left and 50 % assistance on the right (100L-50R);
- 50 % Assistance on the left and 100 % assistance on the right (50L-100R).

PUI results during the customization process were graphically represented by means of PUI matrixes, which allowed the choice of level of assistance to be made, see Fig. 6.3

Training procedure

After a session of familiarization, 10 days of training were performed three times per week (40 minutes each day). The main goal of the training was to improve the comfortable gait velocity. According to this aim, pre and post each training session the 10 meter walking test (MWT) was performed with and without the Achilles. The training session followed a specific procedure that is further described the Appendix E.

Biomechanical assessment

The biomechanical assessment was based on the following measures:

- Ankle joint kinematics (recorded with the Achilles ankle encoders);
- Ankle assistive torque (recorded with the Achilles torque sensors);
- Stance/swing phases duration (recorded with the Achilles sensorized insoles);
- Muscular activity of the Tibialis Anterior (TA), Soleus (SO), Gastrocnemius (GA), Rectus Femoris (RF), Biceps Femoris (BF), Vastus Lateralis (VL) (recorded with surface EMG sensors).
- GRFs and spatio-temporal parameters (recorded with force plates).
- Walking speed was measured in clinical assessment (10MWT) with a chronometer.

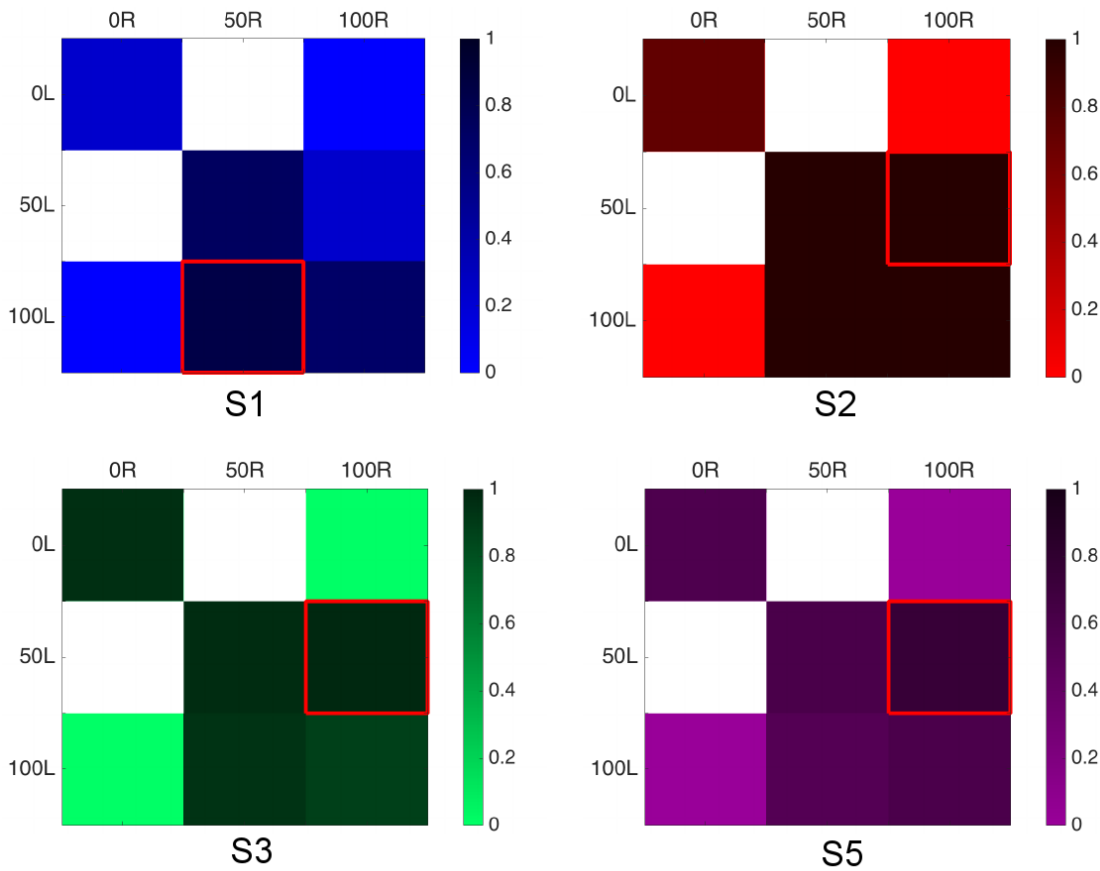


Figure 6.3 – Results of the customization process: PUI matrixes for the 4 test pilots (S1, S2, S3 and S5). Red square highlights the selected NMC assistance configuration.

6.2. I : NMC for incomplete SCI on the Achilles exoskeleton

Clinical assessment

For the enrolment process (T0), neurological status was assessed using the American Spinal Injury Association (ASIA) and the ASIA Impairment Scale (AIS). AIS levels C and D reflect incomplete motor lesions. Test pilots underwent a battery of clinical evaluations before (T0) and after 10 training sessions (T2), as detailed in Table 6.2. Furthermore, the 10MWT was assessed before and after each training session, with and without the use of Achilles.

Table 6.2 – Overview of the clinical scales used during the training. Details concerning each scale can be found in the Appendix E

	T0	10 Training sessions	T2
Asia Impairment Scale	✓		
Spasticity and Related Symptoms (MAS, SCATS, SPASM Frequency Scale)	✓		✓
Muscle Force(MMT hip, knee, ankle)	✓		✓
Pain (VAS)	✓		✓
Balance (Berg Balance Scale)	✓		✓
Walking index for SCI (WISCI)	✓		✓
10MWT	✓	✓	✓

The results of the PUI indicate that each pilots choosed the highest level of assistance (100) on their most affected leg, while still trying to minimize left/right assistance asymmetry (50% assistance on the less affected leg).

Results

Walking speed

Gait speed improvement was considered as the primary outcome of the study. We focused on two different assessments: short path speed (10MWT) and long distance speed (6 Minutes Walking Test (6MWT)).

All test pilots at T0 were not able to perform the 6MWT without the Achilles, while for the 10MWT, no difficulties were reported. Clinical walking assessments reported in Fig. 6.4 demonstrate improvements of the gait speed after training at both time tests without (10MWT) and with (6MWT) the Achilles, and in particular for the short distance speed. It is necessary to stress that already at T1 (i.e. after 5 sessions) the speed was improved for both tests, demonstrating an unexpected rehabilitative effect of the training. Furthermore, during each training day the 10MWT was performed with and without the Achilles, before and after 40 minutes of

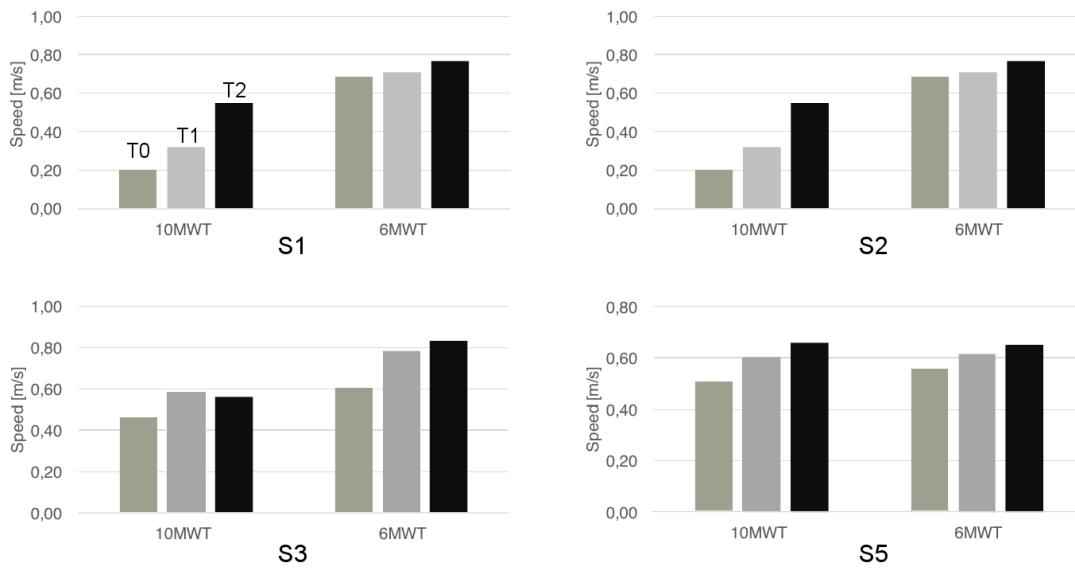


Figure 6.4 – Average 10MWT without the Achilles and 6MWT with the Achilles.

training. Data related to the test without Achilles (i.e. “free walking”) highlight a progressive improvement in the performance for all the test pilots. In particular, the most evident reduction in 10MWT score was obtained during the first 5 sessions, thus suggesting an early effect of training on gait performance. During the last 5 training sessions, a slight improvement was also reported. For all the test pilots between T0 and T2 (i.e. after 10 training sessions) an improvement of gait speed was obtained.

Results of 10MWT recorded with NMC are in line with speed improvements recorded without the Achilles (Figures 6.4 and 6.5). Again, improvements during the first 5 sessions are more striking.

Ankle kinematics

Ankle joint angle and torque data are reported in Fig. 6.6 for the 4 test pilots. Conventionally, dorsiflexion is negative and plantarflexion is positive. The variability of the curves demonstrates that NMC does not force the ankle joint towards a predefined trajectory. Rather it provides torque assistance without imposing a stereotyped motion. Each test pilot preserved his walking features and his peculiar asymmetries while healthy subjects, as expected, showed a higher symmetry. No significant differences were observed between T0, T1 (after 5 training sessions) and T2 (after 10 training sessions) assessments. Comparing test pilots data with respect to the healthy subjects, we noticed that the angle of the less affected ankle (right for S1 and left for S2, S3 and S5) was closest to the healthy subject’s path. In particular, S1 right ankle (less affected) was very close to the healthy trajectory. S2 had both ankle joints kinematics very similar to the healthy one, except for an offset likely due to the initial robot calibration

6.2. I : NMC for incomplete SCI on the Achilles exoskeleton

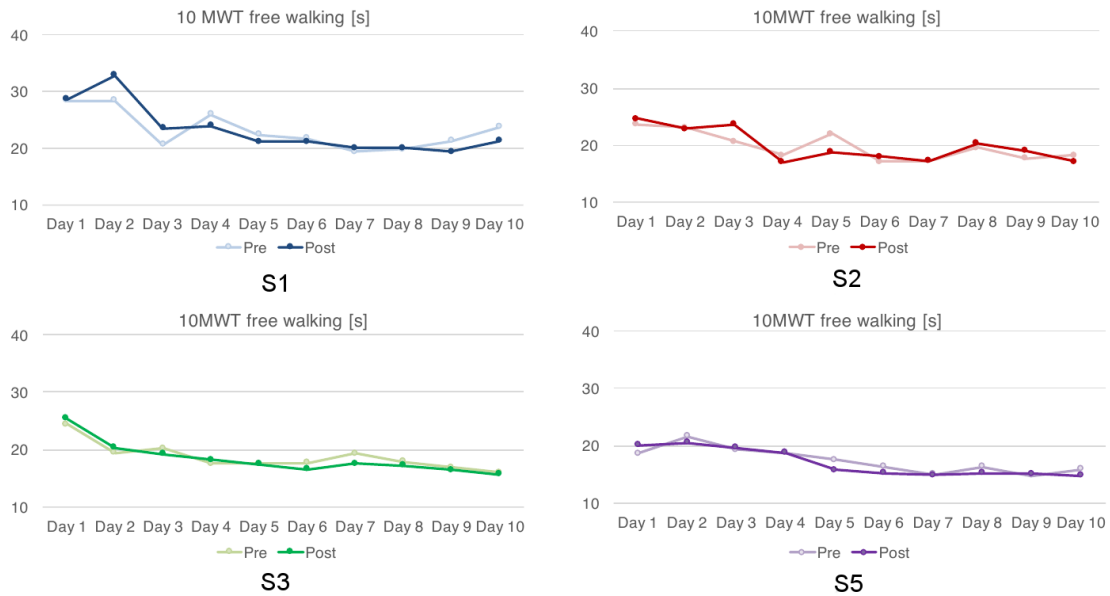


Figure 6.5 – 10MWT during walking with Achilles for each training session. Pre and post training measurements are reported.

affected by a non- physiological standing posture. S3 and S5 had kinematic patterns quite different from the healthy subjects, with a pronounced asymmetry for S5 (the most affected test pilot, showing the worst scores for MMT). It is worth noticing that S3 and S5 had very similar kinematic patterns on the right (most affected) leg, with an ankle ROM higher than healthy subjects and a relevant increase of dorsiflexion during late stance. This last effect is due to a torque saturation in the Achilles. Indeed, a limit of around 60 Nm was imposed and the plantarflexion torque required for the push-off was not properly delivered by the robot; as a counter-action test pilots magnified dorsiflexion by an accentuated leg forward progression (ankle passive dorsiflexion).

Summary of achievements

Taken together, the Achilles experiment on group I test pilots allowed us to develop a systematic method for the customization of the NMC walking controller, allowing it to cope with specific neurological and motor features of each single test pilot. Thanks to this method, we successfully implemented the customization process on 4 test pilots for the subject-specific tailoring of Achilles controller. We evaluated the performances of the training of the 4 test pilots in the use of Achilles based on clinical, biomechanical and psychological measurements, and report a significant improvement of walking speed while wearing the Achilles, after 5 and 10 training sessions.

Chapter 6. Applications

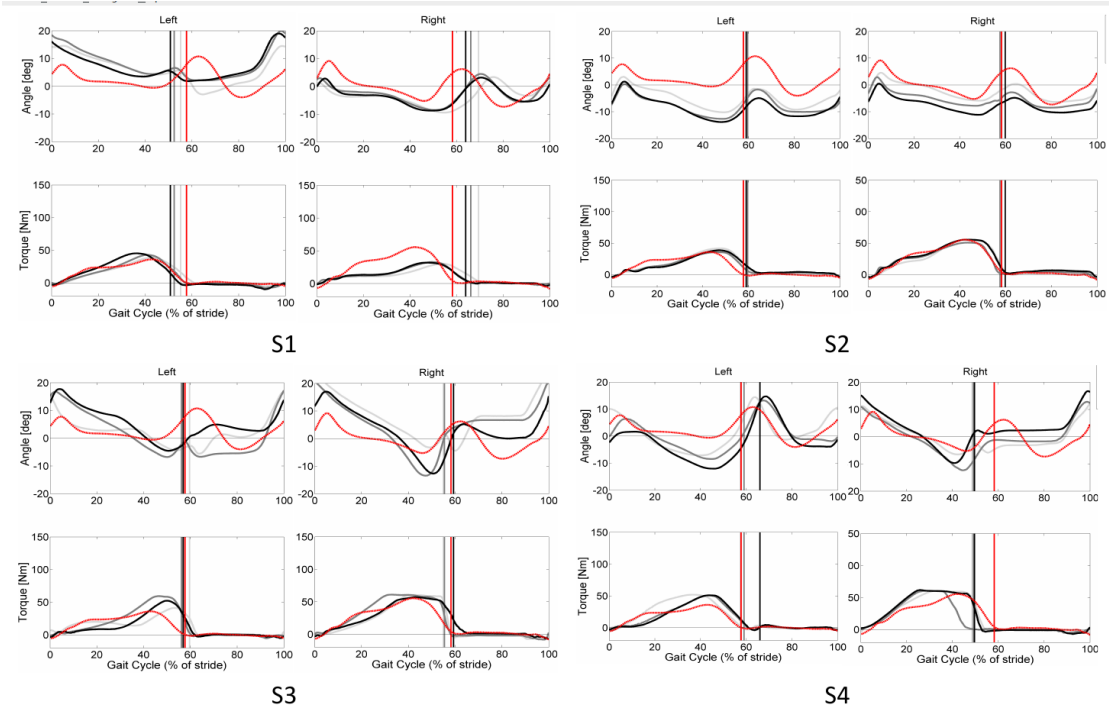


Figure 6.6 – Ankle kinematics and Achilles assistive torque for the 4 test pilots. Light grey: T0; Grey: T1; Black: T2; Red: healthy subjects. Dorsiflexion is negative and plantarflexion is positive. The vertical lines correspond to lift-off.

II : NMC for incomplete SCI on the WE1 exoskeleton

Pilots general information

The test pilots of this set of experiment are the same as those in the previous section and presented in Fig. 6.1. The test pilots are referred to as S1 to S4.

Objectives

We present herein the implementation of the NMC for WE1, which requires the ankle and knee modules. Tests were performed on group I test pilots by our consortium partner at the Santa Lucia Foundation. We also provided a simple user interface for the NMC and assistance when needed. The objectives of the experiments performed on the WE1 are to demonstrate the use of the MNC to control a wearable exoskeleton (WE1) and to assess its effects on SCI group I test pilots. More specifically, we aimed at:

- Implementing the NMC on the wearable exoskeleton WE1. Here we used the ankle and knee modules to control the WE1 device, which actuates the wearer's ankle and knee joints.
- Achieving subject-specific customization of balance and walking controller.
- Investigating the effects of the controller on the gait of those with SCI (group I test pilots).
- Assessing NMC assistance using kinematics (from motion capture and WE1), joint torques (measured from WE1 or from inverse dynamics), ground reaction forces (GRFs), and electromyography (EMG) analyses.

Methods

An overview of the timing of the protocol is reported in Fig. 6.7 , in which the different phases are highlighted. 1) The anthropometric adaptation, which includes the modification of the robot mechanical configuration (insoles, links, cuffs) to adapt it the anthropometric features of the user. 2) The Training, which include a first phase (phase 1) to perform walking customization (i.e. selection of the best NMC walking settings, based on the PUJ, as described in Section 5.3.2, and a second phase (phase 2), to use of WE1 with the selected NMC setting for 5 training sessions (details on the training sessions can be found in the Appendix E).

Pre-training data (T0) was recorded after the NMC gains were customized according to the protocol defined in Section 6.3.3. T0 data includes shod trials (without wearing WE1), zero impedance mode (ZIM) with WE1, and NMC with WE1. See Table 6.3 for a summary of the walking conditions. Then the test pilots had five training sessions with the same gains. Finally,

Chapter 6. Applications

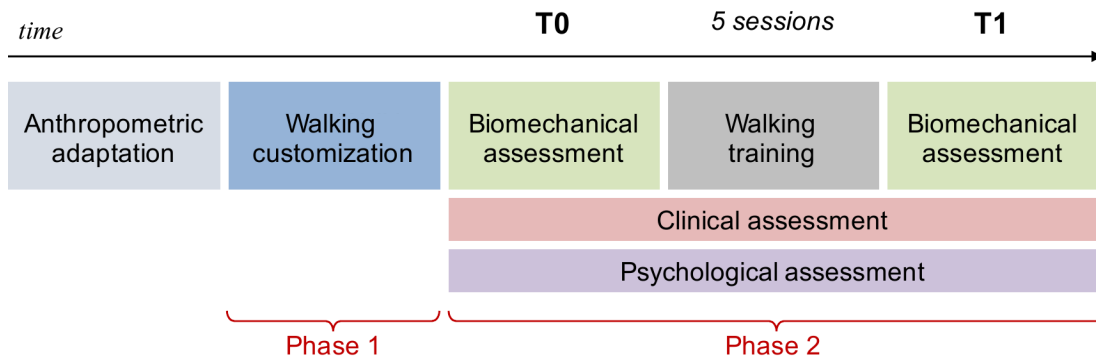


Figure 6.7 – Overview of the timing for the experimental protocol for the clinical evaluation of the WE1.

post-training gait (T1) was measured with WE1 and NMC. The NMC gains were unchanged for all training sessions and trials.

Table 6.3 – Walking condition labels and meaning (W: walking, F: free, R: robot, Z: ZIM).

Condition	Meaning		
W-F-T0	Walking	Without wearing WE1 (shod)	Pre-training
W-R-Z-T0	Walking	Wearing WE1, in zero impedance mode (ZIM)	Pre-training
W-R-T0	Walking	Wearing WE1, with controller assistance (NMC)	Pre-training
W-R-T1	Walking	Wearing WE1, with controller assistance (NMC)	Post-training

NMC customization procedure

Since the WE1 only has actuation at the ankle and knee, we tailored the NMC to the device by using only the ankle and knee components of the full controller. To provide ankle plantarflexion and dorsiflexion, the soleus and tibialis muscles were also included. The biarticular gastrocnemius produced ankle plantarflexion and knee flexion, and the vastus induced knee extension. Muscles governing hip flexion (hip flexors) or hip extension (gluteus) and the bi-articular hamstring muscle were excluded. In the context of the WE1, the NMC muscle action limiter can be used to augment or reduce the level of assistance from each joint (i.e. the vastus for the knee; the soleus and tibialis anterior for the ankle) and from the bi-articular gastrocnemius muscle (Fig. A.2). Additionally, the soleus and tibialis anterior may be modified separately to yield the level of plantarflexion or dorsiflexion, respectively, needed (Fig. A.3). The vastus contribution can also be changed to produce more knee extension assistance. As no muscle solely actuates knee flexion in this controller, modifications to that action will be through the gastrocnemius. A summary of the customizable parameters for WE1 are presented in Table 6.5.

The gains optimization procedure for the customization purpose is performed based on the PUI, as described in Section 5.3.2.

6.3. II : NMC for incomplete SCI on the WE1 exoskeleton

Table 6.4 – NMC adjustable parameters for WE1.

Step	Assistance type	Involved joints	Symmetry	Quantity rescaled	Assisted motion	% of the maximum value**
1	Overall	Knee/ Ankle	Yes	Nominal resultant torque	Knee flexion/extension and ankle dorsi/plantarflexion	100%-70%-40%-0%
2	Biarticular	Knee and Ankle		Gastrocnemius	Knee flexion and ankle plantarflexion	
3-6	Single joint*	Knee	No	Vasti	Knee extension	
		Ankle		Tibialis anterior and soleus	Ankle dorsi/plantarflexion	
7	Push off	Ankle	Yes	Gastrocnemius length	Ankle dorsiflexion	98%-99%-100%***
8	Ankle flexion			Tibialis anterior	Ankle dorsiflexion	100%-70%-40%-0%
9	Ankle extension			Soleus	Ankle plantarflexion	

* Hierarchically, from the less affected to the most affected.

** The maximum value is set experimentally and is the one that still allows comfortable walking. The amount of decrease is based on pre-assessed perceivable variations.

*** A decrease in the gastrocnemius length means an increase in the push-off assistance.

Chapter 6. Applications

Table 6.5 – Measurements and instruments used for walking biomechanical assessment. W-F: walking free, W-R: walking with the robot

			Walking condition	
			W-F	W-R
Measured quantity	Joint angles	Hip	Optoelectronic motion capture system	Optoelectronic motion capture system
		Knee		WE1 encoders
		Ankle		
	Assistive torques	Knee/ankle	Inverse dynamics torques from motion capture system	WE1 torque sensors
	Spatio-temporal parameters	Stance/swing duration	WE1 sensorized insoles and/or force plates	WE1 sensorized insoles
		Velocity, step length, step width	Force plates	
	GRFs	AP, ML, V		
	EMG	TA, SO, GA, RF, BF, VL	Surface EMG sensors	

Biomechanical assessment

The biomechanical measurements performed during walking are reported in Table 6.5.

Clinical Assessment

Similarly to the experiment on the Achilles (Section 6.2), test pilots underwent a battery of clinical evaluations before and after 5 training sessions, as detailed in Table 6.2 and the Appendix E. Furthermore, during each training session, the 10MWT was assessed before and after the training, with and without the use of WE1.

Results

Walking speed

During gait training, test pilots walked with their self-selected assistive aid, according to their WISCI level. Test pilots walked at a wide range of speeds with NMC assistance, from a minimum of 0.21 m/s to a maximum of 1.08 m/s (speeds are summarized in Table 6.6, and Fig. 6.8 and 6.9). All test pilots achieved with a faster maximum walking speed with NMC assistance than without (both while wearing WE1 (ZIM, W-R-Z-T0) and without (shod, W-F-T0)). Interestingly, for S2 and S3, the NMC condition (W-R-T0) also led to the fastest mean speed. The 5 training sessions had no major effects on speed improvements.

Walking speed can be changed by adjusting step length, step frequency, or a combination of

6.3. II : NMC for incomplete SCI on the WE1 exoskeleton

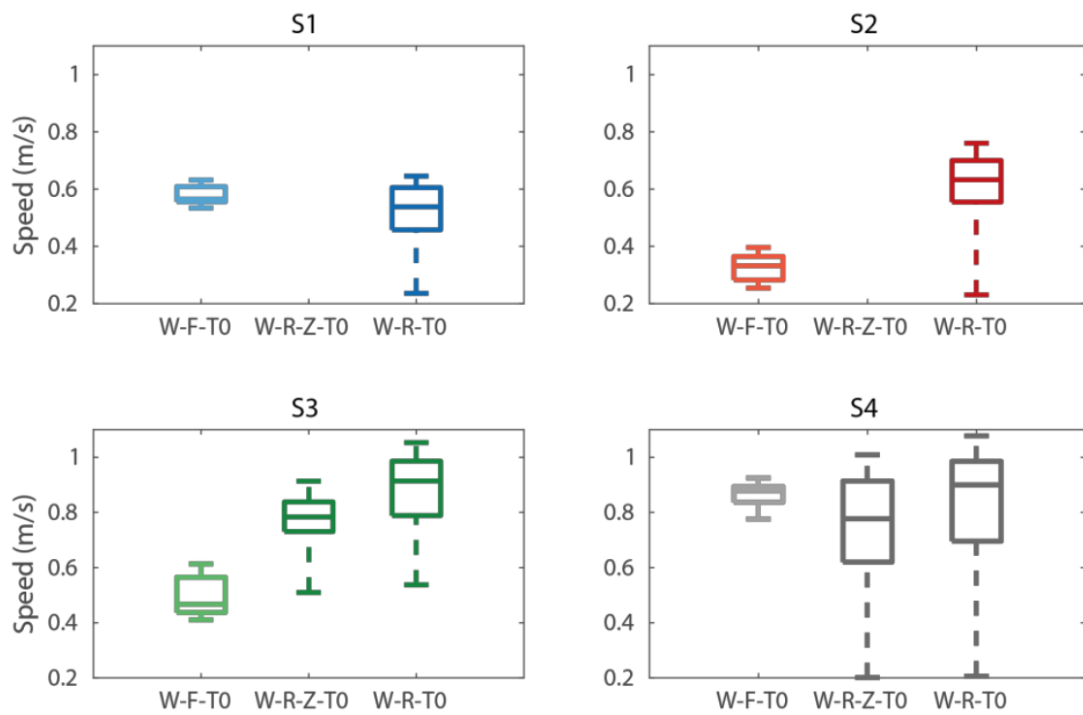


Figure 6.8 – Boxplot of walking speeds at T0. The middle line in the box is the median speed while the bottom and top edges represent the 25th and 75th percentile, respectively. The whiskers extend to the minimum and maximum speeds. Strides with stride times $t < 0.8$ s and $t > 3$ s and speeds < 0.2 m/s were discarded to avoid any turning or very small steps at the beginning or end of the trial.

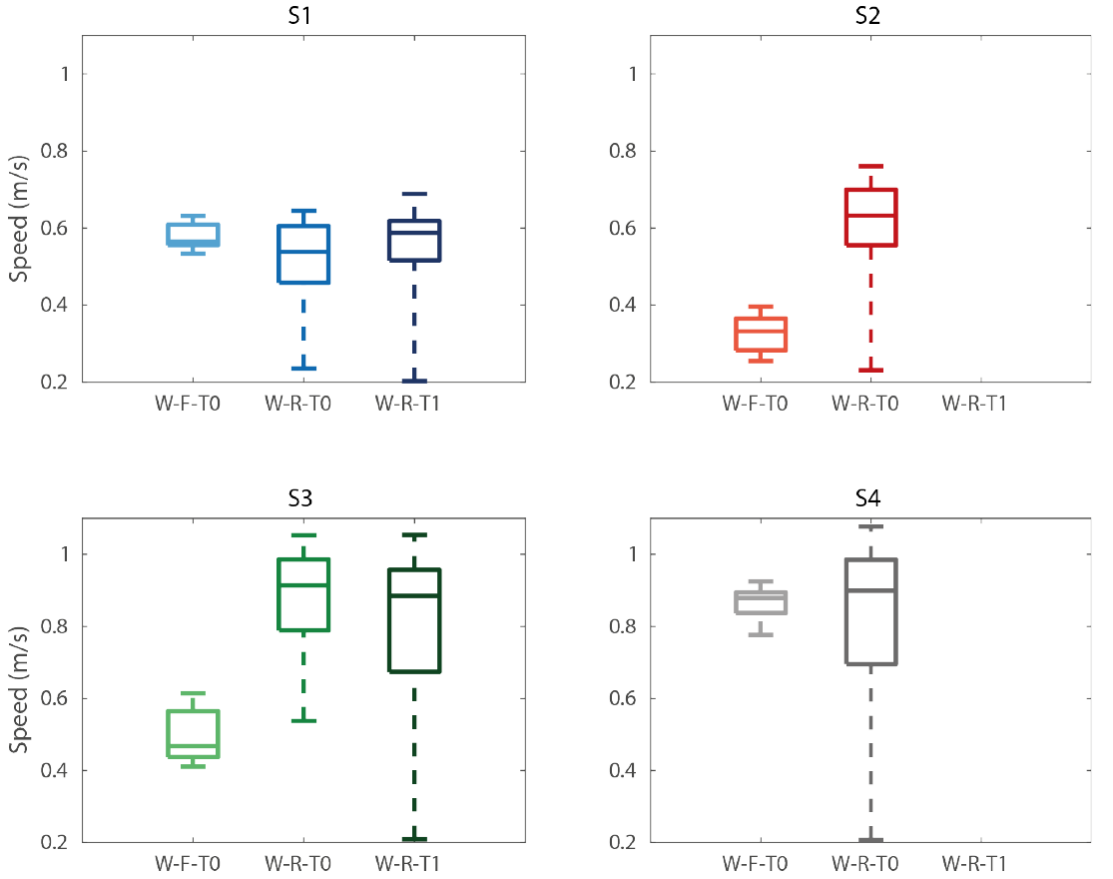


Figure 6.9 – Boxplot of walking speeds. The middle line in the box is the median speed while the top and bottom edges represent the 25th and 75th percentile, respectively. The whiskers extend to the maximum and minimum speeds. Strides with stride times $t < 0.8$ s and $t > 3$ s and speeds < 0.2 m/s were discarded to avoid any turning or very small steps at the beginning or end of the trial.

6.3. II : NMC for incomplete SCI on the WE1 exoskeleton

Table 6.6 – Range of walking speeds for each condition. Strides with stride times $t < 0.8$ s and $t > 3$ and speeds < 0.2 m/s were discarded to avoid any turning or very small steps at the beginning or end of the trial.

Test pilot	Condition	Speed (m/s)		
		Min	Mean \pm SD	Max
S1	W-F-T0	0.53	0.58 \pm 0.03	0.63
	W-R-T0	0.24	0.52 \pm 0.11	0.65
	W-R-T1	0.20	0.54 \pm 0.12	0.69
S2	W-F-T0	0.25	0.33 \pm 0.05	0.40
	W-R-T0	0.23	0.61 \pm 0.12	0.76
	W-R-T1	--	--	--
S3	W-F-T0	0.41	0.50 \pm 0.07	0.61
	W-R-T0	0.54	0.87 \pm 0.15	1.05
	W-R-T1	0.21	0.80 \pm 0.21	1.05
S4	W-F-T0	0.78	0.86 \pm 0.04	0.92
	W-R-T0	0.21	0.81 \pm 0.24	1.08
	W-R-T1	--	--	--

both. For healthy individuals, the preferred speed and step length relation can be characterized by a power law [31] (see Section 6.4.2 for details), which represents the compromise between the cost of swinging our legs and the cost of body center of mass redirection. We determined the changes in step length with speed for the SCI test pilots to evaluate how close they were to healthy gait (Fig. 6.10) by calculating the exponent β for the equation $L = v^\beta$ where L is stride length and v is walking speed. For healthy individuals, β is 0.54 ± 0.1 (mean \pm standard deviation)[31]. The relationship between gait speed and stride length showed interesting results, as presented in Fig. 6.10. For S1 and S4 walking in free mode, stride length was almost not dependent on the speed (poor fits to the equation due to a small speed range), while for S2 and S3 stride length varied almost linearly with speed in the same condition. Similarly to what happened for S2 and S3 in W-F condition, all the test pilots nearly linearly modified the stride length with speed when walking in W-R condition. This data indicates higher speed variability for the whole cohort in the W-R condition in comparison to W-F condition, thus demonstrating that WE1 allowed users to freely self- select speed, due to the intrinsic features of NMC.

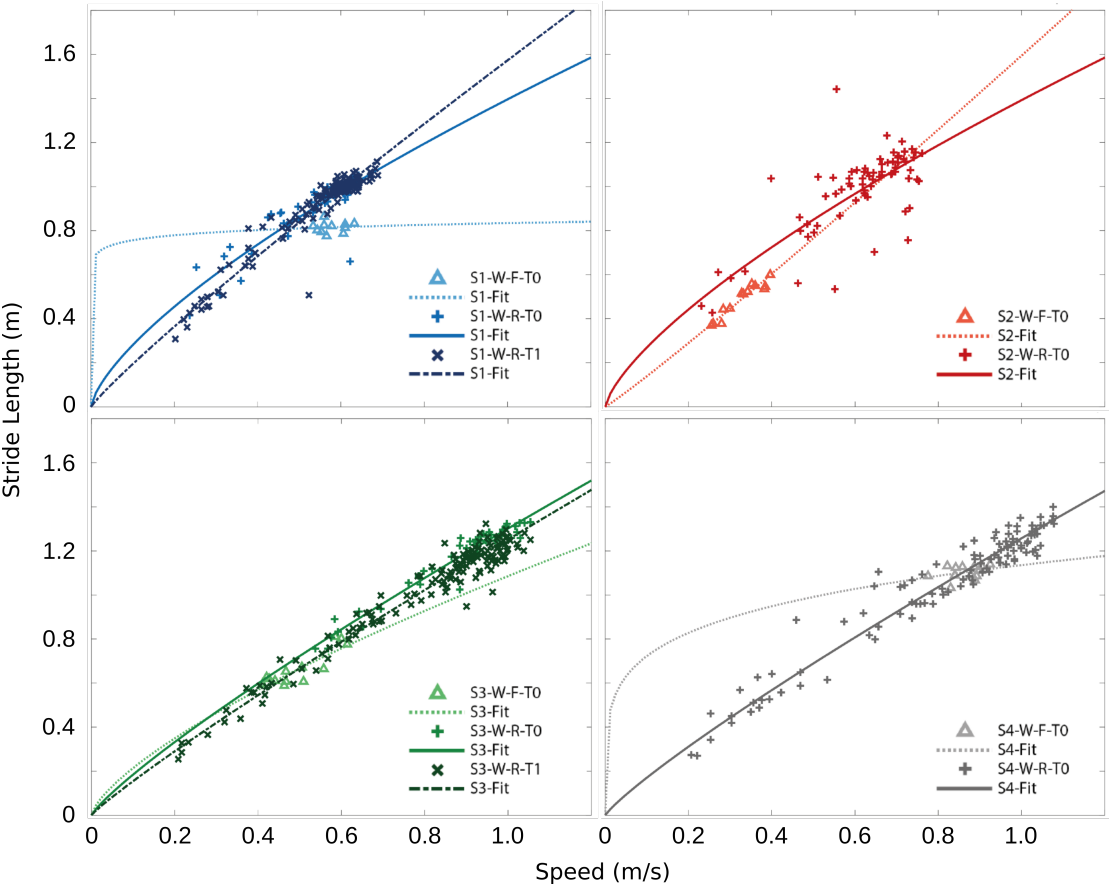


Figure 6.10 – Speed and stride length for each subject for the W-F-T0 (triangle), W-R-T0 (plus), and W-R-T1 (cross) conditions and fits (to the log of speed and stride length; dotted, solid, and dash-dotted lines).

6.3. II : NMC for incomplete SCI on the WE1 exoskeleton

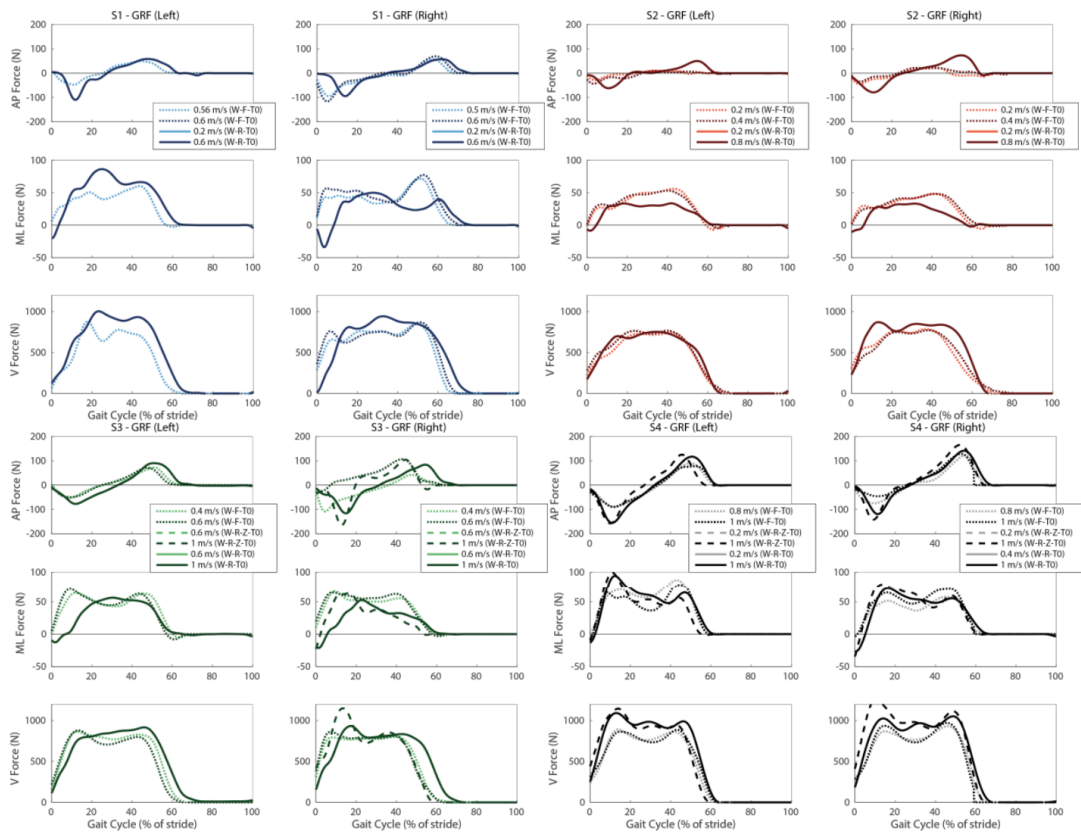


Figure 6.11 – Ground reaction forces for each subject for W-F-T0 (dotted), W-R-Z-T0 (dashed), and W-R-T0 (solid) conditions for two different speeds (fast: dark, slow: light). Missing forces indicate that those strides were taken while not on a force plate.

Ground Reaction Forces, joint kinematics and measured torques

The NMC did not negatively alter the test pilots' ground reaction forces (GRFs, Fig. 6.11), as W-R-T0 GRFs were similar in profile with W-F-T0 shod conditions. While qualitatively there was no clear trend among test pilots, NMC did not necessarily lead to more impulsive (and thus unpleasant) collisions at heel-strike (see loading rates for GRF vertical). W-R conditions had greater vertical ground reaction forces on average, due to the additional weight of the WE1 device. NMC conditions (W-R-T0) had greater peak fore-aft forces, signifying larger braking and propulsive forces. S3 had a shallower vertical force loading rate with NMC than without, indicating a smoother impact at heel-strike. For both S3 and S4, the zero impedance condition (W-R-Z-T0) had the greatest loading rate and highest impact.

Test pilot joint kinematics and kinetics were similar to healthy gait (Fig. 6.12), although some differences did exist. The NMC provided peak ankle plantarflexion torque for all test pilots to assist in ankle push-off, but the overall ankle range of motion remains small. Knee angles were similar in profile, with the exception of WE1's end stop preventing S1 and S4 from

overextension. Hip angles, which were not controlled by NMC, were not perturbed and were similar in profile to W-F-T0 conditions (except for the slow speeds of S4). For W-R-T0, there was little knee extension torque and more knee flexion torque during early stance. Compared to the tests performed on the Lopes, see Section 6.4, where knee flexion torque is missing during mid to late stance, here the knee flexion is present, presumably because of the existing gastrocnemius in the ankle module.

Differing methods for recording kinematics between W-F-T0 and W-R conditions may account for some of the disparities in joint angles. For the W-R conditions, ankle and knee kinematics and torques were measured from WE1. These conditions also include hip kinematics calculated from motion capture of a reduced marker set but no hip torques. For the W-F-T0 condition, joint kinematics were measured fully from motion capture (OptiTrack, NaturalPoint, Corvallis, OR, sampling frequency 120 Hz), and joint torques were calculated from inverse dynamics (Opensim [40]) using motion capture and ground reaction forces (BTS Engineering, Brooklyn, NY USA, sampling frequency 500 Hz). For almost all subjects (except S3), there is an offset in mean hip angle between W-F-T0 and W-R-T0. Nevertheless, with the exception of the left knee for S2, WE1 and motion capture measured angles (ankle and knee) are within similar ranges.

Summary of achievement

The neuromuscular controller (NMC) was successfully implemented and tested on the WE1 device with four group I test pilots presenting different anthropometric dimensions, levels of lesion and walking abilities. Results indicate that the NMC can support gait for a large range of speeds and is capable of generating healthy-like gait for test pilots, in terms of kinematics and torques. Using only a fixed set of controller gains tailored to each user's needs, the diversity of gaits achieved demonstrates the versatility and capability of a bio-inspired controller. In the following Sections, we will evaluate whether these results can be extended to other exoskeletons and a group of test pilot presenting more severe walking impairment (group II).

6.3. II : NMC for incomplete SCI on the WE1 exoskeleton

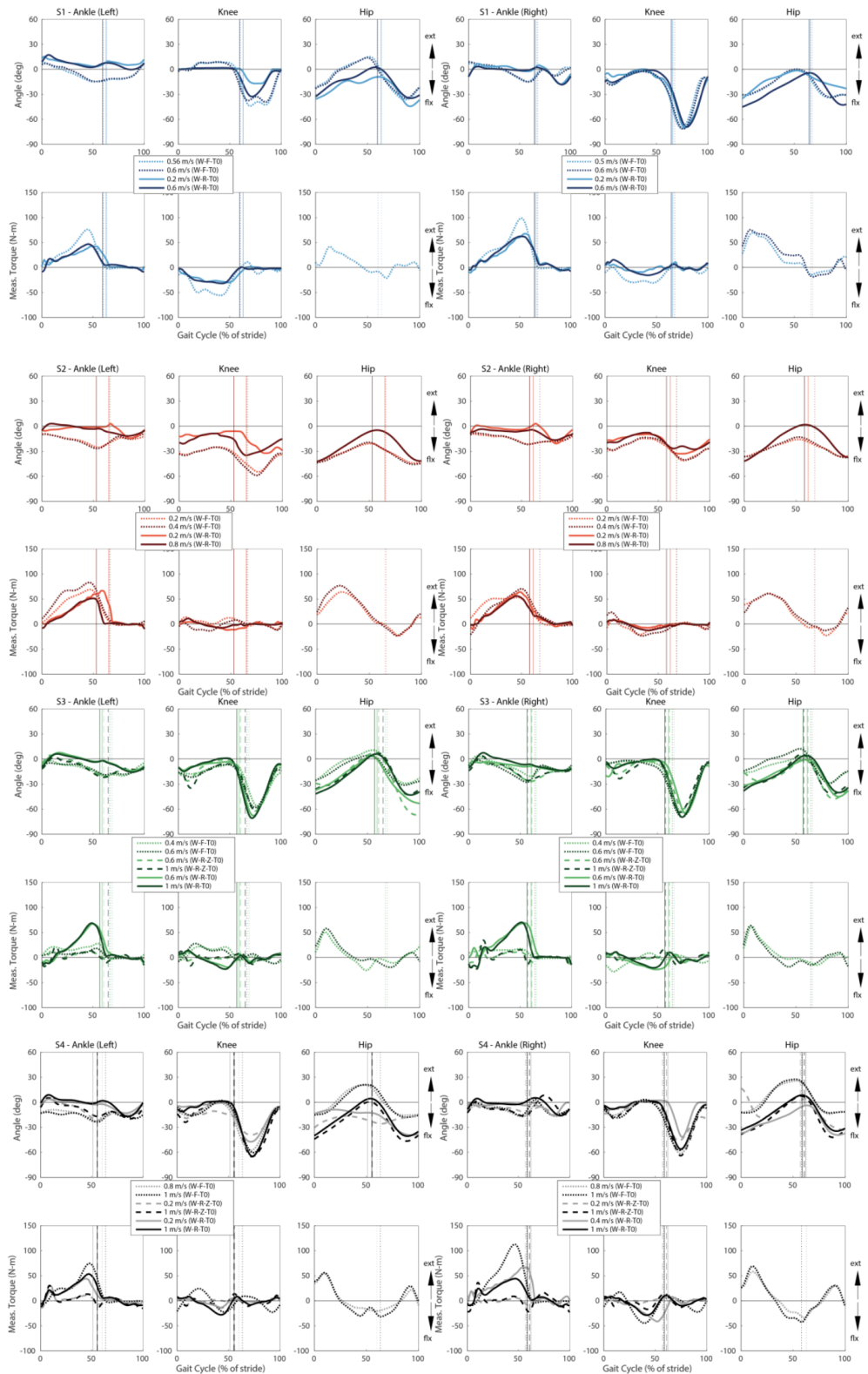


Figure 6.12 – Joint angles, torques, and power for each subject for walking conditions W-F-T0 (dotted), W-R-Z-T0 (dashed), and W-R-T0 (solid). Average strides at two different speeds (fast: dark, slow: light). Toe-off indicated by vertical lines. Positive: extension, negative: flexion.

IV : NMC for complete SCI on the LOPES gait trainer

Introduction

The challenges of developing an effective controller for assistive and rehabilitative robotic devices stem from both incomplete knowledge of healthy neurophysiology and biomechanics and the difficulty in translating such knowledge, however incomplete, into control algorithms. While observed properties of human gait can be reproduced (e.g. joint trajectories), it is unclear how to produce gait that can adapt to a variety of situations and terrains. For individuals with impaired motor functions, active and natural interaction between user and device is crucial for promoting motor recovery and increasing brain plasticity [160, 176, 175]. Therefore developing a controller that is safe and intuitive to operate, responsive to the user's intentions, and adapts to any walking situation is an unsolved but necessary challenge.

Controllers of assistive exoskeletons generally uses predefined movement patterns. This may entail imposing a specific walking pattern (e.g. early versions of Lokomat [32]), which does not require active user involvement and thus may encourage slacking [180] and reduce motor recovery capacity. Another class of controllers mitigates this problem by assisting the subject when needed (e.g. when the subject's movement is deviated from the desired pattern [14, 194]). This can be achieved by modulating the stiffness and damping properties of the controller, and knowing these properties allows controller actions to be stable and predictable. However, references trajectories for a variety of speeds and situations are needed to extend walking beyond one particular set of motion.

User intention is another challenge, and some simple and unambiguous user interface solutions include manual inputs (e.g. push-button) or voice commands. However, these user-activated gaits may be too generic and therefore susceptible to the lack of interaction discussed previously. They also do not address multi-joint level human-machine interaction. However, requiring the user to command lower levels of control (e.g. actuate multiple degrees of freedom) can also lead to high cognitive demands [204]. Hence there is a need to find the right balance among reducing the degrees of freedom to be controlled, effective subject involvement, and adaptability.

One interesting approach to encourage shared control that is amenable to different gait conditions is myoelectric control, which uses electromyographic activity (EMG) to generate command signals. Myoelectric control does not require reference signals, and users can actively command their device with modulation of their own muscle signals [68, 70]. However, this method relies on clean and reliable signals from functional muscles, which will often be impractical or even impossible to obtain with paraplegics due to their motor control problems.

To promote positive shared user-machine control, bio-inspired controllers that mimic the user's own neuromuscular system are one potential solution. Current approaches include leveraging complex musculoskeletal models with virtual Hill-type muscles [97] activated by reflexes [79]. This model has no predetermined patterns of movement, and walking emerges

from the interaction of body dynamics, reflex loops, and virtual muscles with the environment. Not only can the model recreate human behavior such as joint kinematics, kinetic measures, and muscle activations, but it can also walk at a variety of speeds and is robust against perturbations and environmental disturbances in simulation [192]. Controller versions of these models, called neuromuscular controllers (NMC) or reflex-based controllers, have also been implemented on lower limb prostheses [62, 202] and on assistive devices [75, 60] with promising results.

We investigated the capabilities of the NMC with a haptic gait trainer worn by subjects with a Spinal Cord Injury (SCI). This is the first known application of this controller on a knee and hip robotic device with SCI subjects. We hypothesize that the NMC's virtual dynamics and few sensory inputs could generate healthy-like gait at several speeds for subjects with a diverse range of walking abilities. With NMC assistance, we anticipate that simulating biological muscle motion could allow active recruitment of the user's own neuromuscular system, possibly for rehabilitation.

Material and Methods

Neuromuscular Controller (NMC)

The NMC control paradigm uses a neuromuscular model (NMM) to derive the reference torque pattern used to drive the exoskeleton. In this contribution, the NMM used is based on the gait simulation proposed by H.Geyer [79], where the torques applied to the different lower limb joints comprise combined contributions from 14 leg muscles (seven per leg). The activity of each muscle is the result of different reflex loops that act depending on the gait cycle. During stance, the reflex loops induce higher activity in extensor muscles to favor weight bearing support. When the swing phase is initiated, the reflexes induce a reduction of extensor activity and an increase of flexor activity (see Fig. 6.13A for a detailed description of the NMC).

The advantages of this controller over other approaches include robustness, modularity, and adaptability. In particular, the NMC:

- does not require filtering of its inputs (as with myoelectric control),
- can be decomposed into relevant modules (e.g. only knee or hip control), allowing for easy adaptation to different exoskeletons
- can be modulate the level of assistance (i.e. through scaling commanded torques) to account for subject-specific conditions, such as between legs (to accommodate for left / right asymmetry), between joints of the same leg (to accommodate for joint level asymmetry), and within joints (to accommodate for muscle weakness, i.e. flexor / extension asymmetry).
- can generate walking at different speeds and on different terrains [191, 192].

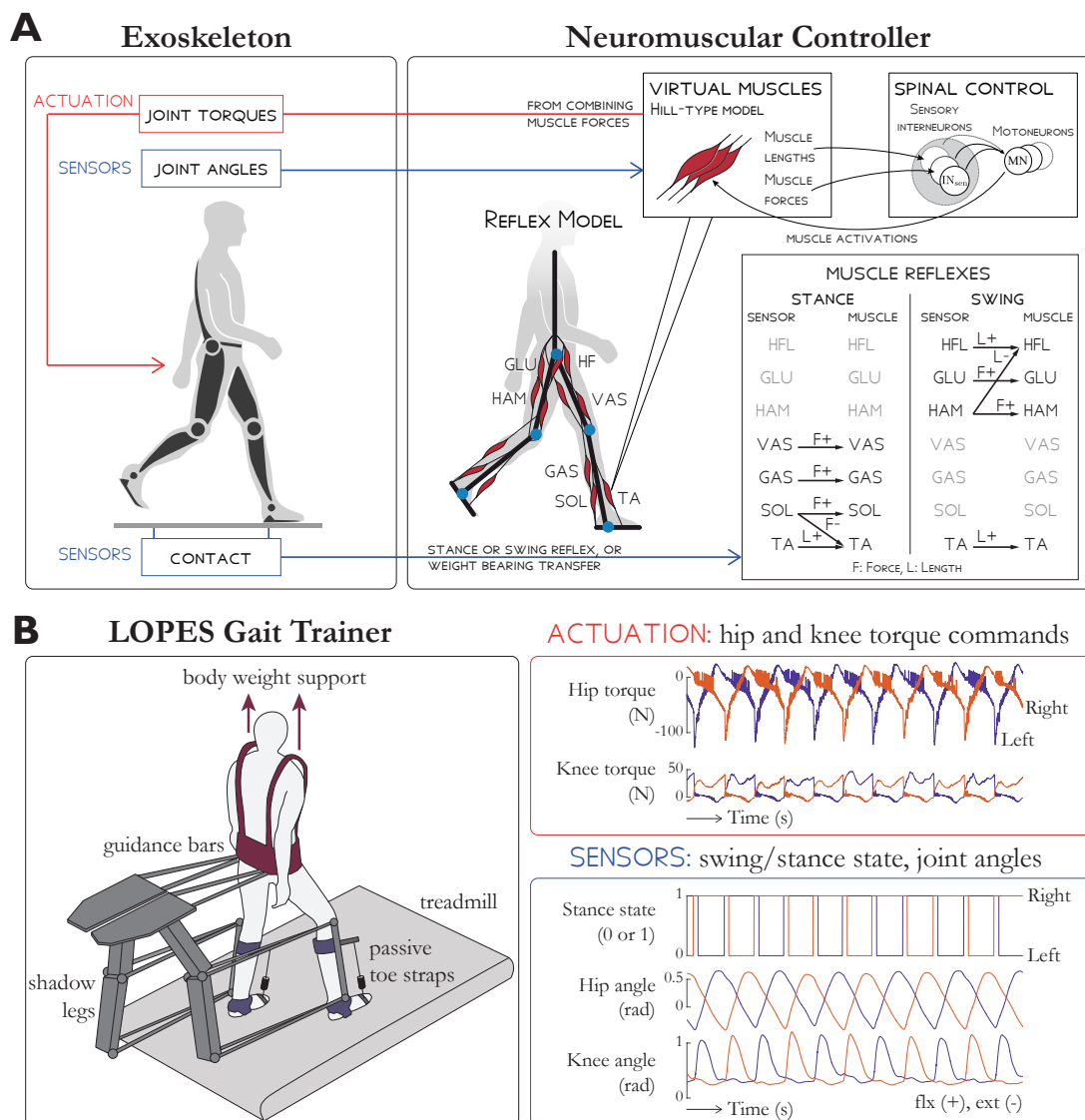


Figure 6.13 – Schematic overview of (A) the NMC and (B) the LOPES gait trainer. (A) Sensors on the exoskeleton are used to detect ground contact. Then, depending on whether the limb is in stance or swing, different reflex rules are activated (shown on the bottom right table). An extra term is added to the hip flexors HFL and hip extensors GLU to facilitate the weight bearing transfer during double support. The reflex loops (which use muscle length, stretching velocity and tendon force) are then combined to stimulate virtual Hill-type muscles which then generate active torques on exoskeleton joints. (B) Subjects in LOPES walk on a treadmill with body weight support. Knee and hip actuation is provided with guidance bars moved by shadow legs, and passive toe straps prevents toe drag. The NMC provides hip and knee torque commands. Sensory input into NMC include stance state, hip angle, and knee angle for both legs. LOPES figure based on [136].

6.4. IV : NMC for complete SCI on the LOPES gait trainer

The last point raises a very interesting aspect of this controller. Instead of constraining a specific motion and resisting against all other external forces, the NMC has the capacity to both work with or against external forces, depending on the direction of the external forces and the current muscle states. For example, during swing at the hip joint, the controller generates a large burst of flexor activity to swing the leg forward. During that period, the NMC's response to an external force on the hip joint would depend on the direction of its application. An extensor torque would act against the controller while flexor torque would act together with the controller. This feature and the ability of the model to produce movement and interaction dynamics in agreement with human locomotion ensures that, barring volitional hindrance by the subject, both the controller and the subject will work in concert. When combined with the modularity aspect of the NMC, this approach allows for easier design of controllers tailored to both the specificity of the subject and of the device.

The virtual muscles of the NMC are the tibialis anterior, soleus, gastrocnemius, vasti muscles, hamstrings, hip flexors, and glutei muscles (Table 6.7). Since the LOPES gait trainer had only knee and hip actuation, we used only the knee and hip NMC modules. This excluded all muscle contributing to the ankle (i.e. the tibialis anterior, soleus, and gastrocnemius). A gain multiplying the normal torque output of the knee and hip controller was used to scale the level of assistance. The gain was applied as a percentage, where 100% was the nominal provided torque and 0% was zero NMC torque, which defaulted to Zero Impedance Mode (ZIM, where the generated torques are to make the device feel as transparent as possible). The assistance gain could also be further tailored to act on specific joints or sides of the body. The nominal torques provided by the controller corresponds to those one needed for a human of 80 kg in mass and 1.8 m in height to walk at 1.3 m/s.

There are two important differences between the NMM proposed by H.Geyer and the one used here for the NMC. First, to reduce the complexity of the sensors to be used, a simplified version of the weight transfer reflex is used that does not require GRFs but only a ground contact information (the activity of the vastus muscles is decreased or increased depending a filtered version of the ground contact information). Second, the trunk balance reflex (proportional-derivative feedback control acting on the trunk to ensure that the trunk stays upright) is not used. This limits the use of NMC for SCI subjects with very good control of their trunk and thus excludes paraplegics with lesions above C7.

Table 6.7 – Virtual muscles of the neuromuscular controller, their actions, and whether or not they were used in LOPES

Muscle	Action	In LOPES?
Gluteus (GLU)	Hip extension	Yes
Hip flexor (HFL)	Hip flexion	Yes
Hamstring (HAM)	Hip extension, knee flexion	Yes
Vasti (VAS)	Knee extension	Yes
Gastrocnemius (GAS)	Knee flexion, ankle plantarflexion	No
Soleus (SOL)	Ankle plantarflexion	No
Tibialis anterior (TA)	Ankle dorsiflexion	No

Experiment

LOPES gait trainer The haptic gait trainer LOPES, see Fig. 6.13B [135] consists of shadow legs that help move the subject and a treadmill. The subject is provided body weight support through a harness and is also attached to the device at the waist and at the shank with leg clamps. Active degrees of freedom include shank flexion/extension, thigh flexion/extension and hip abduction/adduction. LOPES can impart up to 70 N-m of knee torque and hip torque [135], within range of biological torques and therefore able to move the lower limbs of a fully paralyzed subject. The pelvis can also be moved in the forward/aft direction and in the frontal plane. Since the ankle is unactuated, passive toe straps in series with springs were used to prevent toe drag.

Participants Seven adult subjects walked with a lower limb gait trainer controlled by the NMC. Of the seven subjects, one was healthy (i.e. no neurological deficits, female, 32 years of age, mass M 58 kg, height L 1.79 m), and the six others had a spinal cord injury (see Table 6.8 for subject information). Neurological status of SCI subjects was assessed using the American Spinal Injury Association (ASIA) and ASIA Impairment Scale. Of the SCI subjects ($N=6$, 2 female, 4 male, 24 to 52 years of age, mass M 69.5 ± 14.9 kg, mean \pm s.d., height H 1.79 ± 0.07 m), two had incomplete injuries (Group I - AIS level C and D) and the others had a complete injury (Group II - AIS level A). All subjects provided written informed consent prior to the study, according to Institutional Review Board procedures.

Table 6.8 – Subject characteristics. SHL is a healthy subject, S1A and S2A are Group I subjects (incomplete injury), and S2A, S2B, S2C, and S2D are Group II subjects (complete injury). Lesion and AIS level from clinical neurological assessment, lesion time is the time from lesion diagnosis to data measurement (in months).

Subject	G	Gen.	Age (year)	W (kg)	H (m)	Lesion level	AIS level	Lesion time (months)
SHL	-	F	32	58	1.79	-	-	
S1A	I	F	35	48	1.65	T12	C	33
S1B	I	M	33	90	1.85	L1	D	18
S2A	II	M	52	82	1.78	T7	A	13
S2B	II	M	25	64	1.85	T11-T12	A	71
S2C	II	M	28	70	1.82	T9	A	49
S2D	II	M	24	63	1.80	T7	A	61

Protocol Subjects walked at a variety of speeds and controller assistance levels, depending on their ability and comfort level. At the beginning of each trial, two experimenters manually maneuvered each leg of the SCI subjects to initiate gait at very slow speeds. Then treadmill speed and controller gains were increased until the subject could walk independently with the controller and without manual assistance. Body weight support (BWS) was also provided, and

6.4. IV : NMC for complete SCI on the LOPES gait trainer

subjects could use the handrail for support. Trials ranged from approximately 2 minutes to 5 minutes long with an average of 112 strides, from which a subset is shown here.

Measurements We evaluated the joint kinematics and muscle activity as well as the joint torques provided by the controller and virtual muscle properties. Knee and hip joint angles and controller torques were measured from LOPES. The LOPES also measures the total ground reaction force, but not the contribution from each leg. Therefore gait event detection provided to the controller was estimated from the vertical linear velocity of the ankle joint and the angular velocity of the knee, similar to the method reported in [149]. We calculated the contribution of handrail usage by subtracting body weight support from the overall bodyweight unloading. Overall unloading was calculated from the average vertical ground reaction force as measured by LOPES and the subject's weight.

We calculated joint power to determine the amount of work performed on the subject by the controller. Joint power (W) was derived from joint angular velocity (time derivative of joint angles) multiplied by joint torques. Joint work (J) was calculated from the integral of positive (or negative) components of power over time over a gait cycle. Virtual muscle lengths, velocities, and activations were determined post-experiment because they were not recorded in situ. We simulated the experiment by sending the controller the same sensory inputs (i.e. joint angles, ground contact) as during the experiment.

Electromyographic (EMG) activity of eight muscles was recorded with surface electrodes from the least affected leg (wired Bagnoli system, Delsys, Boston, MA, USA). The muscles measured were the tibialis anterior (TA), soleus (SOL), gastrocnemius medialis (MGAS), vastus lateralis (VL), rectus femoris (RF), biceps femoris (BF), semitendinosus (ST), and gluteus maximus (GMAX). EMG signals were recorded at 1000 Hz. In post-processing, all signals were high-pass filtered with a 20 Hz cutoff frequency (fourth-order Butterworth filter, zero-lag). They were then full-wave rectified and low-pass filtered at 10 Hz (zero-lag) to obtain the linear envelope. Each EMG signal was then normalized by its maximum amplitude over all conditions to obtain a maximum activation of unity.

Analysis We were primarily interested in whether or not NMC-controlled LOPES could recreate healthy-like gait in SCI subjects. To assess this question, we compared the joint angles and the provided joint torques of NMC walking against joint angles and biological joint torques from healthy shod walking. We also compared EMG patterns of SCI subjects with the healthy subject in LOPES and with the virtual muscle activations of the model to assess changes in muscle activity. As a crude method of evaluating energetic optimality, we investigated the speed-step length relation of SCI subjects with NMC. Finally we further studied two SCI subjects, one with an incomplete lesion to compare walking with ZIM and NMC, and another with a complete lesion to study how changing walking speed affected the NMC.

Since each subject had different levels of walking abilities and impaired behavior (experimental

Chapter 6. Applications

conditions summarized in Table 6.9), controller settings and treadmill speed varied, making inter-subject comparisons difficult. Therefore only qualitative assessments in magnitudes and trajectories between healthy NMC, SCI NMC, and healthy shod were made for joint angles, torques, and powers at a particular speed and gain. For S1B, S2C, and S2D, this condition was at 0.6 m/s and 100% gain. S2C data was compared at a faster speed (0.7 m/s) because this subject still needed manual assistance at 0.6 m/s. In contrast, S1A and S2A data were compared at a lower speed and gain. S2A was only able to walk with a combination of NMC and manual assistance. We only show data of the same leg from which EMG measurements were made but acknowledge some small asymmetrical behavior could exist.

Table 6.9 – Subject experiment settings in NMC-controlled LOPES. EMG leg indicates from which leg EMG measurements were recorded. BWS is body weight support provided by LOPES as a percentage of body weight. AS is amount of arm support exerted by the subject as a percentage of body weight. Speed is the walking speed exhibited in Fig. 6.15 and 6.16, and the range of speeds for Fig. 6.14 and Fig. 6.17 are shown parenthetically. Speed Ind. specifies the speed in which subjects did not need manual assistance. Speed* is healthy shod walking speed chosen for comparison against walking with NMC.

Subject	EMG Leg	BWS (%BW)	AS (%BW)	NMC Act (%)	Speed (m/s)	Speed Ind. (m/s)	Speed* (m/s)
SHL	R	0	0	100	1.0	0	1.0
S1A	L	31	12	40	0.4 (0.15-0.5)	0	0.3
S1B	L	36	38	100	0.6 (0.4-1.4)	0.6	0.6
S2A	R	60	24	30	0.35	none	0.3
S2B	L	24	34	100	0.6 (0.3-0.6)	0.5	0.6
S2C	R	21	48	100	0.7 (0.4-1.0)	0.7	0.6
S2D	R	38	30	100	0.6 (0.4-1.1)	0.6	0.6

A simple burst detection algorithm was used to determine if EMG patterns contained meaningful or noisy signals. Similar to Di Fabio's method [41], we first calculated a 50 ms baseline of non-activity for each muscle signal. Then we evaluated whether or not there was a consecutive 25 ms window of activity that was greater than the mean plus three times the standard deviation of the baseline activity. If this activity existed, then the signal was deemed a viable measurement.

The average EMG traces were also compared against activation signals of its corresponding virtual muscle. Since the NMC is a simplification of the human musculoskeletal system, the vastus lateralis was compared against the modeled vasti activation, the rectus femoris against the hip flexors, biceps femoris and semitendinosus with the hamstring, and the gluteus maximus against the glutei muscle group. Although some subject EMG signals did not contain any activity, it was conceivable that the virtual muscle activations could compensate for the lack of motor function.

For comparison with NMC gait, healthy shod joint measures were derived from one subject (female, 31 years of age, mass M 65 kg, height H 1.63 m) walking on a treadmill at 0.3 m/s, 0.6

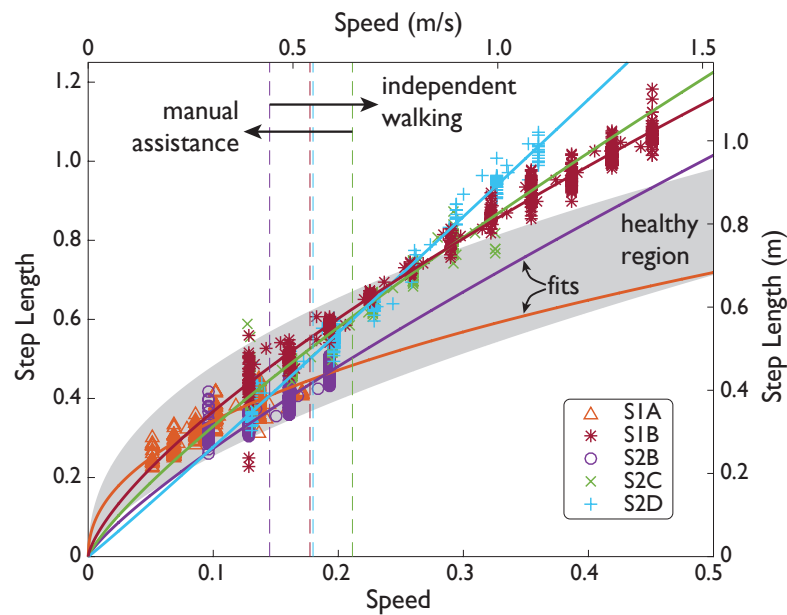


Figure 6.14 – SCI speed and step length over a range of speeds. Subject data (symbols) shown in normalized units (normalized by subject leg length L , and gravity g) and SI units. Manual assistance threshold (dashed lines) indicates the slowest speed included in subjects’ fit (solid lines).

m/s, and 1.0 m/s. We derived kinematics and inverse dynamics (Opensim, Stanford, CA, USA) from motion capture measurements (Phoenix Technologies, Visualeyex, Canada) and ground reaction forces from an instrumented dual-belt treadmill (Motekforce Link, Amsterdam, the Netherlands).

We made two quantitative comparisons across multiple subjects and trials to determine the general behavior of the NMC. First, we assessed whether the NMC could reproduce the speed-step length relation found in healthy gait [83] and second, the relation between speed and joint work [51]. The first relation represents energetically optimal changes in step length with speed. Healthy subjects have been found to walk with a step length s following the power law $s = \alpha v^\beta$ with β typically reported to be 0.54 ± 0.10 [31]. To calculate exponent β (and offset α), we applied a linear regression of $\log s = \log \alpha + \beta \log v$ for each SCI subject for all trials without manual assistance (see Table 6.9 for speed ranges). Since S2B did not walk without manual assistance, his data was excluded from this analysis.

We also determined the relation between speed v and joint work W . Past studies [233] have found that total joint work should be proportional to speed $W = v^{0.28}$. However, it is unclear if the same relation holds for individual joints. Instead we simply performed a linear regression on $W = \alpha + v\beta$ to determine the trend β to understand how NMC torques change with speed.

To further illustrate the effect of NMC speed-related changes, we showed biomechanical

measures from S2D walking at 0.8 m/s, 0.9 m/s, and 1.0 m/s at a constant assistance level of 100%. We also compared the joint trajectories of NMC-controlled gait with the controller inactive (i.e. ZIM) with S1A, who was the only SCI subject to have walked without assistance manually provided by the experimenters.

Analysis was performed on a stride-by-stride basis with each measure calculated as the average over all strides within a condition. All values for comparisons across subjects (i.e. speed, step length, joint work) were analyzed in dimensionless form. We performed linear regression to determine speed-related trends for step length and for joint work. Regression coefficient β was statistically significant if its P-value was less than 0.05 ($P < 0.05$). Normalization was performed using base units of body mass M , leg length L , and gravity g . Leg length L was calculated as $0.530H$ [33]. Step length was normalized by L , speed by \sqrt{gL} , and work by MgL . For reporting purposes, statistical data were converted from dimensionless units to SI units using mean normalization constants of $L = 0.9508\text{ m}$, $\sqrt{gL} = 3.05\text{ ms}^{-1}$, and $MgL = 629\text{ J}$.

Results

With NMC-controlled LOPES, the SCI subjects were able to walk at various speeds (from 0.6 m/s to 1.4 m/s), faster than typical for ambulatory SCI subjects (e.g. average speed from 0.34 m/s to 0.88 m/s [211]). In comparison, only one of the SCI subjects could walk unsupported in LOPES (S1A at 0.4 m/s in ZIM). Their joint angle trajectories were similar to healthy humans, but joint torques were not, due to the lack of ankle actuation in the device and thus active control. For SCI subjects, body weight support unloaded 21% to 60% of their body mass M and use of handrails contributed an additional 12% M to 48% M .

Joint kinematics and kinetics and comparisons with healthy data

The NMC was successful in producing healthy-like walking patterns. NMC joint angles and torques agreed reasonably well with healthy kinematic data and biologically produced torques (Fig. 6.15, first four rows). Differences were found between NMC-provided torques (for both SCI and healthy) and biological torques produced by healthy subjects, including a lack of knee flexion torque near mid-stance and greater hip moment near toe-off. Hip extension torque at heel-strike was also missing. Despite these discrepancies, joint angle trajectories did not seem greatly affected. The torque differences also translated into differences in joint powers (Fig. 6.15, fifth and sixth row), notably more positive hip power around toe-off. On average, more hip work was delivered than knee work (Fig. 6.15, last row).

The interaction between the subject and the NMC-controlled LOPES influences the NMC-provided torques and thus overall gait behavior. For example, healthy subject SHL required less assistance than the SCI subjects. Therefore despite the faster speed and generally larger range of motion, NMC provided SHL with similar or smaller knee and hip torques than for other subjects with the same gain (S1B, S2B, S2C, and S2D) but walking at slower speeds. We

6.4. IV : NMC for complete SCI on the LOPES gait trainer

also expected the NMC to provide less torque at small gains and slow speeds. Indeed NMC delivered relatively small torques and therefore work to S1A and S2A, both of whom walked at slow speeds (0.4 m/s and 0.35 m/s respectively) and low gain (40% and 30% respectively).

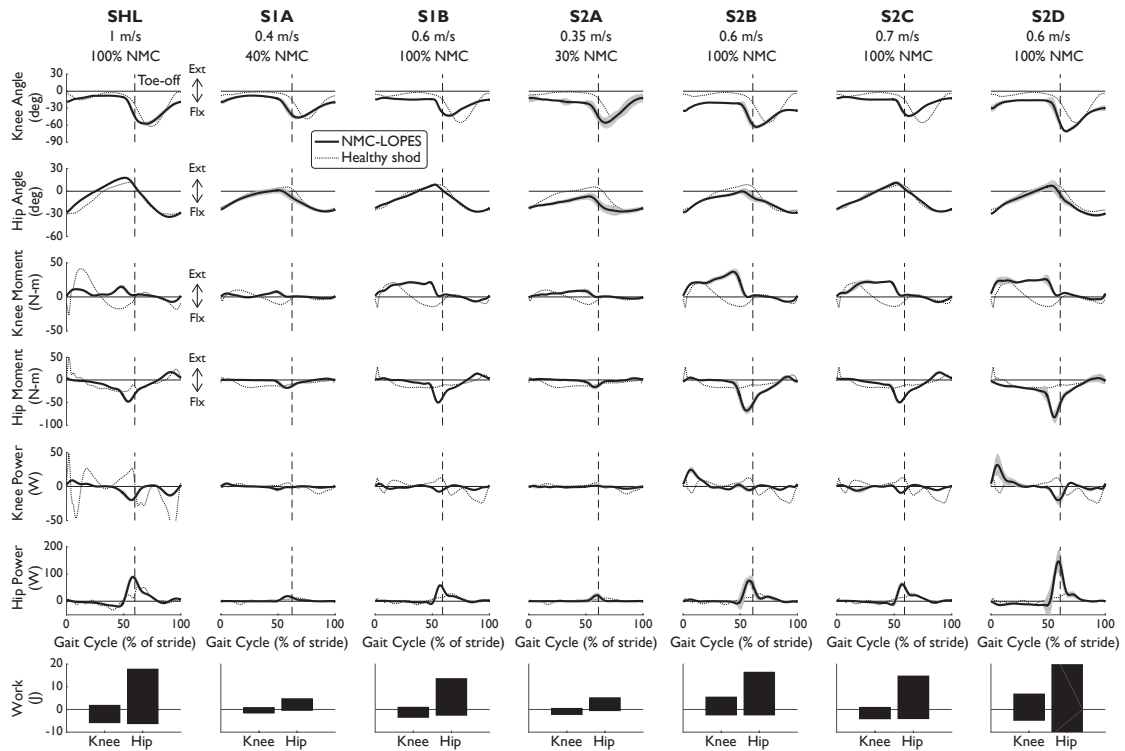


Figure 6.15 – Knee and hip angles and NMC generated moments, torques, power, and work from seven subjects walking with NMC and LOPES. Mean (solid line) and standard deviation (shaded) trajectories are shown along with healthy shod walking (dotted line, see Speed Matched in Tab. 6.9) for comparison. Trajectories are shown as a percentage of gait cycle (% of stride) of one leg (corresponds to "EMG leg" in Table 6.9). Toe-off indicated by dashed vertical line. Ext: positive, Flx: negative.

EMG patterns (Fig. 6.16) indicated that the NMC controller could be inducing rhythmic activation patterns in leg muscles of complete SCI subjects. This could be an expression of remaining reflex pathways that are activated by the movement generated by the legs. This is a very promising results that indirectly provides evidence of remaining functional networks below the lesion.

For three subjects with complete paraplegia, meaningful muscle activity was found at the tibialis anterior and medial gastrocnemius. While these muscles were not modeled in the controller and ankle dorsiflexion/plantarflexion was not an actuated degree of freedom in LOPES, the subsequent walking motion may have activated these muscles, intentionally or not by the subject. Unsurprisingly, systematic muscle activity was found in all muscles measured for the healthy subject. EMG activity was also detected for all measured muscles for S2B

(complete injury), and perhaps this stems from this subject's comparatively low lesion level (T11-T12).

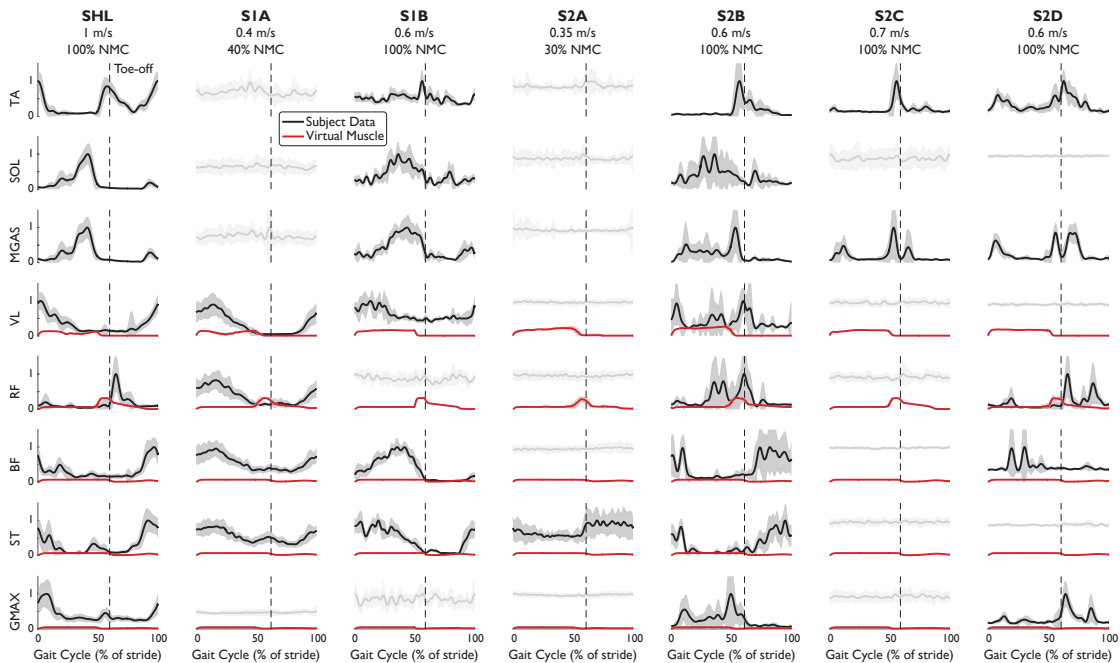


Figure 6.16 – EMG patterns from eight leg muscles of subjects walking with NMC. EMG signals which have met the burst criteria (mean: solid black line), and noisy measurements (light grey) are shown (standard deviation: shaded). Superimposed (red) is muscle activation provided by the virtual muscles in NMC. Trajectories are shown as a percentage of gait cycle (% of stride). Toe-off indicated by dashed vertical line.

While the virtual muscles could serve to supplement missing biological function, the virtual muscles do not seem to differ greatly among subjects, even between SHL and S2A, who only had activity in one muscle. For all subjects, activation signals provided by the virtual muscles were greater for the vasti muscles and hip flexors (compared with subjects' rectus femoris) but small for the hamstring and glutei. The virtual muscle activities are also generally not similar to SHL's EMG activity. This could be due to the weight transfer simplification, which now produces muscle activities that differs from previously reported in simulation [79, 59].

As walking speed increased (along with increases in NMC gain up to 100% assistance), the NMC produced longer step lengths and more joint work. Subjects walked with step lengths that resembled the power law found empirically in healthy gait but were not as energetically optimal due to relatively longer step lengths at faster speeds (Table 6.10). Four subjects demonstrated the power law with $\beta=0.70\pm0.17$ (mean \pm s.d., mean $R^2=0.84$), and one other exhibited a more linear trend ($\beta=1.03$, $R^2=0.98$). Unlike the other subjects who exhibited the power law, S1A showed a shallower increase in step length. This is likely related to fitting to the subject's slow range of speeds (up to 0.4 m/s). For the subjects who exhibited the power law, the average step length at 1.6 m/s was approximately 17% greater than for a healthy human,

this can be explained by the effect of body weight support.

NMC produced greater joint work in response to increases in treadmill speed, more notably at the hip than at the knee (Fig. 6.17, Table 6.10). On average, positive work trend was 5.1 times greater for the hip than for the knee, and 2.7 times greater for negative work. For significant trends ($p < 0.05$), we found that positive hip work increased at a rate from $2.86 \text{ Wm}^{-1}\text{s}$ (S1A) to $63.0 \text{ Wm}^{-1}\text{s}$ (S2B) with mean goodness of fit $R^2 = 0.46$. Negative hip work trend ranged from $-26.6 \text{ Wm}^{-1}\text{s}$ (S2D) to $-1.50 \text{ Wm}^{-1}\text{s}$ (S1A) with mean $R^2 = 0.56$. For the knee, positive work coefficient ranged from $2.44 \text{ Wm}^{-1}\text{s}$ (S2C) to $15.4 \text{ Wm}^{-1}\text{s}$ (S2B) with mean $R^2 = 0.12$, and negative work was from $-13.3 \text{ Wm}^{-1}\text{s}$ (S2B) to $-2.30 \text{ Wm}^{-1}\text{s}$ (S2C) with $R^2 = 0.35$.

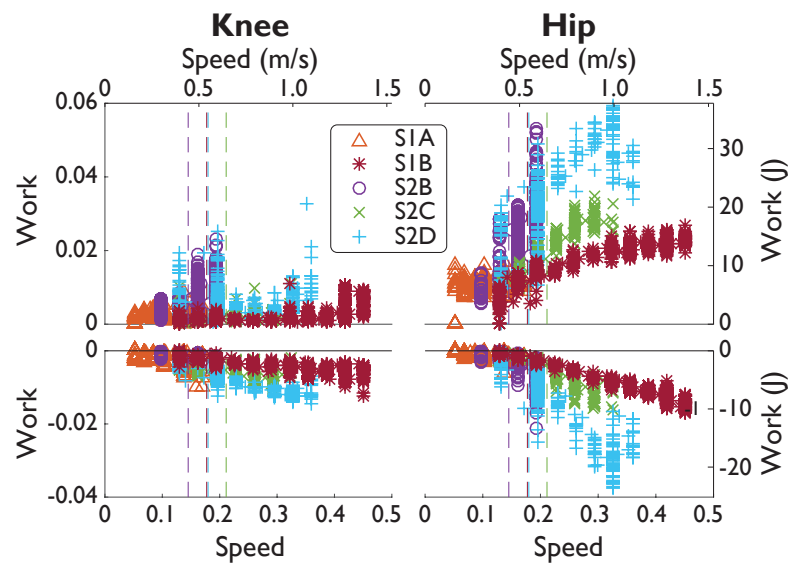


Figure 6.17 – SCI positive and negative joint work over a range of speeds. Subject data (symbols) shown in normalized units (normalized by subject mass M , subject leg length L , and gravity g .) and in SI units. Manual assistance threshold (dashed lines) indicates the slowest speed included in subjects' fit (fits not shown).

Subject S1A (incomplete injury): 40% NMC gain versus ZIM

S1A was the only subject to have walked with LOPES in both ZIM and with the NMC. S1A walked at 0.15 m/s in ZIM and with 40% of NMC assistance. Due to problems in step detection for this subject, only seven strides were analyzed for the NMC condition at this speed while 50 strides were analyzed for zero impedance mode. However, the variability of step parameters are similar for both conditions. NMC served to create shorter strides when compared against zero impedance mode. The average step length with NMC ($0.21 \pm 0.01 \text{ m}$) was shorter than without ($0.28 \pm 0.03 \text{ m}$), as demonstrated by ankle trajectories (Fig. 6.18A). In contrast, the average step width with NMC ($0.26 \pm 0.02 \text{ m}$) was slightly wider than the zero impedance mode ($0.23 \pm 0.03 \text{ m}$). The NMC created a larger range of motion for the knee but reduced motion

Chapter 6. Applications

Table 6.10 – Step length s and knee and hip joint work (positive W^+ and negative W^-) fit parameters, goodness-of-fit, and statistical significance of trend values. Coefficients β and offsets α from linear regression to $s = \alpha\nu^\beta$ or $W = \alpha + \nu\beta$. Significant coefficients are indicated by asterisk if $p < 0.05$. Coefficients and offsets reported in dimensionless units using base units of body mass M , leg length L , and gravitational acceleration g . Coefficients β and offsets α from linear regression to $s = \alpha\nu^\beta$ or $W = \alpha + \nu\beta$. Significant coefficients are indicated by asterisk if $p < 0.05$. Coefficients and offsets reported in dimensionless units using base units of body mass M , leg length L , and gravitational acceleration g .

Parameter	Subject	Coefficient $\beta \pm \text{CI}$	Offset $\alpha \pm \text{CI}$	R^2	P
s	S1A	0.4591 ± 0.0301	0.9880 ± 0.0688	0.8203	0.0000*
	S1B	0.7141 ± 0.0095	1.9007 ± 0.0108	0.9837	0.0000*
	S2B	0.8152 ± 0.0710	1.7865 ± 0.1234	0.6657	0.0000*
	S2C	0.8160 ± 0.0455	2.1572 ± 0.0625	0.8932	0.0000*
	S2D	1.0297 ± 0.0174	2.9703 ± 0.0255	0.9815	0.0000*
W_{knee}^+	S1A	-0.0021 ± 0.0052	0.0023 ± 0.0006	0.0032	0.4284
	S1B	0.0138 ± 0.0023	-0.0020 ± 0.0008	0.2722	0.0000*
	S2B	0.0777 ± 0.0257	-0.0040 ± 0.0046	0.1211	0.0000*
	S2C	0.0113 ± 0.0082	-0.0005 ± 0.0021	0.0478	0.0068*
	S2D	0.0129 ± 0.0088	0.0034 ± 0.0022	0.0313	0.0043*
W_{knee}^-	S1A	-0.0185 ± 0.0071	-0.0001 ± 0.0008	0.1165	0.0000*
	S1B	-0.0107 ± 0.0015	-0.0010 ± 0.0005	0.3555	0.0000*
	S2B	-0.0672 ± 0.0066	0.0090 ± 0.0012	0.6132	0.0000*
	S2C	-0.0107 ± 0.0093	-0.0041 ± 0.0024	0.0335	0.0241*
	S2D	-0.0328 ± 0.0030	0.0006 ± 0.0007	0.6483	0.0000*
W_{hip}^+	S1A	0.0204 ± 0.0103	0.0083 ± 0.0012	0.0711	0.0001*
	S1B	0.0339 ± 0.0020	0.0082 ± 0.0007	0.7565	0.0000*
	S2B	0.3173 ± 0.0483	-0.0288 ± 0.0086	0.3942	0.0000*
	S2C	0.0851 ± 0.0127	-0.0038 ± 0.0033	0.5399	0.0000*
	S2D	0.1258 ± 0.0140	0.0081 ± 0.0035	0.5495	0.0000*
W_{hip}^-	S1A	-0.0107 ± 0.0031	-0.0000 ± 0.0004	0.1906	0.0000*
	S1B	-0.0434 ± 0.0014	0.0056 ± 0.0005	0.9140	0.0000*
	S2B	-0.1088 ± 0.0184	0.0145 ± 0.0033	0.3451	0.0000*
	S2C	-0.0767 ± 0.0109	0.0108 ± 0.0028	0.5614	0.0000*
	S2D	-0.1383 ± 0.0087	0.0175 ± 0.0022	0.7912	0.0000*

for the hip, contributing to shorter step lengths (Fig. 6.18B). EMG activity seemed similar in magnitude and activation pattern, except for the gluteus muscle, where the mean activity was slightly higher on average (Fig. 6.18C).

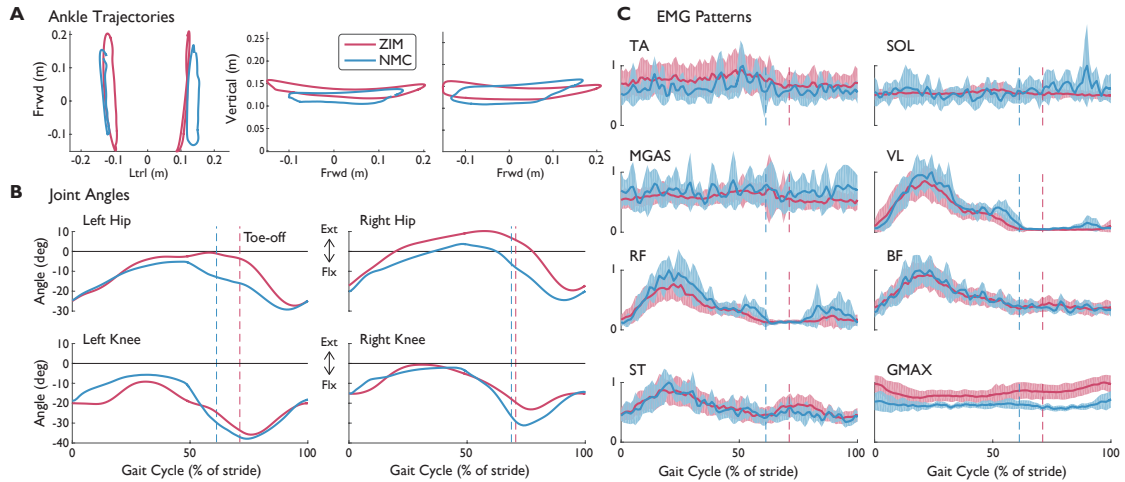


Figure 6.18 – (A) Left and right ankle trajectories, (B) knee and hip angles, and (C) EMG patterns with standard deviations (shaded) from S1A (incomplete SCI injury) with NMC assistance and without (ZIM) at 0.15 m/s. Trajectories are shown as a percentage of gait cycle (% of stride). Toe-off indicated by dashed vertical line. Ext: extension, Flx: flexion

Subject S2D (complete injury): Speed-related changes at 100% NMC gain

We observed that NMC’s gait adaptations to different speeds were similar to observations of healthy subjects walking at different speeds. In particular, in response to treadmill speed changes, the NMC automatically modulated the torques exerted on the subject. We evaluated speed-related changes for S2D, who walked at 0.6 m/s, 0.9 m/s, 1.0 m/s at 100% of NMC assistance. The increase in walking speed produced greater step lengths (0.51 ± 0.02 m, 0.82 ± 0.02 m, 0.89 ± 0.02 m from slowest to fastest speed) while step width changes showed no trend (0.24 ± 0.03 m, 0.31 ± 0.02 m, 0.27 ± 0.02 m).

Speed increases led to greater magnitudes in joint angle, similar to healthy humans (Fig. 6.19). In addition, NMC provided more peak torque, especially at the hip, as humans would increase biological torques to walk faster. While little changes were observed in peak powers, positive and negative work did increase with speed (with the exception of positive knee work).

We investigated the muscle force, contractile velocity, and length from NMC’s virtual muscles (Fig. 6.20). The speed-related increase in torque was produced mainly by changes in the length of the virtual muscles rather than by velocity. In congruent with how greater speeds induce longer strides, the hip extension muscles (i.e. hamstring and glutei muscles) were more contracted at fast speeds than slow speeds around maximum hip extension (approximately 50% of gait), and the hip flexor muscles were more extended. The vasti muscle did not show

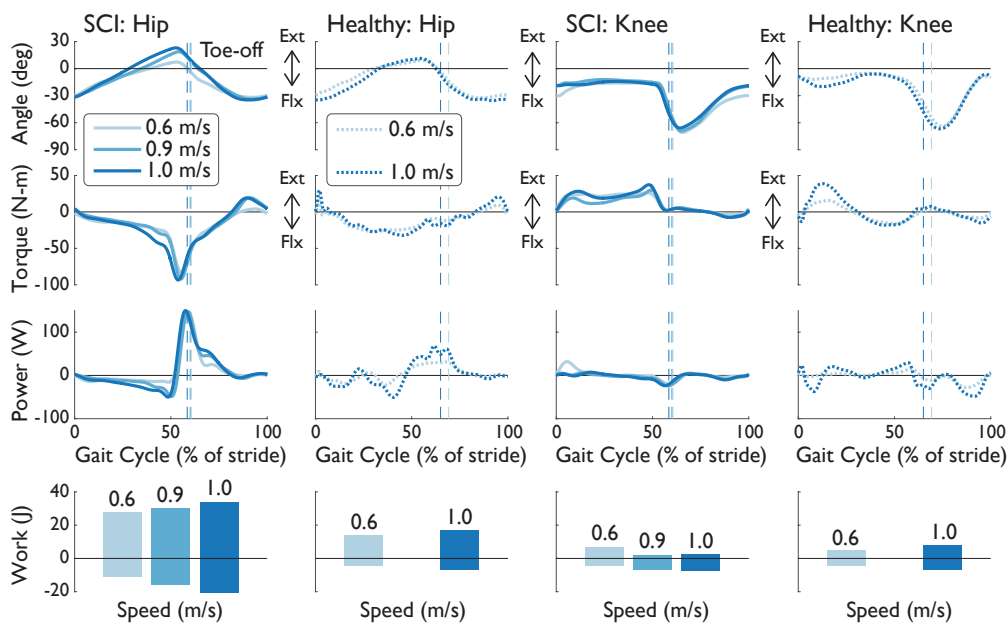


Figure 6.19 – Knee and hip angles, moments, powers, and work from the right leg of S2D (complete SCI injury) while walking with NMC and LOPES. Mean trajectories (solid line) are shown with healthy shod walking (dashed line) at similar walking speeds. Trajectories are shown as a percentage of gait cycle (% of stride). Toe-off indicated by dashed vertical line. Ext: extension, Flx: flexion

much change in length except near heel-strike at the slowest speed. In contrast to the changes in muscle length, there was no visible trend from the contractile velocity of the virtual muscles. The noise-like behavior in these signals are from integration of differential equations in the muscle model [59]. Muscle forces also seem to be affected by speed, but peak forces do not seem proportional to speed.

Discussion

Our preliminary results demonstrated the versatility of the NMC. With very few sensors, SCI subjects were able to walk at multiple speeds, including near healthy speeds, despite the lack of ankle actuation. NMC gait kinematics resembled those of healthy shod walking. With no predefined settings for multiple walking speeds, the NMC also adjusted step length similarly to healthy humans as speed changed. Meaningful EMG activity was also detected in several muscles of SCI subjects, possibly implying functional engagement of the subjects' own muscles.

Several factors could explain the observed differences between NMC-generated torques and biological torques. One source of disparity is the neuromuscular model (NMM), the basis of the controller, generates human-like walking in simulation but cannot fully capture human

6.4. IV : NMC for complete SCI on the LOPES gait trainer

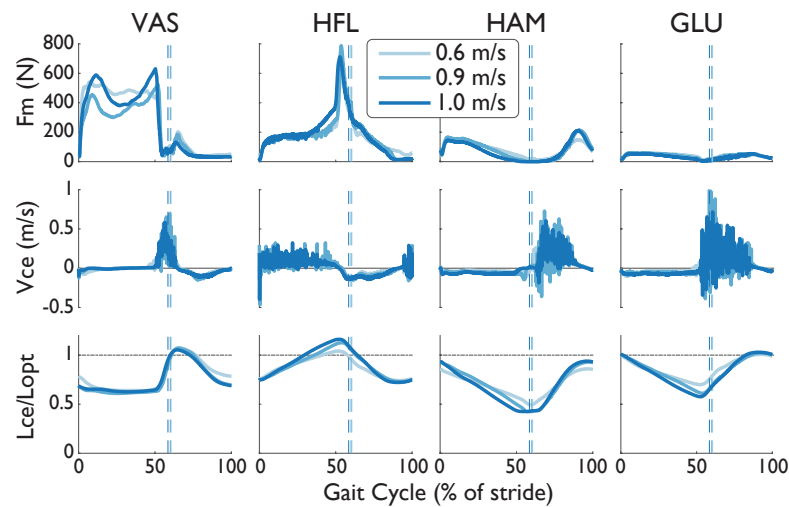


Figure 6.20 – Muscle force (F_m), contraction velocity (V_{ce}), and length (L_{ce}) from four virtual muscles of the NMC with S2D (complete SCI injury) walking in LOPES. The length of the contractile element has been normalized by the optimal length L_{opt} (dashed-dotted line). Trajectories are shown as a percentage of gait cycle (% of stride). Toe-off indicated by dashed vertical line.

behavior. For example, compared with biological torques, the model produces a greater hip flexion torque near toe-off, which we also observed with NMC-generated torques. In addition, model parameters from NMM simulation were directly applied to the controller, and therefore user-machine interactions were not taken into account.

The lack of ankle actuation is another compelling reason for the differences in NMC and biological torques. For the knee disparities, the virtual biarticular gastrocnemius muscle, which provides knee flexion, was also omitted in the NMC for implementation in LOPES. While the virtual hamstring muscle can also provide knee flexion, nominal behavior of the full NMC model (i.e. with ankle) is a burst of muscle activity in the gastrocnemius but little in the hamstring during peak knee flexion [79]. Therefore, without the virtual gastrocnemius muscle, NMC's ability to produce knee flexion torque is reduced. No virtual muscles were missing at hip joint and therefore abnormal behavior was not expected. As expected NMC hip angles were also very similar to healthy angles. The differences in torques at the hip joint could be a result of altered dynamics due to lack of actuation at the ankle. An other reason could be the simplification of the weight bearing algorithm (see Sec. 6.4.2), which affects the virtual vasti muscles, glutei muscles, and hip flexors. The major discrepancies in hip torques occurred during double support (e.g. near early stance and toe-off), which coincides with weight transfer from one leg to the other.

Differences in step length trends between SCI gait and healthy gait with increased speed could be partially explained by body weight support and the use of handrails. These subjects had 21% to 38% of their body weight unloaded and their use of handrails also provided an

additional 12% to 48% of support. S3D, the subject with the linear trend, had the highest body weight support provided by LOPES. Body weight support has been shown to affect gait kinematics at 75% of BW [210], and the reported effect on stride length (at greater speeds) was a significant but small increase relative to zero bodyweight support.

Although walking speed was regulated by the treadmill, the NMC is reactive controller that acts only in the sagittal plane and thus gait adjustments could be made by healthy subjects by changing step time or step width. For the SCI subjects, less adjustments were possible due to their impairment, but subjects did employ their arms (as indicated in the previous paragraph) by imparting forces on the handrails. Some arm use may be in response to an unfamiliar device and controller and the fear of tripping. However, some SCI subjects also used their arms to utilize their upper body to assist in propelling their legs forward and in making small lateral corrections. We feel this was unnecessary, as the NMC would swing the leg as soon as it was unloaded, but we did not test this controller on a completely passive subject. We also did not directly quantify or study upper arm effort, but we did ask subjects to decrease their reliance on the handrails if possible.

Pronounced EMG patterns were detected from both incomplete and complete SCI subjects. Some patterns seemed similar to healthy (e.g. TA, BF, and ST of S2B) while others were more aberrant (e.g. MGAS of S2C and S2D). While these patterns may have been induced by the uncontrived NMC gait dynamics, it is difficult to separate in the present study these findings from EMG activity previously found with coordinated stepping movements by physiotherapists [43] and a fixed gait pattern by a driven gait orthosis [42]. Nonetheless, as the previous studies have noted, subjects' muscle activities in both the actuated joints of the LOPES and the passive ankle are likely the result of systematic load receptor input during each stride. The implication and veracity of this finding deserves further investigation.

There were some limitations to this study. We could not compare the NMC against the device's ZIM because SCI subjects were unable to walk without assistance. In addition to testing a small number of subjects, SCI subjects also could not be evaluated at the same speeds and controller settings because each had unique neurological symptoms, and controller gains were manually tuned for their specific walking ability. A different investigation with healthy subjects with the NMC would be appropriate to more fully evaluate the NMC and its ability to lessen the energetic burden of walking (e.g. less metabolic cost). However, as our aim is to restore gait in paraplegic subjects, the controller fared well despite the lack of ankle actuation.

Due to limitations in experimental set up, we also did not evaluate how walking in LOPES affects healthy gait. In particular, we compared NMC to shod walking but did not evaluate how biological joint torques for a healthy subject walking in LOPES (calculated from inverse dynamics) under ZIM would differ from shod walking. In addition, some of the differences between NMC and shod joint angles could be due to dissimilarities between LOPES-measured angle and kinematics from motion capture.

The NMC was not optimized for subject anthropometry to provide subject-specific assistance

6.4. IV : NMC for complete SCI on the LOPES gait trainer

or at multiple walking speeds. Although subject-NMC interaction allowed for slow walking speeds, the NMC cannot function at speeds slower than 0.6 m/s in simulation. These issues are to be addressed in future work. However, the controller did produce healthy-like gait in paraplegic subjects of different anthropometry and walking abilities and at multiple speeds, thus demonstrating high robustness. These additional features may, therefore, not be necessary.

We also conducted this study on a treadmill, but using the same controller on a wearable exoskeleton overground, especially for subjects with inadequate volitional hip control, poses new challenges. Indeed, the treadmill moves the subjects' feet, which could aid in initiating or sustaining gait. The NMC is also better suited for walking at normal to fast speeds. Therefore new algorithms, likely with pre-determined gait patterns, will be needed to help initiate and terminate gait and to increase speed up to around 0.6 m/s. These preset algorithms can be combined with the NMC to maintain gait during transient behavior or slow walking (e.g. increased contribution from preset patterns) or during normal to fast speeds (e.g. when the NMC can fully take control).

III : NMC for complete SCI on the WE2 exoskeleton

The preliminary results of the experiments on the WE2 presented here were performed at the Santa Lucia Foundation, by Symbitron's clinical partners in close collaboration with the hardware and control team. We did not perform these experiments, but since they are based on the implementation of our NMM, and are key to confirm our hypotheses, they are included here for completeness.

Pilot general information

The test pilots of this set of experiment are part of the cohort presented in the previous Section 6.4 and described in Table 6.8. For simplicity, the two test pilots involved in the test on WE2, S2B and S2C, are renamed here S1 and S2, respectively.

Objectives

We present herein the implementation of the NMC for WE2, which requires the ankle, knee and hip modules. Tests were performed on group II test pilots by our consortium partner at the Santa Lucia Foundation, and aimed at:

- Perform preliminary tests on healthy subjects to check the reliability of the WE2, to set up the testing environment (body weight support, walking aids) and safety measures, and to optimize experimenters' procedures in mounting the robot, assisting walking and helping test pilots.
- Identify subject-centered configurations of the WE2 controllers and the walking training for the use of WE2 with the group II test pilots.
- Identify and fixing the WE2 issues (team of TUDelft and UTwente).
- Demonstrate WE2 acceptability, effectiveness in assisting walking and current limitations and needs for improvements.

Methods

Training procedure

Preliminary tests were performed by the experimenters to optimize subsequent tests with SCI subjects. The detailed procedure can be found in the Appendix E

Compared to the Lopes gait trainer presented in the previous section, here the test pilots are free walking. To provide body weight support (BWS) and allow test pilots to move freely and provide a forward trust to help initiate the movement (similar to the Lopes' treadmill), the test pilots were equipped with the dynamic multidimensional overhead body weight support system FLOAT [206]. Each training session of the two test pilots were organized as follows:

- Psychological assessment (~10 min)
- Robot mounting (~15 min)
- Balance exercises (~5 min)
- Walking training (~45 min with intermediate resting periods, as needed)
- Robot un-mounting (~5 min)
- Skin check of the trunk, pelvis and lower limbs (~2 min)
- Psychological assessment (~10 min)

The walking training phase had the following objectives:

- To optimize human-robot interaction thus increasing the comfort perceived by the test pilots.
- To decrease the BWS with the final target of walking without any help from the FLOAT.
- To increase the autonomy of the test pilots, i.e. moving from the use of parallel bars to the use of crutches, taking the control of the device by means of buttons in the handle and receiving less and less physical assistance from the spotters.
- To customize and tune controllers to optimize the walking pattern. Since each test pilot is unique, has specific residual functions and performance and peculiar human-robot interaction strategies, the customization of WE2 assistance became important to obtain an effective interaction with WE2, with the highest benefits for the user. Possible regulations of the walking patterns included:
 - Speed
 - Step length
 - Foot clearance
 - Flexion/extension of hip, knee and ankle and adduction/abduction of the hip
 - Type of controller (i.e. more emphasis on the TC or NMC)
- To increase speed that could be managed by the test pilots, based both on faster legs motions and/or on an increased cadence due to a higher frequency of step triggers
- To Increase the step length that could be managed by the test pilots.

The actual duration of the activities depended on the reliability of the robot, on the resting needs of the test pilots and, in general, on possible different experimental issues. In many cases training sessions needed to be interrupted due to technical problems, thereby preventing a proper finalization of the training. Besides the data collected by the WE2, when possible, the walking performance was also measured by means of a chronometer. This was not possible in the cases when several technical errors interrupted frequently the WE2 functioning thus leading to a discontinuous walking. More detailed features of the training can be found in the Appendix E.

WE2 customization procedure

For the WE2, the customization concerned the adaptation of the WE2 mechanical configuration (foot plates, links and cuffs) to the anthropometric features of each test pilot. This was performed in two steps:

- Initial configuration based on anthropometric measures retrieved by an expert physical therapist (before the first training session Tr1, so at a time indicated as Tr0).
- Configuration refinement after the first fitting of the WE2 occurring at Tr0 (normally happening at Tr1).

The different adjustable parts of the WE2 as well as the selected settings for two different test pilots are shown in Fig. 6.21.

Clinical Assessment

Test pilots underwent a battery of clinical evaluations before and after the training. Clinical scales used for the assessment are:

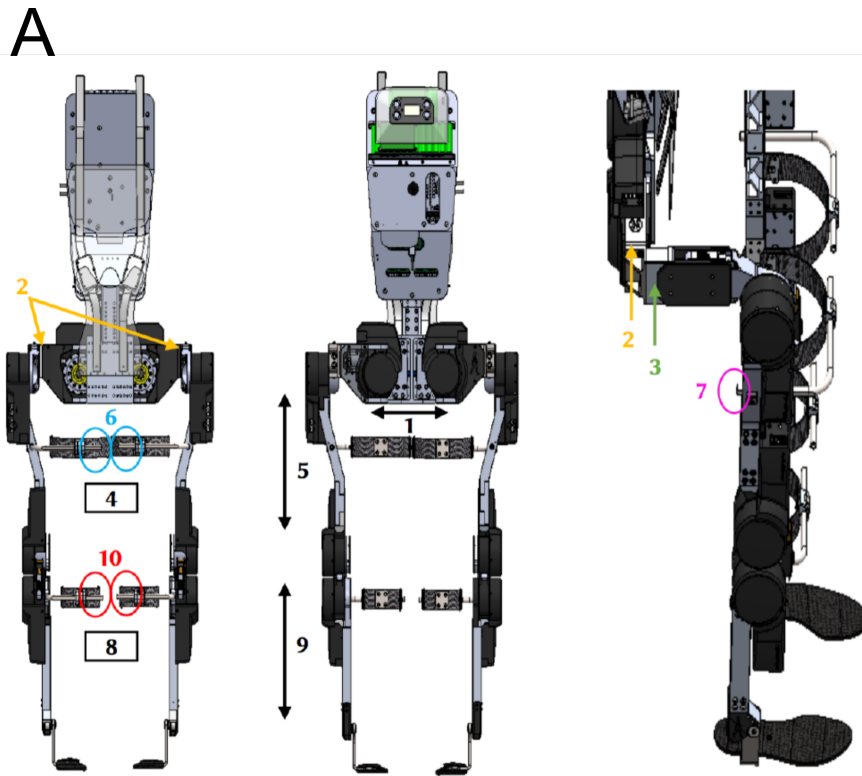
- The Modified Ashworth Scale (MAS), for spasticity assessment, rates from 0 to 4 (0: no increase in muscle tone, 4: affected part(s) rigid in flexion or extension).
- The Penn Spasm Frequency Scale (PSFS): a self-reported measure on a 5- point scale developed to augment clinical ratings of spasticity and provides a more comprehensive assessment of spasticity (scores are 0 = no spasm; 4 = spasms occurring more than 10 times per hour).
- The Spinal Cord Assessment Tool Clonus Scale (SCATS): uses passive dorsiflexion to assess clonus. It is rated on a 4-point scale that ranges as follows: 0 = no reaction; 1 = mild lasting < 3 sec; 2 = moderate lasting 3-10 sec; 3 = severe lasting > 10 sec.

Since test pilots had complete lesions and no muscular activity was preserved below the lesion level, no tests on muscular force were performed.

The test revealed that S1 presented no spasticity at the hip joints, while a medium level of spasticity and spasms was measured for knee and ankle joints. For S2, a high degree of spasticity, clonus and spasms were measured for knee and ankle joints. All these scales were also used after WE2 training to check possible positive or negative effects due to WE2 usage. No modifications were recorded for both subjects.

Results

The high number of technical issues slowed down the experiments and prevented a proper training of S1 and S2. Indeed, especially at the beginning of the training activity, the low



B

	Component			Test Pilot	
	Name	Units		S1	S2
Pelvis	Center width	-	(1)	Minimum	Minimum
	Back piece (ML)	[mm]	(2)	20	0
	Side piece (AP)	[mm]	(3)	10	10
Thigh	Cuff size	-	(4)	6	6
	Length	[mm]	(5)	230	280
	Front bar length	[mm]	(6)	37	22
	Side bar length	[mm]	(7)	24	32
Shank	Cuff size	-	(8)	5	4
	Length	[mm]	(9)	220	210
	Front bar length	[mm]	(10)	41	35
Foot plates	Size			44	44

Figure 6.21 – NMC adjustable parameters for WE2. A) Graphical representation of the WE2 exoskeleton with the different adjustable part numbered from 1-8, B) The chosen parameters for the two involved test pilots.

Chapter 6. Applications

reliability of WE2 caused highly frequent faults and only few steps were finalized between two consecutive disabling events. In some cases only very few steps were performed despite long session durations. This effect reduced the motivation of the test pilots and, most importantly, did not allow to really train them in using the WE2 autonomously. Hence, the first part of the training was performed with the use of parallel bars (a first attempt of employing crutches was unsuccessful) and a requiring important effort produced by the pilot's arms (for S1, as S2's personal strategy was to solely use his legs to walk). One of the main issues in this phase was the limited amount of torque that WE2 joints, the knee in particular, could produce. This caused WE2 to stop when the BWS was below around 30-40 kg. The attempt of increasing knee stiffness and/or extension and using NMC on the ankle to increase push-off thus unloading knee joints, was not significantly effective.

Following technical intervention on WE2, the device performances were significantly improved and made the WE2 capable of withstanding almost the full weight of the pilot + WE2 with a minor contribution of the FLOAT. Also, the frequency of occurrence of the other technical errors was significantly reduced. Therefore, the functioning of WE2 became less discontinuous and the performance of the pilots (mainly S1) increased. This solution greatly improved the functioning of the WE2 and made it possible to move from parallel bars to crutches. This also provided the test pilots with the possibility of triggering steps by themselves. In turn, this resulted in a decrease of BWS support and help from the spotters, and in a slight increase of step speed.

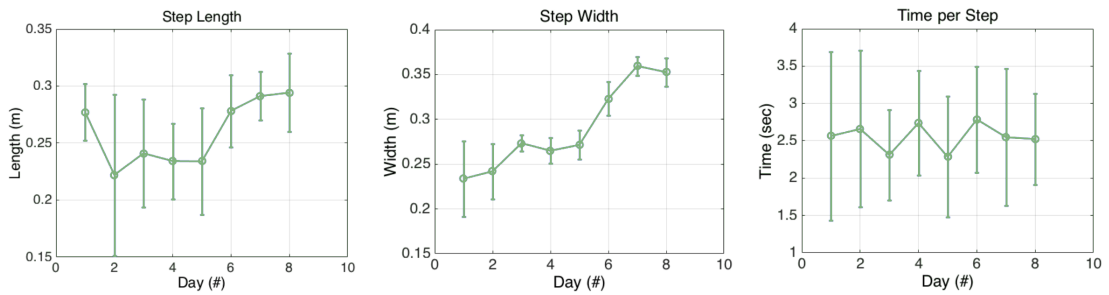
More specifically, nine training sessions were performed by S1 and significant improvements were observed: at the beginning of the training 40 kg of BWS, parallel bars and help from spotters were needed while at the end of the training S1 could walk with only 10 kg of BWS (i.e. negligible help from the FLOAT), with crutches and minor external physical assistance. A horizontal helping force (50 N) was added to compensate for FLOAT inaccuracy in seconding test pilot walking. Speed was not significantly increased along the training since the occurrence of several technical failures prevented the real increase of performance in terms of spatio-temporal parameters.

Four training sessions were performed by S2 and minor improvements were observed: BWS was only reduced from 40 kg to 30 kg (also for S2 a horizontal helping force of 50 N was added). The change from parallel bars only occurred at the last training session when a mechanical problem in the left adduction/abduction hip actuator forced the end of the training and did not allow to test technical improvements introduced. Nonetheless, a slight minor improvement in the spatio-temporal parameters was recorded.

No adverse effects were noted in terms of spasticity, clonus and spasms for both test pilots (MAS, PSFS and SCATS scores were the same before and after training) thus suggesting a safe usage of the WE2.

Fig. 6.22 reports step length, step width and step time for S1 and S2 along the training. The variability in the data is due to intra-session changes in the walking conditions (e.g. reduction

S1



S2

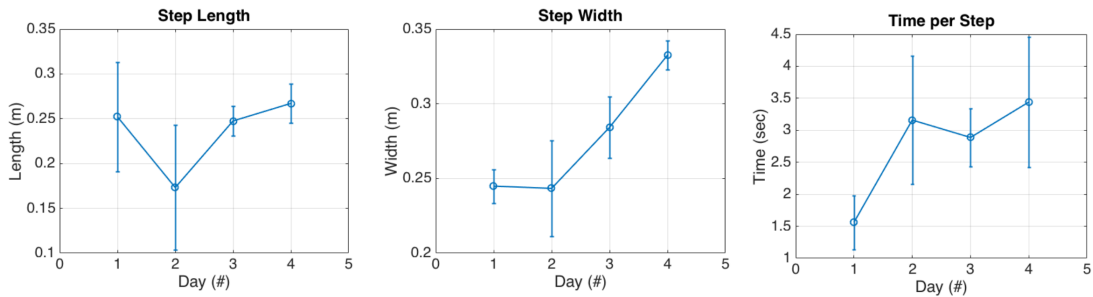


Figure 6.22 – WE2 experiment - Speed, Step length and time per step across the experiment for the two subjects.

of BWS) and test pilot usage of upper limbs. A slight increase in step length and width can be observed over the training sessions, while step time remained almost constant.

Summary of achievement

Despite technical issues, WE2 demonstrated to be effective in enabling complete SCI subjects to walk. The prototype iteratively underwent technical improvements driven by the results of the experiment on the test pilots. The extensive testing with SCI subjects was extremely useful to unveil the limitations of WE2, some of which could not be identified in advance with healthy subjects, as some of the technical issues were masked by their active contribution the the motion. Some of the technical problems were totally solved, others were only mitigated and will require additional attention.

Along the training activities, WE2 proved to successfully assist walking with increased autonomy and decreased effort. WE2 mechanics and control were properly adapted to the specific needs of the two test pilots. The successful customization allowed the subjects to walk initially with parallel bars and finally with crutches, with decreasing BWS and external help from the experimenters.

Outlook

Seeking an understanding of some of the basic control principles used by the neuromuscular system to generate locomotion, we have developed different models (NMM), presented in part I of this thesis. Specifically, the results presented in Chapter 2 demonstrated the inherent robustness to perturbations of a reflex model and their striking similarity with human walking. The models presented in Chapter 3 leverage on this robustness to create qualitative gait changes, such as gait speed modulation, suggesting that the design of exoskeletons based on such models would allow the wearer to induce gait speed changes without having to change the control parameters.

Interestingly reflex maps can be represented with as little as 4 signals found by non-negative matrix factorization (98% correlation between the original signals and the reconstructed ones, data not shown). Since motoneurons are a simple linear combination of feedback pathways, the same conclusions are valid when analyzing the motoneurons signals. This low dimensional representation is also found in humans EMG patterns [29, 50], where only 4 signals, the so-called “motor-primitives”, are necessary to faithfully represent the EMG patterns of adult human walking. A logical next step would thus be to exploit this low dimensional structure when modeling the feedforward components. In other words, one could model the CPGs as a set of motor-primitives that can be combined together to generate the different motoneurons states. Therefore, instead of viewing the CPG as a feedback predictor, one would view it as a motoneuron predictor. The hypothesis would be that the modulation of the timing, amplitude and duration of the motor-primitive would offer a better control of the gait, in terms of speed, stride length, gait transition and adaptation to increasing/ decreasing slope.

The stability of the reflex model tells us that the generate dynamical system have large basin of attraction. This means that the system can handle relatively large disturbances. This offers nice property that allows to switch online between different set of parameters, or switch part of the control to complete different control scheme (e.g. to generate more complex reflex behavior such as stumbling correction reflex), or as we presented in this work add a feedforward signal to modulate speed or step length. Improving the muscle model as discussed in Section 5.5.1 has a strong potential to increase the stability of the model even further, which could lead to the generation of more versatile feedforward control scheme as discussed in Section 3.4.2.

The implementation of our NMM model on a controller (NMC) was demonstrated for human healthy subject and was confirmed with experiment on SCI subjects with different devices in

part II of the thesis. Overall, the bio-inspired NMCs demonstrated remarkable versatility in generating gait patterns tuned to the subjects' dynamics and producing near-physiological gait at near-normative speeds. The positive SCI subject-machine interaction stemmed from replacing the subject's impaired function with dynamical virtual muscles that require few sensors to generate gait. The controller scheme was tested on different devices with similar results, suggesting that the only required feature the exoskeleton needs to run an NMC is to provide good torque control capabilities and ground contact information (on/off).

These preliminary but auspicious results have important implications towards the exploitation of natural walking dynamics through understanding human biological behavior in the design of controllers for wearable devices that are amenable to various environmental conditions and promote intuitive and unobtrusive human-machine interaction.

Although our model and resulting controller architectures are largely bio-inspired, the optimization process itself is not biologically relevant. Upon optimization, our NMM model showed striking similarities with human walking, but it is unlikely that the brain relies on a PSO algorithm to fine-tune the different sensory-interneurons-motoneurons connections. Therefore, what could be the optimization process used by the brain? Is the same process used across the whole animals kingdom?

Unguligrade animals can walk within minutes to hours following birth, while rodents require days and humans around a year to achieve this locomotor skill. At first glance, such an observation suggest that even among mammals, the optimization process used by the brain to generate locomotion is not conserved. However, Garwicz and al. observed that despite the large differences in brain capacity existing across mammals, all species apparently begin to walk at the same stage of their brain development [76]. They demonstrated a linear correlation between brain development stage and the period from conception to walking. This observation suggests that some of the mechanisms underling the onset of locomotion may be shared across species. If this is true, then - since this brain development machinery allows some mammals to walk almost immediately after birth - it implies that the *in-utero* development phase may be sufficient to wire up the network allowing locomotion and standing features. Assuming that this developmental machinery is implemented as a learning mechanism and not as a fully wired-up network in the genome, one can start approaching the question of motor development in a whole new perspective. The first consequence of this assumption is that the optimization procedure do not necessarily include walking *per se* in any form. In other words, learning to walk may not require actual walking. Instead, something else must be happening *in-utero* to prepare for walking before the actual walking happens (once the animal is born). Based on this hypothesis, one can try to reverse engineer this procedure by looking at the environments faced by the organism during its development, the motor behavior *in-utero* and the features learned *in-utero* (this can be observed by looking at different mammals that can walk and stand right after birth such as giraffes, horses or cows).

In-utero, the body faces very specific forces due to its immersion in an aqueous liquid. Indeed,

movements in water are damped and gravitational forces are negligible. This means that keeping a specific position in water requires much less energy, while moving requires more energy because of water's viscosity. It is therefore "harder" to produce a movement *in-utero* than *ex-utero*. Assuming that the *in-utero* stage is long enough to allow the network to converge to some optimum, this optimum should be good enough to produce (hesitant) standing and walking (<https://www.youtube.com/watch?v=XM-taq1dbJs>), as it is the case for for most ungligrade. It would not be surprising if this process is common among several species, as being able to move right after birth is a key survival feature for many species. One can then suppose that the *in-utero* stage should train the body to generate coordinated movements to control the legs to push against the ground (to allow standing up), as well as a retraction mechanism (to allow the leg to swing). Assuming that the *in-utero* stage has an optimum, what would be maximized?

Spontaneous motor activities (SMA) are known to arise both *in-* and *ex-utero*. A SMA is defined as a spontaneous firing of a motoneuron pool, while all other muscles are not active. A link between SMAs and motor learning has been suggested [156] and a simulated spinal cord [130], where SMAs were combined with hebbian learning, produced jumping behavior of a simulated human leg musculoskeletal system. In the present context, those results are only partially compatible with the *in-utero* environment. Indeed, learning was performed without contact. However the optimized solution was still able to produce jumping behavior very easily, which is a very good initial condition to learn contact, where the body learns to push and retract their legs. Interestingly, nothing related to jumping behavior, or contact was included in the optimization, yet a jumping behavior was easily obtained.

Taken together, these observations suggest that the wiring and optimization of the locomotion system in mammals is not solely performed *ex-utero*, but that some pre-optimization processes may be performed *in-utero*, although the environment do not resemble that of the *ex-utero* walking environment. This must be true at least for some mammals, as they are able to walk within minutes following birth, and in an evolutionary perspective, this may hold true for humans. This suggests that our models optimizations may benefit from optimization performed in an *in-utero*-like environment. One should keep in mind, however, that humans brain is far from fully developed *in-utero*, and it is clear that wiring and optimization must also occur *ex-utero*. We therefore believe that a combination of optimization procedures both in *in-utero*- and *ex-utero*-like environments would benefit the developed models, both in a biological point of view and in terms of performances. Moreover, walking is not only spinal. Vertebrate animals show fascinating locomotor abilities which are the results of the interplay between the environment, the biomechanics, the spinal cord, and modulation from higher control centers. How the different structures interact to generate meaningful behavior is an active field of research. Understanding key principles could have strong impact in different fields related to medicine and robotics (e.g. improved rehabilitation procedures, predicting surgery outcome, facilitated human-robot interaction such as exoskeleton).

Appendix **Part III**

A Software

C++ Spinal dynamics library: See <https://gitlab.com/srill-fb99/spinaldynamics>

C++ NeuroMuscular toolkit: See <https://gitlab.com/cppNeuroMuscularToolkit>

Biorob Reinforcement learning toolkit: See <https://gitlab.com/srill-fb99/deep-rl-biorob>

Simulink/Matlab neuromuscular controller

See https://gitlab.com/symbitron_simulink_nmc

While most of the modelling is done in Webots using the `cppNeuroMuscularToolkit`, control is done with Simulink with XPC Target (for LOPES) and Etherlab (for Achilles) using the NMC Simulink library. Much emphasis has been placed on facilitating the creation of NMC controllers for use on any lower limb exoskeleton device. The library has been successfully tested in the experiment presented in the Applications.

Library description

The library is designed starting from the Simulink model provided by H.Geyer [79]. The model uses feedback rules connecting different sources of sensory information with virtual Hill-type muscles, which in turn generate effective joints torques. A state machine is used to switch between two sets of feedback rules: one to generate the stance phase control (mainly extensor muscles activity) and one to generate the swing phase control (mainly flexor muscles activity). Ground sensors placed under the feet are used to detect the state transition (takeoff and touchdown). The generation of the gait cycle is done through reflexes represented by a sequence of time delayed reactions. The control can be separated in three layers: the muscle, sensor and joint layers.

Sensor modules

The sensor modules are used to connect the sensory stream to the controller. The sensor modules transform sensory input mainly by adding a delay modelling the nerve conductivity. The sensory output, e.g. ground contact detection and joint angles, can then be used by the control modules and the state machine. The sensory modules are listed in Table 2.

Joint modules

Geyer's Simulink model uses artificial ligaments which are provided by the joint modules. They take as input the concatenated vector of torques of the muscles attached to the corresponding joints together with its angle and angular velocity. The angle and angular velocities are used to create, if needed, an over-extension prevention torque to limit the joint angle range. In order for the model to be easily used by external researchers, the knee sensor has the negative sign embedded in the block, so that only the concatenation has to be done by the user to limit the error.

Muscle control modules

The modular structure of the control architecture permits the creation of different local control modules. Those modules can then be combined to generate different controllers. Two types of control modules exist: reflex modules and CPG modules. Reflex modules correspond to reflex loops in the NMM and CPG to the feedforward component presented in 3. Reflex control modules are generated by merging and modularizing the actuation and control layers of the original Simulink model. More specifically, the model is separated in modules regrouping the muscle actuation and control module (explained below). It takes as input the outputs of the NMC sensor modules and the angle of the corresponding joint(s) and output torques. Note that to improve modularity, the HFL Muscle module is present twice. One is combined with the HAM Muscle to be used when creating a controller to actuate both the hip and the knee joint. The other module is present for cases where the hip is controlled alone. For simplicity, SOL and TA are regrouped into one module as well. All the modules simply output the torque to be applied to one or several joints. The different reflex modules available are shown in Fig. 5.3. The separation in a control¹ and an actuation block² is done to facilitate the addition of a CPG observer. This can simply be done by incorporating it on the signal of interest. A feedback observer can be designed by incorporating the CPG on the feedback going out of the actuation block.

¹Control Block: Block which calculates the stimulation to apply on the muscle depending on the environment information and the muscle force and/or length feedback.

²Actuation Block: Block which calculates the torque to apply on the joint depending on the joint angle and the stimulation to apply estimated from the control block

CPG modules

In the NMC, CPGs are viewed as state estimators. More specifically the CPG is composed of a feedback predictor which is modeled as a dynamical system reproducing the average shape and amplitude of the original feedback signal. The dynamical system implemented is a morphed oscillator (MO) and is capable of speed modulation with a simple augmentation of the frequency. This oscillator is able to produce any shape, as long as this shape can be represented by a function that is both 1-periodic and differentiable. A CPG module can be applied to any data stream, provided that it receives the ground information of the leg on which it acts. It will then learn the steady state signal, which can then be used in a feedforward manner alongside the data stream that it estimates. The combination of the original data stream and the feedforward signal from the CPG is generated by the following procedure described in Chapter 3.

Example of Ankle Knee reflex modules used with WE1

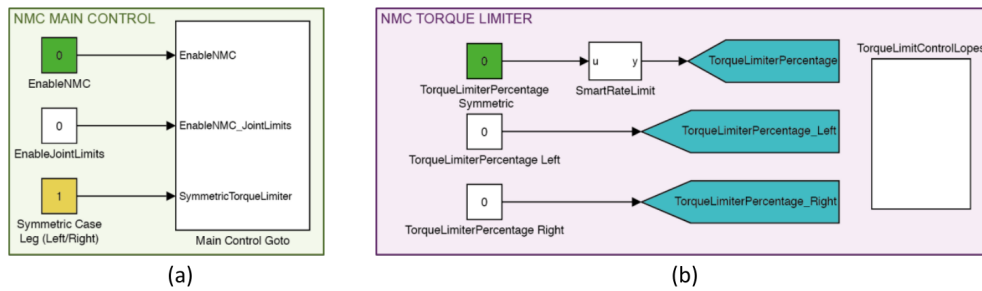


Figure A.1 – Highest level of NMC control. (a) NMC main control panel enables or disables the NMC and is used to toggle between symmetric or non-symmetric gains for the left and right legs. (b) Torque limiter percentage for both legs or specific to the left or right legs.

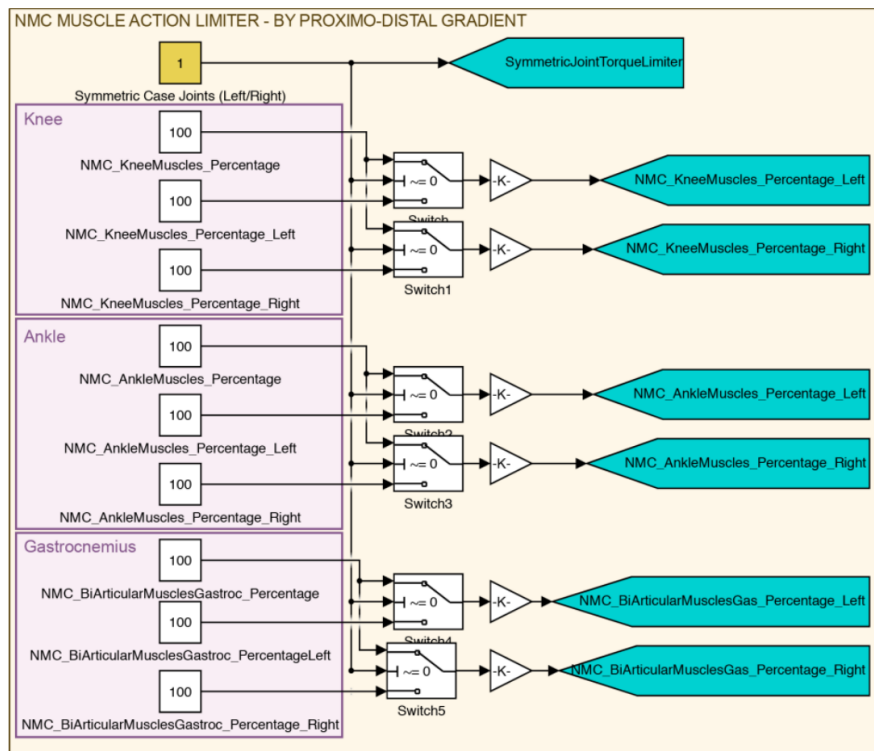


Figure A.2 – Torque limiter by joint (proximal-distal) with the ability to target the left and right sides separately.

1.1. Simulink/Matlab neuromuscular controller

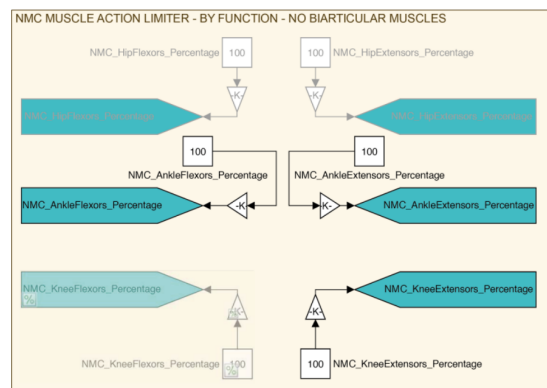


Figure A.3 – Torque limiter by muscle action (i.e. flexion, extension).

B Hardware

Ethercat

As was already decided in the first year of the project, the real-time control of the Wearable Exoskeleton will be done using EtherCAT. In this way we can easily combine several modules (EtherCAT slaves), which is according to our goal of developing a modular system. Furthermore, it contributes to the requirement of a minimal wire solution for the wearable exoskeleton. The main etherCAT slaves (stack) are placed in the backpack of the exoskeleton together with the pc that runs the different models for the control of the EtherCAT slaves. Some off-the-shelf EtherCAT slaves could be used (e.g. for the motor control), but also during the course of the project, some EtherCAT slaves have been developed/built for specific hardware components of the wearable exoskeleton such as the instrumented soil used to detect ground contact.

Etherlab and Symbitron wiki

To control the EtherCAT slaves in real-time, EtherLab in first instance has been selected as the EtherCAT master, because it is open-source and easily communicates with the hardware and the Matlab Simulink control models. The installation of EtherLab was not described extensively anywhere, therefore a master student and some Symbitron members went through all the installation steps and have documented the required steps and especially the problems they encountered. The resulting installation manual has been put on the Symbitron wiki (www.symbitron.eu/wiki) to easily share it with the other Symbitron members, but also to share it with other people who want to use EtherLab. The Symbitron wiki is therefore open for everyone, but editing is only possible after creating an account with permission of the website manager. The Symbitron wiki shows up in the first hits on Google when searching for "EtherLab" and is the first hit when looking for "Etherlab installation".

Low level simulink library

To control the different slaves, Matlab Simulink models are being used. For each EtherCAT module a Simulink library block has been created. These blocks can be directly inserted in a Matlab Simulink model and by putting the correct slave number in the blocks the data from the blocks can be read out or data can be sent to the slaves. To be able to (1) share the different Simulink models among the consortium, (2) to be able to use them on different pc's (development pc and control pc) and (3) to have version control, a Symbitron GIT repository is being used. This GIT repository is being stored on Bitbucket. Bitbucket not only provides the hosting of the repository, but also allows for issue tracking for every project. The Symbitron repository is only open for Symbitron members or on request.

Exoskeleton devices

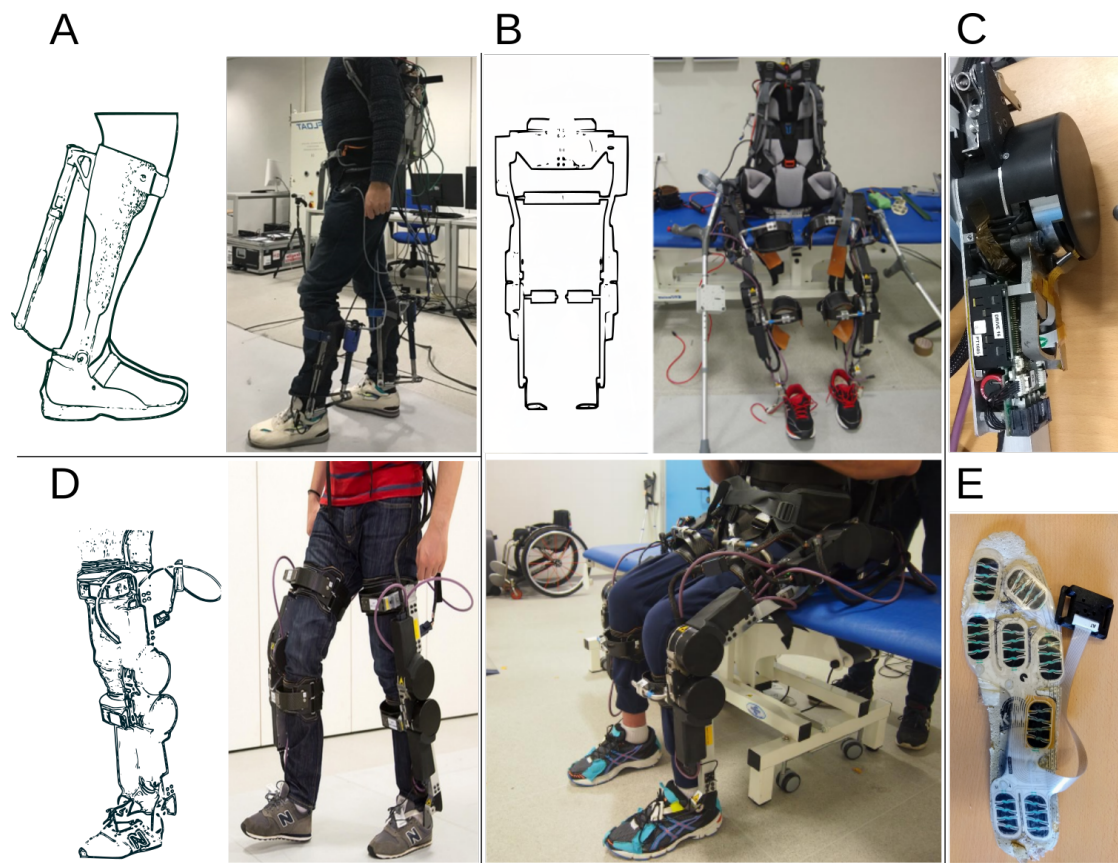


Figure B.1 – Picture of the different exoskeletons. A) Achilles, B) WE2, C) Joint actuator, D) WE1, E) IEE Instrumented Soil used for ground contact detection.

C Mathematical models

Musculoskeletal system

All experiments are done using an implementation of the NMM library (a freely accessible C++ library that we developed to simulate neuromuscular models¹) on the Webots robotic environment platform [137]. This webots implementation² is based on an anthropometric model of human lower body (see Fig. C.1, anthropometric data from [225]).

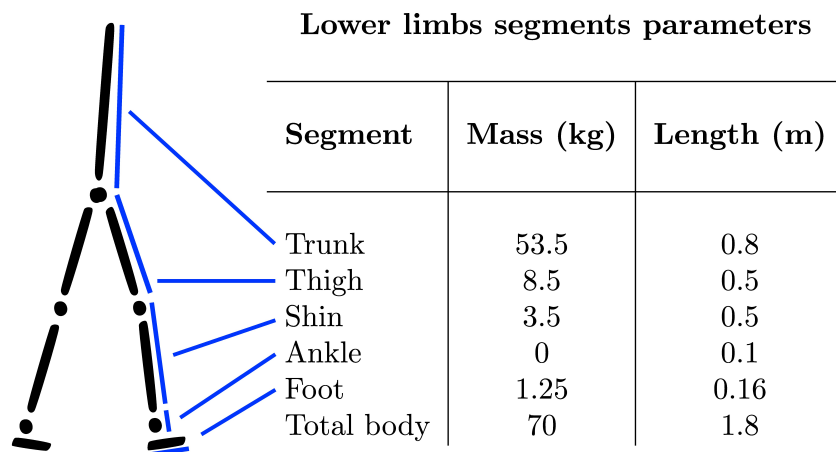


Figure C.1 – Segments weight and length distribution based on anthropometric data from [225].

Ligament model

In animals, a ligament forms the joint that maintains two bones together. It also ensures that the angle formed by the bones stays within a given range. Its action is against the movement and engages only when the angle is beyond a certain limit, which depends on the joints (see

¹The NMM library can be found online at <https://bitbucket.org/efx/libnmm>

²The Webots implementation of the NMM library can be found online at <https://bitbucket.org/efx/sml>

Appendix C. Mathematical models

Table C.1). Ligaments are modeled as non linear spring damper acting as soft limit on the joints [79, 183]. When the angle goes beyond the limit of the joint and the angular speed is not big enough to bring back the joint in its normal range a force is generated. The resulting torque $\tau_j^{ligament}$ acting on joint j is modeled as :

$$\tau = \begin{cases} k \cdot \Delta\phi \cdot (1 - \omega/\omega_{ref}) & \text{if } \Delta\phi > 0, \omega/\omega_{ref} > -1 \\ 0 & \text{else} \end{cases} \quad (C.1)$$

Where $k = 17.19[Nm/rad]$ is the spring damper stiffness, $\omega_{ref} = 1.74 \cdot 10^{-2}[rad/s]$ is the reference angular speed, used to normalize the joint angular speed, $\Delta\phi$ is the angle by which the joint limit is exceeded (i.e. difference between the actual angle and the limit angle, the axes are chosen so that $\Delta\phi > 0$ when the joint limit is passed) and $\omega[rad^{-1}]$ is the angular speed (the axes of rotation are chosen so that $\omega > 0$ when the angle is going toward the joint limit angle).

Note that this model of non linear spring damper is also used in the model of H.Geyer to model the ground reaction forces to foot contacts. Here the contact of the robot with the ground are managed by the physical simulator of Webots.

Table C.1 – Range of joints angle outside of which soft limit engages. The soft limit models the action of ligaments to work against unnatural movement, thus preventing injuries [79].

Joint	θ_{min}	θ_{max}
HIP	20°	230°
KNEE	45°	175°
ANKLE	70°	130°

Muscle model

The muscle model is based on the Hill model [97] and was developed by H.Geyer [80]. A muscle is modeled together with its respective tendon (called muscle tendon unit, or MTU). An active, contractile element (CE) with two passive parallel elements (buffer elasticity BE and parallel elasticity PE) form the muscle, see Fig. C.2. The active element represents the muscle active contractile element, while the two passive elements model the physical properties of the muscle fibers. The BE element prevents the muscle from collapsing, while the PE prevents the muscle length from going beyond a certain length. The tendon is modeled as a passive element in series with the muscle, called series elasticity (SE). The full mathematical formulation can be found in [80]. The signal sent to the muscle by the motoneuron is related to the activity of the muscle with a first order differential equation accounting for neural delays,

see Section 2.2.1.

The force of a specific muscle j is linked to its activation level A_j by:

$$F_{CE} = F_{\max} \cdot f_l(l_{CE}) \cdot f_v(v_{CE}) \cdot A_j \quad (C.2)$$

Where : F_{CE} is the muscle force, F_{\max} is the maximum force generated by the muscle, f_l and f_v respectively models the length-force and velocity-force relationship capturing main biological features of muscles, f_l and f_v equation can be found in [80]. Given the muscle diagram depicted in Fig. C.2 and applying Newton's third law of motion, we have that the net force generated by the muscle tendon unit (F_m) equals the force of the tendon F_{SE} :

$$F_m = F_{SE} = F_{CE} + F_{PE} - F_{BE} \quad (C.3)$$

The only unknown variables are the length and speed of the contractile element from which all muscle variables can be derived. Details on how v_{CE} is calculated can be found in [80]. l_{CE} is then derived by integrating v_{CE} .

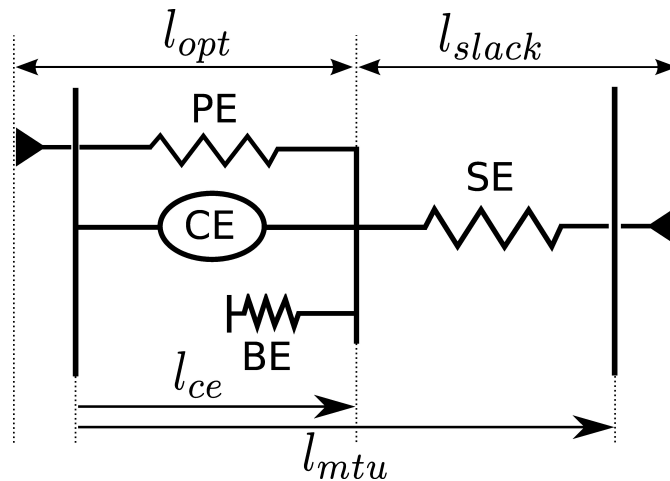


Figure C.2 – Schematic view of a muscle tendon unit (MTU) adapted from [79]. In normal walking condition (no overextension nor overflexion), only the serial element (SE) and the contractile element (CE) are active. Two other passive elements are added in parallel of CE: BE that engages if tendon is slack (i.e if $l_{mtu} - l_{CE} = l_{SE} < l_{slack}$), preventing muscle collapse, and PE, that engages when the muscle stretches beyond its optimal length (i.e if $l_{CE} > l_{opt}$), preventing the muscle to extend beyond a certain length.

Sensors model

There are four different type of sensors (see Fig. C.3):

- Muscle sensors (type 1): There are two muscle feedback types. A muscle length feedback,

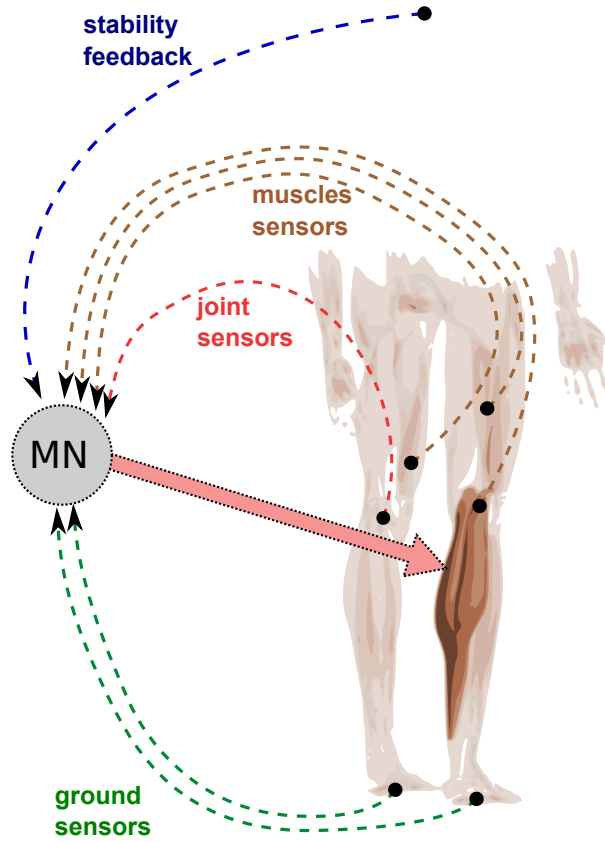


Figure C.3 – Schematic view of the different sensors that can be combined to finally generate the activity of a motoneurons that will in turn activate a MTU.

modeling the muscle spindle, and a muscle force feedback, modeling the Golgi tendon. The muscle length feedback equation for a given MTU m ($Fb_l(m)$) is defined as follow:

$$Fb_l(m) = \frac{l_{ce}^m}{l_{opt}^m} - l_{offset}^m \quad (C.4)$$

Where the exposant m refers to a specific MTU and l_{offset}^m is a parameter found by optimization. l_{ce}^m , l_{opt}^m are respectively the ce length and the ce optimal length of MTU m .

The muscle force feedback equation for a given MTU m ($Fb_f(m)$) is defined as follow:

$$Fb_f(m) = \frac{F_{mtu}^m}{F_{max}^m} \quad (C.5)$$

Where F_{mtu}^m corresponds to the current force generated by the mtu m . F_{max}^m corresponds to the maximum force that can be generated by the mtu m .

- Joint overextension/flexion prevention sensor (type 2): This sensor is used to prevent knee joint overextension. Its intensity is proportional to the difference between the maximum tolerated angles and actual joint angle, and its direction is always against the movement. It is therefore modeled as a simple correction term proportional to the differences between max tolerated angles ϕ^{off} and actual joint angle ϕ . The sensors output for a joint j is given by:

$$Fb_o(j) = \begin{cases} (\phi_j - \phi_j^{off}) & \text{if } \Delta\theta > 0, \omega/\omega_{ref} > -1 \\ 0 & \text{else} \end{cases} \quad (C.6)$$

- Ground sensor (type 3): As in the original model [79], there are two sensors under each foot that feel the reaction forces of the ground, located at the toe and heel position. In our case, the heel and toe sensors are provided by a Webots module called a TouchSensor that returns the cumulative force currently exerted on the sensor's body. Then, as in the original model, the value returned by the ground sensor is defined as being equal to the sum of the toe and heel sensors normalized by the total weight of the model. In order to ensure a smooth variation of the sensors values, the output of the sensors is modeled as linear differential functions of the reaction forces. For instance, the equation governing the toe sensor output is given by

$$\frac{dF}{dt} = \tau f \quad (C.7)$$

Where F is the sensors feedback, f is the reaction force and $\tau = 100$ is the convergence speed. The ground feedback (Fb_g) on side s is defined as being equal to the sum of the two ground sensors normalized by the total weight of the model:

$$Fb_g(s) = k_{bw} \frac{F_{toe_ground}^s + F_{heel_ground}^s}{M \cdot g} = k_{bw} \frac{F_{ground}^s}{M \cdot g} \quad (C.8)$$

Where g is the gravity, M the mass of the model, s is the side (i.e ipsilateral if feedback acts on motoneurone of the same side and contralateral otherwise) and k_{bw} is a parameter found by optimization.

- Stability sensor (type 4): The stability sensors are used to ensure stability. They measure the angle of the trunk in world coordinate and is used by stability feedback to bring the trunk toward a reference angle. These feedbacks are proportional-derivative control adapted to act on muscles and can be viewed as abstract models of descending pathways responsible for balance control originating from the cerebellum and the vestibular system. The feedback acts on the muscles in order to bring the angle of a joint toward a reference angle δ_{ref} . The feedback is given by :

$$Fb_s = \left\{ k_p \cdot (\delta - \delta^{ref}) + k_d \dot{\delta} \right\}_{\pm} \quad (C.9)$$

Where δ corresponds to the actual joint angle we want to bring toward a reference angle and δ_{ref} is the reference angle.

The sign of the brackets depends on the action of the muscles on the trunk; Negative if the action of the muscle is in the direction of positive angle changes and positive otherwise [220]. In the reflex model, this feedback is used to maintain the trunk straight. This is done by sending a signal to hip muscles (i.e. GLU, HAM and HF) during stance phase. In order to account for the fact that only the leg in contact with the ground can be used to stabilize the trunk, the stability feedback signal is combined with the ground sensors of the same leg, allowing the leg bearing most of the weight (i.e. more stable) to be used to maintain the trunk. It has been shown that this combination of the stability feedback and ground sensors is not necessary if during double stance support the stability feedback is applied only to muscles of the leg in stance end phase (st_{end}) [220].

CPG models

Fig. C.4 presents a possible classification of the existing models, according to three different types of CPG architectures:

1. the “Recurrent neural network based CPG (RNN CPG)”
2. the “Half center oscillator based CPG (HCO CPG)”
3. the “Abstract oscillator based CPG (AO CPG)”

The type of architecture chosen will strongly influence the properties of the generated CPG, therefore a judicious choice of CPG architecture is critical in the development of a controller, and strongly depends on its application, see Table C.2. Indeed, a high level of abstraction will be favoured to create robotic CPGs, while low level of abstraction will be generally required to answer biological questions. In this section, we describe the most common models used as building block of CPG networks for the three different architectures.

While neuron-based CPGs use non oscillatory building blocks, half-center oscillator based CPGs and abstract oscillator CPGs use simple oscillators as building blocks. The half-center CPG use biologically inspired half-center oscillator as building blocks, while abstract CPGs use abstract mathematical oscillators, with neither biophysical nor cellular basis, but that have been proven useful to study complex networks of CPGs and to simplify the development of robot models.

Neuron models and RNN CPG

While neurons are very elaborate structures that exhibits extremely complex behaviors, neuron models must be considerably simplified, in order to obtain analytical descriptions or numeri-


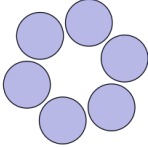

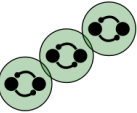
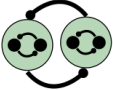

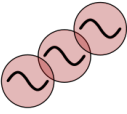
CPG architecture		CPG Model
 Neuron	 Recurrent Neural Network	Ring Model ^C
 Half Center oscillator	 Unit burst Network  Single, 2, 3 Level HCO	Matsuoka ^A Eckeberg Model ^D Ryback ^B Miller and Scott
 Abstract oscillator	 Abstract oscillator Network	Hopf oscillators ^E Phase oscillator ^F Van der Pol Rayleigh

Figure C.4 – Possible classification of the existing models, according to three different CPG architectures type: 1. the “neuron based CPG”, where the building blocks of the CPG networks are not oscillators but neuron models. Therefore the oscillation appears at the level of the network (due to the connection) but the units themselves are not oscillators 2. the “half-center oscillator based CPG”, where the building blocks of the CPG network are half-center oscillators (notable implementation are the UBN and the single,two and three level HCO and, 3. the “abstract CPG”, where the building blocks of the CPG are abstract oscillators that focus on the mathematical convenience of the formulation (explicit phase control, easy generation of arbitrary shape and arbitrary phase relation between the building blocks) rather than on the biological relevance of the model.

Appendix C. Mathematical models

	RNN CPG	HCO CPG	AO CPG
Arbitrary pattern	Optimization	Multi-level HCO	DMPs, Morphing
Synchronization	Global entrainment <i>difficult to predict</i>	Global entrainment	Frequency learning Phase resetting
Phase control	Implicit	Implicit	Explicit

Table C.2 – List of properties relative to each CPG type. RNN CPG stands for recurrent neural network based CPG, HCO CPG for half-center oscillator based CPG and AO CPG for abstract oscillator based CPG.

cally tractable systems, given the computational constraints of embedded systems. Neuron models ranges from the most detailed biophysical description of neurons, to relatively abstract formal spiking or firing rate neuron models. As such, these neuronal models do not show any intrinsic capacity to oscillates, but once coupled together, limit cycle behavior can emerge. In the field of neural networks, this kind of CPG networks are called RNN. The most notable example of such CPG network is the ring model, developed by Székely and Gurfinkel [89]. This CPG model has the form of a RNN and is a highly conceptual model allowing the generation of different locomotor patterns. It is usually composed of a closed chain of groups of neurons (at least two extensors, two flexors and one bifunctional) that projects to motoneurons and determine the order of activation of muscles, hence allowing specific locomotor patterns. Upon descending signal, the system becomes activated through the inhibition of inhibitory neurons (which are active at rest), thus inducing the disinhibition of the chain. The activity within the ring is propagated based on the propagation of an inhibitory drive that travels at a speed that depends on the excitability of each connection. Different neuron models can be used as building block of a neuron based CPG. Below are described the most common ones, categorized as either biophysical, formal spiking or firing rate models.

Biophysical models are detailed models mainly used to investigate how action potentials are formed and, at the level of the CPGs, to understand how rhythm is generated. Although they have been successfully used to implement small CPG networks, their relative complexity (i.e. high degree of nonlinearity, high number of variables, elevated computational cost) make them poor candidates for implementation in robots. The initial model, developed by Hodgkin and Huxley’s [98] to explain the ionic mechanisms underlying the initiation and propagation of action potentials in the squid giant axon is probably the most successful and widely used model of biophysical neurons. Since then, several models, such as the FitzHugh-Nagumo [112] or the Morris-Lecar [116] have been developed, that can qualitatively reproduce the Hodgkin and Huxley model properties, while the equations describing the models are significantly simplified allowing, for instance, effective phase plane analysis through a 2D dimension reduction.

From formal spiking neuron models to firing rate population models. Although detailed biophysical neuron models can reproduce electrophysiological measurements with high fidelity, they are difficult to analyse and are computationally expensive. More abstract formal spiking neuron models, such as the integrate-and-fire or the spike response models [77] have been largely used to study network dynamics and to implement more complex CPG networks. In these models, the action potential is generated by a threshold process; the neuron fires whenever the variable (representing the membrane potential) reaches a specific threshold. The most common formal spiking neuron model, the leaky integrate-and-fire model, is a simple resistor-capacitor circuit, in which the leakage term is due to the resistor and the integration to the capacitor. Although they are too abstract to reproduce all the dynamical features found in real neurons, they can be fully analyzed mathematically and allow the simulation of very large networks. An example of spiking neuron model is the one developed by E.M. Izhikevich [111], who utilized bifurcation methodologies to create a simple 2D system of ordinary differential equations that exhibit most of the observed bursting behavior of neurons, hence recapitulating the biological value of biophysical models, while being as computationally efficient as other formal spiking neuron models.

However, most of the CPG models developed tend to be based on non-spiking neurons – i.e. firing-rate neuron models. Firing-rate neuron models, instead of describing the individual spikes emitted by a neuron, represent the firing rate of a neuron or group of neuron (i.e. the “envelope” of the spiking activity) and can therefore be described using a variable that is continuous with time, providing advantageous mathematical simplicity. These models are well suited to describe the behaviour of group of a neuron, where the global impulse frequency changes slowly compared to the impulse intervals [77]. The Leaky-integrator or the neuron model of the Matsuoka oscillator [131] (see next section) are such models.

HCO CPG

The architecture presented in this section is based on the bio-inspired Half-Center oscillator (HCO) model. Conceptual models were initially proposed by Sherrington to describe a network of reciprocal inhibition, and later by Brown to explain his model of locomotion. The model was further developed by Lundberg [125], who described how spinal interneurons involved in flexion reflexes could participate in the locomotor circuitry.

It is conceptually based on the property of two neurons without intrinsic rhythmogenicity to produce a rhythmic output when coupled. The rhythmogenicity of the coupling is based on reciprocal inhibition, that is, neurons mutually inhibiting each other; the activity of the first group excites, for instance, extensor motoneurons and inhibits the antagonist group (i.e. flexor), preventing their excitation. After a period of depression due to a fatigue mechanism, the second group becomes excited and activates the antagonist group of muscle (flexor), while inhibiting the first half-center, which in turn inhibits extensors, thus driving an alternating two phase pattern. Each CPG must therefore contain two groups of excitatory interneurons (i.e. the half-centers) that project to flexor or extensor motoneurons. Inhibitory interneurons

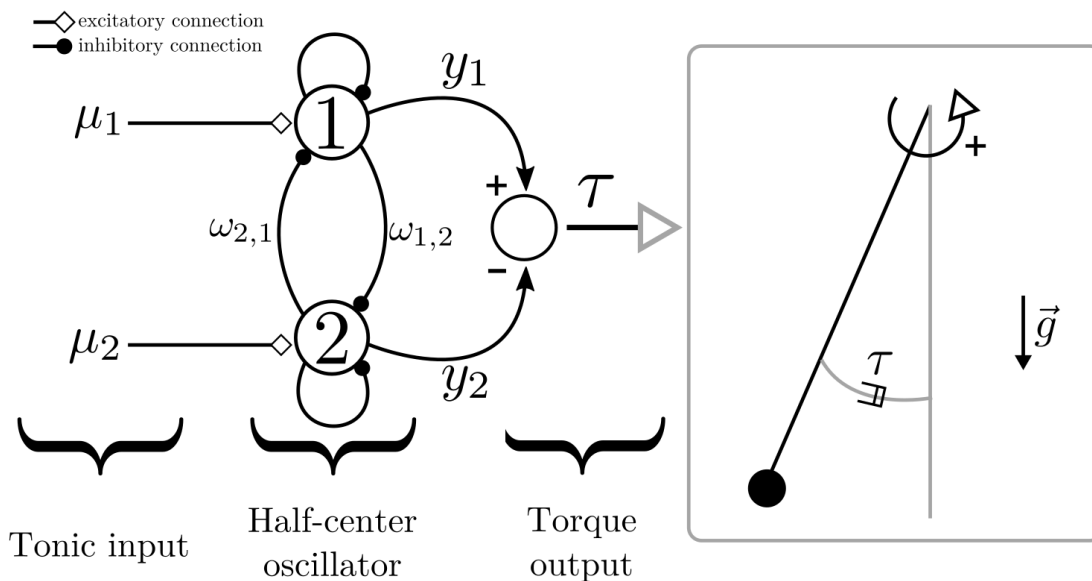


Figure C.5 – Simple pendulum controlled by an HCO. Two non-oscillatory leaky-integrators are connected by inhibitory connections to each other. A self inhibitory connection is also used to ensure the emergence of an oscillation. The parameters of the system are the connection weights and the tonic input. The output of the leaky-integrators is then combined to generate a torque (each unit acting on the opposite direction). The design of the network will favor the emergence of a alternation of activity between the two units and therefore generate a swinging behavior of the pendulum.

enforcing a mutual inhibition between the two groups are used to have only one center activated at the time, and a mechanism of “fatigue” is needed to gradually reduce the activity of the active half-center. Fig. C.5 gives a simple example of an HCO used to drive a pendulum.

Relatively similar to the HCO, the Miller and Scott model (MS) [139] proposes that the alternating mechanism is not due to fatigue, but rather to a specific type of inhibitory neurons present in the spinal cord, the Renshaw cells.

Single, two and three level HCO. To account for the complex locomotor patterns observed in different animals that fail to be recapitulated in the HCO, a two-level half-center model has also been proposed [177], in which both half-centers (i.e. extensor and flexor) send motor commands to bifunctional motoneurons, allowing changes in the pattern structure. This allows a separation between the rhythm and the pattern generation. Many more complex models have since emerged from this model, such as the multi-level half-center models [132] where the phase and frequency of extensor / flexor phases is controlled by a half-center rhythm generator (RG), which projects to a pattern formation (PF) layer that distributes the rhythmic input among the motoneurons. The activation of a specific PF population will excite motoneuron populations and inhibit other PF populations.

Unit burst network (UBN). Based on the physiological observation that CPGs do not simply generate alternation between flexor/extensor activity (i.e. as represented by the half-center model), but can elicit more complex patterns of motoneuron activity in absence of sensory input, Grillner proposed a new conceptual view of CPGs as a network of bursting units, presenting the following properties: 1) each unit CPG can burst by itself or produce tonic output and 2) the connections between unit CPGs assure the coordination. Therefore, in this model, the CPGs consist of multiple coupled oscillators (i.e. modules) [86]. The connections between these units can be both excitatory or inhibitory in nature, and their activity, coupled during normal walking, can be individually controlled by supraspinal centers.

One extensively used UBN is based on Matsuoka's oscillator proposed to describe the autonomic oscillatory behavior observed in neural systems, such as respiration or heartbeat [131]. The model uses firing rate neurons models (represented by piecewise linear differential equations) that receive excitatory stimuli from outside of the network (i.e. from the environment, enabling synchronisation of the oscillator with external signals) and inhibitory stimuli from inside the network (to drive the oscillating patterns). The general equation of a Matsuoka oscillator is defined as follow :

$$\dot{u}_i = \frac{1}{\tau_u} * \left(-u_i + \sum_j^N w_{ij} h(u_j) - \beta v_i + u_0 + S_i(t) \right) \quad (\text{C.10})$$

$$\dot{v}_i = \frac{1}{\tau_v} * \left(-v_i + h(u_i) \right), h(u) = \max(u, 0) \quad (\text{C.11})$$

where, u_i is the state of the i th neuron; v_i is represents the self inhibitory connection of the i th neuron; u_0 is an external input; w_{ij} is a connecting weight from the j th neuron to the i th neuron; τ_u and τ_a are the time constants of the inner state and the self inhibitory connection respectively. S_i is a sensory input to the i th neuron. An example of connection matrix is given in the Section 4.2.

Thanks to its simple neuronal model, the behavior and properties of the CPG emerging from the interaction of several neurons is easy to predict. Matsuoka showed that three different types of topologies can ensure that the neural network produces sustained stable oscillation: 1) lateral inhibition networks of linearly arrayed neurons, 2) symmetrical inhibition networks and 3) cyclic inhibition networks. Consequently, depending on the number of neurons and the network topology, the CPG network can produce many different patterns. This property largely explain why this model has been extensively used both in neuro-mechanical modelling studies of CPG and in robotic applications, to study the dynamical interaction between CPGs and the environment.

AO CPGs

By “abstract oscillator” we mean a dynamical system representing oscillators that 1) do not have a neuron basis, 2) the equations that describe them are not based on neuronal properties, but are purely mathematical representations of oscillatory behaviors used for their mathematical convenience. The final output, that is, the behavior of the whole population of coupled oscillators, is comparable to that obtained when coupling biologically relevant oscillators models, as this dynamic depends mostly on the topology and type of coupling, rather than on the individual mechanisms that drive the oscillation. These types of models are well-suited to study the coordination between different oscillatory centers and can be used to investigate the emergence of complex coordinated patterns of muscle activity, such as those occurring during locomotion. These models are also well-suited for robot applications as they have simple tractable behavior, intrinsic stability, permit intuitive and flexible coupling, while they still allow coupling with external sources, such as sensory information. In this section, we will review the most common abstract mathematical oscillators used to implement CPG networks and highlight their advantages and drawbacks.

1. Amplitude controlled phase oscillator (ACPO)

An ACPO is the simplest model of mathematical oscillator and is defined, in polar coordinate, as follow:

$$[\dot{\theta}, \dot{r}]^T = [\omega, -c \cdot (r - r_0)]^T \quad (\text{C.12})$$

θ and r are respectively the phase and radius of the oscillator. This system represents a limit cycle with an infinite basin of attraction, in the form of a perfect circle of radius r_0 and intrinsic frequency of ω [22], c is the convergence rate of the r toward r_0 . The advantage of this oscillator comes from its simple polar expression (i.e. θ, r are independent), but its trivial structure limits its dynamics (i.e. no bifurcation, see below), which is why more complex oscillators are often preferred.

2. Hopf oscillator

An interesting property of dynamical systems are bifurcations, which are qualitative changes in the dynamics of the system produced by varying structural parameters. A special type of bifurcation that has been widely used in the context of locomotion is the Hopf bifurcation, whose equations can be represented as follow:

$$[\dot{\theta}, \dot{r}]^T = [\omega, (\mu - r^2) \cdot r]^T \quad (\text{C.13})$$

where, θ, r are independent, and corresponds to the phase and radius of the oscillator respectively. ω is the frequency of the oscillation and μ is a structural parameter whose value determine the topology of the system. In certain conditions (when μ sign changes from negative to positive), a Hopf bifurcation occurs. The Hopf bifurcation is characterized by the transition from a fixed point to a limit cycle. In the context of locomotion,

this property is interesting as it allows switches from a resting state (i.e. a fixed point) to locomotion (i.e. a limit cycle). The Hopf oscillator is an abstract dynamical model developed to study and utilize this specific kind of bifurcation.

3. Van der Pol oscillator

The Van der Pol oscillator is a classical example of relaxation oscillator (i.e. switching between a fast and a slow dynamics) that has been often used in biological modeling. It was initially developed to describe electronic circuits containing vacuum tubes, and can be viewed as a simple RLC circuit to which an active nonlinear element has been inserted (for instance the vacuum tube, to replace the passive resistance) and can be represented by the following equation:

$$\ddot{x} + \mu \cdot (x^2 - \alpha) \cdot \dot{x} + \omega^2 \cdot x = 0 \quad (\text{C.14})$$

where μ affects the shape of the waveform, α controls the amplitude of the oscillations and ω the frequency of the oscillations. This model is appreciated for the modeling of locomotion, as the control of the amplitude and frequency of the oscillations is simplified, the physical parameters μ , ω and α being directly associated with the oscillatory behavior. Note that this relation is relatively complex and therefore simpler model such as the Hopf or the ACPO model are usually preferred.

4. Rayleigh oscillator

Originally designed to simulate clarinet oscillations, the Rayleigh oscillator has also been used to model CPGs, and is defined mathematically as follow:

$$\ddot{x} + \mu \cdot (\dot{x}^2 - 1) \cdot \dot{x} + \omega^2 \cdot x = 0 \quad (\text{C.15})$$

The Rayleigh oscillator is relatively similar to the van Der Pol oscillator, except for one key aspect; in an electrical point of view, an increase in voltage would imply an increase in the frequency in the case of the van der Pol oscillator, while in the Rayleigh oscillator it implies an increase in amplitude.

D Supplemental experiments

Neuromuscular ankle controller modeled as an impedance controller

While the modular nature of the NMC design enables control for subject-specific pathologies, controller parameters for subject-specific tuning, such as muscles properties and reflex loops connection weights, are still hard to optimize, mainly due to lack of reliable in-vivo measurement tools. To facilitate subject-specific tunability, we also investigated the modulation of stiffness and damping by comparing the NMC ankle module (presented in Chapter 4 to an impedance controller.

To facilitate tuning of subject-specific parameters, the NMC was compared against impedance controllers derived from a simulated perturbation experiment. The underlying motivation for using a variable impedance model comes from the fact that the stiffness and damping of muscles can be modified based on their intrinsic mechanical properties and the regulations from central nervous system (e.g. reflexes) [24, 71]. These variable muscle impedances can be transferred to the joint level and estimated using torque and angle measurements in perturbation experiments. Such subject-specific estimation of impedance can help to adapt the NMC to the subjects with different muscle mechanical properties and level of motor deficits.

Fig. D.1 shows the estimated stiffness and damping of the ankle across the gait cycle. During the stance phase of the gait, the stiffness damping model was a good approximation of the NMC (correlation of estimated torque with simulated torque > 0.9 except at 2.5% and 17.5% of gait cycle). However, the impedance model was not as representative for the swing phase ($0.4 < \text{correlation coefficient} < 0.7$).

Comparison of the estimated stiffness and the amount of joint torque both in simulations (the linear fit $R^2 > 0.87$) and in the Achilles experiments (Fig. 4.2) verified the existence of a strong linear relationship. This observation is in harmony with previous findings in upper limb impedance [201].

Appendix D. Supplemental experiments

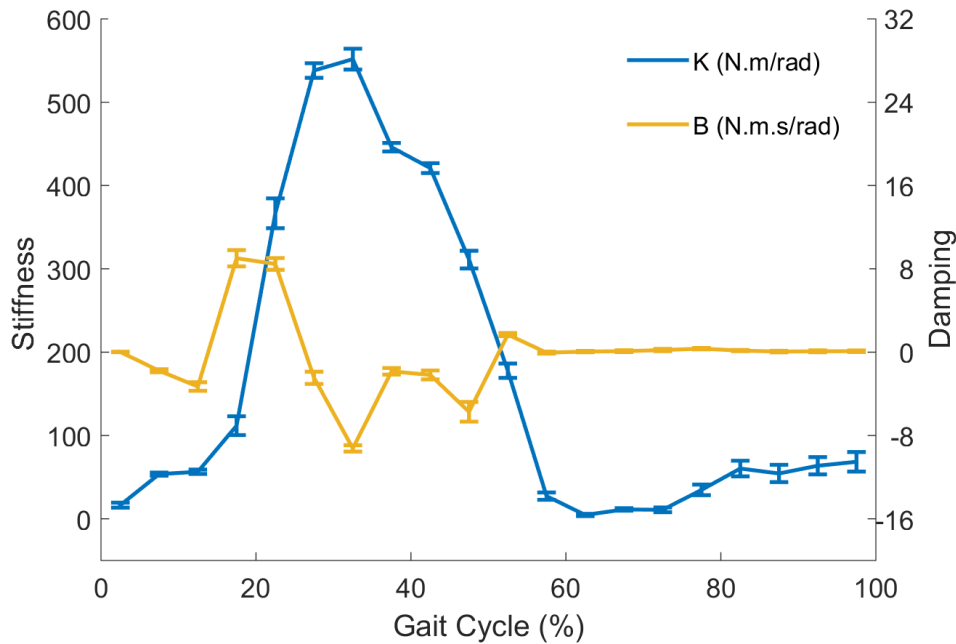


Figure D.1 – Estimated stiffness and damping during gait cycle for the KB-model (the expected value and 3 times standard deviation of estimates). The impedance model was obtained through torque perturbations experiments of different amplitudes applied to the ankle to provide a displacement in joint angle. The perturbations produced deviations in joint angle and torque. These deviations were then processed and used to identify the ankle joint impedance. The impedance model fitted to the reflex controller is the following: KB-model with both variable stiffness and damping components ($\tau = -K(t) \cdot (\theta(t) - \theta_t(t)) - D(t) \cdot (d\theta(t) - d\theta_t(t))$). The correlation (defined as the Pearson correlation between the response torques produced by the reflex controller and by the model) was used to assess the capability of the model to reproduce the response torque produced by torque perturbation.

E Clinical aspects

This last annex is devoted to present some important clinical aspects of the experiments. This will include information on the subjects and inclusion / exclusion criteria, on the tailoring method, and on the assessment methods.

Subjects

Three different categories of subjects were involved in the experiments with the NMC. An healthy group for preliminary testings and two groups of SCI subjects: incomplete and complete paraplegics, the individual groups and their inclusion/exclusion criteria are given below

Incomplete paraplegics

The inclusion criterion where the following :

- 18–75 years old
- incomplete (at cervical, thoracic or lumbar level AIS C or D at the time of inclusion)
- traumatic/non-traumatic first-ever spinal cord lesion
- at least 6 months after lesion
- ability to ambulate over ground;
- evidence of preserved cognitive functions (Mini-Mental State Examination score >26).

Exclusion criterion includes but are not limited to :

- untreatable chronic pain
- untreatable severe spasticity (Ashworth scale score >3),
- severe reduction in lower limb joint's range of motion,
- contraindications for lower extremities weight bearing (pelvic or leg fracture, chronic jointpain, etc.).

Complete paraplegics

Inclusion criteria for test pilots' selection were the following:

- 18–75 years old
- traumatic/non-traumatic first-ever spinal cord lesion, at least 6 months after lesion
- sensory/motor complete lesion (AIS A or B at the time of inclusion) at thoracic or lumbar level
- evidence of preserved cognitive functions (Mini-Mental State Examination score >26).

Exclusion criteria were:

- progressive or not spinal related neurological diseases; symptomatic orthostatic hypotension or 30-mmHg drop when upright; presence of spine-stabilizing devices for whom treating surgeon contraindicates gait; contraindications for lower extremities weight bearing (pelvic or leg fracture, chronic joint pain, etc.); untreatable chronic pain; untreatable severe spasticity (Ashworth scale score >3); severe reduction in lower limb joint's range of motion; pressure sore stage 2 or higher; skin injuries or problems such as blisters, burns, wounds from operation, or other superficial wounds; debilitating disease prior to SCI that causes exercise intolerance and limits mobility-related self-care and instrumental activities of daily living; premorbid major depression or psychosis, suicide attempt caused the SCI, unlikely to complete the intervention or return for follow-up; participation in another research.

Assessments

All experiments involving paraplegics subjects from Symbitron were assessed with a standard procedure involving clinical, psychological and biomechanical assessments. Description is taken from technical reports of the Symbitron, under the authorization of the consortium members.

training procedure

Achilles

The first 10 minutes of each session were devoted to wear the Achilles and to familiarize with it. Test pilots were asked to perform some ankle movements (dorsal/plantar flexion) while maintaining sitting position or knee movements (flexion/extension). After this preliminary phase, test pilots were asked to stand up and start specific balance training propaedeutic for stance/swing phases (zero torque mode for the Achilles). The exercises were devoted to properly distribute the body weight on the lower limbs. A Physical Therapist (PhT) asked the pilots to transfer the body weight in latero-lateral (from the left side on the right one,

and vice versa) and in antero-posterior direction (from forward to backward each side) while maintaining the heels in contact with the ground. To increase the difficulty of the exercises, the PhT asked the pilots to alternatively lift the heel from the ground while doing the latero-lateral transfer of the body weight to reproduce the stance/swing phase of the gait. All these exercises were done both with eyes open and with eyes closed. The last part of the training was devoted to train walking: test pilots were asked to walk with the NMC setting selected during the customization phase according to the body weight transfer scheme previously learned, for instance shifting in a physiological way the body weight from one side to the other and from the back to the front. The PhT asked test pilots to progressively increase the gait speed modifying as little as possible the spatial parameters of the gait (i.e. step length, step width).

WE1

Test pilots were asked to perform some lower limb movements such as dorsal/plantar flexion, knee flexion/extension while sitting and wearing the WE1 to become familiarized with the device. After this preliminary phase, test pilots were asked to walk for 20 minutes with the NMC setting selected during the customization phase by shifting in a physiological way the body weight from one side to the other and in the meanwhile from the back to the front. The PhT asked test pilots to focus on perceiving movements guided by WE1 at each joint. Since WE1 NMC is conceived to provide assistance without forcing pre-defined joint trajectories and only compensating residual functional abilities, test pilots had to properly learn how to walk with the customized level of assistance in order to interact with the WE1 in the best possible way. In particular, test pilots had also to learn how to manage WE1 assistance without counteracting the robot. Finally, the PhT provided verbal instructions for helping test pilots in progressively increasing the gait speed.

WE2

Preliminary tests were performed by the experimenters to optimize subsequent tests with SCI subjects, in terms of:

- **Training Safety:**
All the preliminary activities to fully ensure the safety of the test pilots were performed.
- **Reliability of the robot:**
Extensive tests with WE2 worn by a healthy subject were carried out to check the reliability of the system, to monitor possible faults and to identify in advance possible contingency actions in case of failures.
- **Emergency measures:**
 - **Un-mounting.** Experimenters were trained, with a healthy subject wearing the WE2, to safely and quickly un-mount the robot in case of possible emergency

Appendix E. Clinical aspects

situations.

- Emergency stop. Experimenters were trained, with a healthy subject wearing the WE2, to promptly press the emergency button in case of any danger occurrence.
- Fall prevention:
The FLOAT1 was used both as safety system and as body weight support. It was preventively verified, by a healthy subject wearing the WE2, to be able to prevent falls: emulated and real falls were successfully avoided by its intervention. Experimenters who were guiding the test pilots during training (so called spotters) were also trained to intervene in parallel to the FLOAT to avoid any dangerous condition.
- Training effectiveness and efficiency:
Experimenters defined in advance the procedures to i)
 - help and train test pilots in the most effective way ii) reduce as much as possible the duration of the experiments iii) find a trade-off between complexity and tolerability, still guaranteeing useful results.
 - Mounting procedure. Experimenters tested the WE2 mounting procedure to reduce as much as possible the stress for the test pilots and the duration of the experiments preparation.
 - Training instructions. Experimenters extensively experienced and tested on themselves the action of the WE2 to properly derive the best instructions to be given to the test pilots during the training activities.
 - Assistance as needed. Experimenters tested the way of providing help during walking with the minimum and most effective amount of intervention, as needed by each test pilot (in some cases two spotters were needed on the two sides of the test pilot, in other cases one spotter behind him was sufficient).

The WE2 walking training sessions had the following features:

- Instructions for handling the WE2 and producing a proper gait were given by an expert physiotherapist, who was in front of the test pilot during walking; 1-2 spotters, according to session-specific and/or pilot-specific needs, were close to the test pilots (laterally or behind) to possibly provide stabilizing physical assistance (normally in the antero-posterior direction) and to intervene in case of falls, emergencies and robot failures; The FLOAT was used as a body weight support (BWS) and a safety measure to react and avoid falls in case of perceived sudden vertical motions.
- Minimum BWS: The case when the FLOAT BWS value was set to 10 kg can be considered as a condition without any support since, due to 5 kg weight of the FLOAT harness connection, the BWS became almost negligible.

- Maximum BWS: The FLOAT was also used to lift the test pilots wearing the WE2 in case of direction changes or after robot failures occurrence. In this case a BWS around 70-80 kg was set.
- Planar force. The FLOAT is capable of providing a planar force along the walking direction; this force (maximum: 50 N) was applied sometimes to compensate for a constraining backward pulling force felt by the test pilots during walking and amenable to the FLOAT inaccuracy in being transparent to the user.
- Parallel bars were used during the initial training sessions since they allowed test pilots to have a very good stabilization aid and to firmly keep the control of their body with the arms. When parallel bars were used, steps were triggered by the experimenter, based on the requests expressed through vocal commands by the test pilots. Alternatively, the experimenter decided himself on the cadence of the steps and just notified the test pilots verbally on the forthcoming triggering of each step.
- Crutches were used in a phase when test pilots had gained a sufficient level of autonomy and mastery in handling the robot and the dynamics of walking. When crutches were used, after devoted training on how to manage them, steps were triggered directly by the test pilot through a button positioned in the right handle. A second button was present to trigger the laststep that terminates gait and a redundant safety button, easily accessible to the test pilot, was included to stop the machine in case of emergency.

Training session were organized as follows:

- Psychological assessment
- Robot mounting
- Balance exercises
- Walking training
- Robot un-mounting
- Skin check of the trunk, pelvis and lower limbs
- Psychological assessment

During balance exercises, tasks mimicking stance/swing phases were performed. The exercises were devoted to properly distribute the body weight on the lower limbs. The physiotherapist asked the test pilots to transfer the body weight in mediolateral direction (from the left side to the right one, and vice versa) and in anteroposterior direction (from forward to backward and vice versa) while maintaining the heels in contact with the ground. Upper limbs movements were asked to be properly synchronized with the weight shifting. To increase the difficulty of

Appendix E. Clinical aspects

the exercises, the physiotherapist asked subjects to alternatively lift the heel from the ground while doing the mediolateral transfer of the body weight to reproduce the stance/swing phase of the gait.

During walking training, test pilots were asked to walk using the previously learned weight shifting ability, for instance shifting in a physiological way the weight from one side to the other and in the meanwhile from the back to the front. The physiotherapist provided verbal instructions for helping test pilots in producing a proper gait pattern with enough feet clearance to enable suitable legs swing. During first steps physiotherapist manually assisted test pilots to understand how to manage body weight movements.

Clinical assessment

- The ASIA Impairment Scale (AIS) from the American Spinal Injury Association (ASIA) is used to assess the neurological status of the spinal cord injury. Level C and D reflect incomplete motor lesions while levels A and B reflect more severe cases. Pilot from group 1 are level C and D and pilot from group 2 are level A and B.
- The Modified Ashworth Scale (MAS) [15] [82] was used to evaluate ankle spasticity. The measure involves applying rapid manual movement of the joint through the range of motion to passively stretch specific muscle groups. A 6-point ordinal scale grades the resistance during the passive stretching. Associated symptoms of spasticity such as spasms, clonus, and pain were scored using the Penn modified Spasm Frequency Scale (PSFS) [154], Spinal Cord Assessment Tool for Spastic Reflexes subscale for clonus assessment (SCATS) [10].
- The Manual Muscle Test (MMT) was used for assessing muscle force bilaterally of the hip, knee and ankle joints, according to the motor strength grades 0-5 of the Medical Research Council (0-5, 0/no movement, 5/normal power).
- The Visual Analogue Scale (VAS) was used for assessing the pain at the lower limbs. The VAS consists of a 10 cm line, with 0 representing “no pain” and 10 representing “the worst pain you can imagine” [162].
- The Berg Balance Scale (BBS) [120] was used to identify and evaluate balance impairments, and it can be considered a reflection of functional activity [11].
- Gait was assessed per the Walking Index for Spinal Cord Injury (WISCI) [48], 10 Meter Walking Test (10MWT) [174], and 6 Minutes Walking Test (6MWT) [159]
 - The 10 Meter Walking Test (10MWT) is a measure of walking velocity on a distance of 10 m measured using a stopwatch. Subjects walk in a straight line. As in the original test description, subjects are asked to walk 2 m before the time was recorded and 2 m after to avoid the bias because of acceleration and deceleration

- The 6 Minutes Walking Test (6MWT) is a measure of distance and represents the maximum distance walked in 6 minutes. Patients are asked to walk at their self-selected speed continuously (without resting). This test is performed on a rectangular, 50 m, indoor track. Walking time tests are performed using a self-selected walking device, if needed [150], and scored using the WISCI.
- The Penn Spasm Frequency Scale (PSFS) [15] is a self-reported measure with items on a 5-point scale developed to augment clinical ratings of spasticity and provides a more comprehensive assessment of spasticity. Scores are
 - 0 = No spasm;
 - 1 = Mild spasms induced by stimulation;
 - 2 = Infrequent full spasms occurring less than once per hour;
 - 3 = Spasms occurring more than once per hour;
 - 4 = Spasms occurring more than 10 times per hour.
- The Spinal Cord Assessment Tool Clonus Scale (SCATS) [10], It uses passive dorsi-flexion to assess clonus. It is rated on a 4-point scale that ranges as follows: 0 = No reaction; 1 =Mild lasting <3sec; 2 = Moderate lasting 3-10 sec.; 3 = Severe lasting > 10 sec.

Bibliography

- [1] Masaki O Abe and Norimasa Yamada. Modulation of elbow joint stiffness in a vertical plane during cyclic movement at lower or higher frequencies than natural frequency. *Experimental brain research*, 153(3):394–399, 2003.
- [2] Mostafa Ajallooeian, Jesse van den Kieboom, Albert Mukovskiy, Martin A Giese, and Auke J Ijspeert. A general family of morphed nonlinear phase oscillators with arbitrary limit cycle shape. *Physica D: Nonlinear Phenomena*, pages 41–56, 2013.
- [3] Donna Anderson, Serge Dumont, Leila Azzaria, Marie Le Bourdais, and Luc Noreau. Determinants of return to work among spinal cord injury patients: a literature review. *Journal of Vocational Rehabilitation*, 27(1):57–68, 2007.
- [4] Shinya Aoi and Kazuo Tsuchiya. Locomotion control of a biped robot using nonlinear oscillators. *Autonomous robots*, pages 219–232, 2005.
- [5] Daisuke Aoyagi, Wade E. Ichinose, Susan J. Harkema, David J. Reinkensmeyer, and James E. Bobrow. A robot and control algorithm that can synchronously assist in naturalistic motion during body-weight-supported gait training following neurologic injury. *IEEE transactions on neural systems and rehabilitation engineering: a publication of the IEEE Engineering in Medicine and Biology Society*, 15(3):387–400, September 2007.
- [6] David Malet Armstrong. The supraspinal control of mammalian locomotion. *The Journal of Physiology*, pages 1–37, 1988.
- [7] Richard Baker. The history of gait analysis before the advent of modern computers. *Gait & posture*, 26(3):331–342, 2007.
- [8] Mark Ballermann and Karim Fouad. Spontaneous locomotor recovery in spinal cord injured rats is accompanied by anatomical plasticity of reticulospinal fibers. *The European Journal of Neuroscience*, 23(8):1988–1996, April 2006.
- [9] Sai K. Banala, Suni K. Agrawal, and John P. Scholz. Active Leg Exoskeleton (ALEX) for Gait Rehabilitation of Motor-Impaired Patients. pages 401–407. IEEE, June 2007.
- [10] Ela N Benz, T George Hornby, Rita K Bode, Robert A Scheidt, and Brian D Schmit. A physiologically based clinical measure for spastic reflexes in spinal cord injury. *Archives of physical medicine and rehabilitation*, 86(1):52–59, 2005.

Bibliography

- [11] Katherine Berg, Sharon Wood-Dauphine, JI Williams, and David Gayton. Measuring balance in the elderly: preliminary development of an instrument. *Physiotherapy Canada*, 41(6):304–311, 1989.
- [12] Steve Berger. Energy consumption optimization and stumbling corrective response for bipedal walking gait, July 2011.
- [13] Lindsay J. Bhargava, Marcus G. Pandy, and Frank C. Anderson. A phenomenological model for estimating metabolic energy consumption in muscle contraction. *Journal of Biomechanics*, 37(1):81–88, January 2004.
- [14] Joaquin A. Blaya and Hugh Herr. Adaptive control of a variable-impedance ankle-foot orthosis to assist drop-foot gait. *IEEE transactions on neural systems and rehabilitation engineering: a publication of the IEEE Engineering in Medicine and Biology Society*, 12(1):24–31, March 2004.
- [15] Richard W Bohannon and Melissa B Smith. Interrater reliability of a modified ashworth scale of muscle spasticity. *Physical therapy*, 67(2):206–207, 1987.
- [16] S. J. Bonasera and T. R. Nichols. Mechanical actions of heterogenic reflexes linking long toe flexors with ankle and knee extensors of the cat hindlimb. *Journal of Neurophysiology*, 71(3):1096–1110, 1994.
- [17] I. A. Boyd. Mammalian muscle receptors and their central actions. *Quarterly Journal of Experimental Physiology and Cognate Medical Sciences*, 58(3):290–293, July 1973.
- [18] J. M. Brockway. Derivation of formulae used to calculate energy expenditure in man. *Hum Nutr Clin Nutr*, 1987.
- [19] T Graham Brown. The intrinsic factors in the act of progression in the mammal. *Proceedings of the Royal Society of London. Series B*, pages 308–319, 1911.
- [20] T Graham Brown. On the nature of the fundamental activity of the nervous centres; together with an analysis of the conditioning of rhythmic activity in progression, and a theory of the evolution of function in the nervous system. *The Journal of physiology*, 48(1):18–46, 1914.
- [21] TJH Brug, F Dzeladini, Amy R Wu, and AJ Ijspeert. Combining a 3d reflex based neuromuscular model with a state estimator based on central pattern generators. In *Converging Clinical and Engineering Research on Neurorehabilitation II*, pages 633–637. Springer, 2017.
- [22] Jonas Buchli and Auke Jan Ijspeert. Distributed central pattern generator model for robotics application based on phase sensitivity analysis. In *Biologically Inspired Approaches to Advanced Information Technology*, pages 333–349. Springer, 2004.

- [23] Jonas Buchli, Ludovic Righetti, and Auke Jan Ijspeert. A dynamical systems approach to learning: a frequency-adaptive hopper robot. In *Advances in Artificial Life*, pages 210–220. Springer, 2005.
- [24] E. Burdet, R. Osu, D.W. Franklin, T. Yoshioka, T.E. Milner, and M. Kawato. A method for measuring endpoint stiffness during multi-joint arm movements. *Journal of Biomechanics*, 2000.
- [25] Farley C T and C R Lee. Determinants of the center of mass trajectory in human walking and running. *Journal of Experimental Biology*, 201:2935–2944, November 1998.
- [26] G A Cavagna, H Thys, and A Zamboni. The sources of external work in level walking and running. *The Journal of Physiology*, 262(3):639–657, November 1976.
- [27] GA Cavagna and R Margaria. Mechanics of walking. *Journal of applied physiology*, 21(1):271–278, 1966.
- [28] B. Cioni, M. Meglio, L. Pentimalli, and M. Visocchi. Spinal cord stimulation in the treatment of paraplegic pain. *Journal of Neurosurgery*, 82(1):35–39, January 1995.
- [29] D. J. Clark, L. H. Ting, F. E. Zajac, R. R. Neptune, and S. A. Kautz. Merging of healthy motor modules predicts reduced locomotor performance and muscle coordination complexity post-stroke. *Journal of Neurophysiology*, 103(2):844–857, December 2009.
- [30] Steven H Collins, Peter G Adamczyk, and Arthur D Kuo. Dynamic arm swinging in human walking. *Proceedings of the Royal Society B: Biological Sciences*, 276(1673):3679–3688, 2009.
- [31] Steven H Collins and Arthur D Kuo. Two independent contributions to step variability during over-ground human walking. *PloS one*, 8(8):e73597, 2013.
- [32] G. Colombo, M. Joerg, R. Schreier, and V. Dietz. Treadmill training of paraplegic patients using a robotic orthosis. *J Rehabil Res Dev*, 2000.
- [33] Renato Contini. Body segment parameters, part ii. *Artificial limbs*, 16(1):1–19, 1972.
- [34] Gregoire Courtine, Bingbing Song, Roland R Roy, Hui Zhong, Julia E Herrmann, Yan Ao, Jingwei Qi, V Reggie Edgerton, and Michael V Sofroniew. Recovery of supraspinal control of stepping via indirect propriospinal relay connections after spinal cord injury. *Nature Medicine*, 14(1):69–74, January 2008.
- [35] Grégoire Courtine, Yury Gerasimenko, Rubia van den Brand, Aileen Yew, Pavel Musienko, Hui Zhong, Bingbing Song, Yan Ao, Ronaldo M Ichiyama, Igor Lavrov, Roland R Roy, Michael V Sofroniew, and V Reggie Edgerton. Transformation of nonfunctional spinal circuits into functional states after the loss of brain input. *Nature Neuroscience*, 12(10):1333–1342, October 2009.

Bibliography

- [36] Laura Marchal Crespo and David J. Reinkensmeyer. Haptic guidance can enhance motor learning of a steering task. *Journal of Motor Behavior*, 2008.
- [37] Piotr Czyżżak and Adrezej Jaskiewicz. Pareto simulated annealing—a metaheuristic technique for multipleobjective combinatorial optimization. *Journal of MultiCriteria Decision Analysis*, 7(1):34–47, January 1998.
- [38] Monica A Daley. Biomechanics: running over uneven terrain is a no-brainer. *Current Biology*, 18(22):R1064–R1066, 2008.
- [39] Monica A Daley, G Felix, and Andrew A Biewener. Running stability is enhanced by a proximo-distal gradient in joint neuromechanical control. *Journal of Experimental Biology*, 210(3):383–394, 2007.
- [40] Scott L. Delp, Frank C. Anderson, Allison S. Arnold, Peter Loan, Ayman Habib, Chand T. John, Eran Guendelman, and Darryl G. Thelen. : Open-Source Software to Create and Analyze Dynamic Simulations of Movement. *IEEE Transactions on Biomedical Engineering*, 54(11):1940–1950, November 2007.
- [41] Richard P Di Fabio. Reliability of computerized surface electromyography for determining the onset of muscle activity. *Physical therapy*, 67(1):43–48, 1987.
- [42] V. Dietz. Locomotor activity in spinal man: significance of afferent input from joint and load receptors. *Brain*, 125(12):2626–2634, December 2002.
- [43] V Dietz, G Colombo, and L Jensen. Locomotor activity in spinal man. *The lancet*, 344(8932):1260–1263, 1994.
- [44] V Dietz, G Colombo, L Jensen, and L Baumgartner. Locomotor capacity of spinal cord in paraplegic patients. *Annals of neurology*, pages 574–582, 1995.
- [45] V. Dietz and J. Duysens. Significance of load receptor input during locomotion: a review. *Gait & Posture*, 11(2):102–110, April 2000.
- [46] M. R. Dimitrijevic, L. S. Illis, K. Nakajima, P. C. Sharkey, and A. M. Sherwood. Spinal cord stimulation for the control of spasticity in patients with chronic spinal cord injury: II. Neurophysiologic observations. *Central Nervous System Trauma: Journal of the American Paralysis Association*, 3(2):145–152, 1986.
- [47] Milan R Dimitrijevic, Yuri Gerasimenko, and Michaela M Pinter. Evidence for a spinal central pattern generator in humans. *Annals of the New York Academy of Sciences*, pages 360–376, 1998.
- [48] PL Dittuno and JF Dittuno Jr. Walking index for spinal cord injury (wisci ii): scale revision. *Spinal cord*, 39(12):654, 2001.

-
- [49] B. H. Dobkin, S. Harkema, P. Requejo, and V. R. Edgerton. Modulation of locomotor-like EMG activity in subjects with complete and incomplete spinal cord injury. *Journal of Neurologic Rehabilitation*, 9(4):183–190, 1995.
- [50] N. Dominici, Y. P. Ivanenko, G. Cappellini, A. d’Avella, V. Mondì, M. Cicchese, A. Fabiano, T. Silei, A. Di Paolo, C. Giannini, R. E. Poppele, and F. Lacquaniti. Locomotor primitives in newborn babies and their development. *Science*, 334(6058):997–999, November 2011.
- [51] J Maxwell Donelan, Rodger Kram, and Arthur D Kuo. Mechanical work for step-to-step transitions is a major determinant of the metabolic cost of human walking. *Journal of Experimental Biology*, 205(23):3717–3727, 2002.
- [52] J Maxwell Donelan, Rodger Kram, and Arthur D Kuo. Simultaneous positive and negative external mechanical work in human walking. *Journal of biomechanics*, 35(1):117–124, 2002.
- [53] J Duysens and KJG Pearson. Inhibition of flexor burst generation by loading ankle extensor muscles in walking cats. *Brain research*, pages 321–332, 1980.
- [54] Berger Dzeladini. Nmm library, June 2013.
- [55] F Dzeladini, A Grappe, C Simpson, AR Wu, and A Ijspeert. Muscle activation variability is inversely correlated with walking speed. In *Converging Clinical and Engineering Research on Neurorehabilitation II*, pages 1025–1029. Springer, 2017.
- [56] Florin Dzeladini. Implementation of a Human Feedback-based Locomotion and its Control by means of a Feedforward Component inspired by Central Pattern Generators. 2013.
- [57] Florin Dzeladini, Nadine Ait-Bouziad, and Auke Ijspeert. Cpg-based control of humanoid robot locomotion. *Humanoid Robotics: A Reference*, pages 1–35, 2018.
- [58] Florin Dzeladini, Andrew Pennycott, Auke Ijspeert, and Etienne Burdet. A neuromuscular model for symbiotic man-machine exoskeleton control accounting for patient impairment specificity. *Proceedings of Werob 2014, The International Workshop on Wearable Robotics*, 2014.
- [59] Florin Dzeladini, Jesse van den Kieboom, and Auke Ijspeert. The contribution of a central pattern generator in a reflex-based neuromuscular model. *Frontiers in Human Neuroscience*, 2014.
- [60] Florin Dzeladini, Amy R Wu, Daniel Renjewski, Arash Arami, Etienne Burdet, Edwin van Asseldonk, Herman van der Kooij, and Auke J Ijspeert. Effects of a neuromuscular controller on a powered ankle exoskeleton during human walking. In *Biomedical Robotics and Biomechanics (BioRob), 2016 6th IEEE International Conference on*, pages 617–622. Ieee, 2016.

Bibliography

- [61] Victor Reggie Edgerton and Susan Harkema. Epidural stimulation of the spinal cord in spinal cord injury: current status and future challenges. *Expert Review of Neurotherapeutics*, 11(10):1351–1353, October 2011.
- [62] Michael F Eilenberg, Hartmut Geyer, and Hugh Herr. Control of a Powered Ankle Foot Prosthesis Based on a Neuromuscular Model. *IEEE Transactions on Neural Systems and Rehabilitation Engineering*, 18(2):164–173, April 2010.
- [63] Jeremy L Emken, Raul Benitez, and David J Reinkensmeyer. Human-robot cooperative movement training: Learning a novel sensory motor transformation during walking with robotic assistance-as-needed. *Journal of NeuroEngineering and Rehabilitation*, 4(1):8, 2007.
- [64] Jeremy L. Emken, Susan J. Harkema, Janell A. Beres-Jones, Christie K. Ferreira, and David J. Reinkensmeyer. Feasibility of Manual Teach-and-Replay and Continuous Impedance Shaping for Robotic Locomotor Training Following Spinal Cord Injury. *IEEE Transactions on Biomedical Engineering*, 55(1):322–334, January 2008.
- [65] Gen Endo, Jun Morimoto, Jun Nakanishi, and Gordon Cheng. An empirical exploration of a neural oscillator for biped locomotion control. In *International Conference on Robotics and Automation*. IEEE, 2004.
- [66] Duygun Erol and Nilanjan Sarkar. Intelligent Control for Robotic Rehabilitation after Stroke. *Journal of Intelligent and Robotic Systems*, 50(4):341–360, November 2007.
- [67] Daniel P Ferris, Joseph M Czerniecki, Blake Hannaford, University of Washington, and VA Puget Sound Healthcare System. An ankle-foot orthosis powered by artificial pneumatic muscles. *Journal of applied biomechanics*, 21(2):189, 2005.
- [68] Daniel P. Ferris, Keith E. Gordon, Gregory S. Sawicki, and Ammanath Peethambaran. An improved powered ankle-foot orthosis using proportional myoelectric control. *Gait Posture*, 2006.
- [69] M. J. T FitzGerald, Gregory Gruener, and Estomih Mtui. *Clinical neuroanatomy and neuroscience*. Saunders/Elsevier, [Edinburgh?], 2012.
- [70] C. Fleischer, C. Reinicke, and G. Hommel. Predicting the intended motion with EMG signals for an exoskeleton orthosis controller. In *2005 International Conference on Intelligent Robots and Systems*. IEEE, 2005.
- [71] David W. Franklin, Etienne Burdet, Rieko Osu, Mitsuo Kawato, and Theodore E. Milner. Functional significance of stiffness in adaptation of multijoint arm movements to stable and unstable dynamics. *Experimental Brain Research*, 2003.
- [72] Dustin D French, Robert R Campbell, Sunil Sabharwal, Audrey L Nelson, Polly A Palacios, and Deborah Gavin-Dreschnack. Health care costs for patients with chronic spinal cord injury in the veterans health administration. *The journal of spinal cord medicine*, 30(5):477–481, 2007.

- [73] R. J. Full and D. E. Koditschek. Templates and anchors: neuromechanical hypotheses of legged locomotion on land. *The Journal of Experimental Biology*, 202(Pt 23):3325–3332, December 1999.
- [74] Andrej Gams, Tadej Petric, Aleš Ude, and Leon Žlajpah. *Performing periodic tasks: On-line learning, adaptation and synchronization with external signals*. INTECH Open Access Publisher, 2012.
- [75] Virginia Ruiz Garate, Andrea Parri, Tingfang Yan, Marko Munih, Raffaele Molino Lova, Nicola Vitiello, and Renaud Ronsse. Walking assistance using artificial primitives: a novel bioinspired framework using motor primitives for locomotion assistance through a wearable cooperative exoskeleton. *IEEE Robotics & Automation Magazine*, 23(1):83–95, 2016.
- [76] Martin Garwicz, Maria Christensson, and Elia Psouni. A unifying model for timing of walking onset in humans and other mammals. *Proceedings of the National Academy of Sciences*, 106(51):21889–21893, 2009.
- [77] Wulfram Gerstner and Werner M Kistler. *Spiking neuron models: Single neurons, populations, plasticity*. Cambridge university press, 2002.
- [78] H. Geyer, A. Seyfarth, and R. Blickhan. Compliant leg behaviour explains basic dynamics of walking and running. *Proceedings of the Royal Society B: Biological Sciences*, November 2006.
- [79] Hartmut Geyer and Hugh Herr. A muscle-reflex model that encodes principles of legged mechanics produces human walking dynamics and muscle activities. *Transactions on Neural Systems and Rehabilitation Engineering*, pages 263–273, 2010.
- [80] Hartmut Geyer, Andre Seyfarth, and Reinhard Blickhan. Positive force feedback in bouncing gaits? *Proceedings of the Royal Society of London B: Biological Sciences*, pages 2173–2183, 2003.
- [81] A M Gordon, A F Huxley, and F J Julian. The variation in isometric tension with sarcomere length in vertebrate muscle fibres. *The Journal of physiology*, 184(1):170–192, May 1966. PMID: 5921536.
- [82] Janine M Gregson, Michael Leathley, A Peter Moore, Anil K Sharma, Tudor L Smith, and Caroline L Watkins. Reliability of the tone assessment scale and the modified ashworth scale as clinical tools for assessing poststroke spasticity. *Archives of physical medicine and rehabilitation*, 80(9):1013–1016, 1999.
- [83] DW Grieve. Gait patterns and the speed of walking. *Bio-Med. Eng.*, 3:119–112, 1968.
- [84] S.E. Grill and W.Z. Rymer. Reflex actions of muscle afferents on fusimotor innervation in decerebrated cats: an assessment of beta contributions. *Experimental Brain Research*, 59(2):282–295, 1985.

Bibliography

- [85] S Grillner and P Zangger. On the central generation of locomotion in the low spinal cat. *Experimental Brain Research*, pages 241–261, 1979.
- [86] Sten Grillner. Control of locomotion in bipeds, tetrapods, and fish. *Comprehensive Physiology*, 2011.
- [87] Sten Grillner, AP Georgopoulos, LM Jordan, PSG Stein, and S Grillner. Neurons, networks, and motor behavior, 1997.
- [88] Sten Grillner and Peter Wallen. Central pattern generators for locomotion, with special reference to vertebrates. *Annual review of neuroscience*, 8(1):233–261, 1985.
- [89] VS Gurfinkel and ML Shik. The control of posture and locomotion. In *Motor control*, pages 217–234. Springer, 1974.
- [90] Maki K Habib, Keigo Watanabe, and Kiyotaka Izumi. Biped locomotion using cpg with sensory interaction. In *International Symposium on Industrial Electronics*. IEEE, 2009.
- [91] S. J. Harkema. Neural plasticity after human spinal cord injury: application of locomotor training to the rehabilitation of walking. *The Neuroscientist: A Review Journal Bringing Neurobiology, Neurology and Psychiatry*, 7(5):455–468, October 2001.
- [92] Susan Harkema, Yury Gerasimenko, Jonathan Hodes, Joel Burdick, Claudia Angeli, Yangsheng Chen, Christie Ferreira, Andrea Willhite, Enrico Rejc, Robert G. Grossman, and V. Reggie Edgerton. Effect of epidural stimulation of the lumbosacral spinal cord on voluntary movement, standing, and assisted stepping after motor complete paraplegia: a case study. *Lancet*, 377(9781):1938–1947, June 2011.
- [93] Kazunori Hase, Kazuo Miyashita, Sooyol Ok, and Yoshiki Arakawa. Human gait simulation with a neuromusculoskeletal model and evolutionary computation. *The Journal of Visualization and Computer Animation*, pages 73–92, 2003.
- [94] T. Hayashi, H. Kawamoto, and Y. Sankai. Control method of robot suit HAL working as operator’s muscle using biological and dynamical information. In *2005 International Conference on Intelligent Robots and Systems*. IEEE, 2005.
- [95] Walter Herzog, Timothy R Leonard, Venus Joumaa, Michael M DuVall, and Appaji Panchangam. The three filament model of skeletal muscle stability and force production. 2012.
- [96] G. W. Hiebert and K. G. Pearson. Contribution of sensory feedback to the generation of extensor activity during walking in the decerebrate Cat. *Journal of Neurophysiology*, 81(2):758–770, February 1999.
- [97] A. V. Hill. The heat of shortening and the dynamic constants of muscle. *Proceedings of the Royal Society B: Biological Sciences*, 126(843):136–195, October 1938.

-
- [98] Alan L Hodgkin and Andrew F Huxley. A quantitative description of membrane current and its application to conduction and excitation in nerve. *The Journal of physiology*, pages 500–544, 1952.
- [99] Matthias Hoffmann, Moritz Mühlenthaler, Sabine Helwig, and Rolf Wanka. Discrete particle swarm optimization for TSP: theoretical results and experimental evaluations. In *Adaptive and Intelligent Systems*, volume 6943, pages 416–427. Springer Berlin Heidelberg, Berlin, Heidelberg, 2011.
- [100] M.A. Holgate, T.G. Sugar, and A.W. Bohler. A novel control algorithm for wearable robotics using phase plane invariants. In *2009 International Conference on Robotics and Automation*. IEEE, 2009.
- [101] Scott L Hooper. Central Pattern Generators. In John Wiley & Sons, Ltd, editor, *Encyclopedia of Life Sciences*. Chichester, April 2001.
- [102] Robert Horowitz, Koscak Maruyama, and Richard J Podolsky. Elastic behavior of connectin filaments during thick filament movement in activated skeletal muscle. *The Journal of cell biology*, 109(5):2169–2176, 1989.
- [103] J C Houk. Regulation of Stiffness by Skeletomotor Reflexes. *Annual Review of Physiology*, 41(1):99–114, October 1979.
- [104] M Igarashi, T O-Uchi, and B R Alford. Volumetric and dimensional measurements of vestibular structures in the squirrel monkey. *Acta oto-laryngologica*, 91(5-6):437–444, June 1981. PMID: 7270114.
- [105] Auke J Ijspeert. Biorobotics: Using robots to emulate and investigate agile locomotion. *science*, 346(6206):196–203, 2014.
- [106] Auke Jan Ijspeert, Alessandro Crespi, Dimitri Ryczko, and Jean-Marie Cabelguen. From swimming to walking with a salamander robot driven by a spinal cord model. *science*, pages 1416–1420, 2007.
- [107] Auke Jan Ijspeert, Jun Nakanishi, and Stefan Schaal. Learning attractor landscapes for learning motor primitives. Technical report, EPFL, 2002.
- [108] Auke Jan Ijspeert, Jun Nakanishi, and Stefan Schaal. Movement imitation with nonlinear dynamical systems in humanoid robots. In *International Conference on Robotics and Automation*, pages 1398–1403. IEEE, 2002.
- [109] Marco Iosa, Augusto Fusco, Fabio Marchetti, Giovanni Morone, Carlo Caltagirone, Stefano Paolucci, and Antonella Peppe. The golden ratio of gait harmony: Repetitive proportions of repetitive gait phases. *BioMed Research International*, 2013:1–7, 2013.
- [110] Marco Iosa, Daniela Morelli, Maria Vittoria Nanni, Chiara Veredice, Tiziana Marro, Alessandra Medici, Stefano Paolucci, and Claudia Mazzà. Functional taping: a promising

Bibliography

- technique for children with cerebral palsy. *Developmental Medicine & Child Neurology*, 52(6):587–589, 2010.
- [111] Eugene M Izhikevich et al. Simple model of spiking neurons. *Transactions on neural networks*, pages 1569–1572, 2003.
- [112] Eugene M Izhikevich and Richard FitzHugh. Fitzhugh-nagumo model. *Scholarpedia*, page 1349, 2006.
- [113] L. E. Kahn, W. Z. Rymer, and D. J. Reinkensmeyer. Adaptive assistance for guided force training in chronic stroke. *Conference proceedings: ... Annual International Conference of the IEEE Engineering in Medicine and Biology Society. IEEE Engineering in Medicine and Biology Society. Annual Conference*, 4:2722–2725, 2004.
- [114] James Kennedy. Particle swarm optimization. In *Encyclopedia of Machine Learning*, pages 760–766. Springer, 2010.
- [115] Youngwoo Kim, Yusuke Tagawa, Goro Obinata, and Kazunori Hase. Robust control of cpg-based 3d neuromusculoskeletal walking model. *Biological cybernetics*, pages 269–282, 2011.
- [116] Hiroyuki Kitajima, Kunichika Tsumoto, Tetsuya Yoshinaga, Kazuyuki Aihara, and Hiroshi Kawakami. Bifurcations in morris–lecar neuron model. *Neurocomputing*, pages 293–316, 2006.
- [117] H.I. Krebs, J.J. Palazzolo, L. Dipietro, M. Ferraro, J. Krol, K. Rankeleiv, B.T. Volpe, and N. Hogan. Rehabilitation robotics: Performance-based progressive robot-assisted therapy. *Autonomous Robots*, 15(1):7–20, 2003.
- [118] Arthur D Kuo. The relative roles of feedforward and feedback in the control of rhythmic movements. *Motor control*, 6(2):129–145, April 2002. PMID: 12122223.
- [119] Benedikt Lauber, Albert Gollhofer, and Wolfgang Taube. Differences in motor cortical control of the soleus and tibialis anterior. *Journal of Experimental Biology*, 221(20):jeb174680, 2018.
- [120] JF Lemay and S Nadeau. Standing balance assessment in asia d paraplegic and tetraplegic participants: concurrent validity of the berg balance scale. *Spinal cord*, 48(3):245, 2010.
- [121] Tim R Leonard and Walter Herzog. Regulation of muscle force in the absence of actin-myosin based cross-bridge interaction. *American Journal of Physiology-Cell Physiology*, 2010.
- [122] Bin-Bin Li, Ling Wang, and Bo Liu. An effective PSO-Based hybrid algorithm for multi-objective permutation flow shop scheduling. *IEEE Transactions on Systems, Man, and Cybernetics - Part A: Systems and Humans*, 38(4):818–831, July 2008.

-
- [123] Guang Lei Liu, Maki K Habib, Keigo Watanabe, and Kiyotaka Izumi. Central pattern generators based on matsuoka oscillators for the locomotion of biped robots. *Artificial Life and Robotics*, pages 264–269, 2008.
- [124] A. Lundberg. Multisensory Control of Spinal Reflex Pathways. In *Progress in Brain Research*, volume 50, pages 11–28. Elsevier, 1979.
- [125] A Lundberg. Half-centres revisited. *Regulatory functions of the CNS. Motion and organization principles*, pages 155–167, 1981.
- [126] Marilyn MacKay-Lyons. Central pattern generation of locomotion: a review of the evidence. *Physical Therapy*, 82(1):69–83, January 2002.
- [127] Laura Marchal-Crespo and David J Reinkensmeyer. Review of control strategies for robotic movement training after neurologic injury. *Journal of NeuroEngineering and Rehabilitation*, 6(1):20, 2009.
- [128] Sergey N. Markin, Alexander N. Klishko, Natalia A. Shevtsova, Michel A. Lemay, Boris I. Prilutsky, and Ilya A. Rybak. Afferent control of locomotor CPG: insights from a simple neuromechanical model: Afferent control of locomotor CPG. *Annals of the New York Academy of Sciences*, 1198(1):21–34, June 2010.
- [129] Jared Markowitz, Pavitra Krishnaswamy, Michael F Eilenberg, Ken Endo, Chris Barnhart, and Hugh Herr. Speed adaptation in a powered transtibial prosthesis controlled with a neuromuscular model. *Philosophical Transactions of the Royal Society B: Biological Sciences*, 366(1570):1621–1631, 2011.
- [130] Hugo Gravato Marques, Arjun Bharadwaj, and Fumiya Iida. From Spontaneous Motor Activity to Coordinated Behaviour: A Developmental Model. *PLoS Computational Biology*, 10(7):e1003653, July 2014.
- [131] Kiyotoshi Matsuoka. Sustained oscillations generated by mutually inhibiting neurons with adaptation. *Biological cybernetics*, pages 367–376, 1985.
- [132] David A McCrea and Ilya A Rybak. Organization of mammalian locomotor rhythm and pattern generation. *Brain research reviews*, 2008.
- [133] T. McGeer. Passive Dynamic Walking. *The International Journal of Robotics Research*, 9(2):62–82, April 1990.
- [134] Cor Meijneke, Wietse van Dijk, and Herman van der Kooij. Achilles: An autonomous lightweight ankle exoskeleton to provide push-off power. IEEE.
- [135] Jos Meuleman, Edwin van Asseldonk, Gijs van Oort, Hans Rietman, and Herman van der Kooij. Lopes ii—design and evaluation of an admittance controlled gait training robot with shadow-leg approach. *IEEE transactions on neural systems and rehabilitation engineering*, 24(3):352–363, 2016.

Bibliography

- [136] Jos Meuleman, Edwin van Asseldonk, Gijs van Oort, J. Rietman, and Herman van der Kooij. LOPES II: Design and evaluation of an admittance controlled gait training robot with shadow-leg approach. *Transactions on Neural Systems and Rehabilitation Engineering*.
- [137] O. Michel. Webots: Professional mobile robot simulation. *Journal of Advanced Robotics Systems*, 1(1):39–42, 2004.
- [138] Matjaž Mihelj, Tobias Nef, and Robert Riener. A novel paradigm for patient-cooperative control of upper-limb rehabilitation robots. *Advanced Robotics*, 21(8):843–867, January 2007.
- [139] S Miller and PD Scott. The spinal locomotor generator. *Experimental brain research*, pages 387–403, 1977.
- [140] Karen Minassian, Ursula S Hofstoetter, Florin Dzeladini, Pierre A Guertin, and Auke Ijspeert. The human central pattern generator for locomotion: Does it exist and contribute to walking? *The Neuroscientist*, 23(6):649–663, 2017.
- [141] M Patricia Murray, Ross C Kory, Bertha H Clarkson, and SB Sepic. Comparison of free and fast speed walking patterns of normal men. *American Journal of Physical Medicine & Rehabilitation*, 45(1):8–24, 1966.
- [142] Jun Nakanishi, Jun Morimoto, Gen Endo, Gordon Cheng, Stefan Schaal, and Mitsuo Kawato. Learning from demonstration and adaptation of biped locomotion. *Robotics and Autonomous Systems*, pages 79–91, 2004.
- [143] Blaine S. Nashold and Harry Friedman. Dorsal column stimulation for control of pain: Preliminary report on 30 patients. *Journal of Neurosurgery*, 36(5):590–597, May 1972.
- [144] Kiisa Nishikawa. Eccentric contraction: unraveling mechanisms of force enhancement and energy conservation. *Journal of Experimental Biology*, 219(2):189–196, 2016.
- [145] Jennifer R Nymark, Suzanne J Balmer, Ellen H Melis, Edward D Lemaire, and Shawn Millar. Electromyographic and kinematic nondisabled gait differences at extremely slow overground and treadmill walking speeds. *Journal of Rehabilitation Research & Development*, 42(4), 2005.
- [146] N.J. O’Dwyer, L. Ada, and P.D. Neilson. Spasticity and muscle contracture following stroke. *Brain*, 119(5):1737–1749, 1996.
- [147] Stephen M. Onifer, George M. Smith, and Karim Fouad. Plasticity After Spinal Cord Injury: Relevance to Recovery and Approaches to Facilitate It. *Neurotherapeutics*, 8(2):283–293, April 2011.
- [148] Jimmy Or. A hybrid cpg–zmp control system for stable walking of a simulated flexible spine humanoid robot. *Neural Networks*, pages 452–460, 2010.

- [149] Ciara M O'Connor, Susannah K Thorpe, Mark J O'Malley, and Christopher L Vaughan. Automatic detection of gait events using kinematic data. *Gait & posture*, 25(3):469–474, 2007.
- [150] M Patrick, P Ditunno, JF Ditunno, RJ Marino, G Scivoletto, T Lam, J Loffree, F Tamburella, and B Leiby. Consumer preference in ranking walking function utilizing the walking index for spinal cord injury ii. *Spinal Cord*, 49(12):1164, 2011.
- [151] Chandana Paul, Mario Bellotti, Sašo Jezernik, and Armin Curt. Development of a human neuro-musculo-skeletal model for investigation of spinal cord injury. *Biological Cybernetics*, 93(3):153–170, September 2005.
- [152] K. G. Pearson. Common principles of motor control in vertebrates and invertebrates. *Annual Review of Neuroscience*, 16:265–297, 1993.
- [153] Keir Pearson, Örjan Ekeberg, and Ansgar Büschges. Assessing sensory function in locomotor systems using neuro-mechanical simulations. *Trends in Neurosciences*, 29(11):625–631, November 2006.
- [154] Richard D Penn. Intrathecal baclofen for severe spasticity. *Annals of the New York Academy of Sciences*, 531(1):157–166, 1988.
- [155] Jacquelin Perry, Jon R Davids, et al. Gait analysis: normal and pathological function. *Journal of Pediatric Orthopaedics*, 12(6):815, 1992.
- [156] Per Petersson, Alexandra Waldenström, Christer Fåhræus, and Jens Schouenborg. Spontaneous muscle twitches during sleep guide spinal self-organization. *Nature*, 424(6944):72, 2003.
- [157] Tadej Petric, Andrej Gams, Auke Jan Ijspeert, and Leon Žlajpah. On-line frequency adaptation and movement imitation for rhythmic robotic tasks. *The International Journal of Robotics Research*, pages 1775–1788, 2011.
- [158] Tadej Petrič, Andrej Gams, Martin Tomšič, and Leon Žlajpah. Control of rhythmic robotic movements through synchronization with human muscle activity. In *International Conference on Robotics and Automation*. IEEE, 2011.
- [159] PA Poole-Wilson. The 6-minute walk. a simple test with clinical application, 2000.
- [160] C.-S. Poon. Sensorimotor learning and information processing by bayesian internal models. In *Engineering in Medicine and Biology Society, 2004*. IEEE, 2004.
- [161] Jerry Pratt, Chee-Meng Chew, Ann Torres, Peter Dilworth, and Gill Pratt. Virtual model control: An intuitive approach for bipedal locomotion. *The International Journal of Robotics Research*, pages 129–143, 2001.

Bibliography

- [162] Donald D Price, Patricia A McGrath, Amir Rafii, and Barbara Buckingham. The validation of visual analogue scales as ratio scale measures for chronic and experimental pain. *Pain*, 17(1):45–56, 1983.
- [163] A. Prochazka, D. Gillard, and D. J. Bennett. Positive force feedback control of muscles. *Journal of Neurophysiology*, 77(6):3226–3236, June 1997.
- [164] A Prochazka and M Gorassini. Ensemble firing of muscle afferents recorded during normal locomotion in cats. *The Journal of physiology*, 507 (Pt 1):293–304, February 1998. PMID: 9490855.
- [165] Dale Purves and Jean-Marie Coquery. *Neurosciences*. De Boeck, Paris [etc.], 2005.
- [166] Marc H. Raibert. *Legged robots that balance*. The MIT Press series in artificial intelligence. MIT Press, Cambridge, Mass, 1986.
- [167] Sandeep Rana, Sanjay Jasola, and Rajesh Kumar. A review on particle swarm optimization algorithms and their applications to data clustering. *Artificial Intelligence Review*, 35(3):211–222, November 2010.
- [168] D.J. Reinkensmeyer. How to retrain movement after neurologic injury: a computational rationale for incorporating robot (or therapist) assistance. pages 1479–1482. IEEE, 2003.
- [169] H. Reisine, J. I. Simpson, and V. Henn. A geometric analysis of semicircular canals and induced activity in their peripheral afferents in the rhesus monkey. *Annals of the New York Academy of Sciences*, 545(1 Representatio):10–20, December 1988.
- [170] Robert Riener, Lars Lünenburger, Saso Jezernik, Martin Anderschitz, Gery Colombo, and Volker Dietz. Patient-cooperative strategies for robot-aided treadmill training: first experimental results. *IEEE transactions on neural systems and rehabilitation engineering: a publication of the IEEE Engineering in Medicine and Biology Society*, 13(3):380–394, September 2005.
- [171] Ludovic Righetti, Jonas Buchli, and Auke Jan Ijspeert. From dynamic hebbian learning for oscillators to adaptive central pattern generators. In *International Symposium on Adaptive Motion in Animals and Machines*. Verlag ISLE, Ilmenau, 2005.
- [172] Ludovic Righetti and Auke Jan Ijspeert. Programmable central pattern generators: an application to biped locomotion control. In *International Conference on Robotics and Automation*. IEEE, 2006.
- [173] J. P. Roll and J. P. Vedel. Kinaesthetic role of muscle afferents in man, studied by tendon vibration and microneurography. *Experimental Brain Research*, 47(2):177–190, 1982.
- [174] Philippe Rossier and Derick T Wade. Validity and reliability comparison of 4 mobility measures in patients presenting with neurologic impairment. *Archives of physical medicine and rehabilitation*, 82(1):9–13, 2001.

- [175] Serge Rossignol. Locomotion and its recovery after spinal injury. *Current opinion in neurobiology*, 10(6):708–716, 2000.
- [176] Paolo M. Rossini and Gloria Dal Forno. Integrated technology for evaluation of brain function and neural plasticity. *Physical Medicine and Rehabilitation Clinics of North America*, 2004.
- [177] Ilya A Rybak, Natalia A Shevtsova, Myriam Lafreniere-Roula, and David A McCrea. Modelling spinal circuitry involved in locomotor pattern generation: insights from deletions during fictive locomotion. *The Journal of physiology*, pages 617–639, 2006.
- [178] Kenneth S. Saladin. *Anatomy & physiology: the unity of form and function*. McGraw-Hill, New York, NY, 6th ed edition, 2012.
- [179] Gregory S. Sawicki and Daniel P. Ferris. Mechanics and energetics of level walking with powered ankle exoskeletons. *Journal of Experimental Biology*, 2008.
- [180] R. A. Schmidt and R. A. Bjork. New conceptualizations of practice: Common principles in three paradigms suggest new concepts for training. *Psychological Science*, 1992.
- [181] Gregor Schöner. A dynamic theory of coordination of discrete movement. *Biological cybernetics*, pages 257–270, 1990.
- [182] William John Schwind. *Spring loaded inverted pendulum running: A plant model*. PhD thesis, University of Michigan, 1998.
- [183] Stephen H. Scott and David A. Winter. Biomechanical model of the human foot: Kinematics and kinetics during the stance phase of walking. *Journal of Biomechanics*, 26(9):1091–1104, September 1993.
- [184] W Scott and J Stevens. Human skeletal muscle fiber type classifications. *Phys Therapy*, 81:1810–1816, 2001.
- [185] A. Seyfarth. Swing-leg retraction: a simple control model for stable running. *Journal of Experimental Biology*, 206(15):2547–2555, August 2003.
- [186] C. S. Sherrington. Flexion-reflex of the limb, crossed extension-reflex, and reflex stepping and standing. *The Journal of Physiology*, 40(1-2):28–121, April 1910.
- [187] Charles Sherrington. *The integrative action of the nervous system*. CUP Archive, 1952.
- [188] XH Shi, Y. Zhou, LM Wang, QX Wang, and YC Liang. A discrete particle swarm optimization algorithm for travelling salesman problem. *Computational methods*, pages 1063–1068, 2006.
- [189] Allan Siegel, Hreday N Sapru, and Heidi Siegel. *Essential neuroscience*. Lippincott Williams & Wilkins, Philadelphia, 2006.

Bibliography

- [190] R.W. Soames and J. Atha. The validity of physique-based inverted pendulum models of postural sway behaviour. *Annals of Human Biology*, 7(2):145–153, January 1980.
- [191] Seungmoon Song and Hartmut Geyer. Regulating speed and generating large speed transitions in a neuromuscular human walking model. pages 511–516. IEEE, May 2012.
- [192] Seungmoon Song and Hartmut Geyer. A neural circuitry that emphasizes spinal feedback generates diverse behaviours of human locomotion. *The Journal of physiology*, 593(16):3493–3511, 2015.
- [193] Shoubao Su, Xibin Cao, and Xukun Zuo. Traveling salesman problems on a cuboid using discrete particle swarm optimization. In Rongbo Zhu and Yan Ma, editors, *Information Engineering and Applications*, volume 154, pages 404–411. Springer London, London, 2012.
- [194] Frank Sup, Amit Bohara, and Michael Goldfarb. Design and Control of a Powered Transfemoral Prosthesis. *The International Journal of Robotics Research*, 2008.
- [195] G Taga, Yousuke Miyake, Y Yamaguchi, and H Shimizu. Generation and coordination of bipedal locomotion through global entrainment. In *International Symposium on Autonomous Decentralized Systems*. IEEE, 1993.
- [196] Gentaro Taga. Emergence of bipedal locomotion through entrainment among the neuro-musculo-skeletal system and the environment. *Physica D: Nonlinear Phenomena*, pages 190–208, 1994.
- [197] Gentaro Taga. A model of the neuro-musculo-skeletal system for human locomotion. *Biological cybernetics*, pages 97–111, 1995.
- [198] Gentaro Taga. A model of the neuro-musculo-skeletal system for anticipatory adjustment of human locomotion during obstacle avoidance. *Biological Cybernetics*, pages 9–17, 1998.
- [199] Gentaro Taga, Yoko Yamaguchi, and Hiroshi Shimizu. Self-organized control of bipedal locomotion by neural oscillators in unpredictable environment. *Biological cybernetics*, pages 147–159, 1991.
- [200] Aya Takeoka, Isabel Vollenweider, Grégoire Courtine, and Silvia Arber. Muscle Spindle Feedback Directs Locomotor Recovery and Circuit Reorganization after Spinal Cord Injury. *Cell*, 159(7):1626–1639, December 2014.
- [201] K. P. Tee, E. Burdet, C. M. Chew, and T. E. Milner. A model of force and impedance in human arm movements. *Biological Cybernetics*, 2004.
- [202] Nitish Thatte and Hartmut Geyer. Toward balance recovery with leg prostheses using neuromuscular model control. *IEEE Transactions on Biomedical Engineering*, 63(5):904–913, 2016.

- [203] A.F. Thilmann, S.J. Fellows, and H.F. Ross. Biomechanical changes at the ankle joint after stroke. *Journal of Neurology, Neurosurgery & Psychiatry*, 54(2):134–139, February 1991.
- [204] Michael R Tucker, Jeremy Olivier, Anna Pagel, Hannes Bleuler, Mohamed Bouri, Olivier Lambercy, José del R Millán, Robert Riener, Heike Vallery, and Roger Gassert. Control strategies for active lower extremity prosthetics and orthotics: a review. *Journal of neuroengineering and rehabilitation*, 12(1):1, 2015.
- [205] Bruno J. Urban and Blaine S. Nashold. Percutaneous epidural stimulation of the spinal cord for relief of pain: Long-term results. *Journal of Neurosurgery*, 48(3):323–328, March 1978.
- [206] Heike Vallery, Peter Lutz, Joachim von Zitzewitz, Georg Rauter, Michael Fritschi, Christophe Everarts, Renaud Ronsse, Armin Curt, and Marc Bolliger. Multidirectional transparent support for overground gait training. In *2013 IEEE 13th International Conference on Rehabilitation Robotics (ICORR)*, pages 1–7. IEEE, 2013.
- [207] Herman van der Kooij, Edwin van Asseldonk, Gijs van Oort, Victor Sluiter, Amber Emmens, Heide Witteveen, Nevio Luigi Tagliamonte, Federica Tamburella, Iolanda Pisotta, Marcella Masciullo, et al. Symbitron: Symbiotic man-machine interactions in wearable exoskeletons to enhance mobility for paraplegics. In *International Symposium on Wearable Robotics*, pages 361–364. Springer, 2018.
- [208] Nicolas Van der Noot, Florin Dzeladini, Auke J Ijspeert, and Renaud Ronsse. Simplification of the hill muscle model computation for real-time walking controllers with large time steps. In *Dynamic Walking Conference. ETH Zurich. Google Scholar*, 2014.
- [209] Nicolas Van der Noot, Auke J Ijspeert, and Renaud Ronsse. Biped gait controller for large speed variations, combining reflexes and a central pattern generator in a neuromuscular model. In *International Conference on Robotics and Automation*. IEEE, 2015.
- [210] HJA Van Hedel, L Tomatis, and R Müller. Modulation of leg muscle activity and gait kinematics by walking speed and bodyweight unloading. *Gait & posture*, 24(1):35–45, 2006.
- [211] Hubertus JA van Hedel. Gait speed in relation to categories of functional ambulation after spinal cord injury. *Neurorehabilitation and neural repair*, 23(4):343–350, 2009.
- [212] Johnathan Van Why, Christian Hubicki, Mikhail Jones, Monica Daley, and Jonathan Hurst. Running into a trap: numerical design of task-optimal reflex behaviors for delayed disturbance responses. In *2014 IEEE/RSJ International Conference on Intelligent Robots and Systems*, pages 2537–2542. IEEE, 2014.
- [213] Huseyin Atakan Varol and Michael Goldfarb. Real-time Intent Recognition for a Powered Knee and Ankle Transfemoral Prosthesis. pages 16–23. IEEE, June 2007.

Bibliography

- [214] Rui Vasconcelos, Simon Hauser, Florin Dzeladini, Mehmet Mutlu, Tomislav Horvat, Kamilo Melo, Paulo Oliveira, and Auke Ijspeert. Active stabilization of a stiff quadruped robot using local feedback. In *Intelligent Robots and Systems (IROS), 2017 IEEE/RSJ International Conference on*, pages 4903–4910. IEEE, 2017.
- [215] Jan F. Veneman, Rik Kruidhof, Edsko E. G. Hekman, Ralf Ekkelenkamp, Edwin H. F. Van Asseldonk, and Herman van der Kooij. Design and evaluation of the LOPES exoskeleton robot for interactive gait rehabilitation. *IEEE transactions on neural systems and rehabilitation engineering: a publication of the IEEE Engineering in Medicine and Biology Society*, 15(3):379–386, September 2007.
- [216] Bart W Verdaasdonk, HFJM Koopman, and Frans CT Van Der Helm. Energy efficient and robust rhythmic limb movement by central pattern generators. *Neural Networks*, pages 388–400, 2006.
- [217] BW Verdaasdonk, HFJM Koopman, and Frans CT van der Helm. Energy efficient walking with central pattern generators: from passive dynamic walking to biologically inspired control. *Biological cybernetics*, pages 49–61, 2009.
- [218] Joachim von Zitzewitz, Michael Bernhardt, and Robert Riener. A novel method for automatic treadmill speed adaptation. *IEEE transactions on neural systems and rehabilitation engineering: a publication of the IEEE Engineering in Medicine and Biology Society*, 15(3):401–409, September 2007.
- [219] Miomir Vukobratovic and Branislav Borovac. Zero-moment point thirty five years of its life. *International Journal of Humanoid Robotics*, pages 157–173, 2004.
- [220] Jack M. Wang, Samuel R. Hamner, Scott L. Delp, and Vladlen Koltun. Optimizing locomotion controllers using biologically-based actuators and objectives. *ACM Transactions on Graphics*, 31(4):1–11, July 2012.
- [221] N. Weidner and M. H. Tuszynski. Spontaneous plasticity in the injured spinal cord—implications for repair strategies. *Molecular Psychiatry*, 7(1):9–11, 2002.
- [222] Peter G Weyand, Bethany R Smith, Maurice R Puyau, and Nancy F Butte. The mass-specific energy cost of human walking is set by stature. *The Journal of experimental biology*, 213(Pt 23):3972–3979, December 2010. PMID: 21075938.
- [223] Patrick J Whelan. Control of locomotion in the decerebrate cat. *Progress in neurobiology*, 49(5):481–515, 1996.
- [224] Matthew M Williamson. *Robot arm control exploiting natural dynamics*. PhD thesis, Citeseer, 1999.
- [225] David A. Winter. *Biomechanics and Motor Control of Human Movement*. John Wiley & Sons, Inc., Hoboken, NJ, USA, September 2009.

- [226] Eric T. Wolbrecht, Vicky Chan, Vu Le, Steven C. Cramer, David J. Reinkensmeyer, and James E. Bobrow. Real-time computer modeling of weakness following stroke optimizes robotic assistance for movement therapy. pages 152–158. IEEE, May 2007.
- [227] Amy R Wu, Florin Dzeladini, Tycho JH Brug, Federica Tamburella, Nevio L Tagliamonte, Edwin Van Asseldonk, Herman Van Der Kooij, and Auke J Ijspeert. A versatile neuromuscular exoskeleton controller for gait assistance: a preliminary study on spinal cord injury patients. In *Wearable Robotics: Challenges and Trends*, pages 163–167. Springer, 2017.
- [228] Amy R Wu, Florin Dzeladini, Tycho JH Brug, Federica Tamburella, Nevio L Tagliamonte, Edwin HF Van Asseldonk, Herman Van Der Kooij, and Auke J Ijspeert. An adaptive neuromuscular controller for assistive lower-limb exoskeletons: A preliminary study on subjects with spinal cord injury. *Frontiers in neurorobotics*, 11:30, 2017.
- [229] Amy R Wu, Florin Dzeladini, and Auke J Ijspeert. Speed-related gait changes in reflex-based neuromuscular models with a cpg extension. *Moment (Nm)*, 100:0, 2017.
- [230] Michel Wyndaele and Jean-Jacques Wyndaele. Incidence, prevalence and epidemiology of spinal cord injury: what learns a worldwide literature survey? *Spinal cord*, 44(9):523, 2006.
- [231] Aaron J. Young, Ann M. Simon, Nicholas P. Fey, and Levi J. Hargrove. Intent recognition in a powered lower limb prosthesis using time history information. *Annals of Biomedical Engineering*, 2014.
- [232] George I Zahalak. Can muscle fibers be stable on the descending limbs of their sarcomere length-tension relations? *Journal of Biomechanics*, 30(11-12):1179–1182, 1997.
- [233] Karl E. Zelik and Arthur D. Kuo. Human walking isn't all hard work: evidence of soft tissue contributions to energy dissipation and return. *J. Exp. Biol.*, 2010.

Florin Dzeladini

Mobile: +41-76-440-8702
E-mail: florin.dzeladini@epfl.ch

RESEARCH INTERESTS	Neural control of locomotion, Artificial intelligence, bio-inspired artificial intelligence, distributed intelligent systems, dynamical system modeling, engineering, machine learning, programming, signal processing, neurosciences, mechatronics
EDUCATION	<p>EPFL, Lausanne, VD, Switzerland</p> <p>M.S., Life Science & Technology February 2013</p> <ul style="list-style-type: none">• Minor in biocomputing• Minor in business management <p>B.S., Life Science & Technology July 2010</p> <p>CMS, Special Course in Mathematics July 2006</p> <p>CIFOM, Le Locle, NE, Switzerland</p> <p>H.S., Computer Science July 2005</p> <ul style="list-style-type: none">• <i>Magna cum Laude</i>, With Honors
ACADEMICS PROJECTS	<ul style="list-style-type: none">• <i>Gait project : Modeling pathological gait</i> 2018-present• <i>Symbitron project : robotics assisted rehabilitation of paraplegic subjects</i> 2013-2018• <i>Bipedal walking modeling</i> 2012• <i>Locomotion prediction of bipedal walking in monkeys</i> 2011• <i>Locomotion modeling of a Cheetah robot</i> 2010• <i>Image Classification using SVM and ANN</i> 2010• <i>Evolutionary neural network on behaviors based controller</i> 2010• <i>Highway traffic modelisation and jam traffic prediction</i> 2010
PROFESSIONAL EXPERIENCE	<ul style="list-style-type: none">• <i>Adivsor at IOV</i> 2018• <i>Adivsor at Aeler</i> 2018• <i>Adivsor at AlpineMining</i> 2017-2018• <i>Startup Development : AlpineMining</i> 2017• <i>Startup Development Festy payment system</i> 2017• <i>Startup Development Guest list management</i> 2017• <i>Adivsor at 1Motion</i> 2012-2018• <i>Job as CTO at Opera incubator</i> july-dec 2017• <i>Job as CTO at Biodyssey SA : Biodyssey</i> 2011-2012• <i>Company Development : 1Motion</i> 2012
CENTER OF INTERESTS	<p>Artistic Jamming & Music composition & Piano playing</p> <p>Environment Vegetable growing</p> <p>Spirtuality Vipassana & Mindfulness & Plant therapy</p> <p>Economics Sustainable entrepreneurship & Cryptocurrenc</p> <p>Sports Hiking & Snowboarding</p>
SKILLS	<p>Computer science Web/App development, server configuration, cryptocurrencies, artificial intelligence</p> <p>Music Composition, piano playing, improvisation & jamming</p> <p>Social Patience, diplomacy, perseverance, enthousiasm</p>

Journal Papers :

- Florin Dzeladini, Jesse van den Kieboom, and Auke Ijspeert. The contribution of a central pattern generator in a reflex-based neuromuscular model. *Frontiers in Human Neuroscience*, 2014.
- Amy R Wu, Florin Dzeladini, Tycho JH Brug, Federica Tamburella, Nevio L Tagliamonte, Edwin HF Van Asseldonk, Herman Van Der Kooij, and Auke J Ijspeert. An adaptive neuromuscular controller for assistive lower-limb exoskeletons: A preliminary study on subjects with spinal cord injury. *Frontiers in neurorobotics*, 11:30, 2017.

Conferences paper :

- Florin Dzeladini, Amy R Wu, Daniel Renjewski, Arash Arami, Etienne Burdet, Edwin van Asseldonk, Herman van der Kooij, and Auke J Ijspeert. Effects of a neuromuscular controller on a powered ankle exoskeleton during human walking. In *Biomedical Robotics and Biomechanics (BioRob), 2016 6th IEEE International Conference on*, pages 617–622. Ieee, 2016.
- F Dzeladini, A Grappe, C Simpson, AR Wu, and A Ijspeert. Muscle activation variability is inversely correlated with walking speed. In *Converging Clinical and Engineering Research on Neurorehabilitation II*, pages 1025–1029. Springer, 2017.
- Florin Dzeladini, Andrew Pennycott, Auke Ijspeert, and Etienne Burdet. A neuromuscular model for symbiotic man-machine exoskeleton control accounting for patient impairment specificity. *Proceedings of Werob 2014, The International Workshop on Wearable Robotics*, 2014,
- Nicolas Van der Noot, Florin Dzeladini, Auke J Ijspeert, and Renaud Ronsse. Simplification of the hill muscle model computation for real-time walking controllers with large time steps. In *Dynamic Walking Conference. ETH Zurich. Google Scholar*, 2014,
- TJH Brug, F Dzeladini, Amy R Wu, and AJ Ijspeert. Combining a 3d reflex based neuromuscular model with a state estimator based on central pattern generators. In *Converging Clinical and Engineering Research on Neurorehabilitation II*, pages 633–637. Springer, 2017.
- Amy R Wu, Florin Dzeladini, Tycho JH Brug, Federica Tamburella, Nevio L Tagliamonte, Edwin Van Asseldonk, Herman Van Der Kooij, and Auke J Ijspeert. A versatile neuromuscular exoskeleton controller for gait assistance: a preliminary study on spinal cord injury patients. In *Wearable Robotics: Challenges and Trends*, pages 163–167. Springer, 2017.
- Amy R Wu, Florin Dzeladini, and Auke J Ijspeert. Speed-related gait changes in reflex-based neuromuscular models with a cpg extension. *Moment (Nm)*, 100:0, 2017.
- Rui Vasconcelos, Simon Hauser, Florin Dzeladini, Mehmet Mutlu, Tomislav Horvat, Kamilo Melo, Paulo Oliveira, and Auke Ijspeert. Active stabilization of a stiff quadruped robot using local feedback. In *Intelligent Robots and Systems (IROS), 2017 IEEE/RSJ International Conference on*, pages 4903–4910. IEEE, 2017.

Reviews :

- Florin Dzeladini, Nadine Ait-Bouziad, and Auke Ijspeert. Cpg-based control of humanoid robot locomotion. *Humanoid Robotics: A Reference*, pages 1–35, 2018.
- Karen Minassian, Ursula S Hofstoetter, Florin Dzeladini, Pierre A Guertin, and Auke Ijspeert. The human central pattern generator for locomotion: Does it exist and contribute to walking? *The Neuroscientist*, 23(6):649–663, 2017.

